THE UNIVERSITY OF CHICAGO

EXPLORING THE SYNTHESIS OF POLY[*N*]CATENANES

A DISSERTATION SUBMITTED TO

THE FACULTY OF THE DIVISION OF THE PHYSICAL SCIENCES

IN CANDIDACY FOR THE DEGREE OF

DOCTOR OF PHILOSOPHY

DEPARTMENT OF CHEMISTRY

BY

MARISSA MICHELLE TRANQUILLI

CHICAGO, ILLINOIS

AUGUST 2022

DEDICATION

This one is for me.

TABLE OF CONTENTS

LIST OF TABLES

LIST OF FIGURES

LIST OF EQUATIONS

LIST OF SYMBOLS AND ABBREVIATIONS

°C	Degrees Celsius
δ (NMR)	NMR Chemical Shift
δ (Equation 2.2)	Pulsed Field Gradient Duration
Δ (Equation 2.2)	Diffusion Delay
γ (Equation 2.2)	Gyromagnetic Ratio of the Nuclei
2EG	Diethylene Glycol
3EG	Triethylene GLycol
4EG	Tetraethylene glycol
Å	Angstrom
ADMET	Acyclic Diene Metathesis
AFM	Atomic Force Microscopy
au	Arbitrary Units
b-	Branched
Bip	2,6-bisbenzimidazolylpyridine
BPA	Bisphenol A
BPZ	Bisphenol Z
c-	Cyclic
ca.	Circa
COSY	Correlated Spectroscopy
CV	Column Volumes
d	Doublet
D (Equation 2.2)	Diffusion Coefficient
DCM	Dichloromethane
DMF	Dimethylformamide
dn/dc	Specific Refractive Index Increment
DOSY	Diffusion Ordered Spectroscopy

$\overline{\boldsymbol{DP}}$	Degree of Polymerization
ESI	Electrospray Ionization
fluoro	Fluorene
h	Sextet
H_{mpy}	*m*-Pyridyl Protons of Bip
HPLC	High Performance Liquid Chromotography
G (Equation 2.2)	Gradient Strength
g	Grams
g mol^{-1-}	Grams per Mole
GPC	Gas Permeation Chromatography
GPZ	Gradient Pulse on the Z-Axis (NMR)
I	Integration
I_g (Equation 2.2)	Integration of Peak at GPZ value = 5
I_g (Equation 2.2)	Integration of Peak at GPZ value = g
K	Kelvin
kg/ mol	Kilograms Per Mole
l-	Linear
m	Multiplet
M–M	Metal–Metal (distance)
m^2 g^{-1}	Square Meters per Gram
m^2 s^{-1}	Square Meters per Second
$\overline{\boldsymbol{M_n}}$	Number Average Molar Mass
MALDI	Matrix-Assisted Laser Desorption/Ionization
MALS	Multi-Angle Light Scattering
MC	Macrocycle
MeOH	Methanol
Meta	α,α′-Dibromo-*m*-xylene
mg	Milligram

MHz	Mega Hertz
min	Minutes
mL	Milliliter
mM	Millimolar (molar^{-3})
mmol	Millimoles
MS	Mass Spectrometry
MSP	Metallosupramolecular Polymer
MW	Molecular Weight
N_c	Number of Chain Ends
nap	2,7-disubsituted naphthalene linker
nm	Nanometers
NMR	Nuclear Magnetic Resonance
NOESY	Nuclear Overhauser Effect Spectroscopy
oligo	Oligomer
ortho	α,α′-Dibromo-*o*-xylene
p	Pentet
para	α,α′-Dibromo-*p*-xylene
PDMS	Polydimethylsiloxane
PGSE	Pulsed-Gradient Spin-Echo
ppm	Parts Per Million
q	Quartet
RI	Refractive Index
rt	Room Temperature
s	Singlet
SEC	Size Exclusion Chromatography
SMFS	Single-molecule Force Spectroscopy
t	Triplet
TEA	Triethylamine

T_g	Glass Transition Temperature
THF	Tetrahydrofuran
TMS	Tetramethylsilane
TOF	Time of Flight
UV	Ultraviolet
UV/vis	Ultraviolet–Visible
wrt	With Respect To
wt%	Weight Percent
xan	3,6-disubstited 9,9-dimethylxanthene linker

ACKNOWLEDGEMENTS

In reviewing my time here in Chicago, I find that I cannot possibly thank everyone who merits thanks, even if I spent every page of this dissertation on acknowledgements. From the academic perspective, I must thank my advisor, Dr. Stuart Rowan, for his guidance as a mentor and for being a genuinely fun person to spend time with outside of the lab. I am grateful to everyone who worked with me on the interlocked project as a whole: Dr. Qiong Wu, Dr. Benjamin Rawe, Dr. Phillip Rauscher, Jerald Hertzog, Laura Hart, Guancen Liu, Molly Sun, and Abigail Dizon. Unfortunately, due to Stuart's propensity for collecting incredible scientists, I cannot list every friend that I have been lucky enough to gain, so I will say more generally: Thank you to every member of the Rowan Group, past and present. Much of the science in this dissertation was made possible with aid from the facilities managers Dr. Phillip Griffin, Dr. Antoni Jurkiewicz, and Dr. Josh Kurutz, whose help I will be forever grateful for. Finally, I would like to thank the members of my committee, Dr. John Anderson and Dr. Mark Levin, for their advice and for taking the time to be interested in my work.

Beyond my academic pursuits, there are many people who should be thanked; however, instead of listing every name, I will do so anecdotally. In pursuit of self-reflection, I often like to ask silly little questions to probe how I perceive myself and others. Recently, a question I have asked myself and my friends is the following, "If you spoke to your high school self, what are three things about you/ your current life that they would not believe?"

In truth, this question came about in a cart-before-the-horse kind of way, as my first answer was the inspiration for the question itself: I would not have believed the quantity, quality, and variety of the people in my life who genuinely care about me. To you all: thank you. Even if our

friendship was a short one or a blip on your radar, it has changed me and I am beyond grateful for each and every one of you.

The only community in Chicago that I would like to thank by name are the Hyde Park Community Players. Thank you for allowing me to be my overly dramatic self and for including me in your family.

Finally, what may seem like the silliest thanks to a reader, but is truly the most important to me, I want to thank the stories that kept me sane through these years. Stories have always been the most important part of how I define myself, regardless of the form of media they are expressed through. I have therefore selected one television show and novel for each year of my time in grad school that was important to me (*note- the selected work was not always released during the year in question, it was selected for when it came into my life, not for when it came into the world). For any future reader of this thesis, feel free to accept this as a list of recommendations:

2016: The X-Files; *Assassin's Apprentice* by Robin Hobb
2017: The Good Place; *The Tao of Pooh* by Benjamin Hoff
2018: Fullmetal Alchemist: Brotherhood; *The Wind-Up Bird Chronicle* by Murakami Haruki
2019: Legion; *The Bear and the Nightingale* by Katherine Arden
2020: Steins;gate; *Mo Dao Zu Shi* by Mo Xiang Tong Xu
2021: Word of Honor; *The Husky and His White Cat Shizun* by Rou Bao Bu Chi Rou
2022: Our Flag Means Death; *The Three-Body Problem* by Liu Cixin

ABSTRACT

Mechanically interlocked polymers (MIPs) derive their name from their unique mechanical bonding motif in which the polymer components are constrained in space but not physically bound to each other. MIPs have received increasing attention of late due to their potential in the fields of molecular machines and smart soft materials. Of these materials, one of the most synthetically challenging architectures is the poly[*n*]catenane, a polymer composed only of interlocking macrocyclic rings, where *n* is equal to the number of interlocked rings. The interlocking macrocycles allow the polymer to display different motions than those seen in a traditionally covalently bound material, suggesting that the poly[*n*]catenane may display uncommon dynamics in solution and unique material properties, such as superior strength and flexibility.

In 2017, the first poly[*n*]catenane synthesis was reported, created from a metallosupramolecular polymer (MSP) template consisting of alternating units of macrocyclic and linear thread-like monomers. Ring closure of the thread components yielded the interlocked polymer and this initial report focused primarily proving the existence of the poly[*n*]catenane structure, while including basic characterization of polymer architecture. This dissertation represents the continuation of that work.

Firstly, the original synthetic process was explored in depth, with a focus on the MSP precursor. This study primarily probed the effects of the reaction concentration on the overall yields and product mixtures of the poly[*n*]catenane. Secondly, a new series of linear thread-like monomers was developed to test the applicability of this method beyond the initial synthesis and determine how the structure of this component changes the final architecture of the

poly[*n*]catenane. Thirdly, a library of new macrocyclic monomers was created to test the effects of both size and rigidity of these components on the overall poly[*n*]catenane synthesis and the formation of unwanted byproducts. Fourth and lastly, steps toward creating more complex poly[*n*]catenane co-polymers and networks have been taken.

Chapter 1: The Synthesis and Material Properties of Polymeric Catenanes

* This chapter was adapted from: Hart, L.F.; Hertzog, J.E.; Rauscher, P.M.; Rawe, B.W.; Tranquilli, M.M.; Rowan, S.J. Material Properties and Applications of Mechanically Interlocked Polymers. *Nature Reviews Materials*. **2021**, *6*, 508-530.

As well as incorporating excerpts from: Liu, G.; Rauscher, P.M.; Rawe, B.W.; Tranquilli, M.M.; Rowan, S.J. *Chem. Soc. Rev*. **2022**, *51*, 4928-4948.

1.1 The History of Interlocking Molecules

Throughout the study of the chemical sciences, the various forms of atomic bonds have acted as a primary driving force behind scientific exploration. In fact, variations between the covalent and ionic bonds are one of the earliest lessons for a chemist, and the importance of the hydrogen bond is emphasized throughout the sciences. The use of new bonding motifs, therefore, creates boundless opportunities for chemists to explore—from synthesis to functionality. Such was the case with the topological bond when it was reportedly first proposed in 1912;[1] this bonding moiety differs greatly from traditional bonding motifs due to the mechanically interlocked nature of the components. Within a topological bond, the components are spatially associated rather than chemically bound (**Figure 1.1**). However, while the components are not themselves

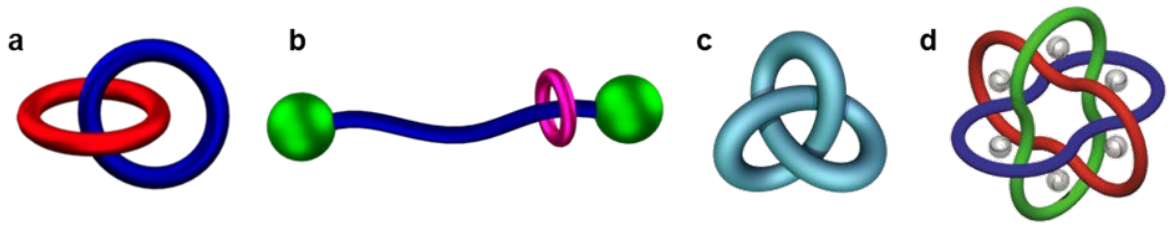

Figure 1.1 Common types of topologically bonded molecules: (a) catenane, (b) rotaxane, (c) knotane, (d) Borromean ring.

covalently bound, the topological bond achieves its robust nature from the fact that the permanent entanglement between components cannot be undone without breaking a covalent bond. As a result, the components are subject to a range of motions[2–4] that cannot be achieved with traditional binding motifs.

However, unlike many bonding motifs, the topological bond occurs very rarely in nature; apart from records of knotted proteins[5,6] and catenated DNA strands,[7,8] topologically bonded materials are primarily created through laboratory synthesis. The absence of a large library of these materials is due in large part to the fact that the entangled form is entropically disfavored during synthesis. In fact, it would take nearly 50 years from the conception of the first interlocked molecule to the initial synthesis in 1960[1] due to both the entropic unfavourability and the complexity of the component synthesis. This first interlocked molecule was a catenane (**Figure 1.1a**): two individual macrocycle rings interlocked in a chain-link fashion. However, it would quickly be followed by the conception[9] and synthesis[10,11] of a rotaxane (**Figure 1.1b**): a macrocyclic ring threaded on to a stoppered axel component. Among the library of topological molecules are also knotanes[12] (**Figure 1.1c**) and Borromean rings[13] (**Figure 1.1d**): self-contained entangled molecules.

As briefly mentioned, the synthesis of these complexes has been a particular challenge for the field, and a selection of synthetic techniques will be discussed in Section 1.2. However, once completed, the topologically linked materials hold great potential for use in a variety of fields due to the range of motions of the components. In the rotaxane for example, the macrocycle is able to rotate around its central axis and undergo translational motion along the axel (**Figure 1.2a**). These motions have been taken advantage of in many materials syntheses.[14–19] For instance, the translation and rotation can be applied in biomedical applications[20–22] and the

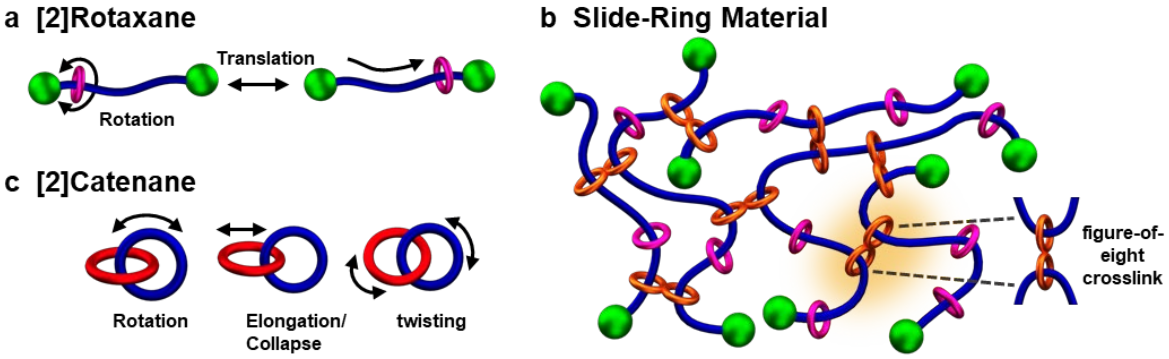

Figure 1.2 (a) The rotational and translations movements observed in the rotaxane topological bond; (b) The slide-ring type material where crosslinking at the mobile macrocycle allows for unique stress dissipation. (c) The three distinct modes of motion accessible to the catenane.

translation of the rings has been exploited in the synthesis of network polymers, where the crosslink is located at the mobile macrocycle (forming a figure-of-eight type crosslink), which have been called slide-ring materials (SRMs, **Figure 1.2b**).[23–26] Within these materials, mobile interlocked crosslinks allow polymer chains to slide through the network like a pulley system, allowing dissipation of stresses in a cooperative manner. This allows for materials that will often display increased toughness and higher extensibility.[19]

The catenane bonding motif has similarly been exploited for a variety of uses. Like the rotaxane, the catenated molecules have primarily been explored in the fields of biological application[27] and polymeric materials.[19,28] The catenane rings are similarly able to rotate along the central axis and translate (collapse/expand) within each other (**Figure 1.2c**). Though the range of translational motion may be lower than that of the rotaxane (depending on the length of the rotaxane axel), the catenane is also able to undergo a third unique motion known as ring twisting (**Figure 1.2c**). Due to these unique motions, there has long been a push to make macromolecular polymeric materials out of catenanes,[28] particularly due to the speculation that polymers composed of only catenane (poly[*n*]catenane) could exhibit a large loss modulus, rapid

stress relaxation, and low activation energy for flow.[29,30] It is worthwhile pointing out that there is little theoretical basis for these conjectures and the theoretical works[31,32] which are sometimes cited as evidence for these properties do not address rheology; however, it is nevertheless reasonable to assume that the large number of interlocking components in these polymers will indeed impart unique or unusual properties on these materials. Unfortunately, the complexities of catenane synthesis have long acted as a barrier to the achievement of these materials.

1.2 Methods for Synthesis of Catenanes

The most basic form of the catenane is composed of only 2 interlocking rings and is named the [2]catenane. Similarly, all catenanes are named for the number of interlocking components they possess, with the largest structure being a polymer composed of *n* interlocking rings, called a poly[*n*]catenane. However, even the synthesis of the most basic [2]catenane has long been a challenge for researchers. The earliest iterations of this structure were formed via statistical assembly, where components were placed in solution and allowed to react without any enthalpic driving force to ensure catenation. The primary example of this synthesis can be seen in the first published catenane structure,[1] where Wasserman and coworkers performed a Clemmensen reduction to form hydrocarbon macrocycles. Within this mixture, the researchers reported "a small but demonstrable yield of a catenane,"[1] though this mixture appears to contain <<1% catenane. Never-the-less, this synthesis inspired researchers to seek enthalpic means to drive catenane synthesis.

To drive the assembly of a catenane beyond statistical assembly, several conditions are required. Firstly, an intermolecular driving force must cause the two components to associate during the synthesis. Secondly, this association must act in such a way that the completed synthesis is an interlocked compound rather than a stacked series. Third and lastly, this

association must be reversible to some extent, such that the components are truly freely moving within each other, rather than bound together. By these criteria, several methodologies have been utilized to create catenanes. Many researchers have made use of known intermolecular, weak, and reversible noncovalent interactions, such as π-π stacking and hydrogen bonding. Similarly, other methods have involved ionic bonding, radical associations, and metal-ligand bonding.[33,34]

1.2.1 Aromatic Donor–Acceptor Interactions

One of the most frequently employed methods for synthesizing catenated molecules incorporates an electron-poor aromatic positively charged element of one of the catenanted rings while the second component contains a contrasting π-electron rich site. During a kinetically driven self-assembly, the two components will naturally π-stack and the open thread-like component may be closed to isolate the [2]catenane.[35,36] This method had been pioneered and employed heavily by Stoddart and coworkers,[37,38] who primarily use a π-electron-accepting cyclobis(paraquat-p-phenylene) ($CBPQT^{4+}$) macrocyclic ring for assembly (**Figure 1.3**).

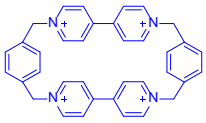

Figure 1.3 Chemical structure of the commonly used cyclobis(paraquat-p-phenylene) (CBPQT4+) ring.

The positively charged viologen component of the $CBPQT^{4+}$ ring has also been shown to radically dimerize in solution, which has been used to creating a homo[2]catenane assembled through radical-radical templating.[39] Advantageously, this $CBPQT^{4+}$ ring can also be used in a thermodynamically driven reaction in where the $CBPQT^{4+}$ ring undergoes a dynamic reaction: a

tetrabutylammonium catalyst is used to reversibly open the $CBPQT^{4+}$ ring which is thermodynamically driven to stack within the corresponding π-electron rich ring.[40]

These donor-acceptor based catenanes have been proposed for a variety of uses as they can be synthesized within water (making them viable candidates for biological applications) and undergo controllable switching for detection or for usage in molecular machines.[41–43] Recently, donor–acceptor based catenanes have even shown weak tendencies to undergo visible light photocatalysis, opening the door to increased charge-transfer utility.[44] In each of these materials, the synthesis method and utility of the final product are directly linked.

1.2.2 Hydrogen Bonding and Halogen Bonding

Hydrogen bonding has also been used to some extent in the synthesis of [2]catenanes and, by extension, more complex polymeric catenane materials. This method was discovered independently by Hunter[45] and Vögtle[46] and both methodologies relied on the presence of amide functionalities to self-assemble the components into a proper template.

This template acted as the base upon which the rings were fully assembled and, once complete, the synthesis yielded fully formed [2]catenane units (**Figure 1.4a**). Analogs of this

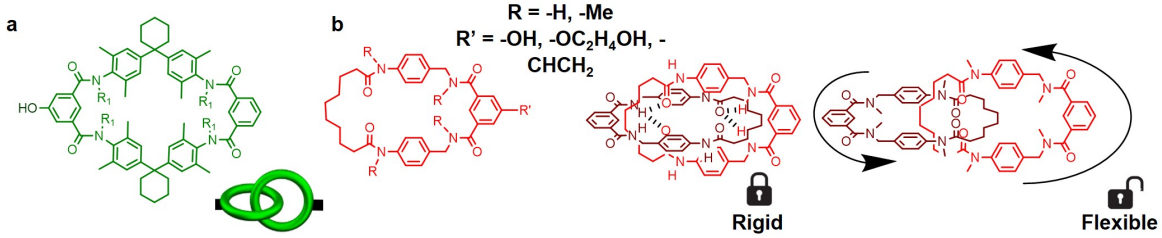

Figure 1.4 (a) Chemical structure of early H-bond templated [2]catenanes; (b) Frequently used H-bond [2]catenane which demonstrates "locking" and "unlocking" abilities based on the H-bond used for synthesis.

system have been adapted over the years,[47–52] the most notable example for this work is pictured in **Figure 1.4b**, which has often been used in the synthesis of polymers containing [2]catenane units (to be discussed in Section 1.3.1).[53,54] The H-bond formation site also allows for a built in switching mechanism: when the R_1 site is populated by a H atom, the [2]catenane is locked in position by H-bonding within the ring (**Figure 1.4b**, Rigid). However, if the H-bond is disrupted by chemical or physical means, the [2]catenane become freely mobile, similar to when R_1 is populated by a methyl group. The difference between the freely mobile and rigid locked catenanes have been exploited in material synthesis (**Figure 1.4b**).[55]

Similar to H-bonding, halogens incorporated into macrocyclic rings can also be used to direct the assembly of a [2]catenane molecule. Though the average strength of a halogen bond is stronger than that of the H-bond, this method is far newer and has not been used with the same frequency. In fact, the only notable examples of this method were developed by Beer and coworkers in the early 2010s.[56,57] The earliest example of this material utilized multiple assembly methods,[57] however the most notable of these examples was able to assemble a [2]catenane via a single N---I bond. Unfortunately, this material was only isolated in 6.5% yield.[56]

1.2.3 Hydrophobic Effects

One of the most common methods for the self-assembly of interlocked components is through the use of hydrophobic effects. This is most commonly seen in the assembly of rotaxane type molecules,[58] in particular cyclodextrin-ethylene glycol type rotaxanes.

The ethylene glycol and cyclodextrin pseudopolyrotaxane assembly is highly efficient and driven by a combination of hydrophobic interactions (between the polymer chain and the hydrophobic pocket of the cyclodextrin) and hydrogen-bonding between adjacent

cyclodextrins.[59] The polyrotaxane is formed when a stoppering reaction is used to "trap" the cyclodextrin rings on the polymer backbone (**Figure 1.5a**).[60] Not long after this original report, a similar approach was used to create a [2]-catenane molecule between cyclodextrin macrocycles and ethylene glycol containing complexes (**Figure 1.5b**), however these compounds have reported generally low yields and do not have the traction of their rotaxane counterparts.[61] More recently, a pseudo-rotaxanes created from the assembled cyclodextrin and ethylene glycol components was closed to form a necklace-like catenane molecule (**Figure 1.5c**), resulting in a high yielding radial polycatenanes.[62,63]

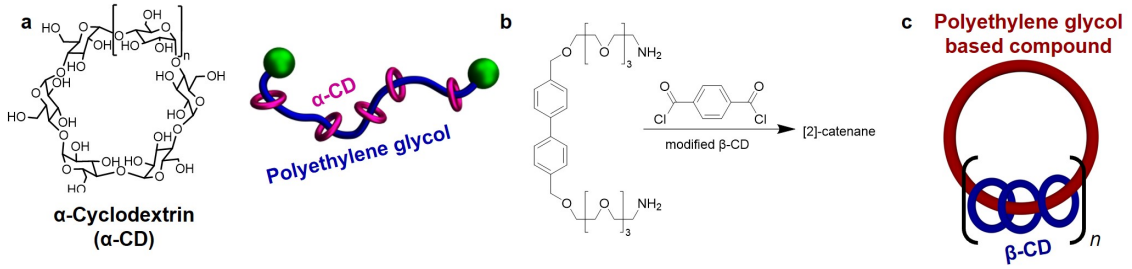

Figure 1.5 (a) Chemical structure of the smallest cyclodextrin molecule, the α-CD as well the commonly seen polyrotaxanes based on this hydrophobic assembly; (b) a [2]-catenane that uses similar ethylene-glycol associations to the hydrophobic pocket of a cyclodextrin based molecule; (c) a radial polycatenane based on chemistry similar to that frequently employed in the synthesis of CD-ethylene glycol polyrotaxanes

1.2.4 Ionic Templating

Unlike the previously discussed methods of catenane synthesis, templated catenane synthesis requires an external compound upon which the catenane is assembled around (**Figure 1.6a**). To create fully mobile complete catenanes, however, these templates must be removable. The two most common methods of templated catenane synthesis utilize ionic assemblies or metal-ligand coordination.

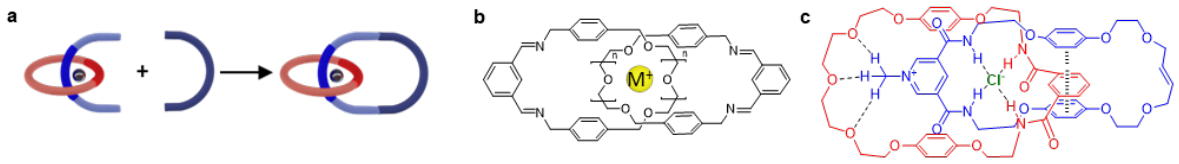

Figure 1.6 (a) Templated assembly involves the components assembling around an external compound upon which catenane synthesis occurs; (b) alkali-metal cation templated [2]catenane based on a crown ether-type pocket between two components; (c) Chloride anion templated [2]catenane formed with aid by π-π stacking and H-bonding.

Alkali-metal cations are known to bind within the pockets of crown-ether materials; similarly, ethylene glycol-based materials can self-assemble around these cations (**Figure 1.6b**).[64–66] However, this templating method does not ensure that the rings are interlocked, as the component conformation around the cation cannot be precisely controlled. Despite this, synthesis of catenanes via this method have been conducted with a series of alkali metal templates (Li^+, Na^+, K^+, Rb^+, Cs^+) and crude materials obtained via this method have shown yields by NMR of up to 81% (Na^+).[67]

Anion templates similarly face a lack of directed assembly when creating catenane materials. However, in conjunction with association complexes (such as the previously discussed H-bonding and halogen bonding),[57,68,69] the anion template may be used to yield catenanes in good yield (up to 78%).[70] These materials exploit the 1:1 association of neutral isophthalamide with halides to yield catenated compounds (**Figure 1.6c**).[71] Anionic templating of [2]catenanes is not confined to halide assemblies, and a catenane that similarly assembles using a nitrate anion has also been reported.[72]

1.2.5 Transition Metal-Ligand Templating

Unlike the ionic templating counterpart, transition-metal (TM) templating of catenanes allow for directed templating due to the more defined nature of the coordination geometry. TM-templated reactions have provided to access a wide range of different interlocked compounds

through the use of tetrahedral,[73] linear,[74] trigonal bipyramidal,[75] square planar[76] and octahedral[77] coordination geometries utilizing a variety of metal ions and ligands (**Figure 1.7a**). TM templating is particularly appealing due to the ease of removal of the templating agent: washing the catenane with a stronger ligand will remove the metal from the final product and result in the freely jointed catenane desired.[78]

TM templated catenane synthesis was pioneered by J.P. Sauvage in 1983 with the first example of a Cu(I) complex used.[73] In this synthesis, the organic macrocyclic components incorporated a hydroxy-functionalized 2,9-diphenyl-1,10-phenanthroline (dpp) ligand, which formed a tetrahedral complex with the ligands were aligned perpendicularly (**Figure 1.7b**). The resulting pseudorotaxane ring was "clipped" closed via an two ether formation reactions, yielding the [2]catenanes in 42%. The copper ion was then removed with the aid of a potassium cyanide wash and the subsequent [2]catenane was extensively characterized.[79,80]

Sauvage would later pioneer the field further through the introduction of a single high yielding metathesis reaction during the catenane ring closing step rather than the lower yielding two step "clipping" method (**Figure 1.7c**). Via this method, the [2]catenane was synthesized at yields of 90%.[81] This metathesis based catenane synthesis has been used extensively with a variety of TM templates, such as Mn^{II}, Zn^{II}, Au^{I}, Fe^{II}, Cu^{I}, Cu^{II}, Co^{II}, Ni^{II}, Cd^{II}, Hg^{II},

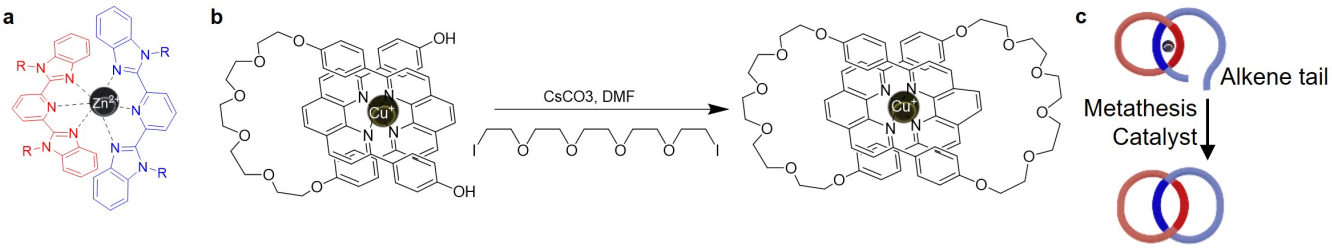

Figure 1.7 (a) Sample of a ligand used in catenane synthesis with octahedral geometry; (b) The first TM templated synthesis of a [2]catenane using Cu(I) and the bidentate phenanthroline ligand; (c) Simple depiction of a metathesis based ring-closing reaction using TM passive metal templating.

Pd^{II}.[27,33,74,76,82] Though the organic framework can vary, the basic synthetic principle of passive metallocatenane synthesis has remain largely unchanged for the last nearly 40 years.[83]

In contrast to this passive templating approach, the TM may also be used as an *active* template where the TM is used to assemble the catenane components *and* complete the ring closing reaction.[84] The first example of this was conducted by Leigh and coworkers in 2009, where a Cu(I) template was used to assemble the macrocycle components.[85] This seminal work by Leigh demonstrated two different methods of using a template to catalyze a ring closing reaction. In the first, the Cu(I) template catalyzed a Cadiot-Chodkiewicz coupling reaction between a alkynyl halide and a terminal alkyne resulting in a [2]catenane at 21% yield (**Figure 1.8**).[85] In the second, the Cu(I) template catalyzed a CuACC "Click" reaction between the azide-alkyne chain ends of the threaded component.[85] Simultaneously, work was published by Saito and coworkers which similarly accomplished an active templated synthesis of [2]catenane using a Glaser coupling between alkyne tails.[86] Since these initial publications, there have been only a few examples of active TM templating in catenane synthesis.[87] Currently, due to the high yields of the metathesis reaction and ease of removal of the template, passive TM templating is one of the most highly used method of catenane synthesis.

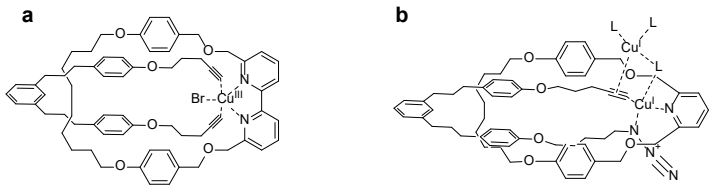

Figure 1.8 Example chemical structures of the mechanism of an active metal templates: (a) Cadiot-Chodkiewicz coupling reaction and (b) azide-alkyne "Click" reaction.

1.3 Selected Polymeric Catenanes

The mechanical bond in a catenane is able to undergo several modes of motion, including elongation, ring twisting and ring rotation (**Figure 1.2c**), and these motions have the potential to influence the properties of a polymeric material. While there are a number of different ways to incorporate catenanes into a polymer architecture, perhaps the most impactful is within the polymer backbone or crosslinking units. **Figure 1.9** shows a selection of such polycatenanes, which include poly[2]catenanes (**Figure 1.9a**), polymeric [2]catenanes (**Figure 1.9b**), Olympic gels (or network catenanes, **Figure 1.9c**) and poly[*n*]catenanes (akin to a macroscopic chain) (**Figure 1.9d**).

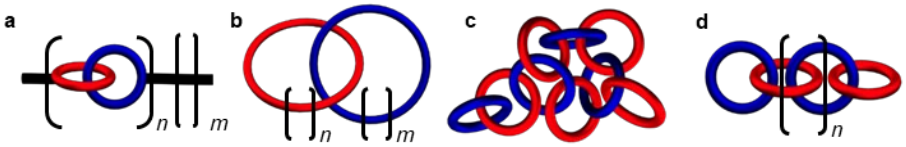

Figure 1.9 Structures of selected polymeric catenanes for discussion: (a) poly[2]catenane, (b) polymeric [2]catenane, (c) network catenane (Olympic gels), and (d) poly[*n*]catenane.

By its very nature, the catenane synthesis must include a ring closing step, a process which is generally not as high yielding as the stoppering reaction frequently employed in (poly)rotaxane synthesis. These lower yields often hinder the formation of catenane-containing polymers on the scale necessary to fully study their thermophysical properties. As a result, theoretical and computational studies have been more influential in characterizing the material properties of such systems. None-the-less, over the years a wide range of polycatenanes have been prepared and, while our understanding of this class of MIPs is not at the level of the polyrotaxanes and SRMs, there are studies that point to the potential advantages of polymers that contain interlocked rings.

1.3.1 Poly[2]catenane

Early polycatenane syntheses employed the polymerization of appropriately functionalized [2]catenane monomers to yield poly[2]catenanes (**Figure 1.9a**).[28] Several reports of this architecture used a functionalized highly aromatic amide-containing [2]catenane (**Figure 1.10a**). [88–90] Early studies focused on the H-[2]catenane (R_1 = H), however the inter-ring hydrogen bonding (between the N-H of one ring and the O=C of the other) hindered ring mobility. Furthermore, this aromatic catenane had limited solubility. To address this issue poly[2]catenanes were prepared using the *N*-methylated catenane (R_1 = Me, **Figure 1.10a**). The bisphenolic *N*-methylated catenane was reacted with a diacid to yield a poly[2]catenane with a number average degree of polymerization ($\overline{DP}$) of 14. Unfortunately, the bulky methyl groups within the rings hindered mobility of the aromatic [2]catenane units. A related larger [2]catenane (**Figure 1.10b**) was able to overcome both the solubility and ring mobility issues of the prior catenane. In this new [2]catenane**,** the rings are large enough that the components are able to freely rotate when the nitrogens are methylated, while hydrogen-bonding in the unmethylated version (R-H) renders the rings immobile (recall **Figure 1.4b, right**).[53,54,91–93]

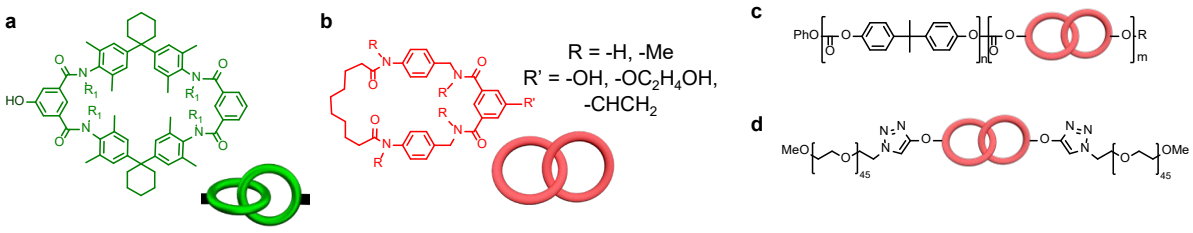

Figure 1.10 (a) Chemical structure of early H-bond templated [2]catenanes used to form poly[2]catenanes. (b) Chemical structure of a [2]catenane used in several poly[2]catenane syntheses, formed by H-bonding as seen in Section 1.2.2. and Figure 1.4; (c) The [2]catenane from (b) incorporated into a bisphenol A polycarbonate (BPAPC) backbone at 10, 20 and 30 wt%; (d) A single molecule of this same [2]catenane incorporated into a polyethylene oxide polymer to create a poly[2]catenane.

This same [2]catenane (with R' = OH) was incorporated into a bisphenol A polycarbonate (BPAPC) backbone at 10, 20 and 30 wt% (**Figure 1.10c**, (10-30 wt%)).[91,92] In BPAPC, two thermal transitions are typically observed at -100 °C and 80 °C via DMA. While the same transitions are observed in this new material (20 wt%), a new sub-T_g thermal transition is observed at -6 °C that was attributed to large conformational changes in the catenane segments, for instance alkyl chain rearrangement or partial ring rotation.

The above study suggests that catenanes within a polymer backbone can elicit effects on the polymer's thermal behavior. However, it also has been shown that the presence of just a single catenane in the polymer chain can impact its overall properties. This was shown with the structure in **Figure 1.10d** in which a poly(ethylene oxide) (PEO, M_n= 2,000 g mol^{-1}) chain was attached to each ring of a single molecule of [2]catenane (though structurally different than the above examples, this system has also been referred to as a poly[2]catenane) .[53] Similar to the studies discussed above, both freely jointed and locked polymers of this PEO based catenane have been investigated. Force extension experiments have shown that the freely-jointed polymer had a smaller persistence length (0.45 ± 0.05 nm) than the locked material (1.0 ± 0.15 nm), suggesting that the presence of a single mobile mechanical bond is enough to significantly enhance the chain mobility.

Related MIPs have been investigated with high T_g polymers attached to a [2]catenane. For example, a single molecule of a catenane with a ligand site for Pd (prepared via Pd(II) templating, see Section 1.2.5) was grafted with polystyrene (M_n= 3,100 gmol^{-1}) (**Figure 1.11**).[94] The polymer with the immobile metal-bound catenane has a T_g of 120 °C. However, the metal free, more mobile polymer has a T_g of 109 °C, only 2 °C above neat polystyrene of a similar

molecular weight. The result suggests that the motion of the catenane is able to offset the physical disruption caused by the bulky catenane rings.

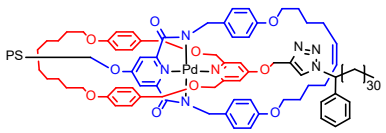

Figure 1.11 Chemical structure of a [2]catenane synthesized by metal templating (Section 1.2.5) within a polystyrene to create a poly[2]catenane structure.

[2]Catenanes have also been incorporated into polymer networks. For example, catenane-containing acetonitrile gels have been prepared by reacting a thiol-containing polyester (M_w= 9,100 gmol^{-1}) with both **Figure 1.10b** unmethylated and methylated catenanes (**Figure 1.12a**).[54,55,95] The thiol-containing polyester was also reacted with a PEG diacrylate to create a control covalently crosslinked acetonitrile gel. Rheological data (**Figure 1.12b**) of the methylated and unmethylated poly[2]catenanes show that the acetonitrile gel of the unmethylated poly[2]catenane is stiffer at ambient conditions as a consequence of the less mobile [2]catenane. In addition, the modulus of the unmethylated poly[2]catenane acetonitrile gel is reduced at high temperature as the hydrogen-bonds are disrupted. In contrast, the methylated poly[2]catenane containing acetonitrile gel is softer at room temperature and shows little temperature sensitivity as there are no hydrogen-bonds to disrupt. In a similar vein, the hydrogen-bonding in the unmethylated catenanes can be disrupted by the addition of acid. As such, the unmethylated poly[2]catenane is pH-responsive, with the protonated poly[2]catenane exhibiting moduli similar to that of methylated poly[2]catenane. In contrast, no pH-sensitive behavior was observed in the methylated poly[2]cateanne nor in the covalently crosslinked gel control. This pH-switching characteristic also affects the stress-strain behavior of the gels (**Figure 1.12c**): the gels with the mobile catenanes were softer and more extensible while the gel with the immobile rings (the

unmethylated poly[2]catenane) possessed a larger elastic modulus and smaller strain-at-break (**Figure 1.12d**). Other [2]catenane-containing networks have also been prepared and exhibit similar trends: namely the properties are highly dependent on the mobility of the catenanes in the network.[96]

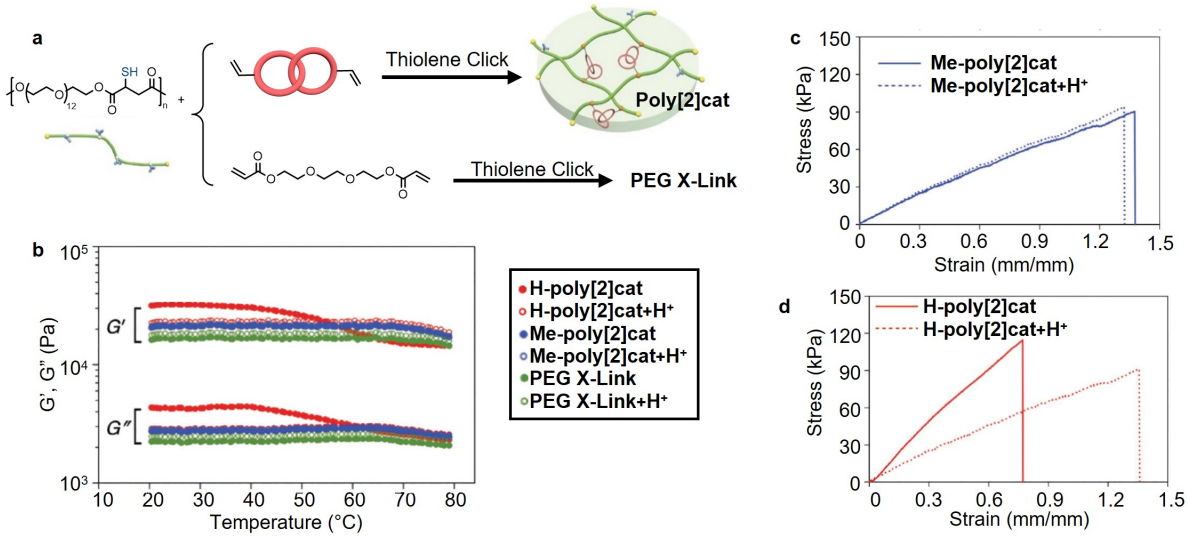

Figure 1.12 (a) Synthesis of [2]catenane containing gels, utilizing the catenane from **Figure 1.10b**, and the synthesis of the covalently crosslinked control (**PEG X-Link**); (b) Temperature sweep rheology for the interlocked and control acetonitrile gels showing softening of hydrogenated poly[2]catenane upon protonation; Stress-strain curves for the methylated poly[2]catenane acetonitrile gel (c) and methylated poly[2]catenane acetonitrile gel (d) in neutral and acidic conditions.

1.3.2 Polymeric [2]catenane

Not to be confused with poly[2]catenanes, a polymeric [2]catenane consists of two cyclic polymers interlocked with a single mechanical bond (**Figure 1.9b**). Early synthesis of polymeric [2]catenanes focused on the use of statistical threading[97] which was low-yielding and the resulting catenanes had to be painstakingly separated from linear and non-catenated cyclic

polymers. Recent efforts have focused on templating strategies that are higher yielding,[98–105] and improved methods of purification.[106]

The most extensive materials characterization of polymeric [2]catenanes to date are studies performed by Advincula and co-workers. In particular, catenated polycaprolactone (PCL) was synthesized via ring expansion to yield two interlocked cyclic polymers, (M_n = 12k g mol^{-1} or 22k g mol^{-1} for the MIPs). Both polymeric [2]catenane materials and their linear PCL counterparts of similar molecular weight (M_n = 11k g mol^{-1} and 21k g mol^{-1}) were subjected to DSC heating and cooling cycles to assess how catenation affects crystallinity. The two catenated materials demonstrated lower degrees of crystallinity (42% and 49%) than the corresponding linear PCL samples (52% and 57%), which was attributed to the self-constrained architecture present in the catenanes that limits the mobility of the polymer chains. In addition, wide-angle X-ray scattering studies showed that PCL formed more compact crystalline structures than the interlocked polymers, again presumably resulting from the permanent entanglements in the MIP.[100]

1.3.3 Olympic Gels and Polycatenane Networks

Network materials consisting only of interlocking rings are known as Olympic gels (**Figure 1.9c**).[2] These networks were first, and still primarily, considered theoretically[2] because they are known to be a synthetic challenge. Some statistical methods of synthesis have been proposed[3,107] and, although simulations have shown that these methods can lead to network formation,[108] such approaches have shown limited success in practice. Therefore, the material properties of Olympic gels have been studied primarily by theory[109] and simulation.[110,111] Several authors[112,113] have argued that the Young's modulus of a catenated network should be related to the average number of catenations (or mechanical bonds) per ring. While this argument and

other similar considerations have been used to estimate the number of catenations per ring in experimentally-realized catenated networks,[112,113] it is not clear under what circumstances the relation is valid. Indeed, when the elasticity of Olympic gels was examined theoretically via scaling arguments, it was found that the stress at small deformations was constant (zero modulus) but large deformations resulted in non-Hookean elasticity, with the force, f, being related to the deformation, λ, as $f \sim \lambda^{2/5}$, in contrast to classical rubbers where the relationship is linear.[109] Such results suggest that Olympic gels will be considerably softer than conventional polymer networks.

In simulations, Olympic gels show a smaller degree of swelling for larger ring sizes,[110,111] a result that is in strong contrast to chemically-crosslinked gels, which show greater swelling when prepared from chains of larger molecular weight (or lower degree of crosslinking). This unusual behavior has a complex topological origin. In particular, ring polymers may be highly entangled without being catenated and these 'non-trapped' entanglements are released when the network swells with solvent, allowing further expansion than if the rings were catenated. However, the probability of finding two nearby non-catenated rings vanishes as the ring size increases – a famous result in knot theory – so that there are fewer non-trapped entanglements and therefore reduced swelling. How these non-trapped entanglements affect material properties such as elasticity and rheology has not yet been examined. Although simulations offer promising avenues for future research, it is important to pay close attention to how the systems are prepared because the method of gel preparation will undoubtedly alter the statistical and topological properties of the network.

One of the few reported synthetic approaches to what has been hypothesized as Olympic-like networks is the thermal polymerization of 1,2-dithiane. This method of polydisulfide

synthesis was intended to target cyclic polymers,[114] however, the unique properties of the materials suggested the presence of catenated structures.[112] A thermally-polymerized sample of polydithiane was fractionated via HPLC, yielding two apparently different architectures: a small molecular weight cyclic polymer, and a potentially interlocked larger molecular weight polydithiane network (**Figure 1.13a**). Interestingly, the viscoelastic properties of the proposed larger molecular weight polydithiane network fractions did not match those of linear analogues (prepared by polymerization of 1,2-dithiane in the presence of a small amount of benzyl mercaptan, **Figure 1.13b**). For instance, the storage modulus of the interlocked polydithiane network fractions remained constant above the melting temperature (from 40-100°C) forming a rubbery plateau while the linear sample flowed at these temperatures. Stress-strain experiments revealed that the polydithiane network fractions were extremely flexible and could be stretched to 3,000% elongation without breaking under load and underwent instant recovery, but the linear standard broke at 800% strain. Since this initial report, materials with similar properties have been synthesized via thermal initiation of cyclic disulfides to make interlocked polymers with aromatic sidegroups[112] and an interlocked copolymer of dithiane and lipoic acid.[115] In these studies, rheological measurements were used as evidence of catenation, even though the relationship between the two is essentially unknown, apart from theoretical considerations which have not yet been tested by simulation. Although the materials are likely catenated, there is no

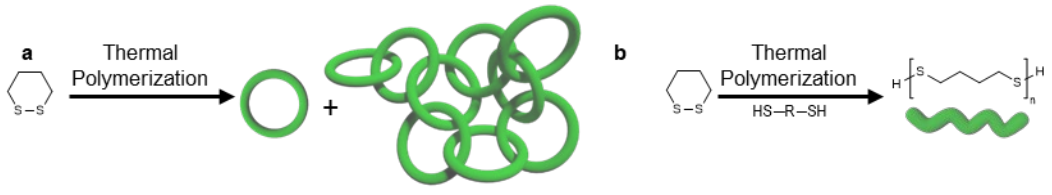

Figure 1.13 (a) Polymerization of 1,2-dithiane, yielding cyclic polymer and the catenated network; (b) Polymerization of linear 1,2-dithiane.

direct evidence supporting this conclusion, so these studies beg the question of how catenation affects rheological behaviour, providing impetus for future studies.

A newer work by Skov and coworkers seems to demonstrate a more targeted approach to synthetic Olympic gels. In this work, α-monovinyl-ω-monohydride telechelic polydimethylsiloxane (PDMS) macromonomers of varying molecular weight (4, 15, 27 g mol^{-1}) were polymerized via a Pt-catalyzed hydrosilylation reaction in the bulk at 80 °C.[116] The resulting mixture was a combination of a catenated network interspersed with individual rings and small catenanes (**Figure 1.14**). After washing the network, the material was softer and more extensible than comparable covalent PDMS networks formed by crosslinking macromonomers of the same molecular weight. For instance, the most durable catenated materials withstood strains of well over 1000% and exhibited a Young's modulus of roughly 0.01 MPa, while the covalent elastomers showed strain-at-break of less than 150% and modulus of ~0.27 MPa. Furthermore, the stress-strain response of the catenated networks at small (<50% strain) and large (> 50% strain) deformations could not be captured simultaneously by classical rubber elasticity theories; rather, a "slip-link" model was required to describe the data.

Although the synthesis of defined Olympic networks has only recently been achieved in the lab, naturally occurring topological networks have been observed in the kinetoplast

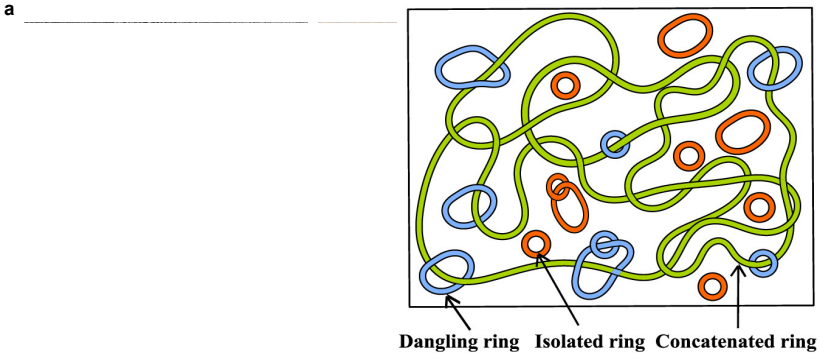

Figure 1.14 Illustrated depiction of the ring structures formed in the synthesis, featuring a network of concatenated rings (green) in addition to catenated "dangling" rings not adding elasticity to the network (blue) and free isolated rings and small catenanes (red).

DNA.[8,117,118] Indeed, vast interlocked networks of several thousand circular DNA molecules have been observed by electron microscopy (**Figure 1.15a**).[7] These interlocked network assemblies bypass the traditional synthetic obstacles and have inspired efforts to synthesize catenated materials from DNA.[119,120] For this methodology, topoisomerase enzymes are employed, which break and reform DNA chains, thereby allowing them to 'pass through' one another. First, the enzymes are introduced to a concentrated solution of DNA rings, so that the rings regularly cross each other, resulting in a dynamic interlocked Olympic gel with transient catenations between the rings. Then, if the enzymes are inhibited in these dynamic DNA gels, the catenated network becomes permanent as the chains can no longer break and reform.[113,121] The linear rheology for both the dynamic (active) and permanent (inactive) gels (**Figure 1.15b**) demonstrates that at timescales shorter than the activity of the topoisomerase, both materials experienced an elastic plateau associated with the interlocked network. However, at the longest time scales, the active (dynamic) gel relaxes all stresses (akin to a polymer solution) while the inactive gel remains solid-like. As a result, by inhibiting or stimulating topoisomerase activity, these materials can switch between the solid-like and fluid-like states. Despite these interesting results, several questions remain unanswered. For instance, the stress-strain behaviour of these

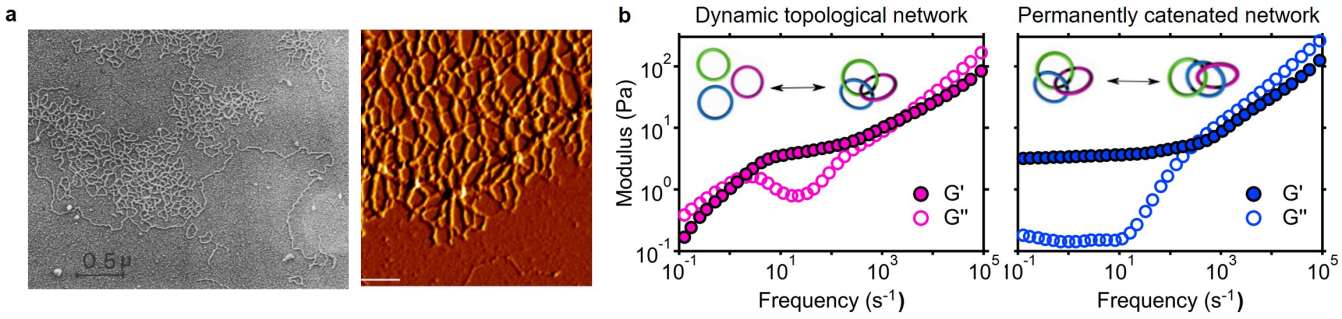

Figure 1.15 (a) Transmission electron microscopy (TEM, left) and atomic force microscopy (AFM, right) taken images of interlocked kinetoplast DNA.; (b) DLS micro-rheology of an Olympic gel prepared using circular DNA and topoisomerase demonstrating multiple dynamical regimes.

gels has not been reported, and it is unclear how the conditions of gel preparation (for example, ring size and DNA volume fraction) affect the resulting material properties. Nevertheless, DNA-based Olympic gels have great potential because they are a facile route to interlocked catenane networks.

1.4 Poly[*n*]catenane

Like their network counterparts, poly[*n*]catenanes consist entirely of interlocked rings (**Figure 1.9d**) and, as indicated above, researchers have in the past speculated that these polymers could exhibit a large loss modulus, rapid stress relaxation, and low activation energy for flow.[29,30] Unfortunately, the synthesis of such polymers is still a major challenge that has inhibited detailed evaluation of their properties.

Historically, the synthesis of [5] and [7]catenanes had been performed in a step-wise approach where rings were added in a consecutive manner.[52,122,123] Although these syntheses were major achievements in catenane research, this approach is not amenable to the synthesis of long polymers, because the number of steps required to achieve even moderate degrees of polymerization is prohibitive. A different approach[124] sought to create a poly[2]catenane with cleavable bridged linkers. Cleavage of the covalent bridges would result in the formation of expanded rings, yielding the desired poly[*n*]catenane. Although bridged poly[2]catenanes and oligo[2]catenanes were successfully synthesized, a poly[*n*]catenane has not be prepared by this method to date.

1.4.1 First Recorded Synthesis

Recently, the metal-templated approach detailed in Section 1.2.5 has been expanded to allow access to poly[*n*]catenanes via the self-assembly of ditopic macrocyclic and thread

components with a metal ion to form a metallosupramolecular polymer (MSP), followed by the ring closing reaction of the thread component and demetallation.[30] A 1:1 solution of macrocycle (**1**) and thread (**2**), which both contain two 2,6-bisbenzimidazolylpyridine (Bip) ligands (**Figure 1.16a**), were mixed with two equivalents of Zn(II) ions to yield the psuedopolyrotaxane MSP (**1·2·Zn(II)$_2$**) (**Figure 1.16b**). Ring closing of **2** was achieved through olefin metathesis of its alkene tails at a concentration of 2.5 mM (wrt. **2**) resulting in a mixture that contains the metallated catenane (**3·Zn(II)$_2$**).[30] Demetallation of **3·Zn(II)$_2$** yielded the first ever poly[*n*]catenane (**3**) as well as several non-interlocked byproducts. Analysis of the interlocked products (obtained in *ca.* 70-80% yield) showed a mixture of linear, cyclic and branched (*c*-, *l*-, and *b*-) poly[*n*]catenanes with an average molecular weight (M_n) of 21.4 kg mol^{-1} corresponding to a $\overline{DP}$ of 14 (**Figure 1.17a**). To isolate the various architectures and sizes, **3** underwent preparatory gel permeation chromatography and the individual fractions were analysed

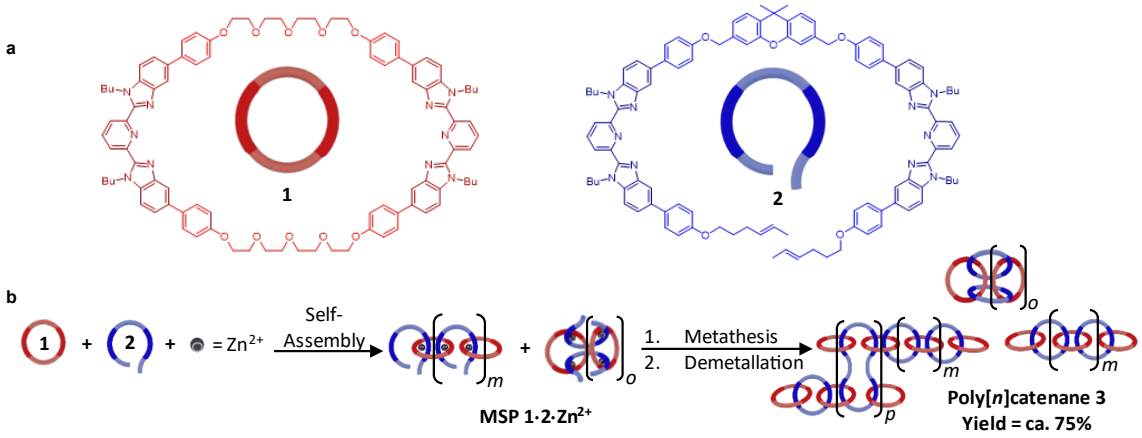

Figure 1.16 (a) Chemical structures and cartoon representations of the macrocyclic (**1**) and thread (**2**) components used in the synthesis the poly[*n*]catenane. The 2,6-bisbenzimidazolylpyridine (Bip) component is darkened for identification; (b) Mixing macrocycle (**1**) and thread (**2**) in a 1:1:2 ratio with zinc di[bis(trifluoromethylsulfonyl)imide] ($Zn(Tf_2N)_2$) results in the self-assembly of metallosupramolecular polymers (**1·2·Zn(II)$_2$**). Reaction with Hoveyda-Grubbs catalyst and subsequent demetallation yields poly[*n*]catenane in ca. 75% yield in three identified architectures: cyclic (top), linear (bottom right), and branched (bottom left).

separately. In the largest M_n fraction, highly branched poly[n]catenanes with up to 130 rings were observed, with an average $\overline{DP}$ of 55. The smaller M_n fractions contained primarily linear and cyclic poly[n]catenanes, with an $\overline{DP}$ of 12 and 8, respectively.

Poly[n]catenane **3** possesses metalloresponsive behaviour as a direct consequence of the metal-templating used in the synthesis. Although the rings are free to rotate when demetallated, they are locked when in the presence of metals which reform the metal–ligand complex in the polymer. The locked arrangement causes large changes in T_g and polymer size. For instance, in linear poly[n]catenanes, an increase of T_g from 97 °C to >160 °C was observed upon metalation with Zn(II) (**Figure 1.17b**). In solution, the same polymers exhibited a 70% increase in hydrodynamic radius (from 3.9 nm to 6.6 nm) upon metalation, consistent with a less flexible structure in the presence of Zn(II).

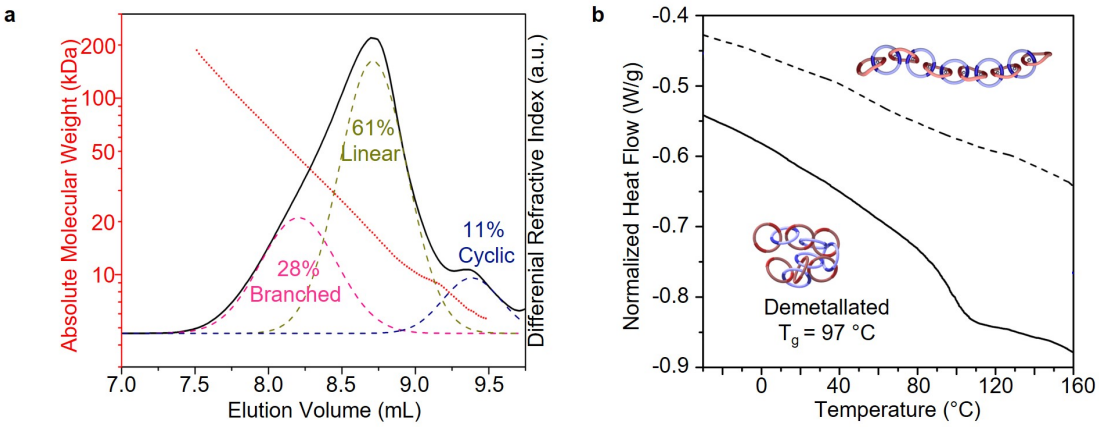

Figure 1.17 (a) The gel permeation chromatography (GPC) trace of poly[n]catenane suggests three unique architectures, identified as branched, linear, and cyclic. (b) DSC of semi-rigid metalated catenane (top) and flexible demetallated catenane (bottom).

1.4.2 Computational Studies

As poly[n]catenane synthesis is still highly challenging, molecular simulations are currently the most productive tool for studying these systems. Over the past two decades, a number of theoretical and computational studies have examined idealized poly[n]catenanes either in solution[31,32,125,126] or the melt.[127,128] In solution, poly[n]catenanes are qualitatively similar to linear polymers at long length scales,[31,125] but recently Dehaghani *et al.*[126] found that the polymer dimensions do not scale with ring size, m, according to the typical good solvent exponent (≈ 0.588), but instead show a somewhat stronger dependence, $R_g \sim m^{0.65}$. Rauscher *et al.*[32] studied the dynamics of poly[n]catenanes in solution and found that ring motion was significantly retarded by the mechanical bonds, both in terms of center-of-mass motion and internal ring relaxations, showing an order of magnitude slow-down relative to free rings. These phenomena are qualitatively similar to those found in entangled polymer melts, suggesting that the unusual dynamics in these MIPs originate from topological effects. However, in poly[n]catenanes these effects are found at short time and length scales, while in conventional linear polymers they occur at longer scales, suggesting that poly[n]catenane materials may have unique dynamical and rheological responses at short time or length scales. Furthermore, the effects are magnified by decreasing the ring size, suggesting that ring size is a key design parameter for these polymers. Interestingly, increasing the ring stiffness only modestly affected the dynamics of the MIPs, which may explain some of the properties of the experimentally-studied poly[n]catenanes: the high rigidity of the segments will result in very high T_g's and the catenation will frustrate packing, resulting in brittle solids. However, the molecule will still be flexible (small and fast) in solution compared to linear analogues.

More recently, a study of model poly[n]catenanes in the melt[127,128] has found that their conformations are highly complex. In particular, the polymers are globular at low DP, which

inhibits inter-chain entanglement; it was estimated that chains of $n \approx 45$ rings are required for polymer chain entanglement, regardless of ring size. The dynamics of the polymers are even more interesting: multiple sub-diffusive regimes are observed in the monomer mean-squared displacement, even though there are no reptation-type dynamics, and the stress relaxation in the systems is extremely fast.[128] These results can be qualitatively explained in terms of a separation of ring-like and chain-like dynamics, but this cannot account for the non-monotonic dependence of the viscosity on the ring size: the viscosity actually decreases with increasing ring size (that is, increasing polymer molecular weight) up to critical ring size above which the viscosity begins to increase (**Figure 1.18**). This behavior deviates strongly from that of ordinary ring polymer melts (**Figure 1.18**) and its cause is not yet known, but it is hypothesized that inter-ring stress (or correlations) are a key factor. Such stress would be large for small rings but become smaller (and relax faster) for larger ones, thus leading to the unusual behavior. These results make it clear that poly[*n*]catenanes are not merely chemical curiosities, but exciting polymer architectures with unexpected dynamical properties.

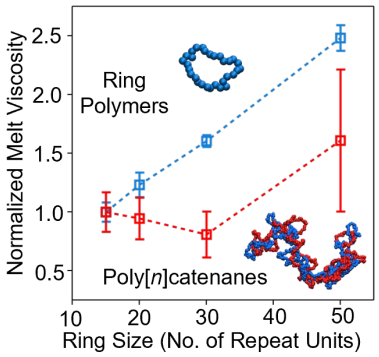

Figure 1.18 Viscosity of ring polymer (blue) and poly[n]catenane (red) melts as a function of ring size as measured by molecular dynamics simulations. Data are normalized by the values at ring size = 15 repeat unit.

1.5 Thesis Scope

This dissertation serves as a record of the progress attained by the author and collaborators in the advancements in our understanding of the synthesis poly[*n*]catenane, modifications to the initial synthesis to yield new, varied poly[*n*]catenane structures, and preliminary efforts to create testable materials that incorporate poly[*n*]catenane components. Chapter 2 investigates the original poly[*n*]catenane synthesis in depth to gain fuller understanding of the reaction precursors and product distributions. This investigation occurs through manipulation of the reaction concentrations and extensive NMR and GPC analysis of the materials.[129] Chapter 3 deals with the other organic component of the poly[*n*]catenane, investigating how small size modifications to the thread (**2**) will affect the MSP and final poly[*n*]catenanes synthesized. Chapter 4 details modifications of the macrocyclic component (**1**) and the effects upon the yield and product distributions of the poly[*n*]catenane materials, with focus on both size and rigidity of the macrocycles used in synthesis. Finally, Chapter 5 reports on the early efforts into making complex poly[*n*]catenane materials and the steps taken toward several new poly[*n*]catenane materials. This chapter will include proposals for further work upon these materials and potential future research directions into this class of poly[*n*]catenanes.

1.6 References

1. Wasserman, E. The Preparation of Interlocking Rings: A Catenane. *J. Am. Chem. Soc.* **82**, 4433–4434 (1960).
2. de Gennes, P.-G. *Scaling concepts in polymer physics*. (Cornell University Press, 1979).
3. Raphaël, E., Gay, C. & de Gennes, P.-G. Progressive construction of an "Olympic" gel. *J. Stat. Phys.* **89**, 111–118 (1997).
4. de Gennes, P.-G. Sliding gels. *Phys. A Stat. Mech. its Appl.* **271**, 231–237 (1999).
5. Craik, D. J., Daly, N. L., Bond, T. & Waine, C. Plant cyclotides: A unique family of cyclic and knotted proteins that defines the cyclic cystine knot structural motif. *J. Mol. Biol.* **294**, 1327–1336 (1999).
6. Virnau, P., Mallam, A. & Jackson, S. Structures and folding pathways of topologically knotted proteins. *J. Phys. Condens. Matter* **23**, 033101 (2011).
7. Renger, H. C. & Wolstenholme, D. R. Form and Structure of Kinetoplast DNA of Crithidia. *J. Cell Biol.* **54**, 346–364 (1972).
8. Borst, P. & Hoeijmakers, J. H. J. Kinetoplast DNA. *Plasmid* **2**, 20–40 (1979).
9. Frisch, H. L. & Wasserman, E. Chemical Topology. *J. Am. Chem. Soc.* **83**, 3789–3795 (1961).
10. Harrison, I. T. & Harrison, S. Synthesis of a stable complex of a macrocycle and a threaded chain. *J. Am. Chem. Soc.* **89**, 5723–5724 (1967).
11. Schill, G. & Zollenkopf, H. Rotaxan-Verbindungen, 1. *Justus Liebigs Ann. Chem.* **721**, 53–74 (1969).
12. Dietrich-Buchecker, C. O. & Sauvage, J.-P. A Synthetic Molecular Trefoil Knot. *Angew. Chemie Int. Ed. English* **28**, 189–192 (1989).
13. Chichak, K. S. *et al.* Molecular Borromean Rings. *Science (80-.).* **304**, 1308–1312 (2004).
14. Koetting, M. C., Peters, J. T., Steichen, S. D. & Peppas, N. A. Stimulus-responsive hydrogels: Theory, modern advances, and applications. *Mater. Sci. Eng. R Reports* **93**, 1–49 (2015).
15. Yui, N., Katoono, R. & Yamashita, A. Functional Cyclodextrin Polyrotaxanes for Drug Delivery. in *Inclusion Polymers* (ed. Wenz, G.) vol. 222 55–77 (2009).
16. Loeb, S. J. Rotaxanes as ligands: from molecules to materials. *Chem. Soc. Rev.* **36**, 226–235 (2007).
17. Loethen, S., Kim, J.-M. & Thompson, D. H. Biomedical applications of cyclodextrin based polyrotaxanes. *Polym. Rev.* **47**, 383–418 (2007).
18. Arunachalam, M. & Gibson, H. W. Recent developments in polypseudorotaxanes and polyrotaxanes. *Prog. Polym. Sci.* **39**, 1043–1073 (2014).

19. Hart, L. F. *et al.* Material properties and applications of mechanically interlocked polymers. *Nat. Rev. Mater.* **6**, 508–530 (2021).

20. Ooya, T. & Yui, N. Polyrotaxanes: Synthesis, structure, and potential in drug delivery. *Crit. Rev. Ther. Drug Carrier Syst.* **16**, 289–330 (1999).

21. Arisaka, Y. & Yui, N. Polyrotaxane-based biointerfaces with dynamic biomaterial functions. *J. Mater. Chem. B* **7**, 2123–2129 (2019).

22. Tardy, B. L., Dam, H. H., Kamphuis, M. M. J., Richardson, J. J. & Caruso, F. Self-Assembled Stimuli-Responsive Polyrotaxane Core–Shell Particles. *Biomacromolecules* **15**, 53–59 (2014).

23. Noda, Y., Hayashi, Y. & Ito, K. From topological gels to slide-ring materials. *J. Appl. Polym. Sci.* **131**, 40509 (2014).

24. Ito, K. Novel entropic elasticity of polymeric materials: why is slide-ring gel so soft? *Polym. J.* **44**, 38–41 (2012).

25. Okumura, Y. & Ito, K. The Polyrotaxane Gel: A Topological Gel by Figure-of-Eight Cross-links. *Adv. Mater.* **13**, 485–487 (2001).

26. Ito, K. Mechanical Properties of Slide-ring Materials. in *Polyrotaxane and Slide-Ring Materials* 44–77 (2016).

27. Gil-Ramirez, G., Leigh, D. A. & Stephens, A. J. Catenanes: Fifty Years of Molecular Links. *Angew. Chem., Int. Ed.* **54**, 6110–6150 (2015).

28. Niu, Z. & Gibson, H. W. Polycatenanes. *Chem. Rev.* **109**, 6024–6046 (2009).

29. Weidmann, J.-L. *et al.* Poly[2]catenanes and Cyclic Oligo[2]catenanes Containing Alternating Topological and Covalent Bonds: Synthesis and Characterization. *Chem. - A Eur. J.* **5**, 1841–1851 (2002).

30. Wu, Q. *et al.* Poly[n]catenanes: Synthesis of molecular interlocked chains. *Science (80-.).* **358**, 1434–1439 (2017).

31. Pakula, T. & Jeszka, K. Simulation of Single Complex Macromolecules. 1. Structure and Dynamics of Catenanes. *Macromolecules* **32**, 6821–6830 (1999).

32. Rauscher, P. M., Rowan, S. J. & de Pablo, J. J. Topological Effects in Isolated Poly[n]catenanes: Molecular Dynamics Simulations and Rouse Mode Analysis. *ACS Macro Lett.* **7**, 938–943 (2018).

33. Evans, N. H. & Beer, P. D. Progress in the synthesis and exploitation of catenanes since the Millennium. *Chem. Soc. Rev.* **43**, 4658 (2014).

34. Taghavi Shahraki, B. *et al.* The flowering of Mechanically Interlocked Molecules: Novel approaches to the synthesis of rotaxanes and catenanes. *Coord. Chem. Rev.* **423**, 213484 (2020).

35. Hamilton, D. G., Sanders, J. K. M., Davies, J. E., Clegg, W. & Teat, S. J. Neutral [2]catenanes from oxidative coupling of π-stacked components. *Chem. Commun.* 897–898

(1997) doi:10.1039/a701048f.

36. Kitajima, K., Ogoshi, T. & Yamagishi, T. Diastereoselective synthesis of a [2]catenane from a pillar[5]arene and a pyridinium derivative. *Chem. Commun.* **50**, 2925–2927 (2014).

37. Ashton, P. R. *et al.* A [2] Catenane Made to Order. *Angew. Chemie Int. Ed. English* **28**, 1396–1399 (1989).

38. Dichtel, W. R. *et al.* Kinetic and Thermodynamic Approaches for the Efficient Formation of Mechanical Bonds. *Acc. Chem. Res.* **41**, 1750–1761 (2008).

39. Barnes, J. C. *et al.* A Radically Configurable Six-State Compound. *Science (80-.).* **339**, 429–433 (2013).

40. Miljanic, O. S. & Stoddart, J. F. Dynamic donor acceptor [2]catenanes. *Proc. Natl. Acad. Sci.* **104**, 12966–12970 (2007).

41. Fang, L., Basu, S., Sue, C.-H., Fahrenbach, A. C. & Stoddart, J. F. Syntheses and Dynamics of Donor−Acceptor [2]Catenanes in Water. *J. Am. Chem. Soc.* **133**, 396–399 (2011).

42. Forgan, R. S. *et al.* Self-Assembly of a [2]Pseudorota[3]catenane in Water. *J. Am. Chem. Soc.* **134**, 17007–17010 (2012).

43. Zhu, Z. *et al.* Controlling Switching in Bistable [2]Catenanes by Combining Donor–Acceptor and Radical–Radical Interactions. *J. Am. Chem. Soc.* **134**, 11709–11720 (2012).

44. Jiao, Y. *et al.* A Donor–Acceptor [2]Catenane for Visible Light Photocatalysis. *J. Am. Chem. Soc.* **143**, 8000–8010 (2021).

45. Hunter, C. A. & Purvis, D. H. Synthesis and structure elucidation of a new [2]-catenane. *J. Am. Chem. Soc.* **114**, 5303–5311 (1992).

46. Vögtle, F., Meier, S. & Hoss, R. One-Step Synthesis of a Fourfold Functionalized Catenane. *Angew. Chemie Int. Ed. English* **31**, 1619–1622 (1992).

47. Iwamoto, H. *et al.* Selective Synthesis of [2]- and [3]Catenane Tuned by Ring Size and Concentration. *J. Org. Chem.* **78**, 5205–5217 (2013).

48. Guidry, E. N., Cantrill, S. J., Stoddart, J. F. & Grubbs, R. H. Magic Ring Catenation by Olefin Metathesis. *Org. Lett.* **7**, 2129–2132 (2005).

49. Kidd, T. J., Leigh, D. A. & Wilson, A. J. Organic "Magic Rings": The Hydrogen Bond-Directed Assembly of Catenanes under Thermodynamic Control. *J. Am. Chem. Soc.* **121**, 1599–1600 (1999).

50. Prakashni, M., Shukla, R. & Dasgupta, S. Rapid and High-Yield Synthesis of [23]Crown Ether: Applied as a Wheel Component in the Formation of Pseudo[2]rotaxane and Synthesis of [2]Catenane with a Dibenzylammonium Dumbbell. *J. Org. Chem.* **86**, 7825–7831 (2021).

51. Marrs, C. N. & Evans, N. H. The rapid synthesis and dynamic behaviour of an isophthalamide [2]catenane. *Org. Biomol. Chem.* **13**, 11021–11025 (2015).

52. Iwamoto, H. *et al.* Synthesis of linear [5]catenanes via olefin metathesis dimerization of pseudorotaxanes composed of a [2]catenane and a secondary ammonium salt. *Chem. Commun.* **52**, 319–322 (2016).

53. Van Quaethem, A., Lussis, P., Leigh, D. A., Duwez, A.-S. & Fustin, C.-A. Probing the mobility of catenane rings in single molecules. *Chem. Sci.* **5**, 1449–1452 (2014).

54. Xing, H., Li, Z., Wu, Z. L. & Huang, F. Catenane Crosslinked Mechanically Adaptive Polymer Gel. *Macromol. Rapid Commun.* **39**, 1700361 (2018).

55. Xing, H. *et al.* Mechanochemistry of an Interlocked Poly[2]catenane: From Single Molecule to Bulk Gel. *CCS Chem.* **1**, 513–523 (2019).

56. Gilday, L. C. *et al.* A Catenane Assembled through a Single Charge-Assisted Halogen Bond. *Angew. Chemie Int. Ed.* **52**, 4356–4360 (2013).

57. Caballero, A. *et al.* A Halogen-Bonding Catenane for Anion Recognition and Sensing. *Angew. Chemie Int. Ed.* **51**, 1876–1880 (2012).

58. Harada, A., Li, J. & Kamachi, M. The molecular necklace: a rotaxane containing many threaded α-cyclodextrins. *Nature* **356**, 325–327 (1992).

59. Fleury, G. *et al.* Synthesis and characterization of high molecular weight polyrotaxanes: Towards the control over a wide range of threaded α-cyclodextrins. *Soft Matter* **1**, 378–385 (2005).

60. Miyake, K. *et al.* Formation Process of Cyclodextrin Necklace−Analysis of Hydrogen Bonding on a Molecular Level. *J. Am. Chem. Soc.* **125**, 5080–5085 (2003).

61. Armspach, D. *et al.* Selbstorganisation von Catenanen mit Cyclodextrineinheiten. *Angew. Chemie* **105**, 944–948 (1993).

62. Higashi, T. *et al.* One-pot synthesis of cyclodextrin-based radial poly[n]catenanes. *Commun. Chem.* **2**, 78 (2019).

63. Morita, K., Motoyama, K., Kuramoto, A., Onodera, R. & Higashi, T. Synthesis of cyclodextrin-based radial polycatenane cyclized by amide bond and subsequent fabrication of water-soluble derivatives. *J. Incl. Phenom. Macrocycl. Chem.* **100**, 169–175 (2021).

64. Tung, S.-T., Lai, C.-C., Liu, Y.-H., Peng, S.-M. & Chiu, S.-H. Synthesis of a [2]Catenane from the Sodium Ion Templated Orthogonal Arrangement of Two Diethylene Glycol Chains. *Angew. Chemie* **125**, 13511–13514 (2013).

65. Wu, Y.-W., Chen, P.-N., Chang, C.-F., Lai, C.-C. & Chiu, S.-H. Synthesizing [2]Rotaxanes and [2]Catenanes through Na + -Templated Clipping of Macrocycles around Oligo(ethylene glycol) Units. *Org. Lett.* **17**, 2158–2161 (2015).

66. Tsai, C.-Y. *et al.* [2]Catenanes Displaying Switchable Gin-Trap-Like Motion. *J. Org. Chem.* **83**, 5619–5628 (2018).

67. Lee, Y.-J., Ho, T.-H., Lai, C.-C. & Chiu, S.-H. Size effects in the alkali metal ion-templated formation of oligo(ethylene glycol)-containing [2]catenanes. *Org. Biomol.*

Chem. **14**, 1153–1160 (2016).

68. Mercurio, J. M., Caballero, A., Cookson, J. & Beer, P. D. A halogen- and hydrogen-bonding [2]catenane for anion recognition and sensing. *RSC Adv.* **5**, 9298–9306 (2015).

69. Brown, A., Langton, M. J., Kilah, N. L., Thompson, A. L. & Beer, P. D. Chloride-Anion-Templated Synthesis of a Strapped-Porphyrin-Containing Catenane Host System. *Chem. - A Eur. J.* **21**, 17664–17675 (2015).

70. Ng, K.-Y., Cowley, A. R. & Beer, P. D. Anion templated double cyclization assembly of a chloride selective [2]catenane. *Chem. Commun.* 3676 (2006) doi:10.1039/b606503a.

71. Sambrook, M. R., Beer, P. D., Wisner, J. A., Paul, R. L. & Cowley, A. R. Anion-Templated Assembly of a [2]Catenane. *J. Am. Chem. Soc.* **126**, 15364–15365 (2004).

72. Langton, M. J. & Beer, P. D. Nitrate anion templated synthesis of a [2]catenane for nitrate recognition in organic–aqueous solvent media. *Chem. Commun.* **50**, 8124–8127 (2014).

73. Dietrich-Buchecker, C. ., Sauvage, J. . & Kintzinger, J. . Une nouvelle famille de molecules : les metallo-catenanes. *Tetrahedron Lett.* **24**, 5095–5098 (1983).

74. Goldup, S. M., Leigh, D. A., Lusby, P. J., McBurney, R. T. & Slawin, A. M. Z. Gold(I)-Template Catenane and Rotaxane Synthesis. *Angew. Chemie* **120**, 7107–7111 (2008).

75. Hamann, C., Kern, J.-M. & Sauvage, J.-P. Zinc(II)-Templated Synthesis of a [2]-Catenane Consisting of a 2,2‘,6‘,2‘ ‘-Terpyridine-Incorporating Cycle and a 1,10-Phenanthroline-Containing Ring. *Inorg. Chem.* **42**, 1877–1883 (2003).

76. Fuller, A.-M. L., Leigh, D. A., Lusby, P. J., Slawin, A. M. Z. & Walker, D. B. Selecting Topology and Connectivity through Metal-Directed Macrocyclization Reactions: A Square Planar Palladium [2]Catenate and Two Noninterlocked Isomers. *J. Am. Chem. Soc.* **127**, 12612–12619 (2005).

77. Loren, J. C., Gantzel, P., Linden, A. & Siegel, J. S. Synthesis of achiral and racemic catenanes based on terpyridine and a directionalized terpyridine mimic, pyridyl-phenanthroline. *Org. Biomol. Chem.* **3**, 3105 (2005).

78. Lewis, J. E. M., Beer, P. D., Loeb, S. J. & Goldup, S. M. Metal ions in the synthesis of interlocked molecules and materials. *Chem. Soc. Rev.* **46**, 2577–2591 (2017).

79. Dietrich-Buchecker, C. O., Sauvage, J. P. & Kern, J. M. Templated synthesis of interlocked macrocyclic ligands: the catenands. *J. Am. Chem. Soc.* **106**, 3043–3045 (1984).

80. Cesario, M., Dietrich-Buchecker, C. O., Guilhem, J., Pascard, C. & Sauvage, J. P. Molecular structure of a catenand and its copper(I) catenate: complete rearrangement of the interlocked macrocyclic ligands by complexation. *J. Chem. Soc. Chem. Commun.* 244 (1985) doi:10.1039/c39850000244.

81. Mohr, B., Sauvage, J.-P., Grubbs, R. H. & Weck, M. High-Yield Synthesis of[2] Catenanes by Intramolecular Ring-Closing Metathesis. *Angew. Chemie Int. Ed. English* **36**, 1308–1310 (1997).

82. Hogg, L. *et al.* A Simple General Ligand System for Assembling Octahedral Metal–Rotaxane Complexes. *Angew. Chemie Int. Ed.* (2004) doi:10.1002/anie.200353186.

83. Colley, N. D. *et al.* One-Pot Synthesis of a Linear [4]Catenate Using Orthogonal Metal Templation and Ring-Closing Metathesis. *Inorg. Chem.* **59**, 10450–10460 (2020).

84. Denis, M. & Goldup, S. M. The active template approach to interlocked molecules. *Nat. Rev. Chem.* **1**, 0061 (2017).

85. Goldup, S. M. *et al.* Active Metal Template Synthesis of [2]Catenanes. *J. Am. Chem. Soc.* **131**, 15924–15929 (2009).

86. Sato, Y., Yamasaki, R. & Saito, S. Synthesis of [2]Catenanes by Oxidative Intramolecular Diyne Coupling Mediated by Macrocyclic Copper(I) Complexes. *Angew. Chemie Int. Ed.* **48**, 504–507 (2009).

87. Langton, M. J., Matichak, J. D., Thompson, A. L. & Anderson, H. L. Template-directed synthesis of π-conjugated porphyrin [2]rotaxanes and a [4]catenane based on a six-porphyrin nanoring. *Chem. Sci.* **2**, 1897 (2011).

88. Geerts, Y., Muscat, D. & Müllen, K. Synthesis of oligo[2]catenanes. *Macromol. Chem. Phys.* **196**, 3425–3435 (1995).

89. Muscat, D., Witte, A., Köhler, W., Müllen, K. & Geerts, Y. Synthesis of a novel poly[2]-catenane containing rigid catenanes. *Macromol. Rapid Commun.* **18**, 233–241 (1997).

90. Muscat, D. *et al.* Synthesis and Characterization of Poly[2]-catenanes Containing Rigid Catenane Segments. *Macromolecules* **32**, 1737–1745 (1999).

91. Fustin, C.-A. *et al.* Mechanically Linked Polycarbonate. *J. Am. Chem. Soc.* **125**, 2200–2207 (2003).

92. Fustin, C.-A., Bailly, C., Clarkson, G. J., Galow, T. H. & Leigh, D. A. Solution and Solid-State Properties of Mechanically Linked Polycarbonates. *Macromolecules* **37**, 66–70 (2004).

93. Fustin, C.-A. *et al.* Mechanically Linked Poly(ethylene terephthalate). *Macromolecules* **37**, 7884–7892 (2004).

94. Ahamed, B. N., Van Velthem, P., Robeyns, K. & Fustin, C.-A. Influence of a Single Catenane on the Solid-State Properties of Mechanically Linked Polymers. *ACS Macro Lett.* **6**, 468–472 (2017).

95. Wang, W. & Xing, H. A novel supramolecular polymer network based on a catenane-type crosslinker. *Polym. Chem.* **9**, 2087–2091 (2018).

96. Xing, H. *et al.* Mechanochemistry of an Interlocked Poly[2]catenane: From Single Molecule to Bulk Gel. *CCS Chem.* **2**, 513–523 (2020).

97. Gan, Y., Dong, D. & Hogen-Esch, T. E. Synthesis and Characterization of a Catenated Polystyrene−Poly(2-vinylpyridine) Block Copolymer. *Macromolecules* **35**, 6799–6803 (2002).

98. Bunha, A. K., Mangadlao, J., Felipe, M. J., Pangilinan, K. & Advincula, R. Catenated PS-PMMA Block Copolymers via Supramolecularly Templated ATRP Initiator Approach. *Macromol. Rapid Commun.* **33**, 1214–1219 (2012).

99. Bunha, A. *et al.* Polymeric catenanes synthesized via 'click' chemistry and atom transfer radical coupling. *Chem. Commun.* **51**, 7528–7531 (2015).

100. Cao, P.-F., Mangadlao, J. D., de Leon, A., Su, Z. & Advincula, R. C. Catenated Poly(ε-caprolactone) and Poly(L-lactide) via Ring-Expansion Strategy. *Macromolecules* **48**, 3825–3833 (2015).

101. Ishikawa, K., Yamamoto, T., Asakawa, M. & Tezuka, Y. Effective Synthesis of Polymer Catenanes by Cooperative Electrostatic/Hydrogen-Bonding Self-Assembly and Covalent Fixation. *Macromolecules* **43**, 168–176 (2010).

102. Bunha, A., Tria, M. C. & Advincula, R. Polymer catenanes via a supramolecularly templated ATRP initiator. *Chem. Commun.* **47**, 9173–9175 (2011).

103. Bunha, A. *et al.* Polymeric catenanes synthesized via "click" chemistry and atom transfer radical coupling. *Chem. Commun.* **51**, 7528–7531 (2015).

104. Cao, P.-F., Mangadlao, J. D., de Leon, A., Su, Z. & Advincula, R. C. Catenated Poly(ε-caprolactone) and Poly(l-lactide) via Ring-Expansion Strategy. *Macromolecules* **48**, 3825–3833 (2015).

105. Ohta, Y., Nakamura, M., Matsushita, Y. & Takano, A. Synthesis, separation and characterization of knotted ring polymers. *Polymer (Guildf).* **53**, 466–470 (2012).

106. Ohta, Y., Nakamura, M., Matsushita, Y. & Takano, A. Synthesis, separation and characterization of knotted ring polymers. *Polymer (Guildf).* **53**, 466–470 (2012).

107. Pickett, G. T. DNA-origami technique for olympic gels. *Europhys. Lett.* **76**, 616–622 (2006).

108. Fischer, J., Lang, M. & Sommer, J.-U. The formation and structure of Olympic gels. *J. Chem. Phys.* **143**, (2015).

109. Vilgis, T. A. & Otto, M. Elasticity of entangled polymer loops: Olympic gels. *Phys. Rev. E* **56**, R1314–R1317 (1997).

110. Lang, M., Fischer, J., Werner, M. & Sommer, J.-U. Swelling of Olympic Gels. *Phys. Rev. Lett.* **112**, 238001 (2014).

111. Lang, M., Fischer, J., Werner, M. & Sommer, J.-U. Olympic Gels: Concatenation and Swelling. *Macromol. Symp.* **358**, 140–147 (2015).

112. Endo, K., Shiroi, T., Murata, N., Kojima, G. & Yamanaka, T. Synthesis and characterization of poly(1,2-dithiane). *Macromolecules* **37**, 3143–3150 (2004).

113. Kim, Y. S. *et al.* Gelation of the genome by topoisomerase II targeting anticancer agents. *Soft Matter* **9**, 1656–1663 (2013).

114. Arakawa, R., Watanabe, T., Fukuo, T. & Endo, K. Determination of cyclic structure for

polydithiane using electrospray ionization mass spectrometry. *J. Polym. Sci. Part A Polym. Chem.* **38**, 4403–4406 (2000).

115. Endo, K. & Yamanaka, T. Copolymerization of lipoic acid with 1,2-dithiane and characterization of the copolymer as an interlocked cyclic polymer. *Macromolecules* **39**, 4038–4043 (2006).

116. Hu, P., Madsen, J., Huang, Q. & Skov, A. L. Elastomers without covalent cross-linking: Concatenated rings giving rise to elasticity. *ACS Macro Lett.* **9**, 1458–1463 (2020).

117. Riou, G. & Delain, E. Electron Microscopy of the Circular Kinetoplastic DNA from Trypanosoma Cruzi: Occurrence of Catenated Forms. *Proc. Natl. Acad. Sci.* **62**, 210–217 (1969).

118. Cavalcanti, D. P., Gonçalves, D. L., Costa, L. T. & de Souza, W. The structure of the kinetoplast DNA network of Crithidia fasciculata revealed by atomic force microscopy. *Micron* **42**, 553–559 (2011).

119. Krasnow, M. & Cozzarelli, N. Catenation of DNA Rings by Topoisomerases. Mechanism of Control by Spermidine. *J. Biol. Chem.* **257**, 2687–2693 (1982).

120. Waldeck, W., Theobald, M. & Zentgraf, H. Catenation of DNA by eucaryotic topoisomerase II associated with simian virus 40 minichromosomes. *EMBO J.* **2**, 1255–1261 (1983).

121. Krajina, B. A., Zhu, A., Heilshorn, S. C. & Spakowitz, A. J. Active DNA Olympic Hydrogels Driven by Topoisomerase Activity. *Phys. Rev. Lett.* **121**, 148001 (2018).

122. Amabilino, D. B., Ashton, P. R., Reder, A. S., Spencer, N. & Stoddart, J. F. Olympiadane. *Angew. Chemie Int. Ed. English* **33**, 1286–1290 (1994).

123. Amabilino, D. B. *et al.* The Five-Stage Self-Assembly of a Branched Heptacatenane. *Angew. Chemie Int. Ed. English* **36**, 2070–2072 (1997).

124. Watanabe, N., Ikari, Y., Kihara, N. & Takata, T. Bridged Polycatenane. *Macromolecules* **37**, 6663–6666 (2004).

125. Brereton, M. G. The statistical mechanics of a concatenated polymer chain. *J. Phys. A. Math. Gen.* **34**, 5131 (2001).

126. Ahmadian Dehaghani, Z., Chubak, I., Likos, C. N. & Ejtehadi, M. R. Effects of topological constraints on linked ring polymers in solvents of varying quality. *Soft Matter* **16**, 3029–3038 (2020).

127. Rauscher, P. M., Schweizer, K. S., Rowan, S. J. & de Pablo, J. J. Thermodynamics and Structure of Poly[n]catenane Melts. *Macromolecules* **53**, 3390–3408 (2020).

128. Rauscher, P. M., Schweizer, K. S., Rowan, S. J. & de Pablo, J. J. Dynamics of Poly[n]catenane Melts. *J. Chem. Phys.* **152**, 214901 (2020).

129. Tranquilli, M. M., Wu, Q. & Rowan, S. J. Effect of metallosupramolecular polymer concentration on the synthesis of poly[n]catenanes. *Chem. Sci.* **12**, 8722–8730 (2021).

Chapter 2: Effect of metallosupramolecular polymer concentration on the synthesis of poly[*n*]catenanes

* This chapter was adapted from: Tranquilli, M.M.; Wu, Q.; Rowan, S.J. Effect of metallosupramolecular polymer concentration on the synthesis of poly[*n*]catenanes. *Chem Sci.* **2021**, *12*, 8722 - 8730.

2.1 Introduction

In 2017[1] the Rowan group reported the first successful synthesis of a poly[*n*]catenane; this polymer was synthesized using two monomers: a macrocyclic monomer (**1**) and thread-like monomer (**2**) that both contain two 2,6-bisbenzimidazolylpyridine (Bip) ligands (**Figure 2.1**). A 1:1 solution of **1:2** were mixed with two equivalents of Zn(II) ions to yield the psuedopolyrotaxane metallosupramolecular polymer (MSP) (**1·2·Zn(II)$_2$**)) (**Figure 2.2**). The ring closing of **2**, to access the metallated poly[*n*]catenanes (**3·Zn(II)**), was achieved through olefin metathesis of its alkene tails at a concentration of 2.5 mM (wrt. **2**). Ideally, the alkene tails of **2** react intramolecularly to undergo a ring closing metathesis reaction, yielding the desired linear poly[*n*]catenanes (***l*-3**) after demetallation. However, studies on the demetallated products showed that in addition to the

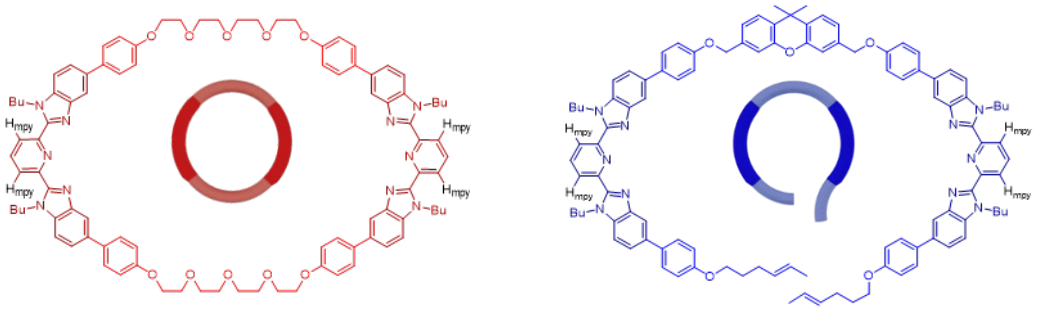

Figure 2.1 The chemical structure of the macrocyclic (**1**) and thread (**2**) components reiterated to emphasize *m*-pyridyl protons (H_{mpy}) indicated in black. The 2,6-bisbenzimidazolylpyridine (Bip) component is darkened for identification.

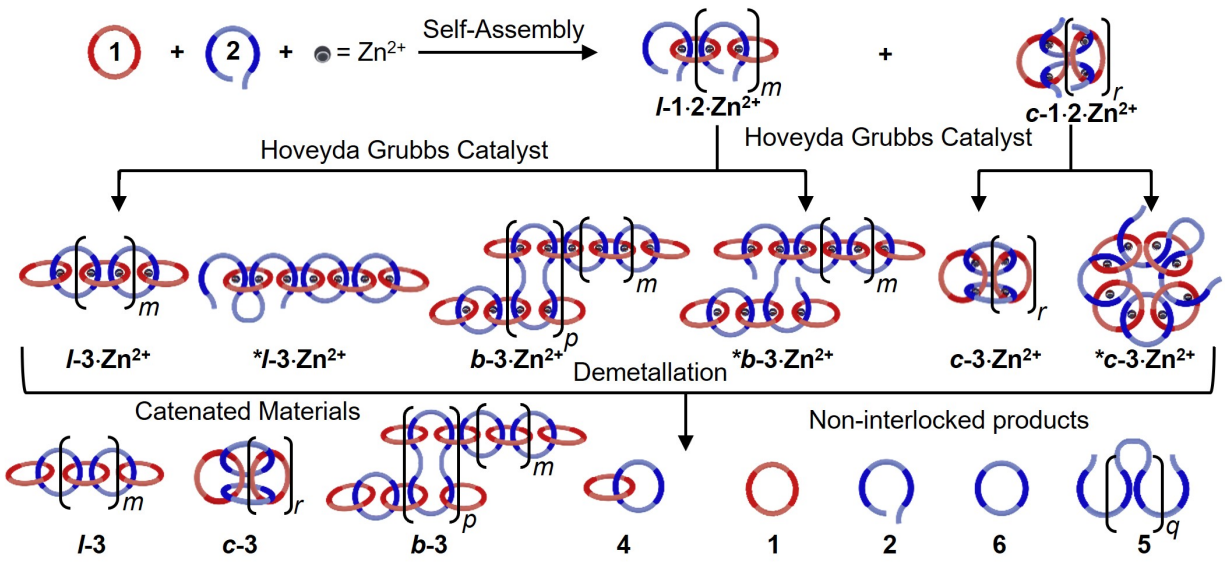

Figure 2.2 Mixing macrocycle (**1**) and thread (**2**) in a 1:1:2 ratio with zinc di[bis(trifluoromethylsulfonyl)imide] ($Zn(Tf_2N)_2$) results in the self-assembly of linear (***l*-1·2·Zn(II)$_2$**) and/or cyclic (***c*-1·2·Zn(II)$_2$**)) metallosupramolecular polymers (MSP). Subsequent reaction of the MSP with Hoveyda Grubbs catalyst can yield a mixture of metallated products (some of which are shown as **3·Zn(II)**) whose distribution depends on the nature of the MSP and concentration of the reaction. Demetallation of these reaction products yields poly/oligo[*n*]catenanes (**3**, **4**) along with recovery of some starting material and some non-interlocked byproducts.

targeted linear poly[*n*]catenane (***l*-3**) the reaction mixture also contained cyclic and branched catenated products (***c*-3**, ***b*-3**) as well as the starting materials (**1**, **2**). In addition, non-interlocked by-products derived from **2** were also observed, namely macrocycle **6** (formed by ring closing of **2**) and oligomer **5**, formed via the Acyclic Diene Metathesis (ADMET) of **2** (which can be formed either via incorrect intramolecular MSP reactions, as in ***l*-3·Zn(II)**, or intermolecular MSP reactions, as in ***b*-3·Zn(II)).** Through a combination of NMR and GPC-MALS (gel permeation chromatography coupled to a multi-angle light scattering detector) studies, it was shown that the overall yield of the interlocked compounds was ca. 75% and, after some purification to remove the non-interlocked products (along with a small amount of low molecular weight interlocked oligomers), the poly[*n*]catenanes were obtained with a number average molar mass ($\overline{M_n}$) of 21.4

kDa. The number average degree of polymerization ($\overline{\boldsymbol{DP}}$) for this reaction was calculated as 14 via Equation 2.1:

$$\overline{DP} = \frac{M_n(obtained\ from\ GPC\ MALS\ analysis)}{(MW(\mathbf{1})+MW(\mathbf{2}))/2} \qquad \text{Equation 2.1}$$

Fractionation of this product allow confirmation that it consisted of a mixture of linear (***l*-3**), cyclic (***c*-3**), and branched (***b*-3**) poly[*n*]catenanes (**Figure 2.2**). It was suggested that the cyclic poly[*n*]catenanes are formed from a cyclic MSP template (***c*-1·2·Zn(II)$_2$**) while the branched poly[*n*]catenanes result from inter-MSP reactions.

This prior study focused primarily on confirming the synthesis of poly[*n*]catenanes. As such, the reaction was primarily carried out at a single concentration (2.5 mM wrt. **2**) and no detailed characterization of the crude product distribution was undertaken. It is reasonable to expect that both the MSP assembly and the ring closing olefin metathesis reaction will be sensitive to monomer concentration. Thus, the goal of this chapter is to build on these prior observations and investigate this reaction in more detail by carrying out the ring closing reactions across a range of monomer concentrations (0.25-10 mM) and analyzing the crude reaction mixtures (after demetallation) to obtain a better understanding of how the reaction conditions impact this synthetic route to poly[*n*]catenanes.

2.2 Increasing the Understanding of the MSP

As the nature of the assembled MSP template is critical to the final product distribution, initial studies focused on obtaining a better understanding of the MSP assembly. A 1:1 mixture of macrocycle **1** and thread **2** in $CDCl_3$ was prepared and titrated with zinc di[bis(trifluoromethylsulfonyl)imide] ($Zn(Tf_2N)_2$). 2D NMR studies[1,2] have shown that the most

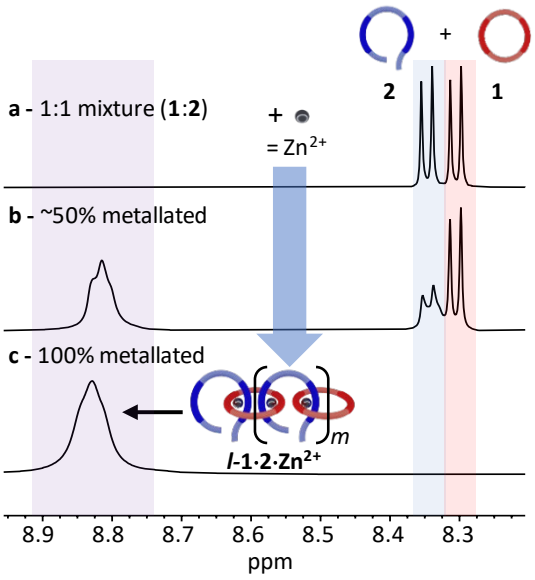

Figure 2.3 The region of the ^{1}H NMR (500 MHz, 298 K) corresponding to the H_{mpy} protons peaks of (a) a 1:1 mixture of macrocycle **1** and thread **2** (in $CDCl_3$), (b) partial metalation of the mixture by titration of $Zn(NTF_2)_2$ (in CD_3CN) and (c) the MSP ***l*-1·2·Zn(II)$_2$** (in 1:5 CD_3CN:$CDCl_3$, 20 mM w.r.t. **2**).

downfield shifted proton corresponds to the meta-proton of the pyridine moiety of the Bip ligands (H_{mpy}, **Figure 2.1**), which appear at 8.30 ppm and 8.35 ppm for **1** and **2**, respectively (**Figure 2.3a**). Coordination of the Zn(II) ions with the Bip ligand can be followed by ^{1}H NMR as the peaks corresponding to H_{mpy} shift to ca. 8.82 ppm (**Figure 2.3b**). It is worthwhile noting that the metal-ligand complex and the uncomplexed ligand are in slow exchange on the NMR timescale, allowing for the amount of free species present to be monitored during the titration. The Zn(II) ions are added into the reaction mixture until all the H_{mpy} peaks around 8.30-8.35 disappear (**Figure 2.3c**). As both Bip moieties in macrocycle **1** cannot bind to the same Zn(II) ion,[2] the only way for all the Bip ligands to bind a Zn(II) ion is the self-assembly of MSP (**1·2·Zn(II)$_2$**) that has alternating **1** and **2** units along its backbone.

In order to better understand if/how the MSP changes with concentration, it was dried and then redissolved in a mixture of acetonitrile-d3 and chloroform-d (1:5) to obtain a series of samples at different concentrations, 0.25 mM, 1.0 mM, 2.5 mM, and 10.0 mM with respect to **2** (**Figure 2.4a**). The mixture of acetonitrile-d3 and chloroform-d (1:5) was selected for the solubility of all metalated poly[*n*]catenane (**3·Zn(II)**) compounds and to mimic the MSP formation conditions. However, since the distribution of products may vary based on solvent, the MSP (**1·2·Zn(II)$_2$**) samples were similarly characterized in d-dichloromethane (**Figure 2.4b**) to confirm that the trends observed were independent of solvent.

The solutions were then characterized using a combination of ^{1}H NMR and diffusion ordered spectroscopy (DOSY). At the highest concentration (10.0 mM), the H_{mpy} appears almost entirely as a one broad peak at around 8.8 ppm (**Figure 2.4a**, Region i) which was assigned to the formation of MSP ***l*-1·2·Zn(II)$_2$** (and/or very large cyclic ***c*-1·2·Zn(II)$_2$**). This peak appears similar to what is seen at 20 mM (**Figure 2.3c**) during sample preparation. There is a slight shift upfield of this peak at this lower concentration, but no free ligand is observed (**Figure 2.4c**). As the concentration decreases, a second set of peaks appear upfield (around 8.67, Region ii in **Figure 2.4a**) which grow in intensity at lower concentrations. The dynamic nature of the Zn(II)/Bip complex results in a ring-chain equilibria existing in these MSPs and, as rings are more likely to be formed at lower concentrations,[3] this suggests that the more upfield shifted Region ii peaks correspond to the cyclic MSP ***c*-1·2·Zn(II)$_2$**.

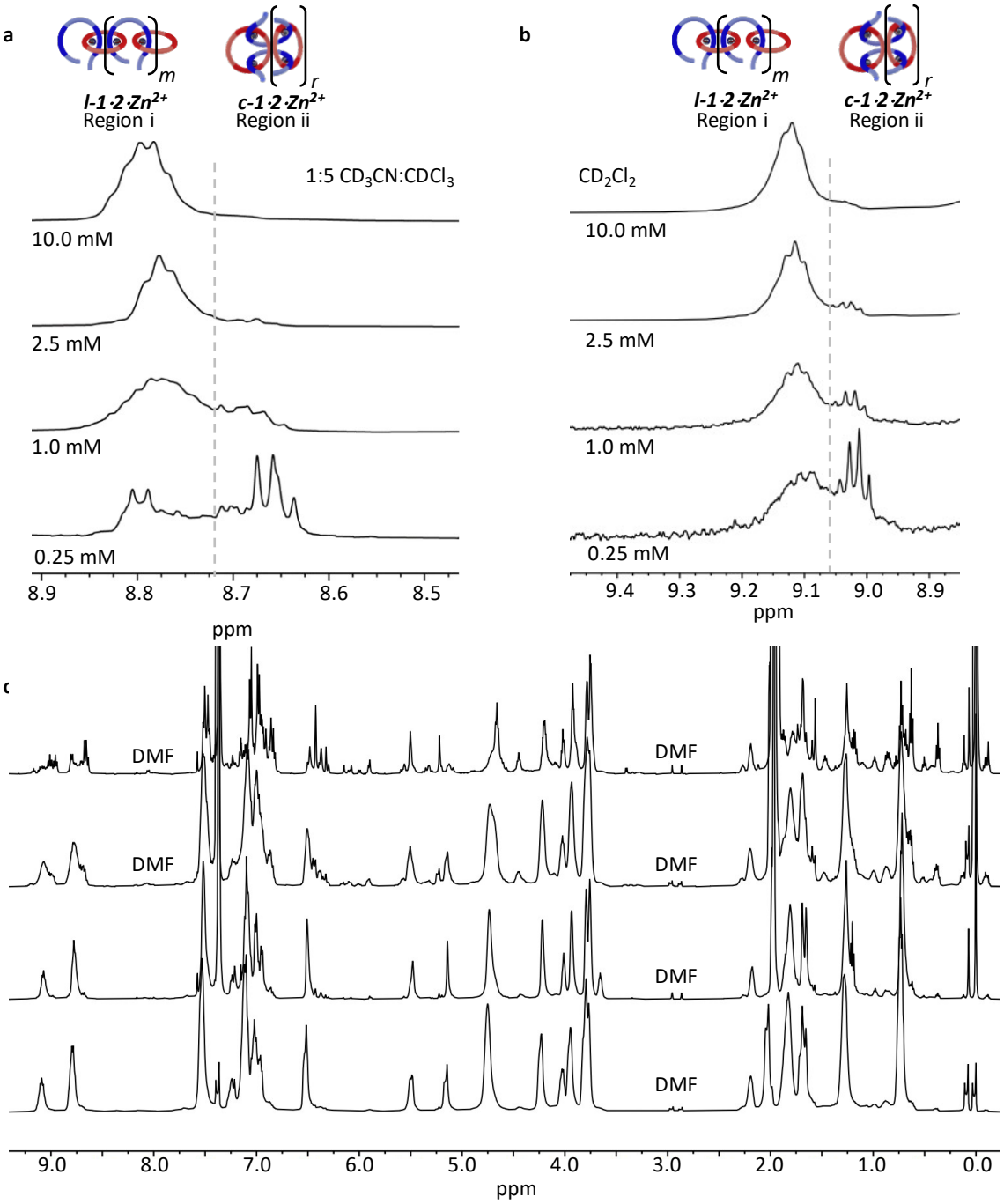

Figure 2.4 (a) Region of the ^{1}H NMR spectra (500 MHz, 1:5 CD_3CN:$CDCl_3$, 298 K) corresponding to the H_{mpy} protons for the MSP (***l*-1·2·Zn(II)$_2$/ *c*-1·2·Zn(II)$_2$**) at 0.25 mM, 1.0 mM, 2.5 mM, and 10.0 mM (w.r.t **2**). (b) Distributions of the MSP protons within the metathesis reaction solvent DCM ^{1}H-NMR of the MSP **1·2·Zn(II)$_2$** (500 MHz, CD_2Cl_2, 298 K) to confirm similarly between d-DCM and 1:5 CD_3CN:$CDCl_3$. (c) Full ^{1}H NMR spectra (500 MHz, 1:5 CD_3CN:$CDCl_3$, 298 K) of the selected MSPs (**1·2·Zn(II)$_2$**).

DOSY NMR of the MSP at the different concentrations was able to provide information on the size of the compounds that correspond to the two regions in the NMR. Diffusion coefficients for the two distinct regions were calculated using the Stejskal-Tanner expression (equation 2.2).[4]

$$\ln \frac{I_g}{I_0} = -D[\gamma^2 \delta^2 G^2 \left(\Delta - \frac{\delta}{3}\right)] \qquad \text{Equation 2.2}$$

Note: the 0.25 mM sample was too dilute to obtain reliable DOSY data.

The diffusion coefficients were calculated via the plots in **Figure 2.5**. Analysis of these diffusion coefficients shows that the values of Region i decrease from 3.3 x 10^{-10} m^2s^{-1} to 7.8 x 10^{-11} m^2s^{-1} as the concentration increases from 1 to 10 mM, consistent with an increase in assembly size/MSP molecular weight with concentration, as would be expected for the linear MSP ***l*-1·2·Zn(II)$_2$**. Region ii, on the other hand, exhibits similar diffusion coefficients for the concentrations tested. In addition, the diffusion coefficient of the Region ii protons (3.0 x 10^{-10} m^2s^{-1}) is similar to the diffusion coefficient of the individual thread (3.0 x 10^{-10}) or macrocycle (3.8 x 10^{-10}), suggesting that the MSP in this region is a more compact structure. Taken together,

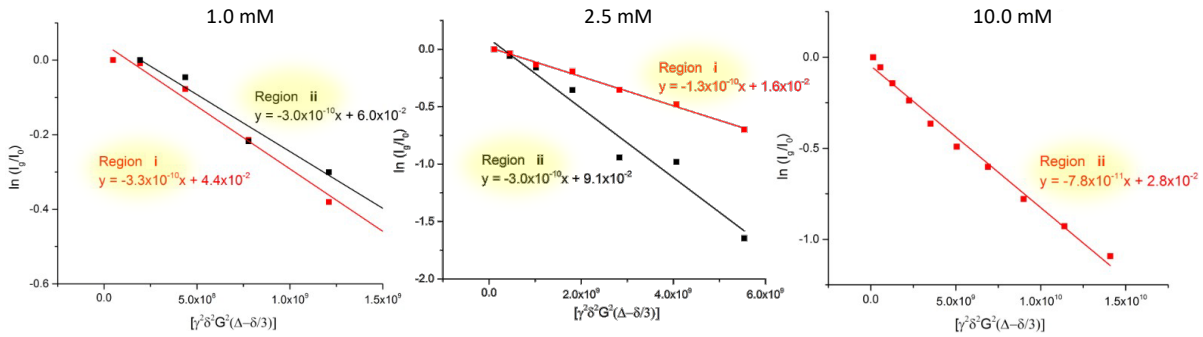

Figure 2.5 Calculation of diffusion coefficients (500 MHz, 1:4 CD_3CN:$CDCl_3$, 25 °C) for MSP **1·2·Zn(II)$_2$** from left to right: 1.0, 2.5, 10.0 mM. For calculation, the slope of the given line corresponds to the diffusion coefficient of the given region and concentration.

this data is consistent with Region ii corresponding to smaller cyclic MSP assemblies (***c*-1·2·Zn(II)$_2$**).

If these two regions in the NMR are representative of cyclic and linear MSPs, then it could be expected that a similar difference in the NMR would be observed in the metallated catenanes. To fully explore this hypothesis, a sample of primarily cyclic polycatenane (***c*-3**) was synthesized. Previous studies of the templating step[1] have demonstrated that the synthesis of cyclic poly[*n*]catenane can be targeted when iron(II) bis(trifluoromethane)sulfonimide (Fe(NTf$_2$)$_2$ is used in place of Zn(Tf$_2$N)$_2$ during the MSP formation step (see the Experimental Section for full synthetic details). This procedure allowed for an isolation of a primarily cyclic sample ***c*-3**. To obtain the primarily linear sample (***l*-3**), a sample of partially purified poly[*n*]catenane (see Experimental Section) underwent preparatory gel permeation chromatography using styrene divinylbenzene beads (40–80 μm bead size, 600–14,000 MW exclusion range). The sample of primarily cyclic poly[*n*]catenane (***c*-3**) and the sample of primarily linear poly[*n*]catenane (***l*-3**) were then metalated using Zn(Tf$_2$N)$_2$ to yield ***c*-3·Zn(II)** and ***l*-3·Zn(II)**. As can be seen in **Figure 2.6**, the ^{1}H NMR of cyclic ***c*-3·Zn(II)** resembles that of the 0.25 mM MSP, with two broad peaks

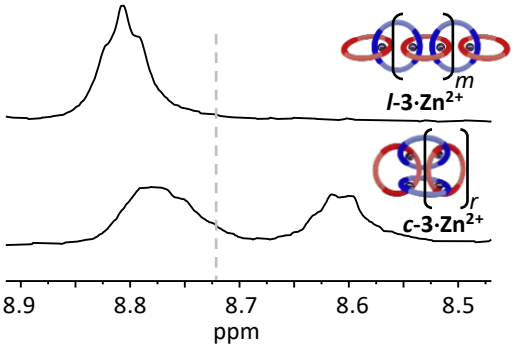

Figure 2.6 Region of the ^{1}H NMR spectra (500 MHz, 1:5 CD_3CN:$CDCl_3$, 298 K) corresponding to the H_{mpy} protons for metalated poly[*n*]catenanes ***l*-3·Zn(II)** and ***c*-3·Zn(II)**.

between 8.60-8.90 ppm. This provides further support to the upfield shifted peaks observed in the more dilute MSPs corresponding to the cyclic assemblies. Likewise, the ^{1}H NMR of ***l*-3·Zn(II)** only shows a broad peak in Region i (around 8.8 ppm) consistent with the MSP at 10.0 mM (**Figure 2.4a**, top) being predominantly linear ***l*-1·2·Zn(II)$_2$**.

2.3 NMR Analysis of Poly[*n*]catenane

To carry out the olefin metathesis ring closing reaction, the MSPs were dried and dissolved in dry dichloromethane to yield a series of samples at 0.25, 0.5, 1.0, 2.5, 5.0, and 10.0 mM, with respect to **2**. The Hoveyda Grubbs catalyst (0.32 mM) was added to each reaction before it was heated to reflux for 48 hrs, with a second addition of the same amount of catalyst after the first 24 hours elapsed. After deactivation of the catalyst, the crude material is demetallated using ethylenediamine.

Figure 2.7a shows the m-pyridyl proton (H_{mpy}) region of the ^{1}H NMR spectra for each of the demetallated crude reaction mixtures. The non-interlocked byproducts are easily identifiable in the NMR, with the macrocycle **1** at 8.31 ppm and the thread **2** and thread-based byproduct **5** around 8.35 ppm. For the interlocked compounds, the H_{mpy}'s shift upfield to between 8.05-8.27 ppm.[1] The integration of these peaks allows determination of the average interlocked yield of each reaction (**Figure 2.7b**, **Table 2.1**). Within this region, a triplet from the **2**/**5** byproducts appears centered at 8.07 ppm which is excluded from the integration to more accurately calculate the yield of interlocked products (**Figure 2.8**). These integrations also allow for a determination of the residual macrocycle (**1**) (**Figure 2.7b**) and residual thread (**2**)/ADMET (**5**) yields (**Table 2.1**). The crude NMRs can also provide preliminary data on the yield of cyclic catenane (***c*-3**). Through previous studies,[1] the cyclic catenane (***c*-3**) was shown to present 50% of it's H_{mpy} peak from 8.05-

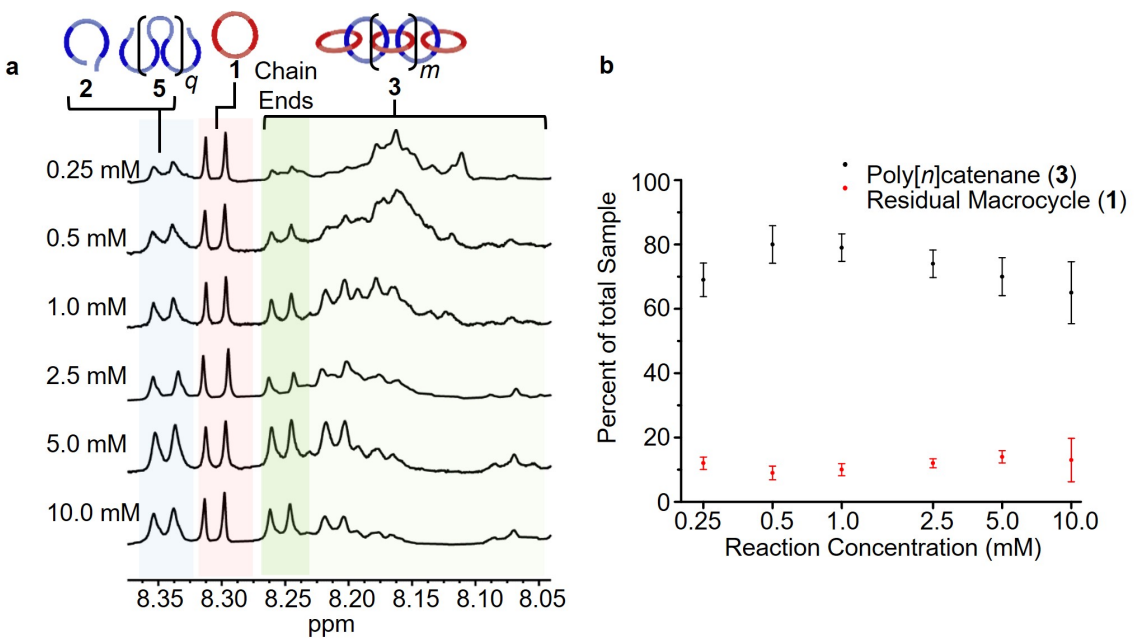

Figure 2.7 (a) Region of the ^{1}H NMR spectra (500 MHz, $CDCl_3$, 298 K) corresponding to the H_{mpy} protons for the demetallated crude reaction mixtures at different concentrations. (b) Average poly[*n*]catenane (**3**) (black) yields and amount of residual macrocycle (**1**) at each reaction concentration. Error bars for data sets taken at 95% confidence interval (n=5).

8.15 ppm, a region where no ***l*-3** or ***b*-3** is seen. Based on this knowledge, the Equation 2.3 can be used to calculated the % cyclic poly[*n*]catenane (***c*-3**) in any given poly[*n*]catenane sample (reference **Figure 2.8** for integrated regions):

$$\%\ Cyclic\ Catenane = \frac{2 \times Integration\ ((8.05-8.15\ ppm) - Triplet\ at\ 8.07\ ppm)}{Integration\ (((8.05-8.27\ ppm) - Triplet\ at\ 8.07\ ppm)} \qquad \text{Equation 2.3}$$

This cyclic yield (**Figure 2.9a**) was found to follow a similar trend to the amount of cyclic MSP (***c*-1·2·Zn(II)$_2$**) given for each concentration (**Figure 2.9b**). The 2.5mM reaction has an average interlocked yield of ca. 73±5 % (n = 5), consistent with the previously reported value.[1] The average interlocked yield remains above 70% for all concentrations except those at the extremes (0.25 mM and 10.0 mM). This is, in part, a consequence of a lower average alkene conversion (87% for both 0.25 and 10.0 mM, c.f. 0.5-2.5mM show ca. 95% conversion, see **Table 2.1**). Presumably at 0.25 mM, the relatively high dilution leads to a decrease in reaction rate and

Table 2.1 Data obtained from analysis of ^{1}H NMR spectra of poly[*n*]catenane samples

Conc. (mM)	Avg. % interlocked yield[a]	Avg. % byproduct **1** remaining	Avg. % byproducts **2** and **5**	% Cyclic ^{1}H NMR[b]	Conversion of Double Bond (% alkene reacted)[c]
0.25	69 ± 5	12	19	52 ± 4	87 ± 5
0.5	82 ± 6	9	9	38 ± 6	94 ± 3
1.0	80 ± 5	10	10	15 ± 3	96 ± 2
2.5	73 ± 5	12	15	7 ± 2	95 ± 2
5.0	71 ± 7	14	15	5 ± 1	91 ± 3
10.0	65 ± 10	13	22	4 ± 2	88 ± 4

(a) Conversion to catenane calculated by integrating H_{mpy} doublets corresponding to non-interlocked products **1** and **5** (8.36-8.28 ppm) against H_{mpy} protons corresponding to **3** (8.28-8.10 ppm). (b) Cyclic conversion calculated via the assumption[1] that only 50% of the cyclic catenane appears in the region 8.05-8.15 ppm where no other catenane appears. Peaks from **5** were considered and removed from the final value when numbers were obtained Equation 2.3. (c) Alkene peaks integrated from 5.62-5.29 ppm, assuming a sample at 100% reaction integrates to 2H.

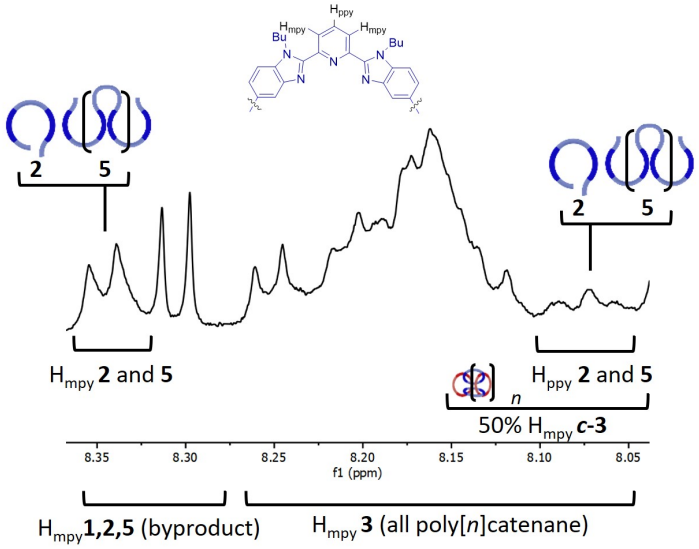

Figure 2.8: ^{1}H NMR spectrum (500 MHz, $CDCl_3$, 25 °C) for an example % poly[*n*]catenane yield and cyclic conversion calculation (0.5 mM sample). In order to determine the size of the triplet at 8.07 ppm the integration of the doublet at 8.35 ppm is used, which is in a 2:1 ratio with the triplet at 8.07 ppm. The contribution from this triplet, based on this integration, is removed from the final catenane conversion calculation and cyclic poly[*n*]catenane (***c*-3**) concentration.

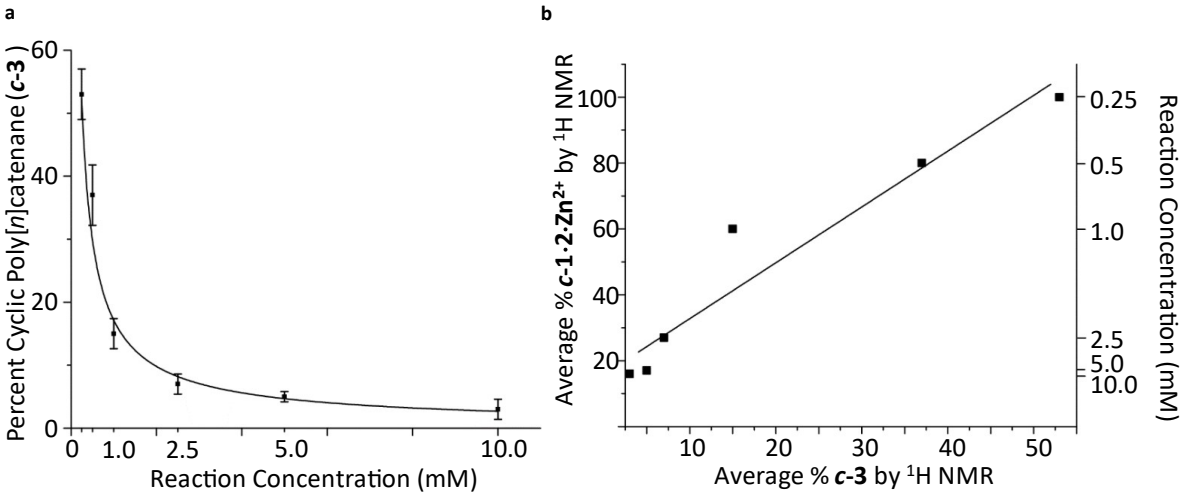

Figure 2.9 (a) Percent yield of cyclic catenane (***c*-3**) calculated via ^{1}H NMR (500 MHz, $CDCl_3$, 25 °C) assuming that 50% of the cyclic catenane protons appear in the region 8.05-8.15 ppm.[1] Peaks from ADMET **5** and residual thread **2** were considered and removed from the final value (see Equation 2.3). (b) Comparison of the amount of cyclic MSP ***c*-1·2·Zn(II)$_2$** at each reaction concentration versus the yield of cyclic poly[*n*]catenane (***c*-3**) at the same concentration (given in (a)). % ***c*-1·2·Zn(II)$_2$** calculated based on the assumption that Region ii of Figure 5a corresponds to 50% of the total ***c*-1·2·Zn(II)$_2$** in each sample.

a slightly lower yield of interlocked materials (69±5%). It is important to note that, at the higher concentrations (5 and 10 mM), a significant amount of insoluble product is obtained during the reaction. This product was still insoluble after demetallation and was only observed to swell in a range of organic solvents, such as chloroform and tetrahydrofuran. These products are assumed to be interlocked networks and are included in the overall interlocked yield in **Figure 2.7b**. None-the-less, at 10 mM, the interlocked yield was only 65±10%. This lower value may result from partial insolubility of the both the MSP and the partially reacted species at these higher reaction concentrations. Additionally, the higher concentration will likely promote inter-MSP reactions, resulting in an increased formation of ADMET polymer **5**.

Preliminary data from DOSY NMR analysis was also collected and analyzed via Equation 2.2. Four samples at each concentration were analyzed (n=4) in order to give the most accurate

representation of the size changes seen at the various reaction concentrations (**Figure 2.10**). These results demonstrated a consistent decrease in diffusion coefficient as the reaction concentration increased, suggesting that the higher reaction concentrations yielded larger products.

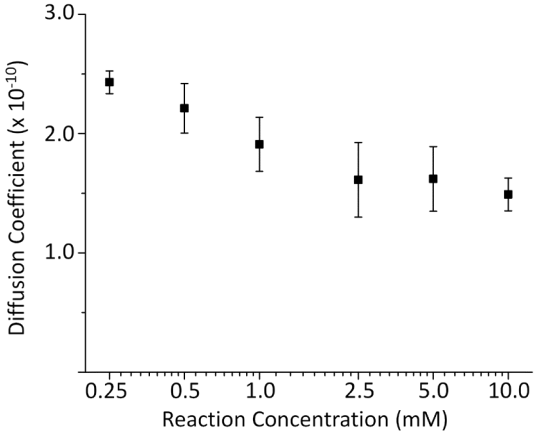

Figure 2.10 Average diffusion coefficients (Equation 2.2) obtained from diffusion NMR studies of the H_{mpy} of the catenanes (500 MHz, $CDCl_3$, 25 °C). Error was calculated based on a 95% confidence (n = 4).

2.4 GPC Analysis of Poly[*n*]catenane Architecture

To fully determine the extent of the size variations between reaction concentrations, the crude products were then analyzed via GPC-MALS. Initial characterizations of the poly[*n*]catenanes via GPC studies were reported in THF,[1] however continued use of this solvent showed interactions between poly[*n*]catenane and the polystyrene/divinylbenzene matrix column within the GPC system. Over time, the poly[*n*]catenane began to drag within the run and obscure the distribution data as well as contaminate the system. Attempts to rectify this within the THF system included utilizing additives (triethylamine (TEA) and trioctylamine (TOA)) in both the sample preparation and the mobile phase, but the additives had no lasting effects.

After the initial THF studies, a new GPC system was purchased to run a mobile phase of DMF+0.1% LiBr. While initial studies in this solvent mixture were promising, the poly[*n*]catenane

began interacting with the LiBr additive and skewing the refractive index trace as well as the MALS trace. Attempts to run the sample in a purely DMF mobile phase led to aggregation of the poly[*n*]catenane samples. After much trial and error, a 1:3 mixture of DMF:THF was proposed to counteract the various issues: the presence of the DMF limited the dragging and the primarily THF mobile phase prevents the aggregation seen in pure DMF. Therefore, any future work on interlocked materials containing the Bip ligand is recommended to continue the use of the 1:3 DMF:THF mobile phase. Beyond the changes to the mobile phase, the new GPC analysis in this study also benefits from a GPC column with better low molecular weight resolution (relative to the prior studies)[1]. This increased resolution results in a clearer picture of the complicated range of products formed during these reactions (**Figure 2.11**). As such, the use of this new GPC protocol allowed new conclusions to be drawn from this data.

Perhaps the most obvious data trend is a move to faster elution times with the reactions carried out at the higher concentrations, confirming the formation of higher molecular weight species in these more concentrated reactions. It is also possible to clearly see the presence of the residual macrocycle **1** in all the GPC spectra, which is consistent with what is observed in the NMR. In an attempt to obtain more information on the reaction products, deconvolution of the GPC traces was explored using a gaussian algorithm[5–7] to fit the data to the minimum number of peaks. All GPC data was processed using OriginPro multiple peak fit gaussian analysis software. Peak centers were chosen based on the apparent peaks seen within the trace (qualitative assessment) as well as maintaining the location consistency of peaks A-I throughout the various samples (elution time consistency of each proposed product). The peak areas and widths were found by optimizing the overall fit to the precise RI trace of the data.

As can be seen in **Figure 2.11**, excellent fits to the experimental GPC trace can be obtained using 6-9 gaussian peaks (depending on the concentration of the reaction). Pure samples of macrocycle **1** and thread **2** were run using the same conditions and eluted at 17.2 minutes and 16.5 minutes, respectively (**Figure 2.12**), allowing those deconvoluted peaks (macrocycle (A, red) and

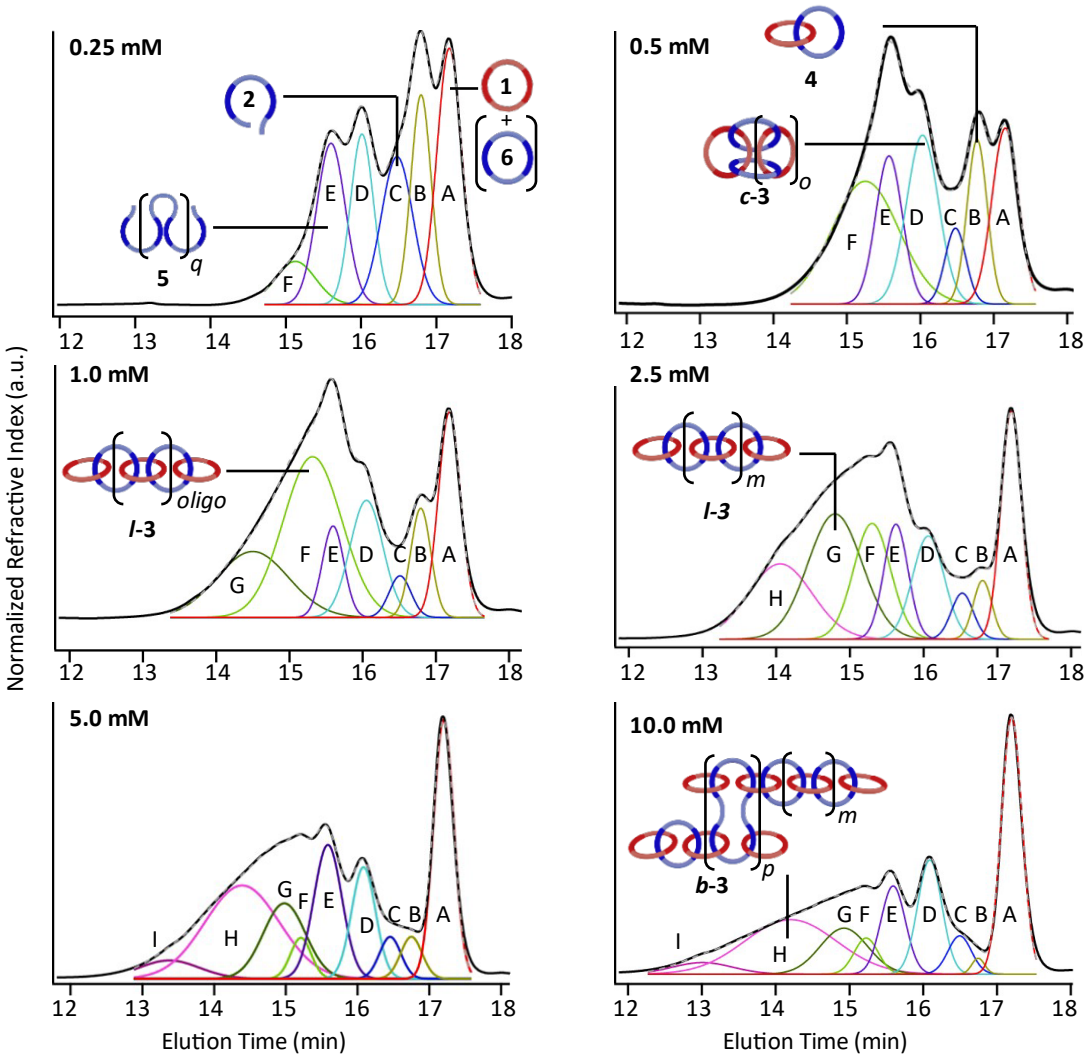

Figure 2.11 GPC refractive index traces for 0.25, 0.5, 1.0 2.5, 5.0 and 10.0 mM (mobile phase - 25% DMF in THF). Each trace shows deconvoluted peaks using a Gaussian Fit with each peak showing its (tentative) assignment. A – Macrocycle (**1**) or ring closed thread (**6**), B – Thread (**2**), C – [2]catenane (**4**), D – cyclic poly[*n*]catenane (***c*-3**), E – ADMET product (**5**), F – oligomeric linear catenane (***l*-3**), G – linear poly[*n*]catenane (***l*-3**), H – branched poly[*n*]catenane (***b*-3**), I – hyper-branched poly[*n*]catenane (***b*-3**).

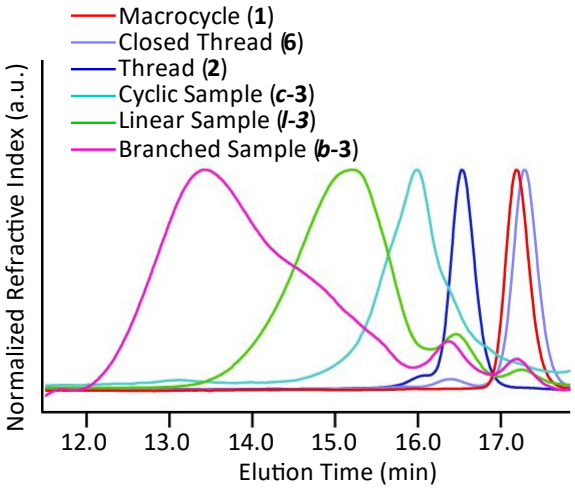

Figure 2.12 GPC traces taken for macrocycle (**1**), thread (**2**), ring closed thread (**6**), the sample made according to literature preparation[1] of cyclic catenane (***c*-3**), the purified primarily linear sample (***l*-3**), and the purified primarily branched sample (N_c = 12, ***b*-3**). Mobile phase - 25% DMF in THF).

thread (C, blue)) to be assigned to these starting materials. In addition, macrocycle **7**, which can be formed by ring closing of thread **2**, elutes ca. 17.3 minutes and as such, if present, would also be present as part of deconvoluted peak A (red).

Between the macrocycle peak (A, red) and the linear thread peak (C, blue) there is a peak that elutes at approximately 16.8 minutes (B, gold in **Figure 2.11**). Based on the elution time of this peak, this compound is more compact than the thread (**2**) but bigger than macrocycles **1** and **6**. MALS data corresponding to this peak (**Figure 2.13**, **Table 2.2**) shows that the molecular weight of this compound is approximately double that of macrocycle peak A. This suggests that peak B either corresponds to a [2]catenane (**4**) and/or possibly the non-interlocked cyclic dimer of thread **2**. The fact that this peak is more prominent at the lowest concentration (0.25 mM, **Figure 2.11** top left), is consistent with either of these assignments.

Peak D (cyan in **Figure 2.11**) elutes at 16.0 minutes and is assigned as the cyclic catenane ***c*-3**, as it corresponds to the elution time of a purified cyclic sample, with an average of 5 rings,

51

Table 2.2 GPC quantitative analysis for crude poly[*n*]catenane samples

Conc. (mM)	$\overline{M_n}^{a}$	$\overline{DP}^{b}$
0.25	6200	4
0.5	9300	6
1.0	13800	9
2.5	15300	10
5.0	16700	11
10.0	15800	10

(a)Values were determined assuming the calculated *dn/dc* of 0.2125. (b) Calculated using Equation 2.1

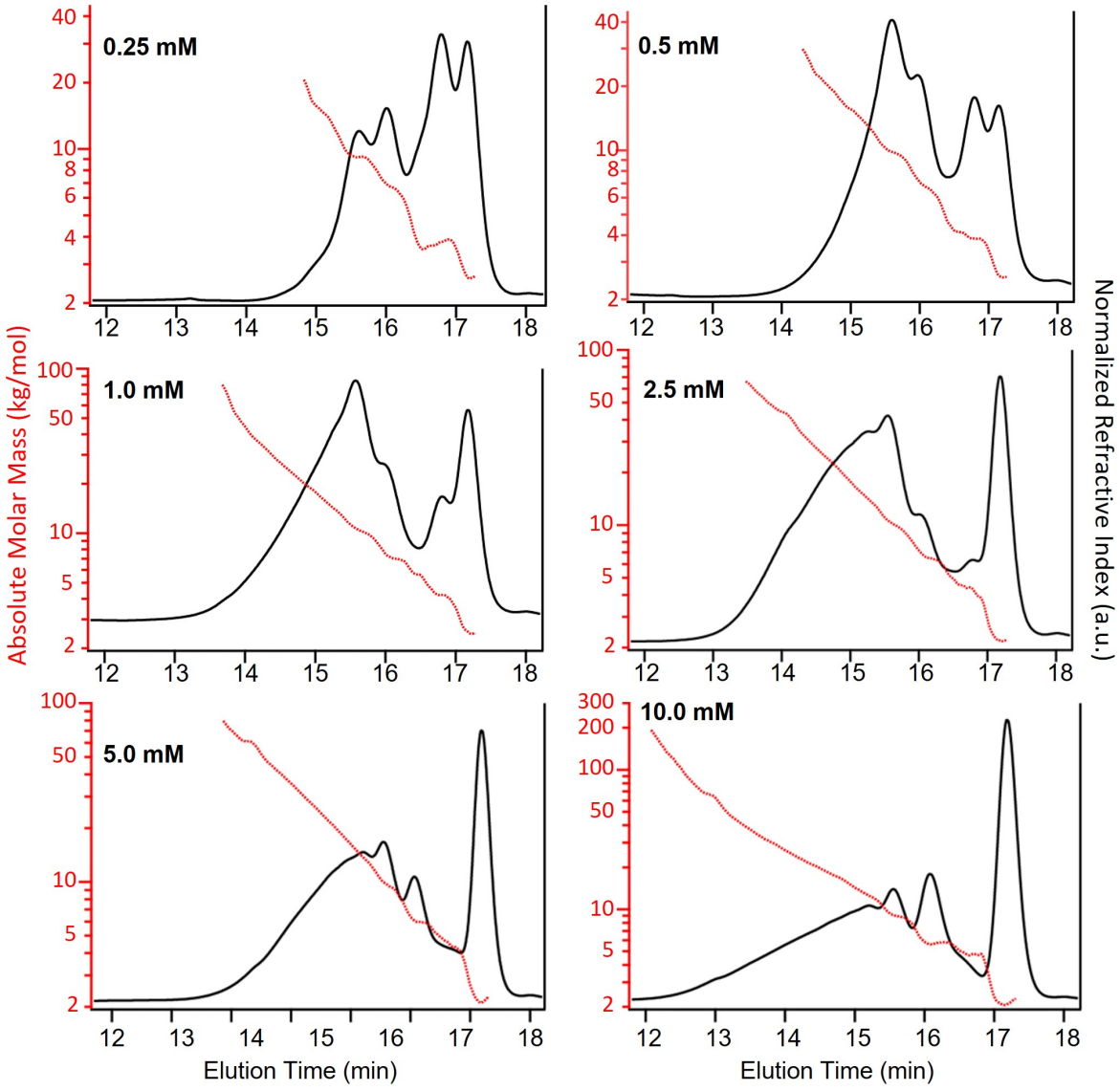

Figure 2.13 Absolute molar mass for the series of samples (0.25, 0.5, 1.0, 2.5, 5.0, and 10.0 mM) determined by MALS-GPC (mobile phase - 25% DMF in THF, 1mL/min at 25 °C).

based on MALS data (**Figure 2.13**).[1] The next identified peak elutes at approximately 15.6 minutes (Peak E, purple, **Figure 2.11**). While this peak does not correspond to any isolated samples, it is tentatively assigned to the ADMET (**5**) product in each of the samples. Based on the previous poly[*n*]catenane characterization,[1] it is proposed that Peaks F, G, H, and I correspond to different populations of linear (***l*-3**) and branched (***b*-3**) poly[*n*]catenanes.

There are a number of different routes that linear poly/oligo[*n*]catenanes can be accessed during the synthesis. **Figure 2.14** highlights two possible routes to these structures, namely incomplete ring closing of the linear (***l*-1·2·Zn**) and cyclic (***c*-1·2·Zn(II)$_2$**) MSPs. It can be expected that at low concentrations (when most of the MSP is the cyclic ***c*-1·2·Zn(II)$_2$**, see above) the majority of the linear catenane will be formed via ***c*-1·2·Zn(II)$_2$** while at higher concentrations the linear catenane will accessed predominantly via ***l*-1·2·Zn(II)$_2$**. If both of these routes occur simultaneously, it can then be expected that there will be two molecular weight populations of linear ***l*-3**. These two populations are tentatively assigned to Peaks F and G (light and dark green) based on the GPC elution time of a sample of purified primarily linear (***l*-3**) poly[*n*]catenane (**Figure 2.12**) that spans both peaks.

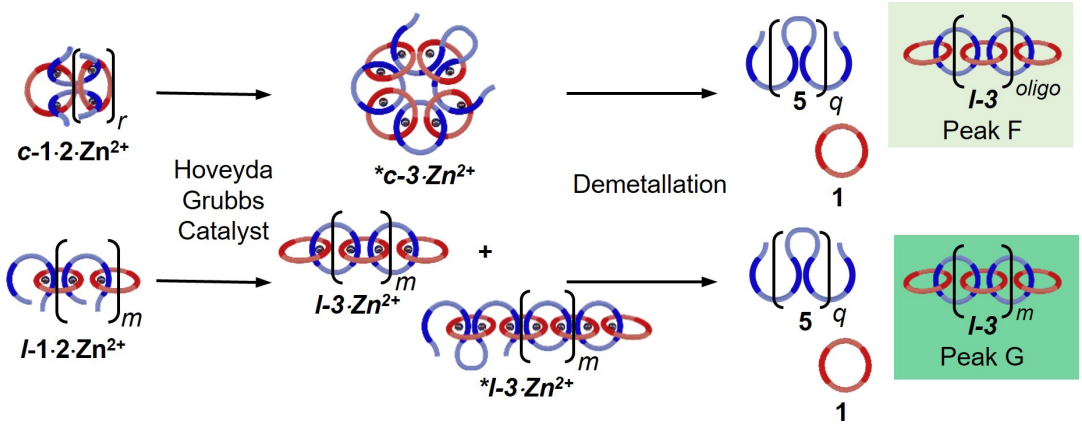

Figure 2.14 Proposed routes to linear poly/oligo[*n*]catenanes (***l*-3**) with different molecular weight populations.

For the 0.25 mM sample, where the MSP is almost exclusively cyclic ***c*-3**, only Peak F is present (15.2 minutes, light green). Based on MALS analysis of this peak, it corresponds to relatively low molecular weight oligomers/catenanes (average molecular weight M_n ca. 8 kg mol^{-1}, **Figure 2.13**). For this reaction, the ^{1}H NMR of the sample shows evidence of catenane chain ends (**Figure 2.7a**), indicating a mixture of linear ***l*-3** and cyclic ***c*-3** poly[*n*]catenanes. As such, it is proposed that Peak F corresponds to the linear oligo[*n*]catenanes ***l*-3** formed from via the cyclic MSP (**Figure 2.14**). This hypothesis is supported by the fact that peak F corresponds to a smaller percentage of the overall product distribution at higher concentrations (**Table 2.3**). NMR of the MSP shows that, as the reaction concentration increases, the MSP shifts from being predominantly cyclic (***c*-1·2·Zn(II)$_2$**) to being predominately linear (***l*-1·2·Zn(II)$_2$**), resulting in a decrease in the yield of this oligomeric linear catenane (***l*-3**) at higher concentrations. As the relative size of peak F decreases with reaction concentration there is a concomitant appearance and increase in the size of Peak G. It is proposed that Peak G corresponds to the higher molecular weight linear catenanes that result from the successful ring-closing of the linear MSP ***l*-1·2·Zn(II)$_2$** (**Figure 2.14**).

Peaks H and I correspond to the largest molecular weights observed in the catenanes. Based on chain end analysis of fractionated samples in prior work and comparison to an isolated branched

Table 2.3 GPC Gaussian deconvolution peak analysis for crude poly[*n*]catenane samples

Reaction conc. (mM)	Peak A (% total area) Macrocycle (**1**)	Peak B (% total area)	Peak C (% total area) Thread (**2**)	Peak D (% total area)	Peak E (% total area)	Peak F (% total area)	Peak G (% total area)	Peak H (% total area)	Peak I (% total area)
0.25	24	17	18	16	18	7	0	0	0
0.5	17	12	6	20	15	30	0	0	0
1.0	16	8	3	14	7	35	17	0	0
2.5	16	4	3	11	10	15	24	17	0
5.0	20	4	4	11	15	3	12	27	4
10.0	26	1	4	14	11	4	11	25	4

poly[*n*]catenane sample (**Figure 2.12**), these peaks are tentatively assigned to branched ***b*-3** poly[*n*]catenanes. Peak H (light pink) at 14.1, begins to appear at 2.5 mM (**Figure 2.10** middle right), where the presence of branched catenanes has already been reported.[1] As the concentration increases further however, a second peak (Peak I, dark pink) at 13.0 minutes is required for the gaussian fit (**Figure 2.11** bottom, **Table 2.3**), suggesting the formation of a new population of highly branched polymers (MALS, $\overline{M_n}$= 60 kg mol^{-1}, $\overline{DP}$= 39 (Equation 2.1)).

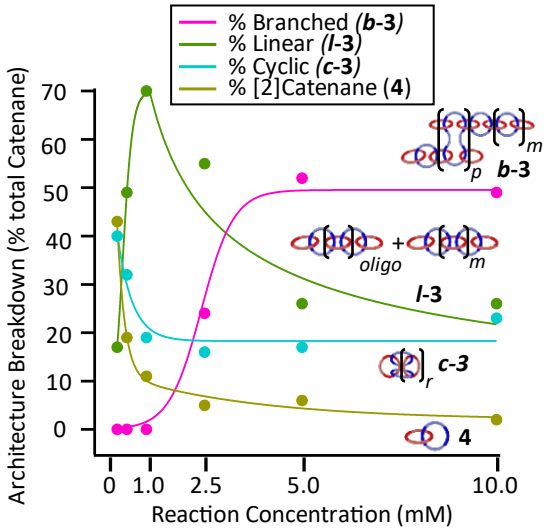

Figure 2.15 Poly/olio[*n*]catenane (***l*-3**, ***c*-3**, ***b*-3** (+ insoluble fraction), and **4**) distribution versus reaction concentration (byproducts are excluded).

Based on these peak assignments, some general trends can be elucidated (**Figure 2.15**, **Table 2.3**) regarding the impact of reaction concentration on product distribution. As may be expected, the [2]catenane (**4**) (and/or cyclic dimer of **2**) and the cyclic (***c*-3**) catenanes are the dominant products at the lowest concentration (0.25 mM). As the reaction concentration increases, the yields of these products drop and eventually plateau for all concentrations above 2.5 mM, consistent with what is commonly observed in polymerizations where ring-chain equilibria are present.[8]

The linear (***l*-3**) catenanes (polymer + oligomer) show a significant increase in yield from 0.25 mM to 1.0 mM (**Figure 2.15**, green) and become the dominant product (70% ***l*-3** at 1.0 mM). However, the linear ***l*-3** formed at 1.0 mM appears to be primarily oligomeric in nature (peak F), presumably a consequence of being formed predominantly from the ***c*-1·2·Zn(II)$_2$** precursor. While increasing the reaction concentration to 2.5 mM results in a slight drop in the overall yield of linear ***l*-3** (**Figure 2.14**), the resulting ***l*-3** now is predominately the higher molecular ***l*-3** fraction (Peak G). As a result, carrying out this reaction at 2.5 mM optimizes both the yield and molecular weight of the linear ***l*-3** products. Between 2.5-5.0 mM the overall amount of linear polycatenane decreases as branched poly[*n*]catenanes ***b*-3** (**Figure 2.11**, pink) start to be formed. It is worthwhile also noting that at the higher concentrations, the larger molecular weight fraction (**Figure 2.11**, Peak G) of linear polycatenane ***l*-3** becomes the dominant linear species. However, the yield of the branched polycatenanes (***b*-3** plus networks as these numbers also include insoluble polymers) quickly dominates the reaction products, becoming the major poly[*n*]catenane formed above 5.0 mM (52% ***b*-3** at 5.0 mM and 48% ***b*-3** at 10.0 mM).

2.5 Chain End Analysis via GPC/NMR Techniques

One way to further elucidate the trends in architecture (and to back up the assignment of the deconvoluted peaks in the GPC) is to determine the number of average value of chain ends (N_c) in each sample. For these samples, cyclic poly[*n*]catenanes have no chain ends ($N_c = 0$), linear poly[*n*]catenanes have $N_c = 2$ and branched poly[*n*]catenanes have $N_c \geq 3$, therefore determination of the average number of chain-ends in the sample can give an idea of the architecture distribution. Using a qualitative assessment of the ^{1}H NMR data in **Figure 2.7**, the chain end region from 8.24-8.27 reflects the observed GPC trends: products formed at low reaction concentrations show diminutive peaks in this region, reflecting fewer chain ends and the primarily cyclic nature of the

materials. However, at the higher reaction concentrations the products show increased prevalence of these chain end peaks consistent with the transition into linear and highly branched materials.

To quantify this, a new set of poly[*n*]catenanes were synthesized and were partially purified using literature procedures before analysis.[1] This purification was performed in an attempt to remove as much of the byproducts as possible, particularly ADMET **5**, to minimize the influence of these byproducts on the reported poly[*n*]catenane molecular weight and calculated Nc.

For this purification, the poly[*n*]catenanes were partially remetallated with Zn(II) ions and the mixture was dried and washed with 2:1 chloroform:hexanes to remove the soluble unmetallated (by)products (full synthetic details in Experimental Section). These samples were then demetallated and analyzed by GPC MALS (using 25 vol% DMF in THF as the mobile phase) and ^{1}H NMR. **Figure 2.16** shows the $\overline{M_n}$ and calculated average number of chain ends (N_c), determined by a combination of the NMR and the GPC-MALS data using previously published[1] Equation 2.4:

$$N_C = \overline{DP} \times \frac{2 \times Integration(\,8.24-8.27\,ppm)}{Integration\,(8.05-8.27)} \qquad \text{Equation 2.4}$$

Where $\overline{DP}$ is taken from Eq. S1.

For example, based on this combination of NMR and GPC-MALS data, the poly[$_n$]catenanes prepared at 2.5 mM have an average number of chain-ends of ca. 2.7, consistent with the product architecture being predominantly linear (***l*-3**) with some branched. In fact, deconvolution of the GPC trace (**Figure 2.17**) shows the dominance of the linear poly[*n*]catenane assigned peak G (50 % of the total catenated material) in this sample.

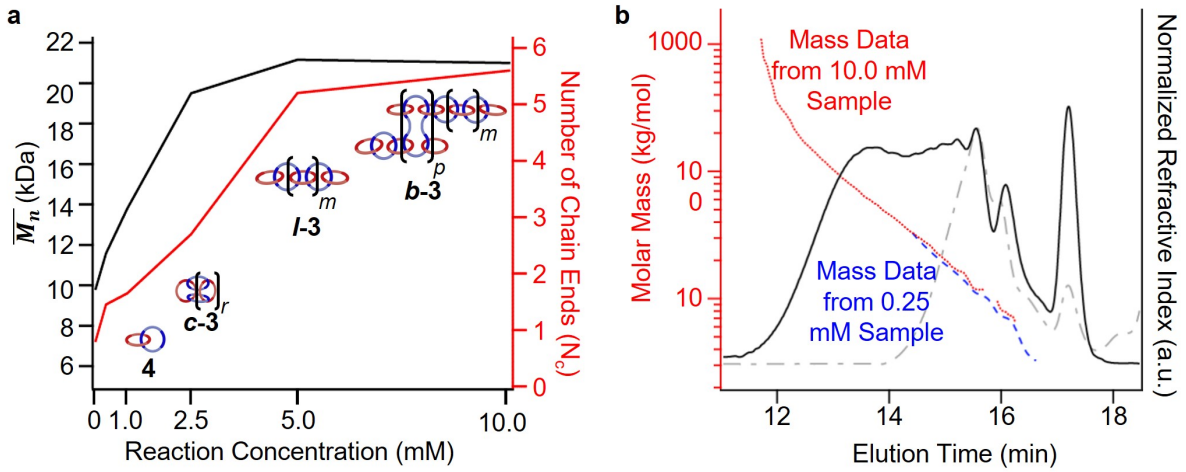

Figure 2.16 (a) Number average molar mass (M_n) determined by GPC-MALS plotted for the reaction concentrations to observe the trends. Number of chain ends (N_c) determined by a combination of GPC-MALS and NMR analysis.[1] (b) GPC RI trace from the 10.0 mM (black) and 0.25 mM (grey, dash) purified sample. Absolute molecular weight (determined by MALS)

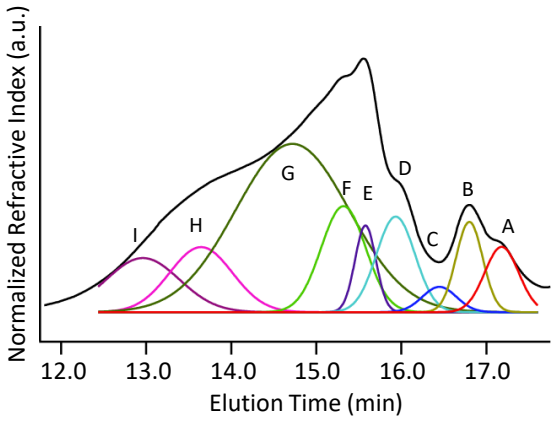

Figure 2.17 Deconvolution of RI trace (mobile phase - 25% DMF in THF, 1mL/min at 25 °C) for a partially purified 2.5 mM concentration sample. Deconvolution performed using a Gaussian fit. Tentative assignments: A – Macrocycle (**1**) or ring closed thread (**6**), B – Thread (**2**), C – [2]catenane (**4**), D – cyclic poly[*n*]catenane (***c*-3**), E – ADMET product (**5**), F – oligomeric linear catenane (***l*-3**), G – linear poly[*n*]catenane (***l*-3**), H – branched poly[*n*]catenane (***b*-3**), I – hyper-branched poly[*n*]catenane (***b*-3**).

The data obtained from the partially purified samples also allows for a more complete analysis of the molecular weight trends throughout the various concentrations with the reduced presence of ADMET **5** (**Figure 2.18**). Consistent with the prior data, lower molecular weights

result from the samples where the primary starting material was the cyclic MSP ***c*-1·2·Zn(II)$_2$**. For these, at 0.25 mM and 0.5 mM, the average molecular weight appeared as 9.8 and 11.6 kg mol^{-1} respectively. These would correspond to catenanes with approximately 6 and 8 interlocked macrocycles. For both of these samples, chain end analysis (Equation 2.4) revealed that the average poly[*n*]catenane contained fewer than 2 chain ends (0.8, 1.5, **Figure 2.16a**) demonstrating that the material was likely a combination of the [2]catenane (**4**), oligomeric ***l*-3**, and cyclic ***c*-3** poly[*n*]catenanes.

At higher concentrations the MSP precursor shifts to a higher percentage of the linear (***l*-1·2·Zn(II)$_2$**) and as such the resulting products now consist of more linear (***l*-3**) and branched (***b*-3**) poly[*n*]catenanes (N_c > 2). This is concomitant with an increase of the $\overline{M_n}$ for the samples: at 2.5 mM the $\overline{M_n}$ is 19.5 kg mol^{-1}, ($\overline{DP}$ ca. 13) and N_c is 2.7. At this reaction concentration, the GPC MALS trace also shows evidence of larger catenanes, with molecular weights up to 100 kg mol^{-1} (**Figure 2.18**).

The highest reaction concentration studied (10.0 mM) produces the highest molecular weight species, $\overline{M_n}$ of 21 kg mol^{-1} ($\overline{DP}$ ca. 14). The poly[*n*]catenanes synthesized here exhibit the largest N_c (5.6), indicative of the presence of a significant amount of highly branched poly[*n*]catenanes. It is important to note that this molecular weight analysis includes the lower molecular weight products (ADMET (**5**), cyclic (***c*-3**), and [2]catenane (**4**)) that were not completely removed during the partial purification step, suggesting that the average size of the linear ***l*-3** and branched ***b*-3** materials is larger than this value.

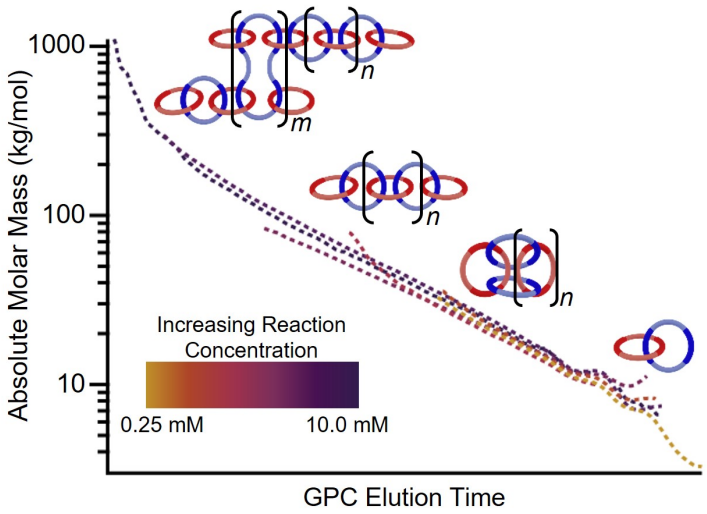

Figure 2.18 MALS data used in tandem with RI trace to determine molecular weight from partially purified samples (mobile phase - 25% DMF in THF, 1mL/min at 25 °C).

For comparison, **Figure 2.16b** shows the GPC-MALS data for these partially purified reactions mixtures that were obtained a 0.25 and 10 mM. The highest molecular weight products obtained at 0.25 mM are ca. 33 kg mol^{-1}. However, the MALS data of products obtained from the 10 mM show evidence of soluble (branched) catenanes up to 1000 kg mol^{-1} (DP > 640), which are the largest reported poly[*n*]catenane compounds to date.

2.6 Experimental

2.6.1 Materials and Methods

Dichloromethane (DCM) was purchased from Acros Organics and distilled over CaH_2 under argon atmosphere before using. Dimethylformamide (DMF, extra dry) was purchased from ACROS was used as received. Deuterated solvents, containing tetramethylsilane (TMS) as internal standard, were purchased from Acros Organics. All other solvents were purchased from Fisher Scientific and used without purification. Zinc di[bis(trifluoromethylsulfonyl)imide] was purchased from Strem Chemicals and stored in a nitrogen desiccator. All other chemicals were purchased

from Sigma-Aldrich and used without further purification unless otherwise mentioned. Preparatory GPC of poly[*n*]catenane was performed using styrene divinylbenzene beads for size exclusion, 1% crosslinkage, 40–80 μm bead size, 600–14,000 MW exclusion range (Bio-Beads S-X1 Support #1522150).

NMR data was acquired on either a 400 MHz Bruker DRX spectrometer equipped with a BBO probe, using Topspin 1.3; or a 500 MHz Bruker Avance-II+ spectrometer equipped with a 1H{19F,13C,31P} QNP probe, using Topspin 2.1. Chemical shifts were calibrated with TMS for all measurements. All Diffusion Pulsed-Gradient Spin-Echo (PGSE) measurements were performed on the 500 MHz spectrometer using the Stejskal-Tanner method.[9] Two identical pulsed field gradients with duration δ = 0.004 s separated by a delay time of either Δ = 0.05413 s (poly[*n*]catenane (**3**) samples, 1.0 mM MSP (**1·2·Zn(II)$_2$**), and 2.5 mM MSP (**1·2·Zn(II)$_2$**) samples) or Δ = 0.1201 s (10.0 mM MSP (**1·2·Zn(II)$_2$**) sample) were incorporated into a spin-echo sequence, one before and the other after the 180° pulse. 1H NMR spectra were recorded in $CDCl_3$ or 1:4 CD_3CN:$CDCl_3$ at 295.5 K without sample spinning. During each experiment, the gradient strength (G) was varied between 0 and 34 G/cm. The gradient was calibrated using a solution of 2% H_2O in D_2O. NMR spectra were processed by either MestReNova software or Bruker Topspin 4.0.6. GPC was performed on a Shimadzu Prominance LC system with PLgel Mixed-D columns using a mixture of 25% HPLC grade dimethylformamide (DMF) and 75% HPLC grade tetrahydrofuran (THF) as the eluent (1mL/min) at 25 °C. Characterization of the eluent occurred using Wyatt Dawn Helios MALS (658 nm laser) and Wyatt Optilab T-rEX refractive index (RI) detectors. The *dn/dc* of poly[*n*]catenane **3** was 0.2125, measured by injecting a series of diluted samples of 5 in 25% DMF/THF solution (concentration: 0.1, 0.2, 0.4, and 0.8 mg/mL)

subsequently into the RI detector until receiving a stable signal for each concentration and processed by Wyatt Astra software.

2.6.2 Synthesis of Procedures

2.6.2.1 Synthesis of 2,6-bisbenzimidazolylpyridine ligand (7)[10]

Step 1 of 4

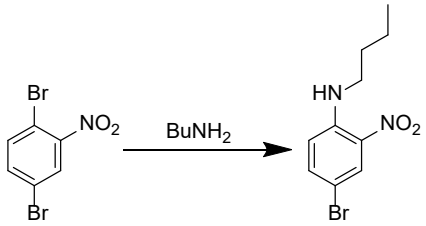

In a 500 mL round bottom flask equipped with condenser and stir bar, 2,5-dibromonitrobenzene (50 g, 178 mmol) and 1-butylamine (150 mL) was added. The mixture was heated up to 85 °C into a homogeneous solution and stirred for 24 hours. The formation of product was indicated by changing to orange color. The reaction mixture was precipitate into 1L of ice-cold water followed by adjusting pH to 7 by 2 M HCl. The product was allowed to stand in the refrigerator overnight before being collected by filtration and purified by recrystallization in methanol to yield the product as a vivid orange crystal in 84% yield. ^{1}H NMR (400 MHz, $CDCl_3$) δ_H (ppm) 8.31 (d, J = 2.4 Hz, 1H), 8.03 (s, 1H), 7.48 (dd, J = 6.8, 2.3 Hz, 1H), 6.76 (d, J = 9.2 Hz, 1H), 3.29 (td, J = 7.1, 5.2 Hz, 2H), 1.71 (p, J = 7.5 Hz, 2H), 1.48 (h, J = 7.5 Hz, 2H), 0.99 (t, J = 7.4 Hz, 3H). ^{13}C NMR (101 MHz, $CDCl_3$) δ_C (ppm) 144.7, 139.0, 129.1, 115.7, 106.3, 43.03, 31.1, 20.3, 13.9. ESI MS: m/z 273.2 ($[M]H^+$)

Step 2 of 4

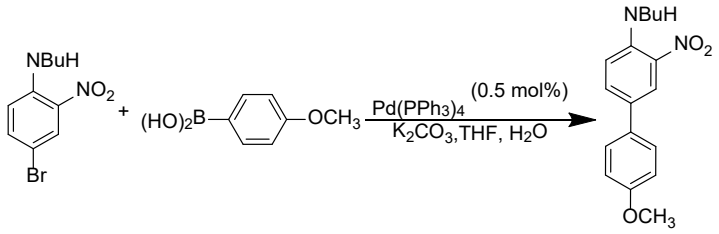

In a 1L round bottom flask equipped with condenser and stir bar, the step 1 product (30.0 g, 110 mmol, 1eq.) was combined with 4-methoxyphenylboronic acid (16.9 g, 110 mmol, 1eq.) and K_2CO_3 (61.3 g, 440 mmol, 4 eq.) and dissolved in a combination of tetrahydrofuran (360 mL) and deionized water (180 mL). To this mixture, a catalytic amount of tetrakis(triphenylphosphine)palladium[0] (0.64 g, 0.55 mmol, 0.5 mol%) was added. The reaction was heated to 80 °C and stirred for 36 h under argon atmosphere. The color of the organic solvent changed from orange to dark red. After allowing to cool down to room temperature, the organic layer was collected and ethyl acetate and water were added. The mixture was filtered and solvent was removed under vacuum. The product was purified by recrystallization in acetonitrile resulting in a red/orange crystal at 80% yield. ^{1}H NMR (400 MHz, $CDCl_3$) δ_H (ppm) 8.38 (d, J = 2.3 Hz, 1H), 8.07 (s, 1H), 7.68 (dd, J = 8.9, 2.3 Hz, 1H), 7.49 (d, J = 8.7 Hz, 2H), 6.97 (d, J = 8.7 Hz, 2H), 6.92 (d, J = 8.9 Hz, 1H), 3.85 (s, 3H), 3.35 (td, J = 7.1, 5.2 Hz, 2H), 1.75 (p, J = 7.2 Hz, 2H), 1.53 – 1.43 (m, 2H), 1.00 (t, J = 7.4 Hz, 3H). ^{13}C NMR (101 MHz, $CDCl_3$) δ_C (ppm) 159.2, 144.7, 135.0, 132.0, 131.7, 128.2, 127.4, 124.0, 114.5, 55.5, 43.0, 31.2, 20.4, 13.9. ESI MS: m/z 301.2 ($[M]H^+$)

Step 3 of 4

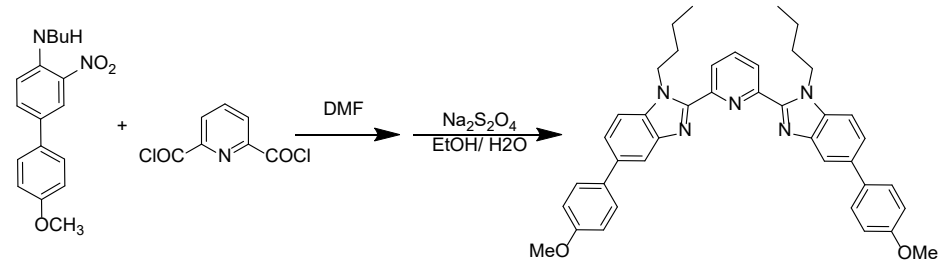

In a 1L round bottom flask equipped with stir bar, the step 2 product (20 g, 78 mmol, 2 eq.) was combined with 2,6-pyridinedicarbonyl dichloride (8.0 g, 39 mmol, 1eq.). The flask was purged with argon followed by the addition of anhydrous DMF (200 mL). The mixture was stirred for 24 h and the red color turns into light orange. After that, 100 mL DMF and a saturated solution of sodium hydrosulfite (33 g, 190 mmol, 5 eq.) dissolved in 5:1 v/v deionized water/ethanol mixture was added into the reaction mixture. After that, a condenser was equipped on the round bottom flask. The temperature was increased to 95 °C under an argon atmosphere and stirred for another 24 hours. After this time the reaction mixture was cooled to RT and neutralized to pH 7 using 1M NaOH. The reaction mixture was cooled in the fridge for several hours to further precipitate additional crude product. The mixture was filtered and the solid filter cake was extracted by boiling chloroform followed by filtration to remove inorganic salts. Chloroform was removed under vacuum and the material was recrystallized in a mixture of chloroform/acetonitrile to yield an off-white solid in 72%. ^{1}H NMR (400 MHz, $CDCl_3$) δ_H (ppm) 8.35 (d, J = 7.9 Hz, 2H), 8.07 (t, J = 7.9 Hz, 1H), 8.03 (s, 2H), 7.65 – 7.60 (m, 4H), 7.58 (dd, J = 8.5, 1.7 Hz, 2H), 7.52 – 7.48 (m, 2H), 7.03 (d, J = 8.7 Hz, 4H), 4.77 (t, J = 7.3 Hz, 4H), 3.88 (s, 6H), 1.75 (p, *J* = 8.2, 7.5 Hz, 4H), 1.15 (h, J = 7.4 Hz, 4H), 0.73 (t, J = 7.4 Hz, 6H). ^{13}C NMR (101 MHz, $CDCl_3$) δ_C (ppm) 159.1, 150.9, 150.2, 143.6, 138.3, 136.3, 135.7, 134.5, 128.6, 125.7, 123.3, 118.3, 114.5, 110.6, 55.5, 44.9, 32.3, 20.0, 13.7. MALDI-MS: m/z 658 ($[M]H^+Na^+$).

Step 4 of 4

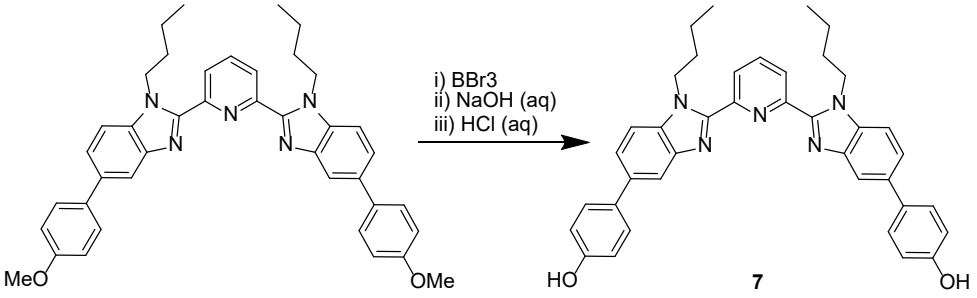

In a 500 mL round bottom flask equipped with stir bar, the step 3 product (10 g, 15.7 mmol) was dissolved in dry dichloromethane (150 mL). BBr3 (10 mL, xs) was added by cannula transfer to the reaction. The mixture immediately turned red in color. The reaction was warmed to RT and was stirred overnight. The reaction was quenched by the dropwise addition of a 1M NaOH solution. An additional volume of a 1M NaOH solution (approx. 1.5 L) was added until the reaction mixture was completely yellow in solution and no red solid was observed. An aqueous solution of HCl was then added until the pH of the suspension was adjusted to 7. The crude product was collected by filtration and purified by recrystallization (chloroform/methanol mixture), to give **7** as a pale yellow solid in 93% yield. ^{1}H NMR (400 MHz, DMSO) δ_H (ppm) 9.50 (s, 2H), 8.38 – 8.30 (m, 2H), 8.25 (dd, J = 8.7, 6.9 Hz, 1H), 7.92 (d, J = 1.6 Hz, 2H), 7.76 (d, J = 8.6 Hz, 2H), 7.62 – 7.53 (m, 6H), 6.92 – 6.84 (m, 4H), 4.80 (t, J = 7.2 Hz, 4H), 1.68 (p, J = 7.3 Hz, 4H), 1.09 (h, J = 7.4 Hz, 4H), 0.66 (t, J = 7.3 Hz, 6H). ^{13}C NMR (101 MHz, DMSO) δ_C (ppm) 156.8, 150.1, 149.6, 142.9, 138.8, 135.4, 135.2, 131.6, 127.9, 125.3, 122.4, 116.6, 115.8, 115.7, 111.3, 79.3, 44.1, 31.7, 19.2, 13.2. MALDI-MS: m/z 630 ([M]Na^+).

2.6.2.2 Synthesis of 4-EG Macrocycle (**1**)[1]

Step 1 of 2

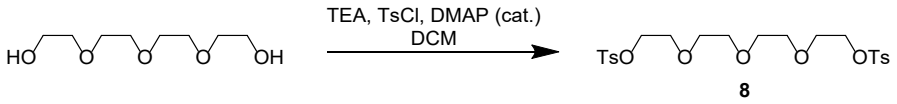

In a 1 L round bottom flask equipped with a stir bar under argon atmosphere, tetraethylene glycol (20.0 g, 103 mmol, 1 eq.) was combined with triethylamine (93.8 g, 927 mmol, 9 eq.), and 4-dimethylaminopyridine (0.25 g, 2.06 mmol, 0.01 eq.) in dry dichloromethane (342 mL) and stirred at 0 °C. 4-Toluenesulfonyl chloride (58.9 g, 309 mmol, 3 eq.) was stirred in dry dichloromethane (342 mL) and added to the reaction flask after it had stirred for some time at 0 °C. The reaction was allowed to slowly warm to rt over 24 hours of reaction after which the solvent was removed. The mixture was redissolved in ethylacetate and filtered to remove salt. Product **8** was purified via column chromatography (80% EtOAc/ hexanes) to yield the tosylated product as a clear viscous liquid in 87% yield. ^{1}H NMR (400 MHz, $CDCl_3$) δ_H (ppm) 7.79 (d, J = 8.9 Hz, 2H), 7.34 (d, J = 8.2 Hz, 2H), 4.15 (t, J = 5.2 Hz, 2H), 3.67 (t, J = 5.4, 4.1 Hz, 2H), 3.56 (s, 3H), 2.44 (s, 3H). ^{13}C NMR (101 MHz, $CDCl_3$) δ_C (ppm) 144.9, 133.1, 129.9, 128.1, 70.8, 70.6, 69.4, 68.8, 21.7. MALDI-MS: 525 m/z ($[M]Na^+$)

Step 2 of 2

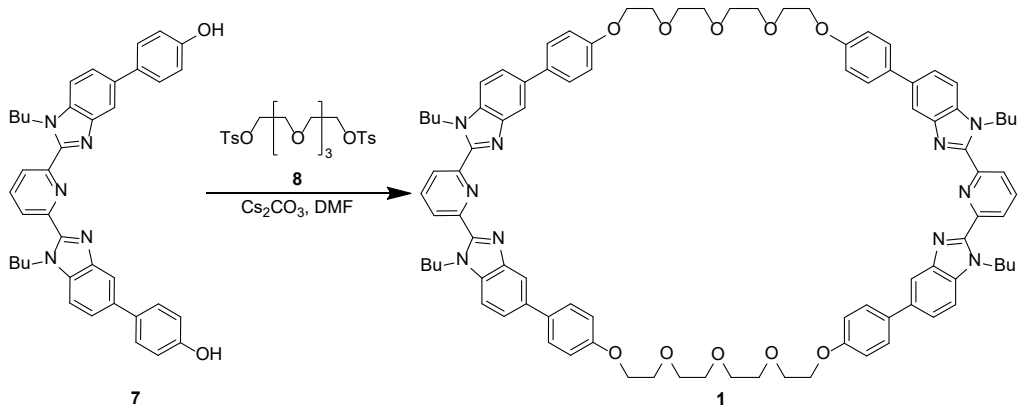

A 500 mL addition funnel containing step 1 material (**8**) (2.03 g, 4.00 mmol, 1eq.) in 500 mL of anhydrous DMF was fitted to a 2 L two-necked round bottom flask containing **7** (2.4 g, 3.95 mmol, 1 eq.) and Cs_2CO_3 (5.2 g, 15.94 mmol, 4 eq.) and a stir bar. The reaction vessel was flushed with argon before anhydrous DMF (500 mL) was added by cannula. The reaction was submerged in a silicone oil bath and heated to 75 °C while rapidly stirring. Over the course of 3 days, the **8** was added dropwise to the reaction vessel. The reaction was stirred at 75°C for an additional 4 days (for a total of 7 days), after which the solvent was removed, the crude product was triturated with $CHCl_3$, and the insoluble salt was removed via filtration. The filtrate was collected and solvent was removed under vacuum. The resulting solid was purified by an iterative combination of column chromatography (TEA pretreated silica gel, 0.5-1.2% MeOH/$CHCl_3$ gradient) and recrystallization (heat-dissolve in $CHCl_3$, add MeOH until product begins to precipitate, allow to settle at -7 °C) to yield **1** as white solid powder in 28% yield. ^{1}H NMR (500 MHz, $CDCl_3$) δ_H (ppm) 8.31 (d, J = 7.8 Hz, 4H), 8.00 (t, J = 7.8 Hz, 2H), 7.98 (dd, J = 1.6, 0.7 Hz, 4H), 7.51 (d, J = 8.7 Hz, 8H), 7.39 (dd, J = 8.4, 1.7 Hz, 4H), 7.26 (d, J = 8.6 Hz, 4H), 6.97 (d, J = 8.7 Hz, 8H), 4.56 (t, J = 7.3 Hz, 8H), 4.13 (t, J = 5.1, 4.2 Hz, 8H), 3.92 (t, J = 5.4, 4.5 Hz, 8H), 3.81 – 3.72 (m, 8H), 1.56 (p, J = 8.0, 7.4 Hz, 8H), 0.96 (h, J = 7.7 Hz, 8H), 0.59 (t, J = 7.4 Hz, 12H). ^{13}C NMR

(101 MHz, $CDCl_3$) δ_C (ppm) 158.3, 150.6, 150.1, 143.5, 138.2, 136.1, 135.5, 134.3, 128.4, 125.6, 123.2, 118.0, 115.1, 110.6, 71.0, 70.0, 67.8, 44.7, 32.2, 19.8, 13.6. MALDI-MS: m/z 1554 ($[M]H^+Na^+$).

2.6.2.3 Synthesis of Xanthene Thread (2)[2]

Step 1 of 5[11]

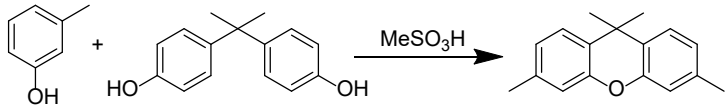

To a 2L flask equipped with a stir bar and water condenser under argon atmosphere, bisphenol-a (20.0 g, 87 mmol, 1 eq.) and methanesulfonic acid (7.57 g, 79 mmol, 0.9 eq.) were combined in m-cresol (600 mL). The reaction was heated at 150 °C for 24 h before being cooled to room temperature after which the m-cresol was removed. 1 M NaOH was then added to the flask and the compound was dissolved in hexanes. The 9,9-dimethyl-9H-xanthene was extracted from the NaOH by hexanes; the organic layer was collected and solvent removed. The material was purified by distillation and then recrystallization, first in ethanol, then in methanol. The final material appeared as white crystals in 36% yield. ^1H NMR (500 MHz, Chloroform-d) δ_H (ppm) 7.28 (d, J = 7.84, 2H), 6.88 (d, J = 8.00, 2H), 6.85 (s, 2H), 2.33 (s, 6H), 1.60 (s, 6H) ^{13}C NMR (101 MHz, $CDCl_3$) δ_C (ppm) 150.3, 137.4, 127.3, 126.1, 124.0, 116.8, 33.5, 32.8, 21.1. ESI MS: m/z 239.2 ($[M]H^+$)

Step 2 of 5

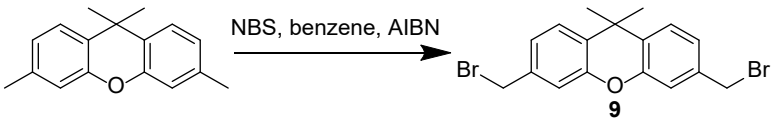

A 50 mL round bottom flask was equipped with a stir bar and condenser. The step 1 product 3,6,9,9-tetramethyl-9H-xanthene (1.00 g, 4.2 mmol) and N-bromosuccinimide (NBS) (1.50 g, 8.4 mol, 2 eq.) were added to the round bottom flask along with a catalytic amount (4 mg, 2.5 mmol, 0.6 eq.) of azobisisobutyronitrile (AIBN). The round bottom was flushed with argon for a period of three minutes and 25 mL of anhydrous benzene was then cannulated into the round-bottom bringing the concentration of the step 1 product to 175 mM. The round-bottom was heated to 75 °C for 18 hrs, after which a precipitate was noted. The reaction was cooled to room temperature and cooled further under refrigeration to remove allow the unwanted material to crash out of solution. The precipitate was removed via filtration and the filtrate was collected. The benzene solvent was removed under reduced pressure to yield an oil. Addition of hexanes to this oil leads to the further precipitation of a white solid. This was filtered again, and the filtrate collected and the solvent removed under reduced pressure to yield an off white powder. This powder was recrystallized from ethanol to yield the 3,6-bis(bromomethyl)-9,9-dimethyl-9H-xanthene (**9**) in a 31% yield. ^{1}H NMR (400 MHz, $CDCl_3$) δ_H (ppm) 7.36 (d, J = 8.0 Hz, 2H), 7.11 (d, J = 8.2 Hz, 2H), 4.46 (s, 4H), 1.60 (s, 6H). ^{13}C NMR (101 MHz, $CDCl_3$) δ_C (ppm) 150.4, 137.3, 130.2, 126.8, 124.0, 117.0, 34.1, 32.9, 32.5.

Step 3 of 5

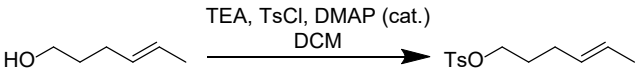

In a 1 L round bottom flask equipped with a stir bar under argon atmosphere, 4-hexen-1-ol (20 g, 200 mmol, 1 eq.) was combined with triethylamine (40.0 g, 800 mmol, 4 eq.), and 4-dimethylaminopyridine (0.24 g, 2.0 mmol, 0.01 eq.) in dry dichloromethane (333 mL) and stirred at 0 °C. 4-Toluenesulfonyl chloride (18.0 g, 300 mmol, 1.5 eq.) was stirred in dry dichloromethane

(333 mL) and added to the reaction flask after it had stirred for some time at 0 °C. The reaction was allowed to slowly warm to rt over 24 hours of reaction after which the solvent was removed. The mixture was redissolved in ethylacetate and filtered to remove salt. Product was purified via column chromatography (gradient from 0-5% EtOAc/ hexanes) to yield the tosylated product as a clear viscous liquid in 82% yield. ^{1}H NMR (400 MHz, $CDCl_3$) δ_H (ppm) 7.79 (d, J = 8.2 Hz, 2H), 7.35 (d, J = 8.0 Hz, 2H), 5.31 (m, 2H), 4.02 (t, J = 6.4 Hz, 2H), 2.45 (s, 3H), 2.00 (q, J = 6.8 Hz, 2H), 1.69 (p, J = 6.5 Hz, 2H), 1.59 (s, 3H). ^{13}C NMR (101 MHz, $CDCl_3$) δ_C (ppm) 144.8, 133.3, 129.9, 129.2, 128.0, 126.6, 70.0, 28.7, 28.3, 21.7, 18.0. ESI MS: m/z 277.1 ($[M]Na^+$)

Step 4 of 5

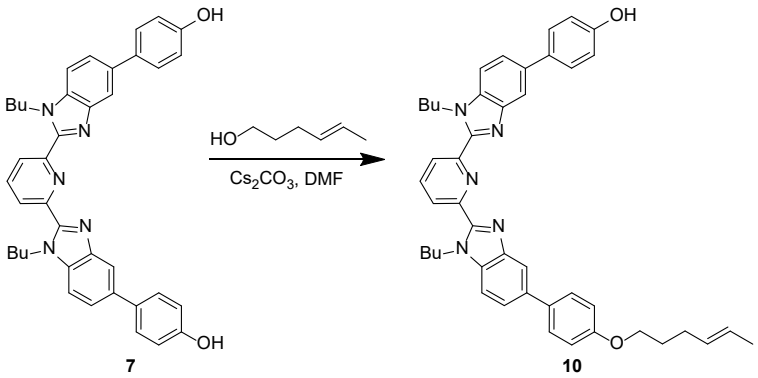

7 10

The step 3 tosylated 4-hexen-1-ol (1.47 g, 6.2 mmol, 0.75 eq.) was combined with **7** (5.0 g, 8.23 mmol, 1 eq.) (Chapter 2.6.2.1), and Cs_2CO_3 (8.0 g, 24.7 mmol, 3 eq.) were added into a 100 mL round bottom flask equipped with stir bar. The flask was flushed with argon and then anhydrous DMF (56 mL) was added by cannula. The reaction mixture was stirred at 72 °C for 24 hours. DMF was then removed under vacuum and the solid was stirred with chloroform and filtered. The filtrate was collected and the solvent removed under reduced pressure. The resulting material was purified using column chromatography (silica gel, chloroform/methanol gradient as eluent (0-3% MeOH/ $CHCl_3$) and recrystallization (chloroform/methanol mixture) to yield yellow crystals of **10** in 53%

yield. ^{1}H NMR (400 MHz, $CDCl_3$) δ_H (ppm) 8.33 (dd, J = 7.9, 1.3 Hz, 2H), 8.06 (t, J = 7.9 Hz, 1H), 8.03 (d, J = 1.7 Hz, 1H), 7.99 (d, J = 1.5 Hz, 1H), 7.63 – 7.46 (m, 8H), 6.99 (t, J = 9.0 Hz, 4H), 5.57 – 5.41 (m, 2H), 4.75 (t, J = 7.3, 1.9 Hz, 4H), 4.02 (t, J = 6.5 Hz, 2H), 2.19 (q, J = 6.9, 6.3 Hz, 2H), 1.88 (dt, J = 8.1, 6.5 Hz, 2H), 1.82 – 1.70 (m, 4H), 1.67 (dt, J = 4.9, 1.4 Hz, 4H), 1.15 (hd, J = 7.4, 2.2 Hz, 4H), 0.73 (t, J = 7.3, 1.3 Hz, 6H). ^{13}C NMR (101 MHz, $CDCl_3$) δ_C (ppm) 158.6, 156.0, 150.8, 150.7, 150.0, 149.9, 143.4, 143.2, 138.5, 136.7, 136.5, 135.5, 135.4, 134.2, 134.0, 130.4, 128.7, 128.5, 125.9, 125.8, 123.4, 118.1, 116.2, 115.1, 110.7, 67.6, 45.0, 32.3, 29.3, 29.1, 20.0, 18.1, 13.7. MALDI-TOF MS: m/z 712 ($[M]H^+$).

Step 5 of 5

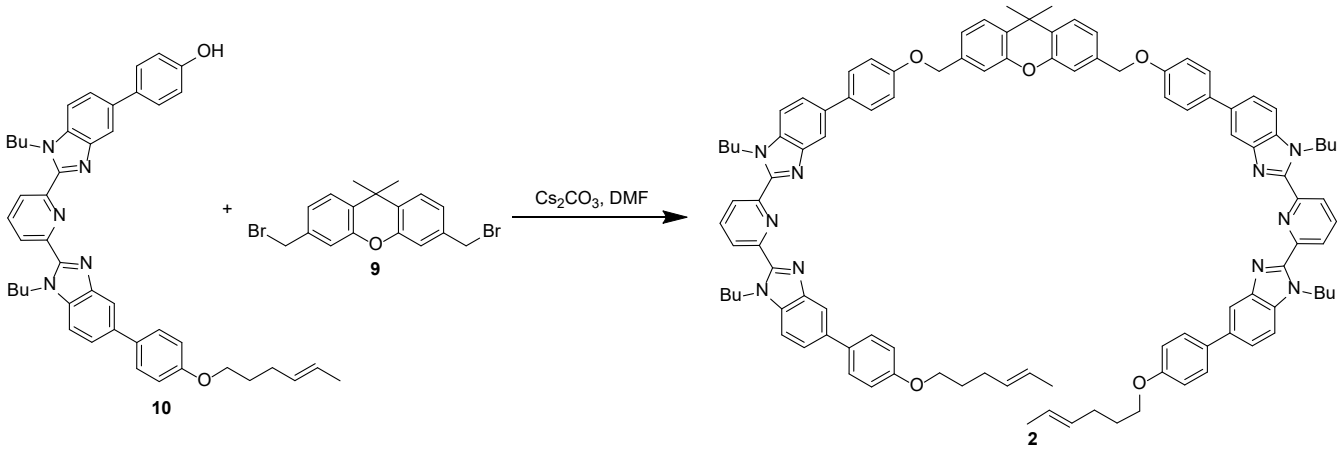

To a 25 mL round bottom flask equipped with stir bar, **9** (step 2) (578 mg, 1.46 mmol, 1 eq.) was combined with **10** (step 4) (2 g, 2.99 mmol, 2 eq.) and anhydrous cesium carbonate (1.93 g, 5.93 mM, 4 eq.), followed by flushing with argon. Then 12.3 mL anhydrous DMF was injected into the reaction. The mixture was stirred at 72 °C for 24 hours. DMF was then removed under vacuum and the solid was stirred with chloroform and filtered. The filtrate was collected and the solvent removed under reduced pressure. The resulting material was purified using column chromatography (chloroform/methanol gradient from 0-3% as the eluent). **2** was collected as a

pale yellow solid in 43 % yield. ^{1}H NMR (500 MHz, $CDCl_3$) δ_H (ppm) 8.37 (d, J = 7.9 Hz, 4H), 8.10 (t, J = 7.9 Hz, 2H), 8.06 (dt, J = 4.6, 1.1 Hz, 4H), 7.69 – 7.58 (m, 12H), 7.53 (dd, J = 8.5, 3.0 Hz, 4H), 7.49 (d, J = 8.6 Hz, 2H), 7.23 (d, J = 7.1 Hz, 4H), 7.14 (d, J = 8.8 Hz, 4H), 7.04 (d, J = 8.8 Hz, 4H), 5.59 – 5.46 (m, 4H), 5.15 (s, 4H), 4.79 (t, J = 7.3 Hz, 8H), 4.05 (t, J = 6.5 Hz, 4H), 2.22 (q, J = 7.0, 6.2 Hz, 4H), 1.91 (p, J = 7.6, 6.8 Hz, 4H), 1.78 (p, J = 7.5 Hz, 8H), 1.70 (d, J = 1.4 Hz, 4H), 1.70 (s, 8H), 1.17 (h, J = 7.4 Hz, 8H), 0.76 (t, J = 7.4 Hz, 12H). ^{13}C NMR (101 MHz, $CDCl_3$) δ_C (ppm) 158.6, 158.2, 150.9, 150.8, 150.6, 150.2, 150.1, 143.6, 138.3, 136.8, 136.4, 136.6, 135.7, 135.6, 134.8, 134.3, 130.4, 129.8, 128.6, 128.5, 126.7, 125.9, 125.7, 123.3, 122.3, 118.3, 118.2, 115.5, 115.4, 115.1, 110.6, 110.5, 69.7, 67.5, 44.9, 34.1, 32.7, 32.3, 29.3, 29.1, 20.0, 18.1, 13.7. MALDI-TOF MS: m/z 1615 ([M]2H$^+$).

2.6.2.4 Synthesis of Poly[*n*]catenane (3)

Step 1 of 3: Metallosupramolecular Polymer (MSP) Assembly

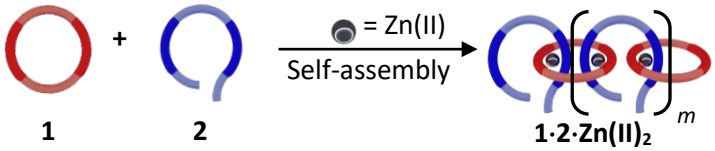

Two separate vials for titration were prepared: the first vial contained **1** (300 mg, 0.20 mmol) in 3 mL $CDCl_3$ and the second vial **2** (317 mg, 0.20 mmol) dissolved in 1 mL $CDCl_3$. The solution of **2** was slowly titrated into the solution of **1**; each addition was monitored by NMR by monitoring the relative integrations of the most downfield shifted doublets for both **1** (8.30 ppm) and **2** (8.35 ppm) as well as the triplets at 4.56 ppm (for **1**) and 4.76 ppm (for **2**). The titration ceased when the two components were at a ratio of 1:1 Zn(II) ions (Zinc di[bis(trifluoromethylsulfonyl)imide] ($Zn(NTf_2)_2$) in deuterated acetonitrile, 0.40 mM) were titrated into the 1:1 mixture and monitored by NMR. The complete disappearance of the doublets at 8.30 and 8.35 ppm (and the corresponding

growth of the peak at 8.9 ppm) indicates that all of the Bip (**7**) units are bound with metal in a 2:1 Bip (**7**):metal ratio. The completed MSP (**1·2·Zn(II)$_2$**) was dried under vacuum (collected as a yellow crystalline solid) and stored at -8 °C.

Step 2 of 3: Poly[*n*]catenane synthesis

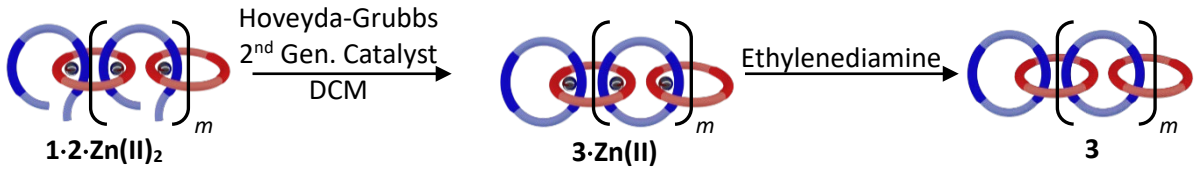

Example procedure for the 2.5 mM reaction: A 10 mL reaction vessel, stir bar, and water condenser were dried overnight at 130°C for use in the catenation reaction. MSP **1·2·Zn(II)$_2$** (60 mg, 0.013 mmol) of was added to the dried vessel and dissolved in 5.2 mL of dried DCM (2.5 mM). The solution was stirred and heated to reflux (45°C) followed by bubbling argon for 30 minutes to remove dissolved oxygen. Then Hoveyda-Grubbs second generation catalyst in DCM (1.0 mg, 0.32 mM) was added to the solution. To account for any solvent evaporation during the bubbling steps additional DCM was added as required to maintain the original concentration (2.5 mM). While still under reflex, the solution was bubbled with argon for additional 30 mins. The Argon purge and catalyst addition was repeated 24 hours after the first addition. The reaction was carried out for a further 24 hours before the solution was cooled to room temperature and ethyl vinyl ether (~1mL) was added to deactivate the catalyst.

To demetallate the reaction products, 50 µL of ethylenediamine was added to the reaction and allowed to stir. The resulting mixture was washed with 5 aliquots of water or until the aqueous wash was no longer basic. The organic layer was passed through a 0.45 µm PTFE syringe filter and the solvent was removed under vacuum. The resulting demetallated reaction mixture was obtained as a yellow or slightly brown solid. The solid material was washed with acetonitrile to

remove residual Hoveyda-Grubbs second generation catalyst before GPC and NMR characterization.

The same procedure was repeated for the reactions carried out at different concentrations (0.25, 0.5, 1.0, 5.0, and 10.0 mM) in DCM. The Hoveyda-Grubbs second generation catalyst was added at a concentration of 0.32 mM for each addition (x2), with the exception of the 10.0 mM samples, which received catalyst at a concentration of 0.64 mM for both additions. The work up for all samples remained the same.

Step 3 of 3: Partial purification of crude reaction mixture

For the partially purified samples, (see **Figure 2.15**) the demetallated reaction mixture was partially re-metalated with $Zn(NTf_2)_2$ until ca. 50% of the poly[*n*]catenane was metalated as observed by NMR. The sample was fully dried under vacuum and washed 5 times with a solution of 2:1 chloroform:hexane to remove the non-metal-containing compounds. The remaining metallated compounds was dissolved in DCM and demetallated using 50 µL of ethylenediamine. The resulting mixture was washed with 5 aliquots of water or until the sample was no longer basic. ^{1}H NMR (500 MHz, $CDCl_3$) δ_H (ppm) 8.28 – 8.13 (m, 8H), 7.98 – 7.82 (m, 12H), 7.46 – 7.19 (m, 34H), 7.03 – 6.93 (m, 4H), 6.90 – 6.76 (m, 8H), 6.71 – 6.62 (m, 8H), 5.39 – 5.26 (m, 2H), 5.09 – 4.98 (m, 4H), 4.64 – 4.42 (m, 16H), 3.94 – 3.76 (m, 12H), 3.70 – 3.49 (m, 24H), 2.16 – 1.97 (m, 4H), 1.78 – 1.37 (m, 26H), 1.10 – 0.86 (m, 16H), 0.65 – 0.47 (m, 24H).

2.6.2.5 Synthesis of Cyclic Poly[*n*]catenane (*c*-3)[1]

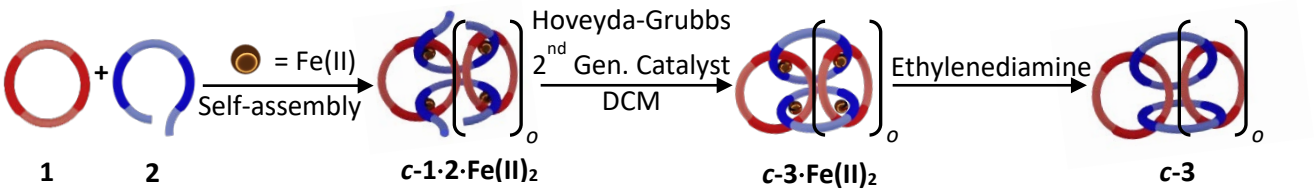

Step 1 of 3

Titration of **1** (30 mg, 0.02 mmol) and **2** (31.6 mg, 0.02 mmol) proceeded as 2.6.2.4. The titration ceased when the two components were at a ratio of 1:1. Fe(II) ions (iron(II) bis(trifluoromethane)sulfonimide ($Fe(NTf_2)_2$) in deuterated acetonitrile (0.40 mM) were titrated into the 1:1 mixture and monitored by NMR. The complete disappearance of the doublets at 8.30 and 8.35 ppm (and the corresponding growth of the peak at 8.9 ppm) indicates that all of the Bip (**7**) units are bound with metal in a 2:1 Bip(**7**):metal ratio. The completed MSP (**1·2·Fe(II)$_2$**) (collected as a deep purple crystalline solid) was dried under vacuum and stored at -8 °C.

Step 2 of 3

A 100 mL reaction vessel, stir bar, and water condenser were dried overnight at 130°C for use in the catenation reaction. MSP **1·2·Fe(II)$_2$** (40 mg, 0.010 mmol) of was added to the dried vessel and dissolved in 40.6 mL of dried DCM (0.25 mM). The metathesis reaction followed the same procedure as 2.6.2.4 Step 2: the solution was stirred and heated to reflux (45°C) followed by bubbling argon for 30 minutes to remove dissolved oxygen. Then Hoveyda-Grubbs second generation catalyst in DCM (7.8 mg, 0.32 mM) was added to the solution. To account for any solvent evaporation during the bubbling steps additional DCM was added as required to maintain the original concentration (0.25 mM). While still under reflex, the solution was bubbled with argon for additional 30 mins. The Argon purge and catalyst addition was repeated 24 hours after the first addition. The reaction was carried out for a further 24 hours before the solution was cooled to room temperature and ethyl vinyl ether (~1mL) was added to deactivate the catalyst. The ring closed product (**3·Fe(II)**) was then demetallated via the addition of 50 µL of ethylenediamine. The resulting mixture was washed with 5 aliquots of water or until the aqueous wash was no longer

basic. The organic layer was passed through a 0.45 μm PTFE syringe filter and the solvent was removed under vacuum. The resulting demetallated reaction mixture was obtained as a brown solid (yield =71% by NMR).

Step 3 of 3

The demetallated reaction mixture was partially re-metalated with $Zn(NTf_2)_2$ until ca. 50% of the poly[*n*]catenane was metalated as observed by NMR. The sample was fully dried under vacuum and washed 5 times with a solution of 2:1 chloroform:hexane to remove the non-metal-containing compounds. The remaining metallated compounds was dissolved in DCM and demetallated using 50 μL of ethylenediamine. The resulting mixture was washed with 5 aliquots of water or until the sample was no longer basic. The sample was dried to yield 87% ***c*-3**.

2.6.2.6 Synthesis of Closed Xanthene Thread (6)[1]

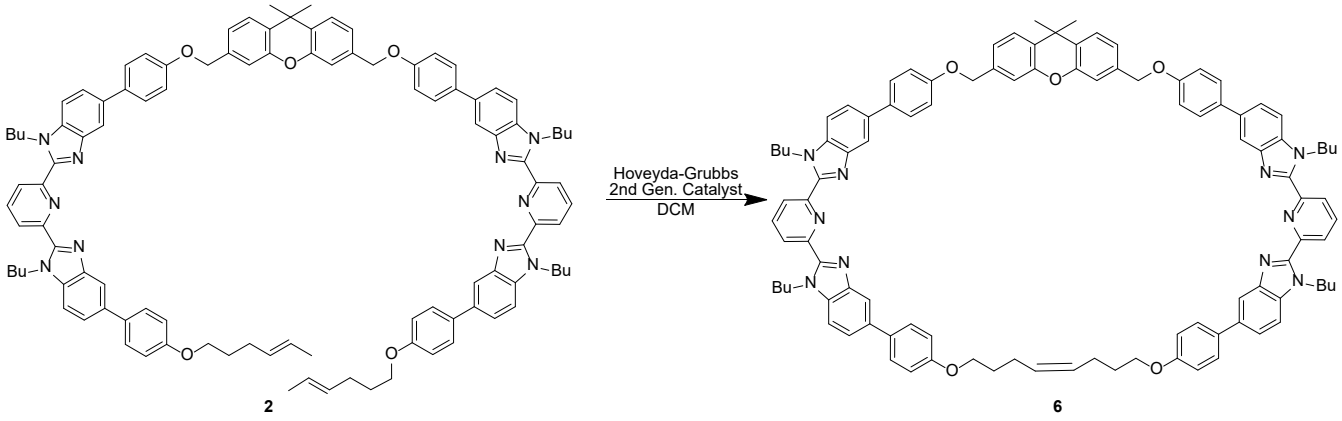

A 100 mL reaction vessel, stir bar, and water condenser were dried overnight at 130°C for use in the metathesis reaction. 150 mg (0.09 mmol) of **2** was added to the cooled round bottom flask and dissolved in 36 mL of DCM. The metathesis reaction followed the same procedure as 2.6.2.4 Step 2: the solution was stirred and heated to reflux (45°C) followed by bubbling argon for 30 minutes to remove dissolved oxygen. Then Hoveyda-Grubbs second generation catalyst in DCM (7.2 mg,

0.32 mM) was added to the solution. To account for any solvent evaporation during the bubbling steps additional DCM was added as required to maintain the original concentration (2.5 mM). While still under reflex, the solution was bubbled with argon for additional 30 mins. The Argon purge and catalyst addition was repeated 24 hours after the first addition. The reaction was carried out for a further 24 hours before the solution was cooled to room temperature and ethyl vinyl ether (~1mL) was added to deactivate the catalyst. After reaction and catalyst deactivation, the solvent was removed under vacuum and the product purified by column chromatography with triethylamine neutralized silica gel and a hexane/chloroform/methanol gradient from 75/25/0 to 0/99/1 (v/v/v) as the mobile phase. Yield: 32%. The product is a light brown solid which is a mixture of cis and trans isomers. ^{1}H NMR (400 MHz, $CDCl_3$) δ_H (ppm) 8.25 (dd, J = 16.4, 7.9 Hz, 4H), 8.04 – 7.89 (m, 6H), 7.59 – 7.35 (m, 16H), 7.42 – 7.28 (m, 2H), 7.13 (d, J = 6.5 Hz, 2H), 7.08 – 6.99 (m, 4H), 6.98 – 6.91 (m, 2H), 6.95 – 6.80 (m, 2H), 5.50 – 5.38 (m, 2H), 5.18 (s, 2H), 5.05 (s, 2H), 4.69 (t, J = 7.3 Hz, 6H), 4.59 (dt, J = 16.1, 7.4 Hz, 2H), 4.05 – 3.89 (m, 4H), 3.02 (q, J = 7.3 Hz, 4H), 2.17 (s, 4H), 1.82 (q, J = 7.1 Hz, 4H), 1.79 – 1.63 (m, 6H), 1.60 (d, J = 4.8 Hz, 4H), 1.34 (t, J = 7.3 Hz, 1H), 1.18 (s, 12H), 1.06 (p, J = 7.4 Hz, 4H), 1.03 – 0.89 (m, 2H), 0.66 (t, J = 7.3 Hz, 4H), 0.65 (s, 2H), 0.56 (ddd, J = 9.9, 6.5, 2.8 Hz, 4H). ^{13}C NMR (126 MHz, $CDCl_3$) δ_C (ppm) 158.33, 157.43, 150.54, 150.49, 149.97, 143.35, 143.30, 138.07, 137.43, 136.12, 135.38, 134.39, 133.98, 130.43, 129.89, 129.22, 128.35, 128.32, 128.27, 126.61, 125.44, 123.17, 121.09, 117.94, 115.62, 114.90, 114.76, 114.49, 110.43, 69.12, 66.69, 44.66, 33.82, 32.49, 32.10, 28.61, 28.49, 19.80, 13.47. MALDI-TOF MS: m/z 1559 ($[M]^+2H^+$).

2.7 References

1. Wu, Q. *et al.* Poly[n]catenanes: Synthesis of molecular interlocked chains. *Science.* **358**, 1434–1439 (2017).
2. Wojtecki, R. J. *et al.* Optimizing the formation of 2,6-bis(N-alkyl-benzimidazolyl)pyridine-containing [3]catenates through component design. *Chem. Sci.* **4**, 4440–4448 (2013).
3. Fox, J. D. & Rowan, S. J. Supramolecular Polymerizations and Main-Chain Supramolecular Polymers. *Macromolecules* **42**, 6823–6835 (2009).
4. Braun, S., Kalinowski, H.-O. & Berger, S. *150 and More Basic NMR Experiments: A Practical Course*. (Wiley-VCH, 1998).
5. Mirmohammadi, S. A. *et al.* The effects of solvent and initiator on anionic ring opening polymerization of ϵ-caprolactone: synthesis and characterization. *Polym. Int.* **63**, 479–485 (2014).
6. Cozza, N., Bonani, W., Motta, A. & Migliaresi, C. Evaluation of alternative sources of collagen fractions from Loligo vulgaris squid mantle. *Int. J. Biol. Macromol.* **87**, 504–513 (2016).
7. Zheng, Y., Huang, Y. & Benicewicz, B. C. A Useful Method for Preparing Mixed Brush Polymer Grafted Nanoparticles by Polymerizing Block Copolymers from Surfaces with Reversed Monomer Addition Sequence. *Macromol. Rapid Commun.* **38**, 1700300 (2017).
8. Semlyen, J. A. Ring-chain equilibria and the conformations of polymer chains. in *Mechanisms of Polyreactions-Polymer Characterization* 41–75 (Springer Berlin Heidelberg). doi:10.1007/3-540-07727-8_3.
9. Stejskal, E. O. & Tanner, J. E. Spin Diffusion Measurements: Spin Echoes in the Presence of a Time-Dependent Field Gradient. *J. Chem. Phys.* **42**, 288–292 (1965).
10. McKenzie, B. M. *et al.* Improved synthesis of functionalized mesogenic 2,6-bisbenzimidazolylpyridine ligands. *Tetrahedron* **64**, 8488–8495 (2008).
11. Caruso, A. J. & Lee, J. L. A New Reaction of Bisphenol A and Preparation of Polysubstituted 9,9-Dimethylxanthenes. *J. Org. Chem.* **62**, 1058–1063 (1997).

Chapter 3: Thread structural effects on the synthesis of poly[*n*]catenanes

* This chapter was adapted from: Tranquilli, M.M.; Rawe, B.W.; Liu, G.; Rowan, S.J. The effect of the thread-like monomer structure on the synthesis of poly[*n*]catenanes from metallosupramolecular polymers. [*submitted*]

3.1 Introduction

The investigations detailed in Chapter 2 on poly[*n*]catenane **3** allowed for significant advancements in the understanding of the poly[*n*]catenane synthesis; however, this investigation was limited by using the same monomeric subunits throughout the synthesis, namely **1** and **2**. Therefore, the next step in increasing the understanding of the efficacy and adaptability of this synthetic method required modifications to the monomeric subunits. Though modifications to both monomers will be detailed in this thesis, the thread-like monomeric subunit **2** (**Figure 3.1**) was the first target of modification because this monomer contains the site (the alkenyl tails) where the

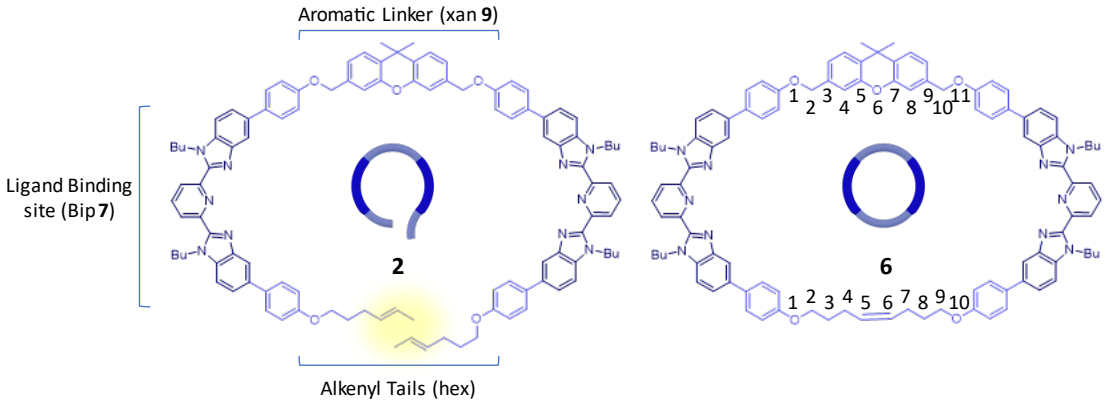

Figure 3.1 The chemical structure for the thread-like monomer **2** used in the synthesis of poly[*n*]catenane **3** composed of three distinct regions: an aromatic linker (**9**), two ligand binding site (**7**) and two alkenyl tails where the ring-closing metathesis reaction occurs (highlighted). Ring-closing of **2** yields the new macrocycle (MC) **6**. The interior count for the aromatic linker and alkoxyl linker in MC **6** is specified.

ring-closing catenation reaction occurs (for modifications to the monomeric subunit **1**, see Chapter 4).

This work is not the first time the thread-component has been investigated. Before the synthesis of the initial poly[*n*]catenane **3**, early [3]catenane synthesis[1] using a similar Bip (**7**) ligand system was performed to test the viability of the structure of **2** and the efficacy of the ring closing reaction. In this study, **2** was designed such that the interior atom count of the aromatic linker and the closed alkoxy linker were approximately the same size (see count in **Figure 3.1**) when macrocycle **6** was formed. At that time, two different aromatic linkers were tested (**Figure 3.2**), however the xanthene-based linker **9** was selected based on its inability to rotate around a central axis, maintaining the C-shaped structure and leading to an increased yield of the catenated product. The results from this study informed the design of this experiment, suggesting that, while changes to the aromatic linker would be worth performing, linkers with high degrees of rotation would not be advantageous to work with.

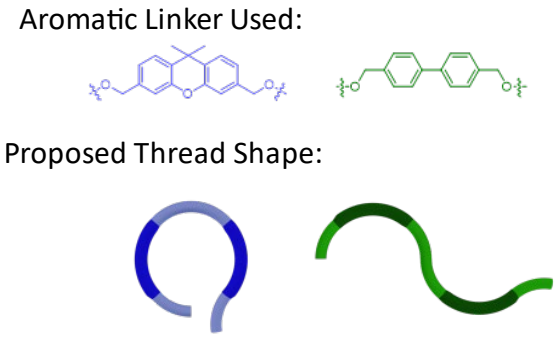

Figure 3.2 Linkers used in previous work[1] and their influence on the ultimate shape of the thread-like monomer.

The initial publication of the poly[*n*]catenane structure,[2] as well as the work detailed in Chapter 2, have detailed the synthesis of a acyclic diene metathesis (ADMET) product **5** in the synthesis of poly[*n*]catenane **3**. This synthesis is proposed to result from inter- or intra- chain thread monomers reactions that do not lead the formation of macrocycle **6** (**Figure 3.3**). Though

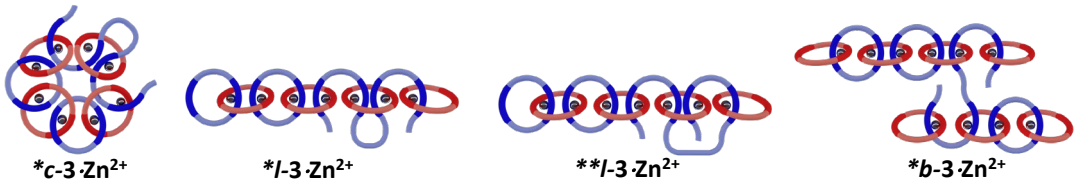

Figure 3.3 Proposed routes to yield the ADMET byproduct **5** during catenane synthesis.

the exact mechanism of this reaction is not certain, it may be assumed that the alkenyl tail length can influence the efficacy of the ring closing reaction as well as the amount of **5** that results in each synthesis.

Based on the prior studies detailed above, three new thread-like monomers were designed and used in the synthesis of the first new poly[*n*]catenane structures.

3.2 Design of new thread-like monomers

The first new thread developed (**11**$_{\text{xan-5}}$, **Figure 3.4**, left) replaces the original 4-hexenyl tails with shorter 3-pentenyl tails, which will result in a shorter alkoxy chain within the closed macrocycle **12**$_{\text{xan-5}}$ (8 atoms). The development of **11**$_{\text{xan-5}}$ sought to understand the alkenyl tail in isolation: if the entire body of the thread remains the same as the original **2**$_{\text{xan-6}}$, will removing a single atom from each alkenyl tail affect the poly[*n*]catenane yield or the final architecture?

A new aromatic linker was selected based on the parameters taken from the literature:[1] a 2,7-disubsituted naphthalene (nap) moiety (**13**) was used in place of **9**. Two new threads were prepared using this shorter naphthalene linker. The first thread to incorporate the nap linker (**14**$_{\text{nap-5}}$) used the same 3-pentenyl tails as **11**$_{\text{xan-5}}$ (**Figure 3.4**, center). This thread was created so that the resulting macrocycle (**15**$_{\text{nap-5}}$) would be similar to **5**$_{\text{xan-6}}$ in its linker: tail interior atom count (9:8 for **15**$_{\text{nap-5}}$ and 11:10 for **5**$_{\text{xan-6}}$). The second thread (**16**$_{\text{nap-6}}$, **Figure 3.4**, right) was created to test

the change of the aromatic linker in isolation, therefore it incorporated the same 4-hexenyl tails as the original material, eventually yielding the closed macrocycle **17**$_{\text{nap-6}}$.

Threads **11**$_{\text{xan-5}}$, **14**$_{\text{nap-5}}$, and **16**$_{\text{nap-6}}$ were synthesized in a similar fashion[2] to the initial thread **2**$_{\text{xan-6}}$ (see Experimental Section).

11$_{\text{xan-5}}$ **14**$_{\text{nap-5}}$ **16**$_{\text{nap-6}}$

Figure 3.4 Chemical structures for the three new thread-like monomers studied in this chapter: **11**$_{\text{xan-5}}$, **14**$_{\text{nap-5}}$, and **16**$_{\text{nap-6}}$.

3.3 Exploring the new MSPs

The new MSP materials were assembled using the process detailed in Chapter 2. In short, a 1:1 ratio of macrocycle (**1**) and the appropriate thread (**11**$_{\text{xan-5}}$, **14**$_{\text{nap-5}}$, or **16**$_{\text{nap-6}}$) was titrated with $Zn(Tf_2N)_2$ (monitoring the H_{mpy} protons) until a 1:1:2 ratio of **1**:**2**:**Zn(II)**$_2$ was obtained, resulting in assembly of the appropriate MSPs, **1**·**11**$_{\text{xan-5}}$·**Zn(II)**$_2$, **1**·**14**$_{\text{nap-5}}$·**Zn(II)**$_2$, and **1**·**16**$_{\text{nap-6}}$·**Zn(II)**$_2$, respectively.

As discussed in Chapter 2, the original MSP **1**·**2**$_{\text{xan-6}}$·**Zn(II)**$_2$ can be characterized using both ^{1}H NMR spectroscopy and diffusion NMR (Diffusion ordered spectroscopy, DOSY). These experiments demonstrated that two distinct populations of the MSP (linear and cyclic) could be observed. Similarly, the three new MSPs were characterized using ^{1}H and DOSY NMR at a series of concentrations (0.25, 2.5, 10.0 mM w.r.t. to **1**, **Figure 3.5**). **Figure 3.5b** shows that, at 2.5 mM

(w.r.t. **1**), each of the new MSPs have peak populations within the regions that have been attributed to *l*- and c-MSP in the original system.[3] This effect is more pronounced at the lowest concentration (0.25 mM, **Figure 3.5a**), where the cyclic population region dominates for all four tested samples. Each MSP was characterized by DOSY NMR at a concentration of 2.5 mM to determine diffusion coefficients of the two distinct regions (**Figure 3.6**). For all MSPs the protons in region i (8.80-8.72 ppm) have diffusion constants around ca. 2.2 x 10^{-10} regardless of thread used (**Table 3.1**). The peaks shifted slightly upfield in region ii (8.62-8.72 ppm) exhibit higher diffusion coefficients (**Table 3.1**) that correspond to lower molar mass assemblies, tentatively assigned to the *c*-MSPs. The data here is consistent with the result from the prior concentration studies carried out on the **1·2$_{xan\text{-}6}$·Zn(II)$_2$** MSP.[3]

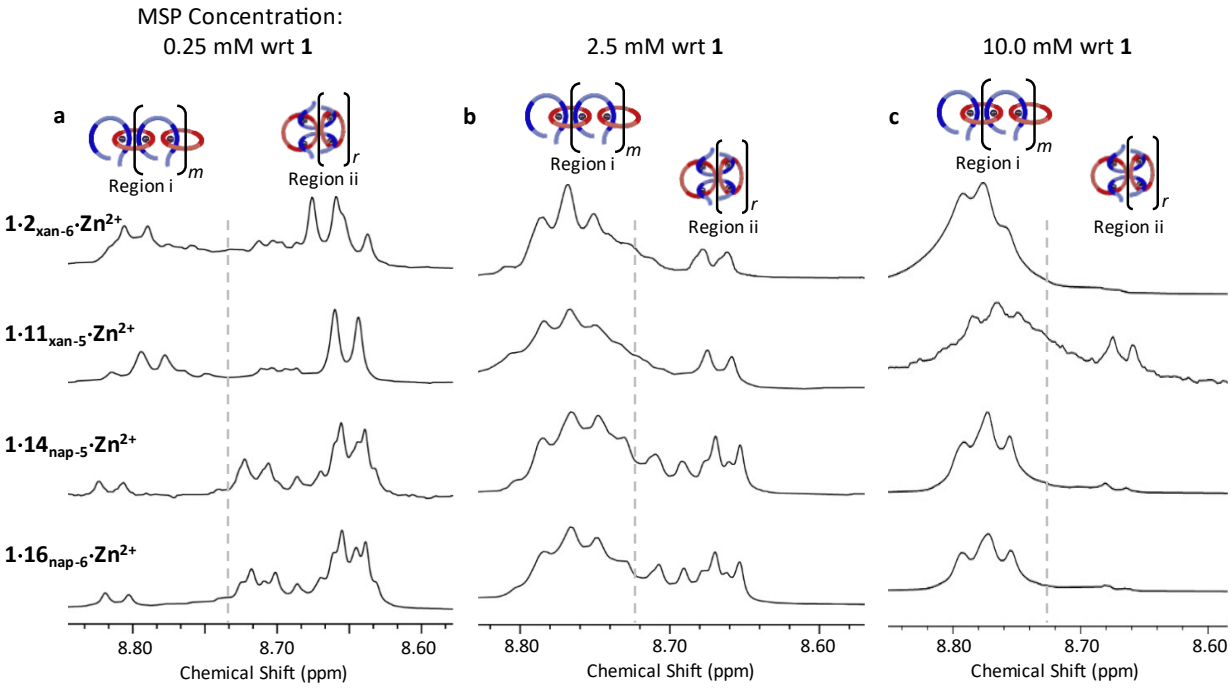

Figure 3.5 ^{1}H NMR for each MSP structure (**1·2$_{xan\text{-}6}$·Zn(II)$_2$**, **1·11$_{xan\text{-}5}$·Zn(II)$_2$**, **1·14$_{nap\text{-}5}$·Zn(II)$_2$**, and **1·16$_{nap\text{-}6}$·Zn(II)$_2$**) taken at (a) 0.25 mM wrt **1**, (b) 2.5 mM wrt **1**, and (c) 10.0 mM wrt **1**.

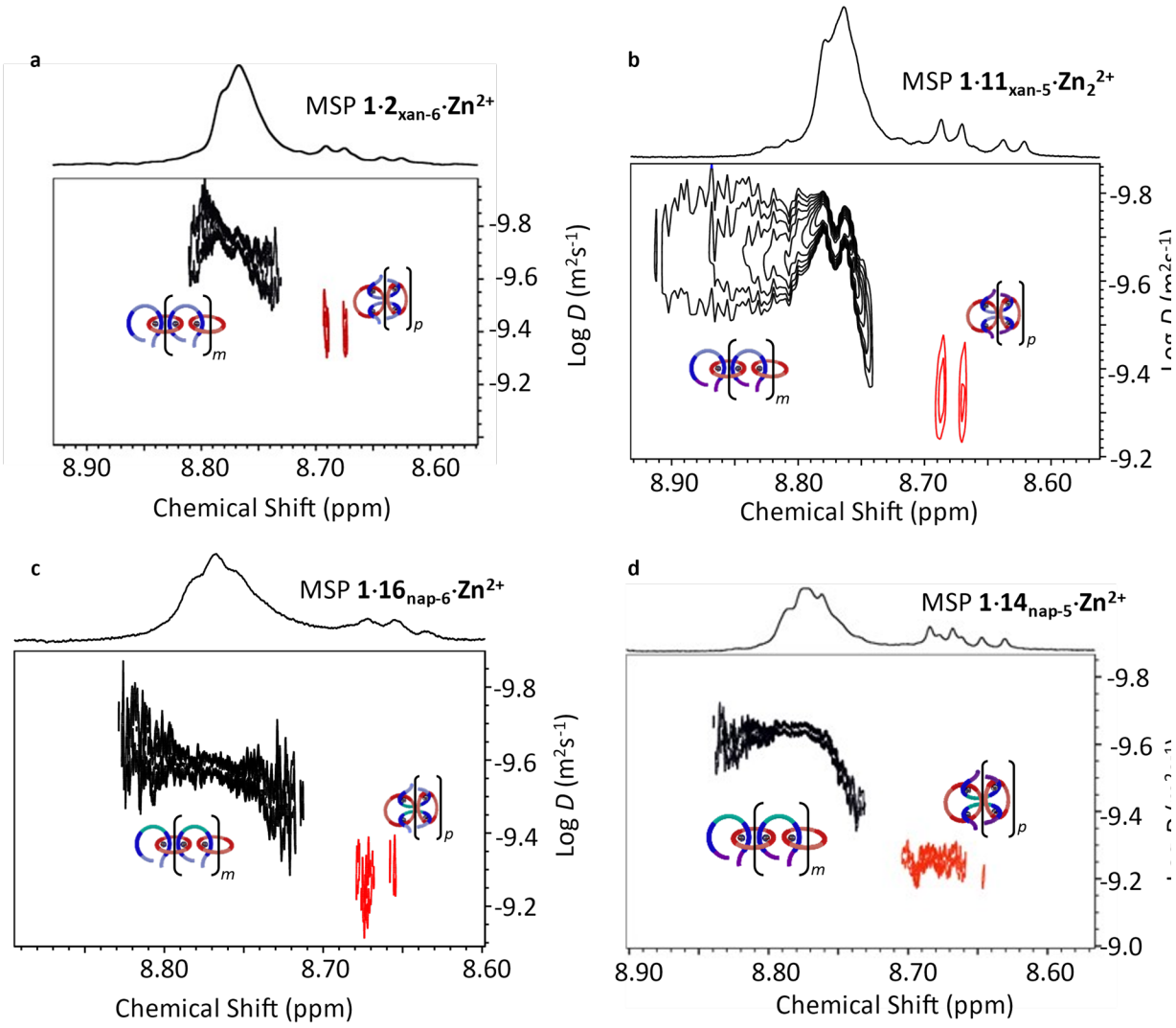

Figure 3.6 DOSY analysis using a direct exponential curve resolution algorithm for each of the MSP samples (**1·2$_{xan-6}$·Zn(II)$_2$** (a), **1·11$_{xan-5}$·Zn(II)$_2$** (b), **1·16$_{nap-6}$·Zn(II)$_2$** (c), and **1·14$_{nap-5}$·Zn(II)$_2$** (d)) at a concentration of 2.5 mM wrt **1**. The data plotted in black corresponds to region i in Figure 3.5 and is currently attributed to the *l*-MSP; the data plotted in red corresponds to region ii in Figure 3.5 and is currently attributed to the *c*-MSP.

Table 3.1 Diffusion Coefficients from DOSY Analysis

MSP	Region i Diffusion Coefficient (x 10^{-10})	Region ii Diffusion Coefficient (x 10^{-10})
1·2$_{xan-6}$·Zn(II)$_2$	2.4	5.5
1·11$_{xan-5}$·Zn(II)$_2$	1.9	4.3
1·14$_{nap-5}$·Zn(II)$_2$	2.3	5.8
1·16$_{nap-6}$·Zn(II)$_2$	2.2	3.8

At the concentration in **Figure 3.5b** (2.5 mM w.r.t. **1**), MSPs based on the xanthene containing threads (**1·2$_{xan-6}$·Zn(II)$_2$** and **1·11$_{xan-5}$·Zn(II)$_2$**) demonstrated similar peak shapes with both containing ~20% of their total MSP in the upfield ("*c*-MSP") region. In contrast, the new naphthalene linker increases the likelihood of forming this *c*-MSP population, where MSP **1·14$_{nap-5}$·Zn(II)$_2$** and **1·16$_{nap-6}$·Zn(II)$_2$** both contain approximately 34% of their MSP peak population in the upfield region. Based on standard ring-chain equilibria[4] it can be expected that, at lower concentrations, a greater amount of *c*-MSP will be formed; consistent with this, at 0.25 mM the naphthalene containing MSPs show over 80% of their peak population in the 8.62-8.72 ppm region while the xanthene containing threads show ~60% (**Figure 3.5a**). Thus, the data suggest that the nature of the aromatic linker (xan vs nap) has a significant effect on the MSP structure, with the shorter naphthalene linker resulting in an increase in the amount of lower molecular weight cyclic MSP. The alkenyl tail appears to have little or no effect on the MSP.

3.4 NMR Analysis of the new poly[*n*]catenane materials

With this information in hand, each MSP was subjected to a ring-closing metathesis reaction over the course of two days, following the procedure detailed in Chapter 2. After deactivating the catalyst and removing the Zn(II) from the resulting product, each of the new catenanes (**18$_{xan-5}$**, **19$_{nap-5}$**, **20$_{nap-6}$**) were characterized by ^{1}H NMR (**Figure 3.7**). This crude ^{1}H NMR spectra is used for preliminary qualitative and quantitative analyses of the new poly[*n*]catenanes, however, before analysis, the interlocked nature of the new materials must be confirmed. Samples of pure ADMET (**21$_{xan-5}$**, **22$_{nap-5}$**, **23$_{nap-6}$**) and ring closed thread (**12$_{xan-5}$**, **15$_{nap-5}$**, **17$_{nap-6}$**) were synthesized for each new thread to confirm the ^{1}H NMR shifts of these compounds (see Experimental Section). Using this data, it was possible to assign the peaks in the NMR of the crude reactions: with peaks ca. 8.35

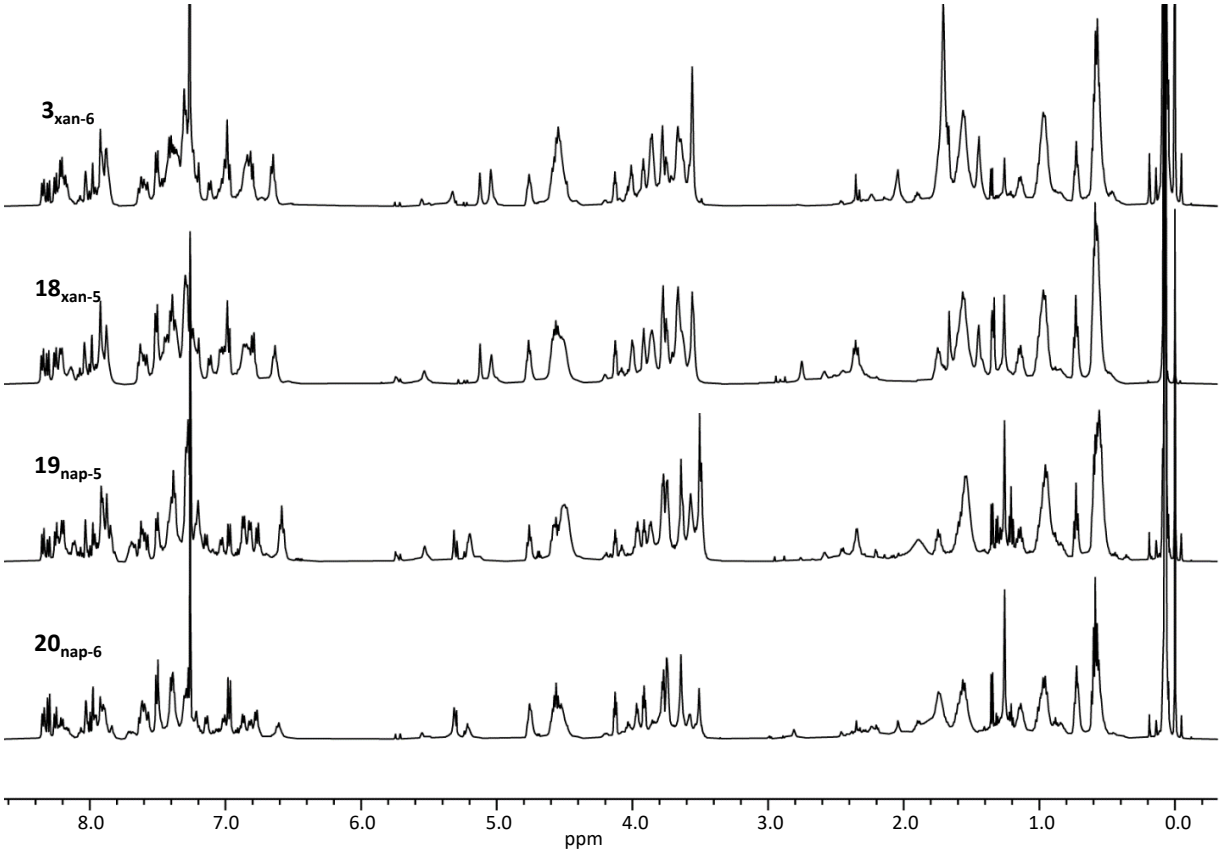

Figure 3.7 ^{1}H NMR for the crude samples of each poly[*n*]catenane explored: **3**$_{\textbf{xan-6}}$, **18**$_{\textbf{xan-5}}$, **19**$_{\textbf{nap-5}}$, and **20**$_{\textbf{nap-6}}$**.**

ppm corresponding to starting thread-like monomer or its ADMET counterpart. Similar to the original system, the peaks around 8.30 ppm corresponded to macrocycle **1** (**Figure 3.8**). In the original poly[*n*]catenane (**3**$_{\textbf{xan-6}}$) synthesis, the region from 8.05-8.27 ppm was shown to correspond to the H_{mpy} for the catenated material. To prove that this region corresponded to a similar interlocked material, a small sample of each new sample was purified via a two-step process. Initially, the samples were fractioned using preparatory gel permeation chromatography (GPC, 1:3 DMF:THF) to remove the residual macrocycle (**1**). Further purification could be achieved by either employing the previously discussed method of partial metalation and

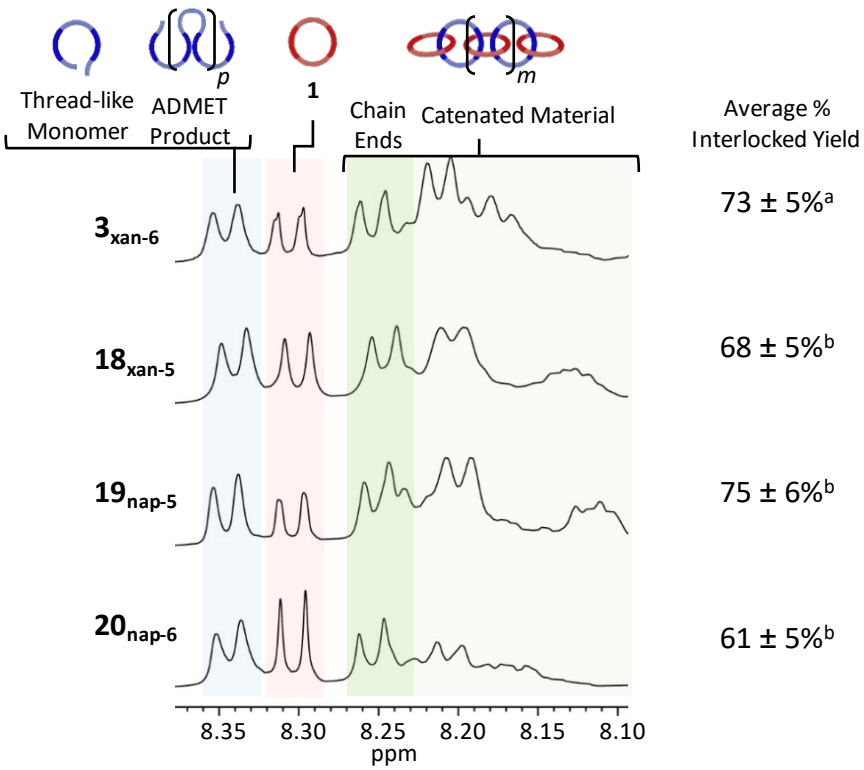

Figure 3.8 ^{1}H NMR (500 MHz, $CDCl_3$, 25 °C) for the crude samples of each new poly[*n*]catenane (**3**$_{xan-6}$, **18**$_{xan-5}$, **19**$_{nap-5}$, and **20**$_{nap-6}$) with a focus on the H_{mpy} region. The byproducts corresponding to thread are highlighted in blue (**2**$_{xan-6}$, **6**$_{xan-6}$, **11**$_{xan-5}$, **12**$_{xan-5}$, **14**$_{nap-5}$, **15**$_{nap-5}$, **16**$_{nap-6}$, and **17**$_{nap-6}$). The residual macrocycle **1** is highlighted in red. The interlocked material (**3**$_{xan-6}$, **18**$_{xan-5}$, **19**$_{nap-5}$, **20**$_{nap-6}$) is highlighted in green.
[a] Error for data set taken at 95% confidence interval (n=5).
[b] Error for data set taken at 95% confidence interval (n=3).

differential solubility (**18**$_{xan-5}$ and **20**$_{nap-6}$) or separated on a preparatory-silica plate (**19**$_{nap-5}$) (detailed in Experimental Section). These resulting purified poly[*n*]catenanes were characterized via ^{1}H NMR and Correlated Spectroscopy (COSY) to fully assign peaks (**Figure 3.9**, **3.10**, and **3.11**). For the purified mixtures containing **18**$_{xan-5}$ and **20**$_{nap-6}$, the ADMET byproduct could not be entirely removed however, the COSY method has allowed for identification of each peak corresponding to this ADMET product. In **Figure 3.9** and **Figure 3.11**, the peaks corresponding to this byproduct are highlighted. The COSY procedure allowed for accurate identification of all

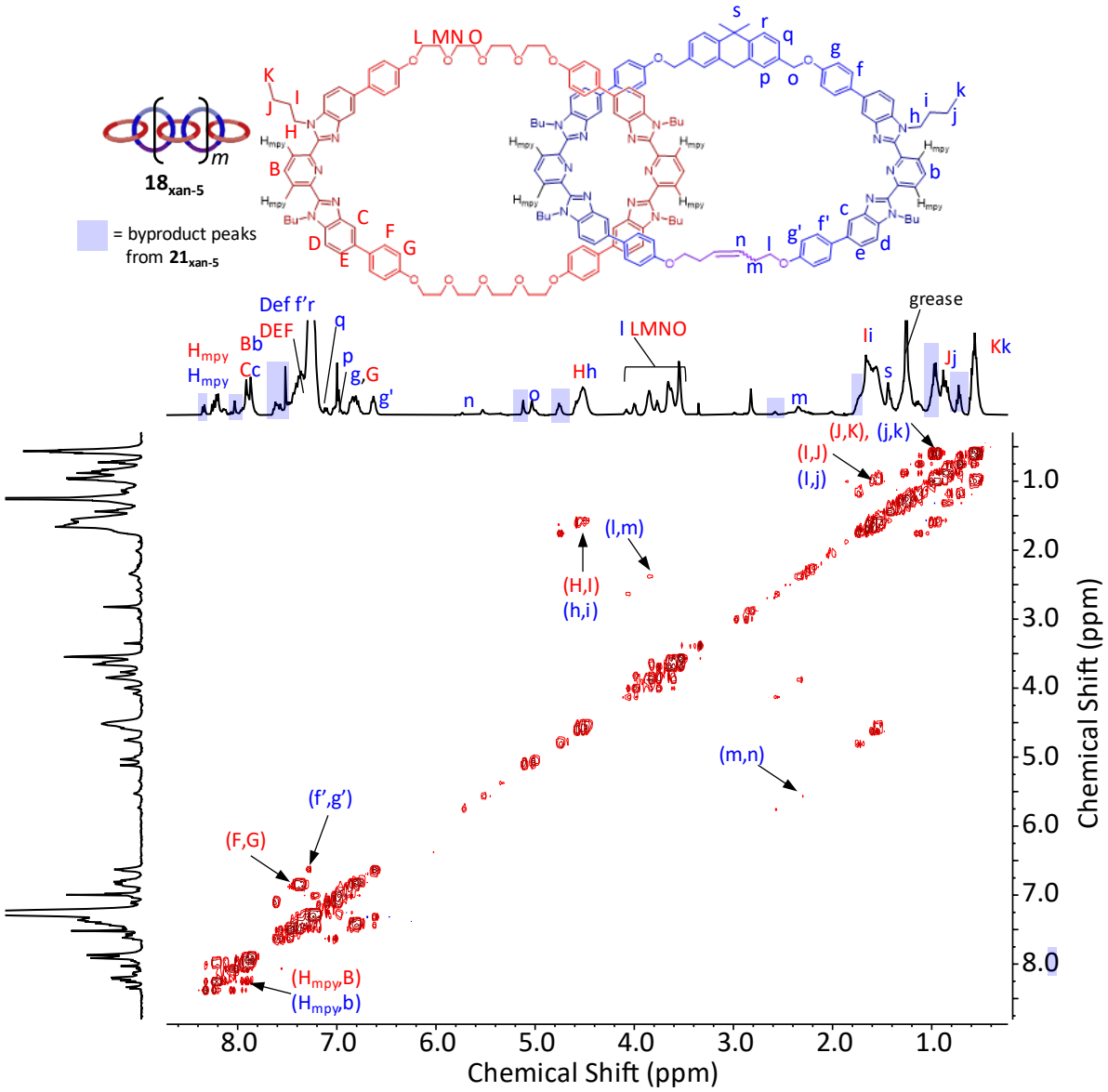

Figure 3.9 ^{1}H-^{1}H homonuclear correlation spectroscopy (COSY) (500 MHz, $CDCl_3$, 25 °C) of **18**$_{xan-5}$ (85% purified, 10 mg/mL). Peaks corresponding to the residual byproduct (**21**$_{xan-5}$) are indicated via blue highlight.

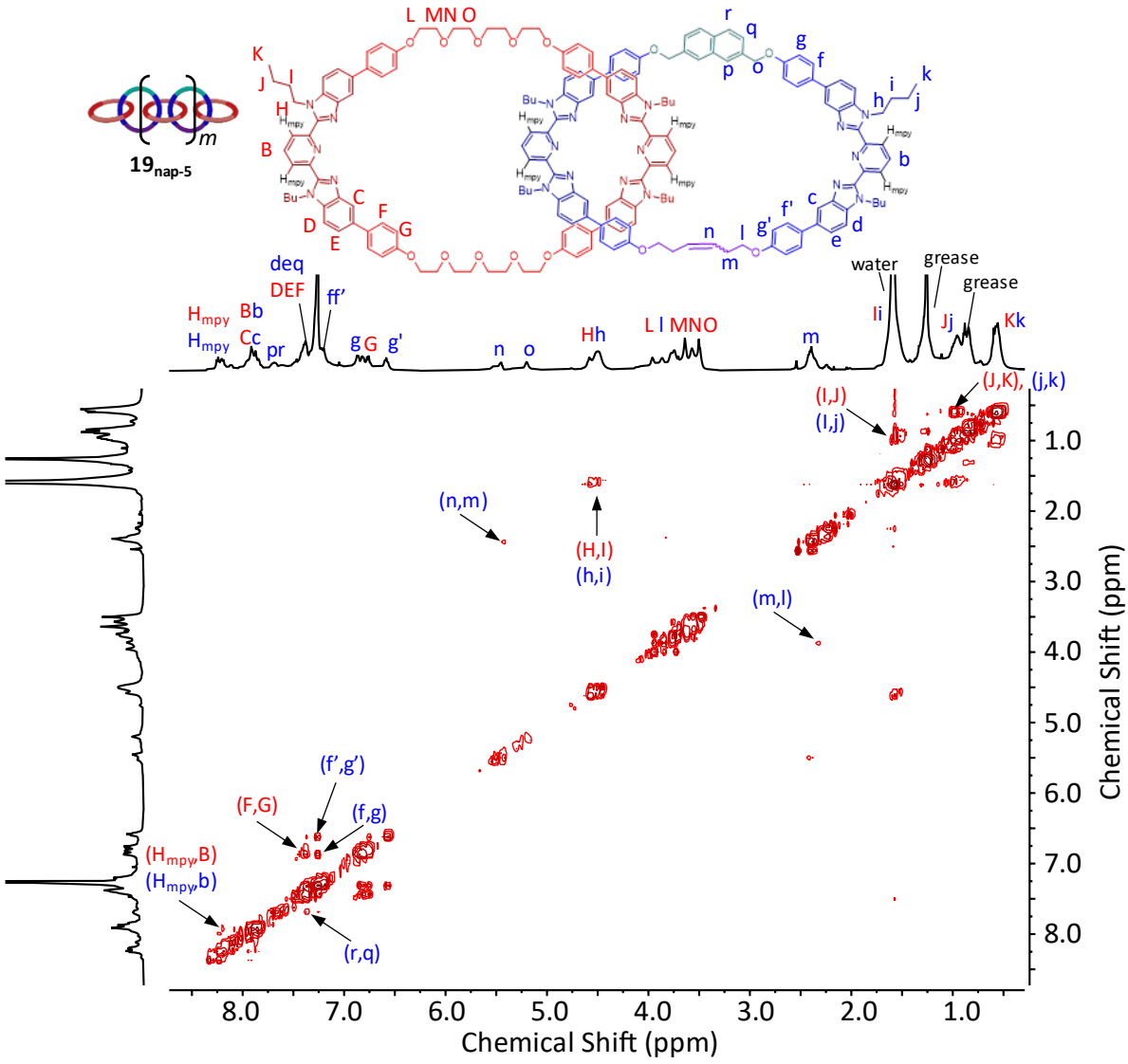

Figure 3.10 ^{1}H-^{1}H homonuclear correlation spectroscopy (COSY) (500 MHz, $CDCl_3$, 25 °C) of **19**$_{\textbf{nap-5}}$ (95% purified, 10 mg/mL).

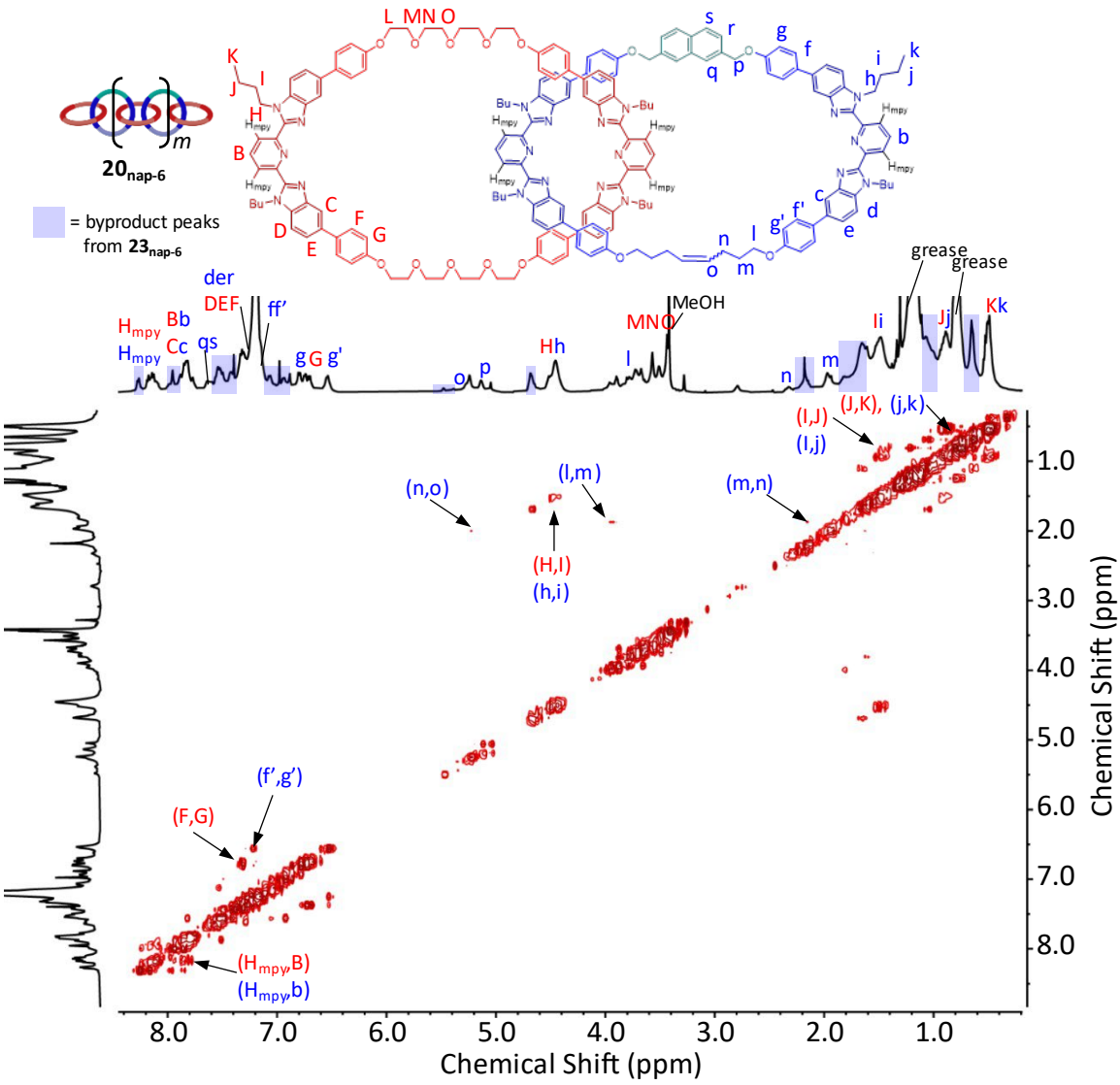

Figure 3.11 ^{1}H-^{1}H homonuclear correlation spectroscopy (COSY) (500 MHz, $CDCl_3$, 25 °C) of **20**$_{nap-6}$ (76% purified, 10 mg/mL). Peaks corresponding to the residual byproduct (**23**$_{nap-6}$) are indicated via blue highlight.

proton assignments; in particular, the COSY data confirms that the peaks above 8.10 ppm do indeed correspond to the H_{mpy} protons in the three new materials.

To confirm the interlocked nature of the new poly[*n*]catenane materials, low temperature Nuclear Overhauser Effect Spectroscopy (NOESY) was employed. NOESY analysis allows for detection of cross-peaks between protons across space (non-bonded) within 5Å. Via this NMR method, cross-peaks between the non-covalently bonded interlocked components can be identified to confirm the interlocked nature of each new material, as was shown in the literature analysis of $\mathbf{3}_{\mathbf{xan\text{-}6}}$.[2] For $\mathbf{18}_{\mathbf{xan\text{-}5}}$, the NOESY analysis can be seen in **Figure 3.12a**, with the cross-peaks between the interlocked components highlighted in **Figure 3.12b**. To prove that these cross-peaks indicate the interlocked nature of $\mathbf{18}_{\mathbf{xan\text{-}5}}$, a mixture of the individual rings that compose the catenane (**1** + $\mathbf{12}_{\mathbf{xan\text{-}5}}$) was also subjected to NOESY analysis as seen in **Figure 3.13a**. The direct comparison of the NOESY of this mixture (**1**+$\mathbf{12}_{\mathbf{xan\text{-}5}}$, **Figure 3.13b**) and the NOESY of $\mathbf{18}_{\mathbf{xan\text{-}5}}$ demonstrates the marked lack of intercomponent cross-peaks in the mixture. Based on this analysis, the catenated nature of $\mathbf{18}_{\mathbf{xan\text{-}5}}$ was confirmed.

Identical analyses were performed for both $\mathbf{19}_{\mathbf{nap\text{-}5}}$ and $\mathbf{20}_{\mathbf{nap\text{-}6}}$. The NOESY of $\mathbf{19}_{\mathbf{nap\text{-}5}}$ can be found in **Figure 3.14**, with the comparison to the mixture of **1** and $\mathbf{15}_{\mathbf{nap\text{-}5}}$ found in **Figure 3.15**. Similarly, the NOESY of $\mathbf{20}_{\mathbf{nap\text{-}6}}$ is analyzed in **Figure 3.16** and compared to a mixture of **1** and $\mathbf{17}_{\mathbf{nap\text{-}6}}$ in **Figure 3.17**.

These extensive NOESY analyses confirm the synthesis of three never-before-seen poly[*n*]catenane structures.

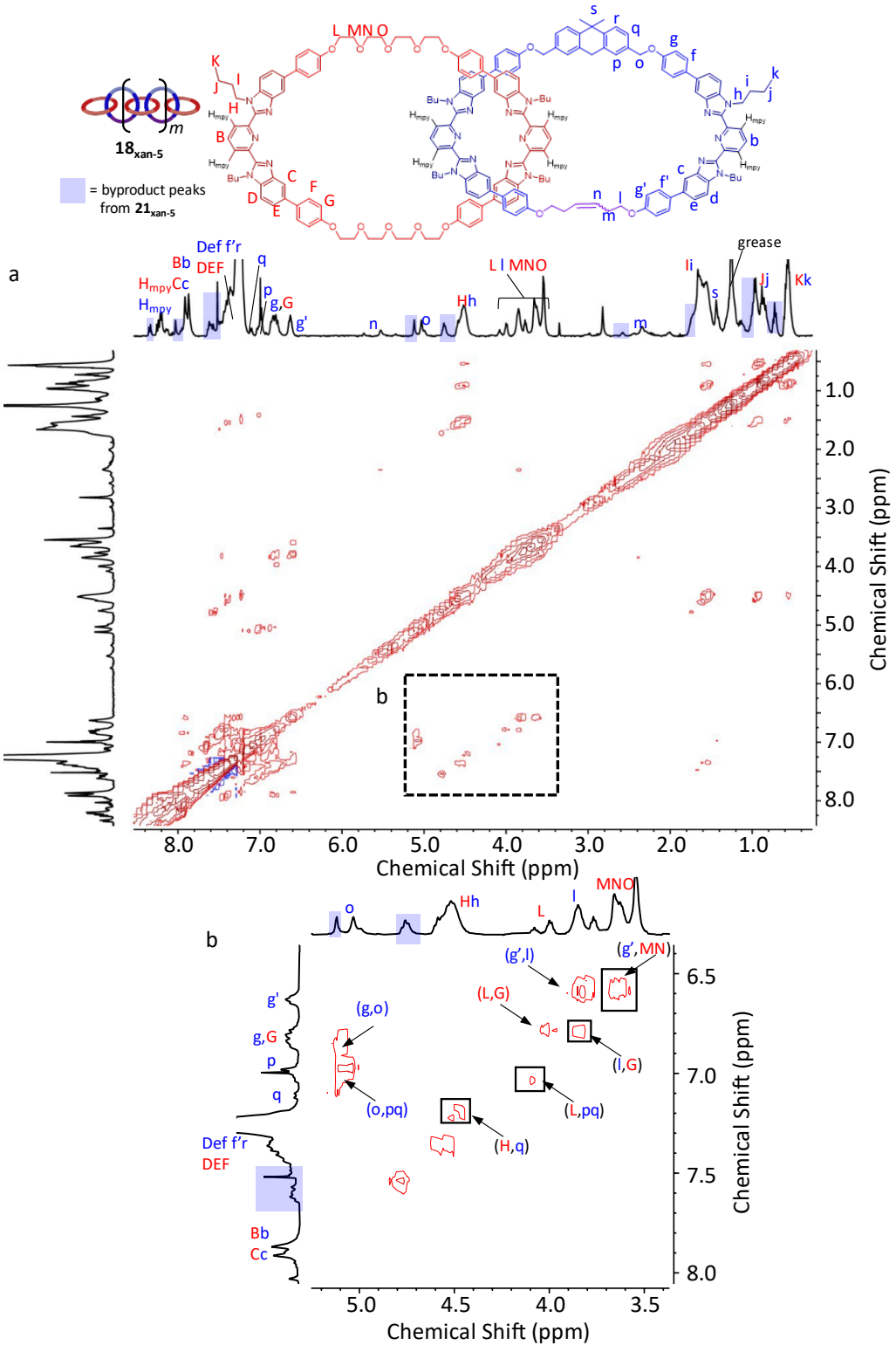

Figure 3.12 Nuclear Overhauser Effect Spectroscopy (NOESY) (500 MHz, $CDCl_3$, -25 °C) of (a) **18**$_{xan-5}$ (85% purified, 10 mg/mL) (b) zoomed in region corresponding to the dashed box in (a) with interlocked cross-peaks indicated by a solid black box in the zoomed region.

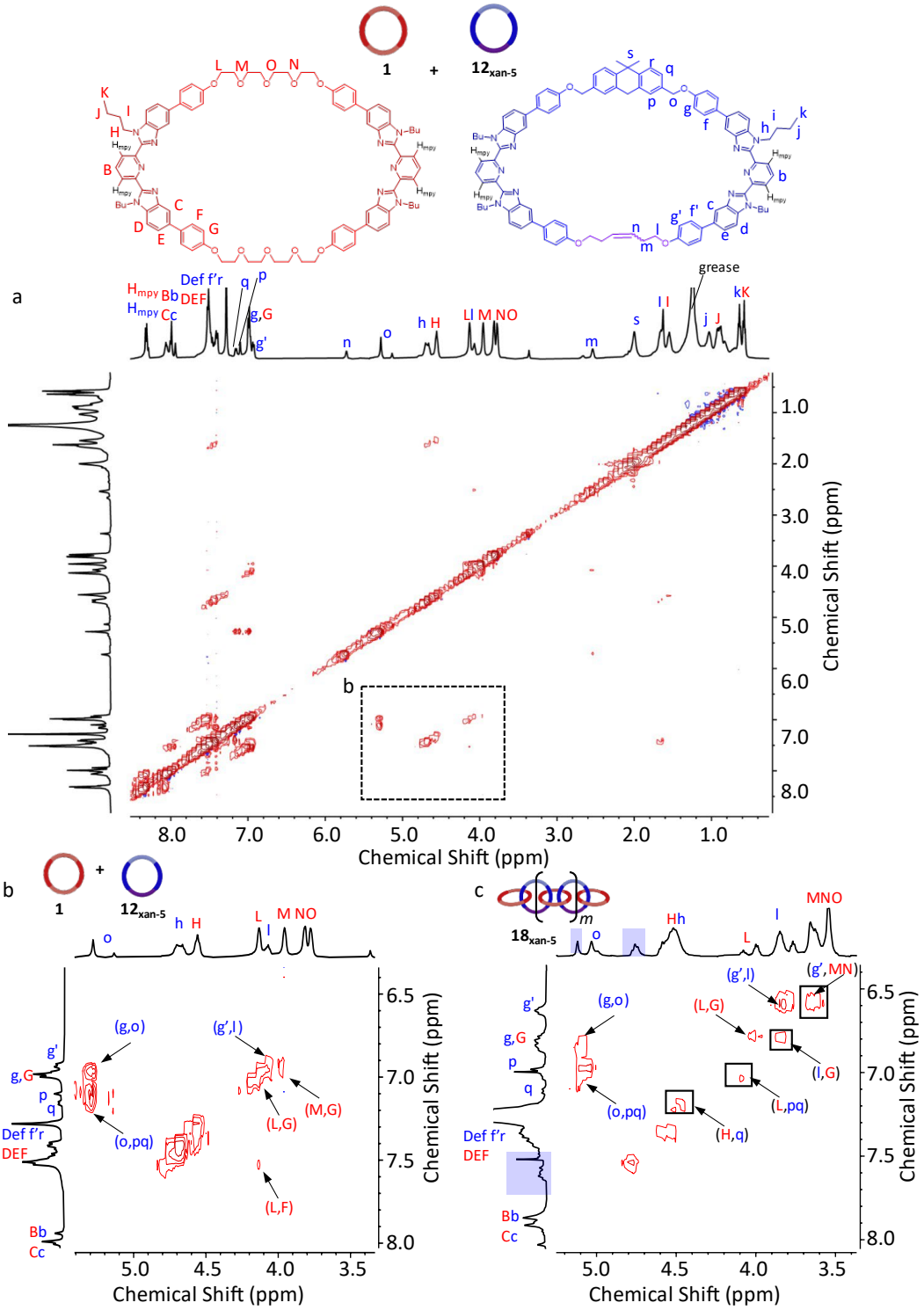

Figure 3.13 Nuclear Overhauser Effect Spectroscopy (NOESY) (500 MHz, $CDCl_3$, -25 °C) of (a) a mixture of **1** and**12**$_{\text{xan-5}}$ (10 mg/mL) for comparison with the interlocked **18**$_{\text{xan-5}}$. (b) zoomed in region (indicated by the dashed box in (a)) of the **1** and **12**$_{\text{xan-5}}$ mixture to compare with (c) the analyzed region of the interlocked material (**18**$_{\text{xan-5}}$) seen in **Figure 3.12**. The inter-macrocycle cross-peaks (highlighted by the solid black boxes) observed in **18**$_{\text{xan-5}}$ (c) are not present in the 1:1 mixture, consistent with the fact that **18**$_{\text{xan-5}}$ has an interlocked structure.

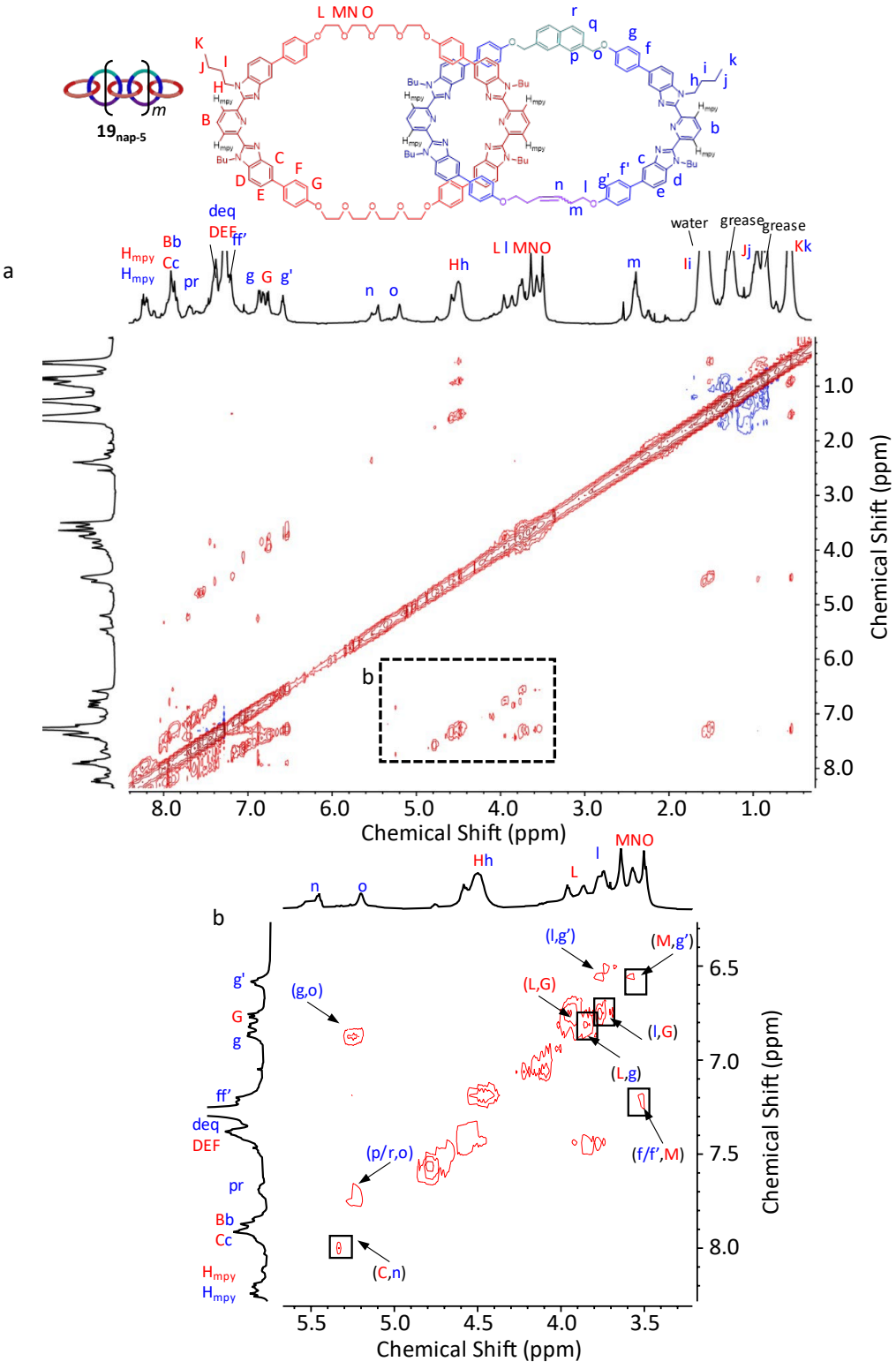

Figure 3.14 Nuclear Overhauser Effect Spectroscopy (NOESY) (500 MHz, $CDCl_3$, -25 °C) of (a) **19**$_{\text{nap-5}}$ (90% purified, 10 mg/mL) (b) zoomed in region corresponding to the dashed box in (a) with interlocked cross-peaks indicated by a solid black box in the zoomed region.

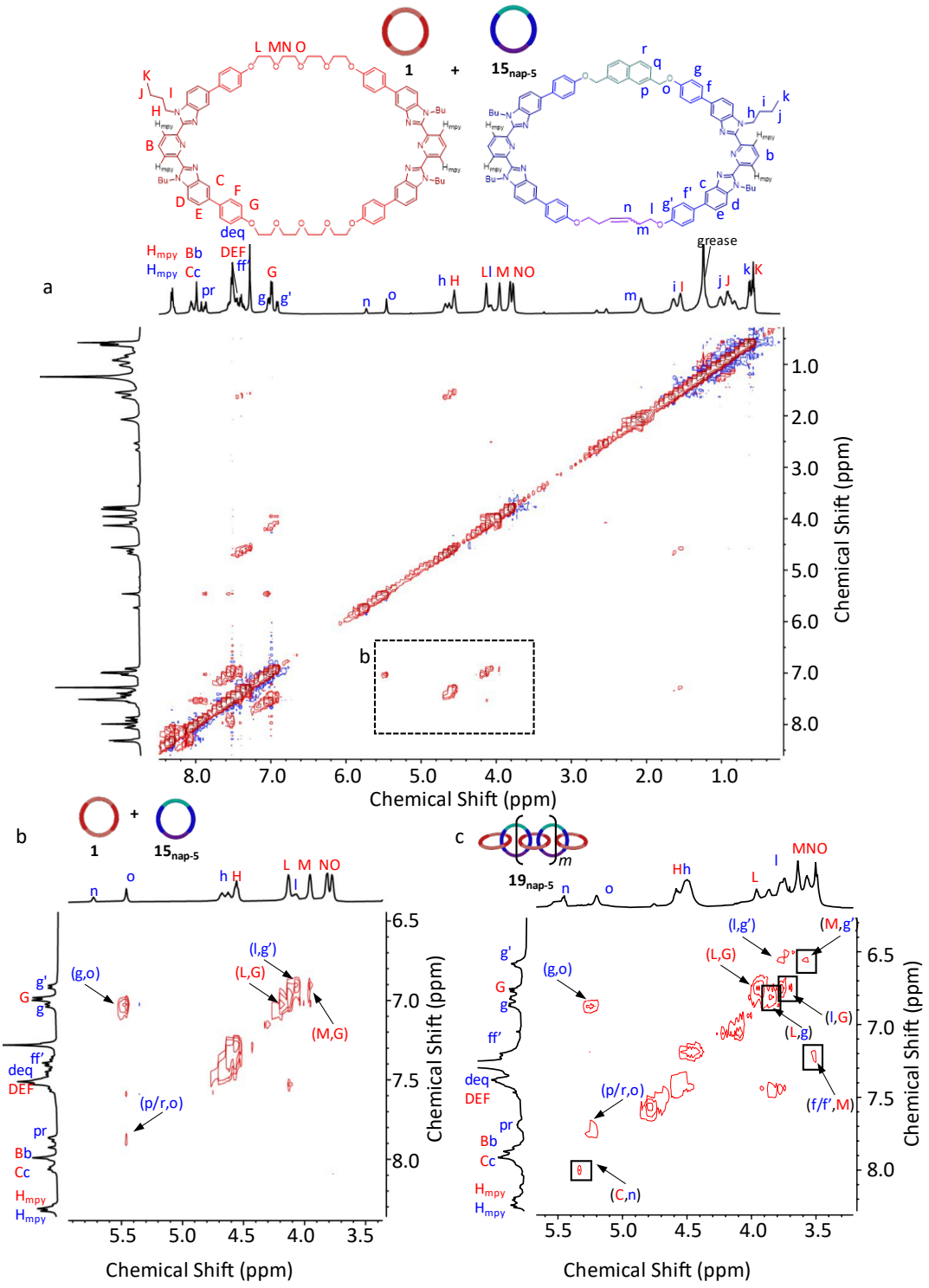

Figure 3.15 Nuclear Overhauser Effect Spectroscopy (NOESY) (500 MHz, $CDCl_3$, -25 °C) of (a) a mixture of **1** and **15**$_{\text{nap-5}}$ (10 mg/mL) for comparison with the interlocked **19**$_{\text{nap-5}}$. (b) zoomed region (indicated by the dashed box in (a)) of the **1** and **15**$_{\text{nap-5}}$ mixture to compare with (c) the analyzed region of the interlocked material (**19**$_{\text{nap-5}}$) seen in **Figure 3.14**. The inter-macrocycle cross-peaks (highlighted by the solid black boxes) observed in **19**$_{\text{nap-5}}$ (c) are not present in the 1:1 mixture, consistent with the fact that **19**$_{\text{nap-5}}$ has an interlocked structure.

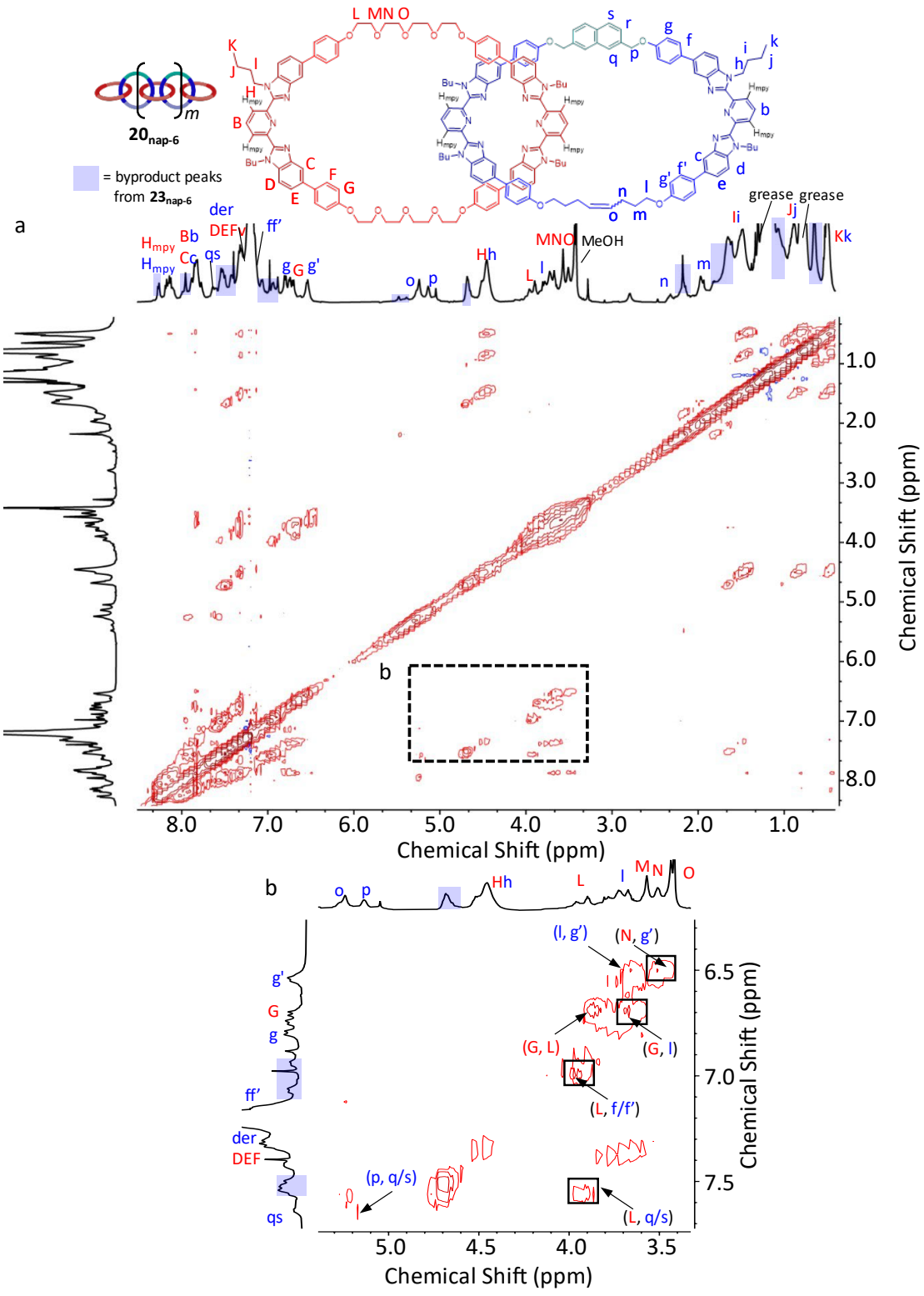

Figure 3.16 Nuclear Overhauser Effect Spectroscopy (NOESY) (500 MHz, $CDCl_3$, -25 °C) of (a) **20**$_{nap-6}$ (76% purified, 20 mg/mL) (b) zoomed in region corresponding to the dashed box in (a) with interlocked cross-peaks indicated by a solid black box in the zoomed region.

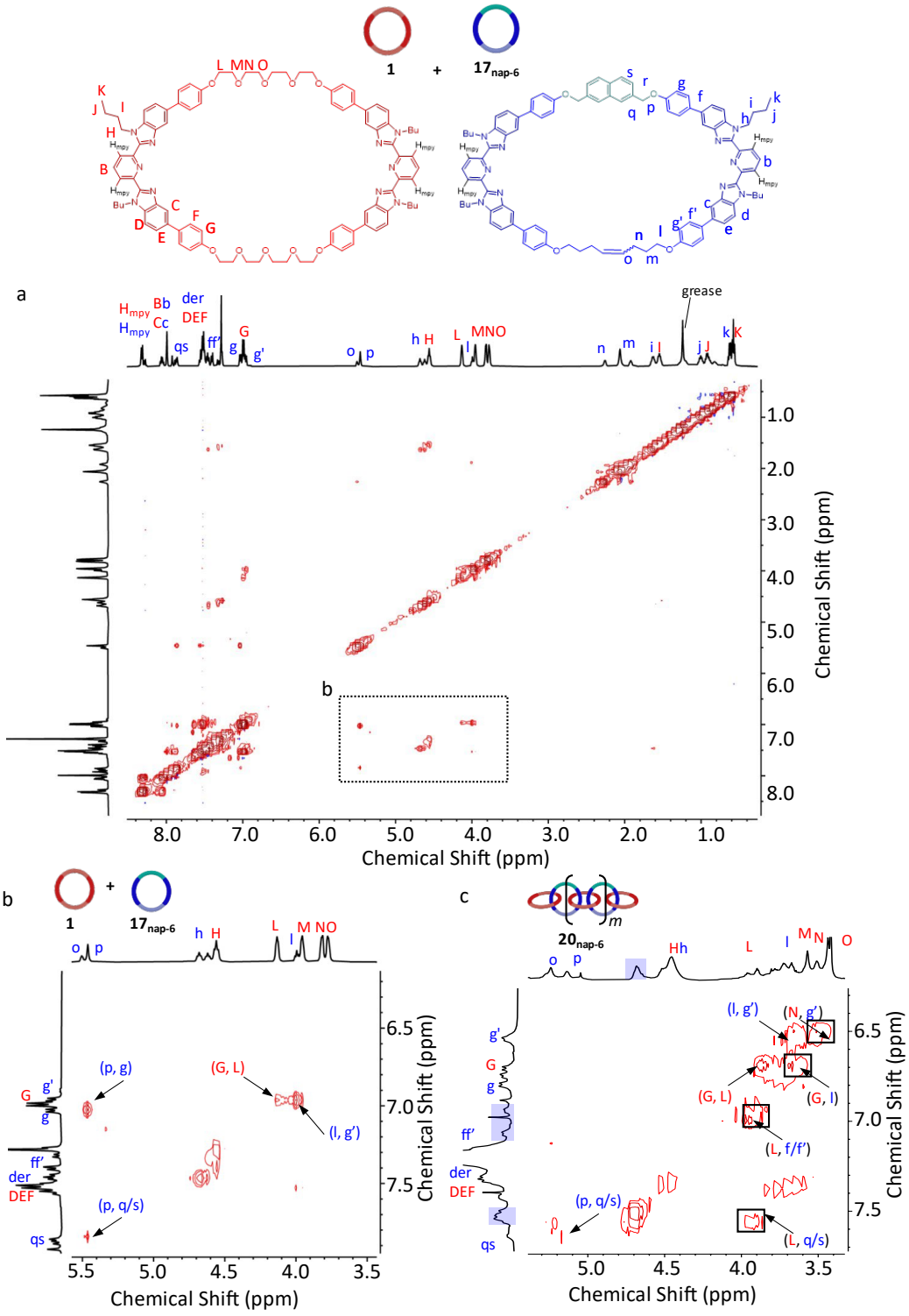

Figure 3.17 Nuclear Overhauser Effect Spectroscopy (NOESY) (500 MHz, $CDCl_3$, -25 °C) of (a) a mixture of **1** and **17**$_{\text{nap-6}}$ (10 mg/mL) for comparison with the interlocked **20**$_{\text{nap-6}}$. (b) Zoomed region (indicated by the dashed box in (a)) of the **1** and **17**$_{\text{nap-6}}$ mixture to compare with (c) the analyzed region of the interlocked material (**20**$_{\text{nap-6}}$) seen in **Figure 3.16**. The inter-macrocycle cross-peaks (highlighted by the solid black boxes) observed in **20**$_{\text{nap-6}}$ (c) are not present in the 1:1 mixture, consistent with the fact that **20**$_{\text{nap-6}}$ has an interlocked structure.

The ^{1}H NMR can also be used to provide information on the polymer chain ends that, in combination with molecular weight data obtained from GPC-MALS, is useful in determining the poly[*n*]catenane architecture.[2] NMR relaxation experiments were carried out on all three new materials. The H_{mpy} peak region (8.10-8.30 ppm) was monitored and T_1 values were determined (**Figure 3.18, Table 3.2**). As was previously shown for **3**$_{\textbf{xan-6}}$,[2] the region corresponding to the singly-threaded chain-ends should have a larger T_1 value than the region corresponding to the doubly-threaded interior rings, on account of the higher mobility of these chain ends. In all three new poly[*n*]catenanes (**18**$_{\textbf{xan-5}}$, **19**$_{\textbf{nap-5}}$ and **20**$_{\textbf{nap-6}}$) the peaks in the region 8.24-8.27 ppm show higher T_1 values than the more upfield shifted protons (**Table 3.2**), consistent with those peaks corresponding to the chain ends for each of new poly[*n*]catenanes.

With the H_{mpy} chemical shifts of the non-interlocked and catenated materials assigned, the crude yield of the three new poly[*n*]catenanes was determined by comparing the integration of the non-interlocked peaks (8.28 – 8.37 ppm) versus the peaks corresponding to the interlocked materials (8.09 – 8.27 ppm). From this analysis it was determined that the yield of **19**$_{\textbf{nap-5}}$ was comparable to the yield obtained for the original system **3**$_{\textbf{xan-6}}$ (ca. 75%) while the yield of the **18**$_{\textbf{xan-5}}$ and **20**$_{\textbf{nap-6}}$ was lower (ca. 68% and 61% respectively) (**Figure 3.8**, **Table 3.3**).

In the original system **3**$_{\textbf{xan-6}}$, the aromatic linker and tail were selected such that the interior of the aromatic linker was a similar length to the closed alkoxy moiety (O to O = 11 atoms vs. O

Table 3.2 T_1 relaxation values for the new poly[*n*]catenanes

Poly[*n*]catenane Sample	T_1 Value	
	Region α (Chain End)	Region β
18$_{\textbf{xan-5}}$	2.01	1.92
19$_{\textbf{nap-5}}$	1.94	1.88
20$_{\textbf{nap-6}}$	2.03	1.95

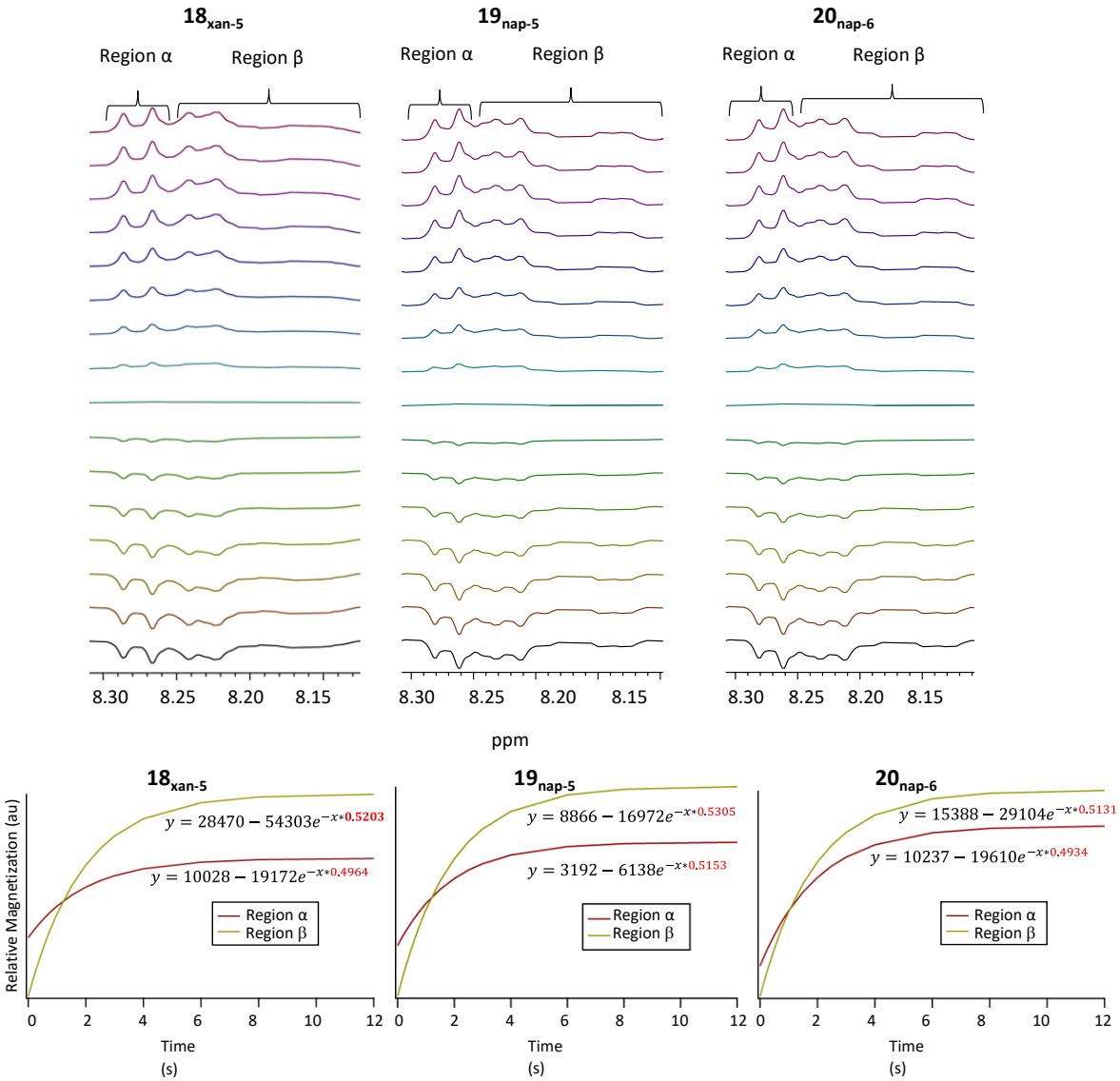

Figure 3.18 ^{1}H NMR relaxation studies on H_{mpy} for all new polycatenane materials. (a) depicts the individual ^{1}H NMR scans taken during the experiment while (b) shows the relative magnetization vs. time calculated from three parameter exponential fit (B+F*exp(-x*G))via the Mestrenova software for each region (α and β). T_1 values taken from 1/G (G highlighted in red), displayed in **Table 3.2**.

to O = 10 atoms, respectively, Figure 2b) with the idea that matching the size of the aromatic linker and alkoxy chains would facilitate the ring closing step. The three new poly[*n*]catenanes have different ratios of aromatic linker to alkoxy chain length (**18**$_{\text{xan-5}}$ (11:8), **19**$_{\text{nap-5}}$ (9:8), and **20**$_{\text{nap-6}}$ (9:10)).

Thus, if matching is the primary factor driving the yield of the poly[*n*]catenane, then it would be expected that **18**$_{\text{xan-5}}$ might be formed in the lowest yield. While the yield does drop slightly relative to the **3**$_{\text{xan-6}}$ (ca. 68 vs ca. 73%), the yield of **18**$_{\text{xan-5}}$ is significantly higher than the apparently closer matched **20**$_{\text{nap-6}}$ (ca. 68 vs ca. 61%). This suggests that other factors, such as, thread rigidity and/or the spatial orientation of the specific thread components, also impact the synthetic yield of the poly[*n*]catenanes. However, while the matching aromatic linker and alkoxy-chain size (through simple atom counting) may not be the only factor in determining the yield, it certainly does to play role, as the **19**$_{\text{nap-5}}$, with both the shorter linker and alkoxy chain, does show an increase in yield (75 ± 6%) and is obtained in approximately the same yield as the original poly[*n*]catenane **3**$_{\text{xan-6}}$.

Table 3.3. Quantitative Data of Poly[*n*]catenane obtained via ^{1}H NMR and GPC-MALS

	Average % product distribution in crude reaction mixture[a]						Poly[n]catenane Architecture **(% based on catenated products)**[g]			
Sample	Interlocked Material	**1**	Thread + ADMET	$\overline{M_n}$[d]	$\overline{DP}$[e]	$\overline{N_c}$[f]	[2]/[3] Cat	Cyclic	Linear	Branched
3$_{\text{xan-6}}$[h]	73 ± 5[b]	12 ± 3[b]	15 ± 2[b]	17700	11	2.9	8	12	51	29
18$_{\text{xan-5}}$	68 ± 5[c]	15 ± 3[c]	17 ± 3[c]	14500	9	4.4	29[h]	8[h]	0[i]	63[i]
19$_{\text{nap-5}}$	75 ± 6[c]	11 ± 4[c]	14 ± 2[c]	18300	12	5.4	22	0	0[i]	78[i]
20$_{\text{nap-6}}$	61 ± 5[c]	17 ± 3[c]	22 ± 2[c]	16000	10	3.0	5	23	45	27

(a) Conversion of MSP to catenane calculated by integrating H_{mpy} doublets corresponding to non-interlocked products **1** and ADMET (**5**$_{\text{xan-6}}$, **21**$_{\text{xan-5}}$, **22**$_{\text{nap-5}}$, or **23**$_{\text{nap-6}}$) (8.36-8.28 ppm) against H_{mpy} protons corresponding to catenane (**3**$_{\text{xan-6}}$, **18**$_{\text{xan-5}}$, **19**$_{\text{nap-5}}$, or **20**$_{\text{nap-6}}$) (8.28-8.10 ppm). (b) Error for data set taken at 95% confidence interval (n=5). (c) Error for data set taken at 95% confidence interval (n=3). (d) MALS data was obtained from the crude catenane samples (n=2) and values were determined assuming the calculated *dn/dc* values for each individual catenane (see SI). (e) Average degree of polymerization was calculated via Eq.2.1, which here correspond to the average number of rings. (f) Average number of chain ends were calculated via Eq. 2.2. (g) Architecture breakdown reported as % of total interlocked material as determined via GPC deconvolution of RI trace data. (h) Value based on the assumption that Peak C is entirely composed of ***c*-18**$_{\text{xan-5}}$. (i) Value based on the assumption that no *l*-poly[*n*]catenane is formed when the pentenyl-based thread-like monomer is used.

3.5 GPC Analysis of Poly[*n*]catenane Architecture

Studies on **3**$_{\text{xan-6}}$ showed that synthesis results in the formation of linear, cyclic and branched poly[*n*]catenane architectures.[2,3] Given that the structure of the thread has an impact on interlocked

yield, it is of interest to determine if the different thread-like monomers play a role in the distribution of the poly[*n*]catenane architecture. To this end, GPC-MALS experiments of the crude reaction mixtures were undertaken and analyzed in conjunction with the ^{1}H NMR data.

The GPC-MALS traces of the three new poly[*n*]catenane crude reaction mixtures (**Figure 3.19**) clearly demonstrate that polymeric materials are formed in all three reactions. The *dn/dc* values of the crude mixtures were obtained to allow determination of the absolute average molecular weight for each sample (**Figure 3.19**, top). When approaching the *dn/dc* values for these polymers throughout the analytical process, a key stipulation to bear in mind is that this value is specific to the material and independent of molecular weight at higher molecular weights. However, at low molecular weights (ie. [2]-[4]catenane, small cyclic catenanes, monomers) the *dn/dc* value has a strong correlation with molecular weight[5] and will therefore be used as an approximation to allow analysis, however the tentative conclusions drawn from smaller molecular weight materials depends largely on ^{1}H NMR data and starting material reference standards.

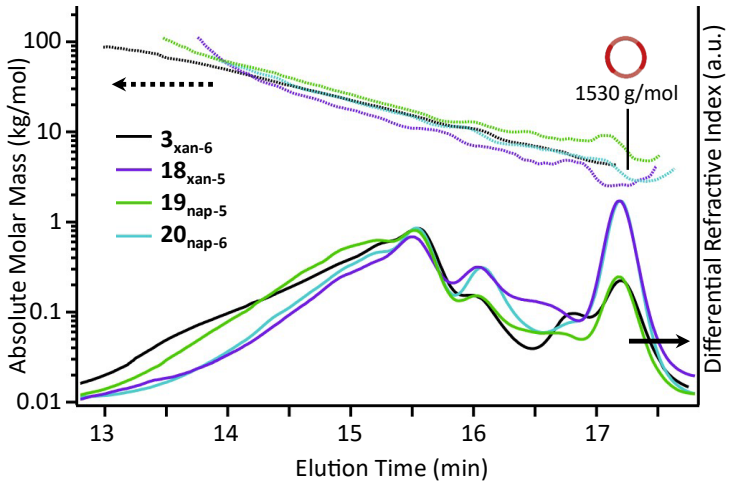

Figure 3.19 GPC (mobile phase - 25% DMF in THF) refractive index traces for **3**$_{\text{xan-6}}$, **18**$_{\text{xan-5}}$, **19**$_{\text{nap-5}}$, and **20**$_{\text{nap-6}}$ (bottom) and absolute molecular weight data as determined by MALS (top).

As would be expected for a step growth polymerization, the data shows that the poly[*n*]catenane obtained in the lowest yield (**20**$_{\text{nap-6}}$) has the lowest observable maximum molecular weight. The GPC traces of all the crude reaction mixtures clearly show that multiple different products with a range of molecular weights obtained (**Figure 3.19**, top); however, differences in the general peak shapes suggest that the different thread-like components do result in different product distributions.

To understand the product distributions in more detail, the GPC traces of the crude reaction mixtures were analyzed via gaussian deconvolution using a procedure similar to Chapter 2. **Figure 3.20a-d** shows the gaussian deconvolution of the crude reaction mixture for **3**$_{\text{xan-6}}$, **18**$_{\text{xan-5}}$, **19**$_{\text{nap-5}}$,

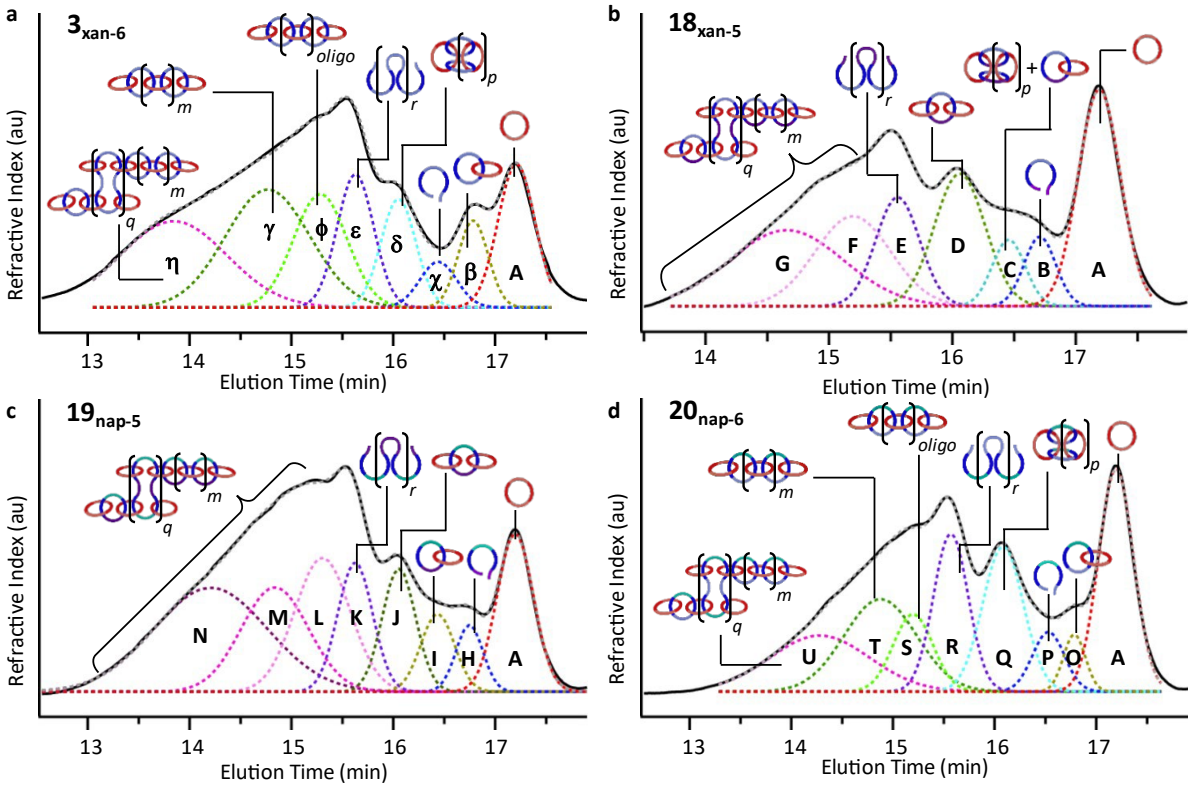

Figure 3.20 GPC (mobile phase - 25% DMF in THF) refractive index traces for a) **3**$_{\text{xan-6}}$, b) **18**$_{\text{xan-5}}$ c) **19**$_{\text{nap-5}}$, and d) **20**$_{\text{nap-6}}$. Deconvolution performed using a gaussian fit, peak assignments made based on GPC analysis shown in Figures 3.22, 3.23, and 3.25. Sum of the deconvoluted peaks fits for (a)-(d) designated by the grey dashed line.

20$_{\text{nap-6}}$, respectively. **Figure 3.20a** shows the assigned peaks based on the prior work.[2,3] For a full analysis of how the peak assignment is made, refer to Chapter 2. In short, each of the peaks within the crude trace can be assigned to tentative architectures using a combination of chain end analysis (^{1}H NMR) and number average molecular weight ($\overline{M_n}$) (GPC-MALS) of the fractionated samples.

The three new poly[*n*]catenane mixtures can also be analyzed in a similar way. For the crude mixture of **18**$_{\text{xan-5}}$, standards of **1** and **11**$_{\text{xan-5}}$ were run and could confidently be attributed to Peaks A and B (**Figure 3.21**). To determine the rest of the deconvoluted peaks, preparatory GPC (1:3 DMF:THF) was employed to isolate fractions of the crude **18**$_{\text{xan-5}}$ mixture. Seven individual fractions were collected and analyzed via ^{1}H NMR (**Figure 3.22a**) and GPC-MALS (**Figure 3.22b**): Fraction 1$_{\text{xan-5}}$ being the first to elute and the highest molecular weight and Fraction 7$_{\text{xan-5}}$ being the last to elute and the lowest molecular weight. For the GPC-MALS analysis of these materials (**Figure 3.22b**), the molecular weight analysis shows strong cohesion at the higher molecular weights, suggesting that the *dn/dc* for this material (0.2042) corresponds to the large

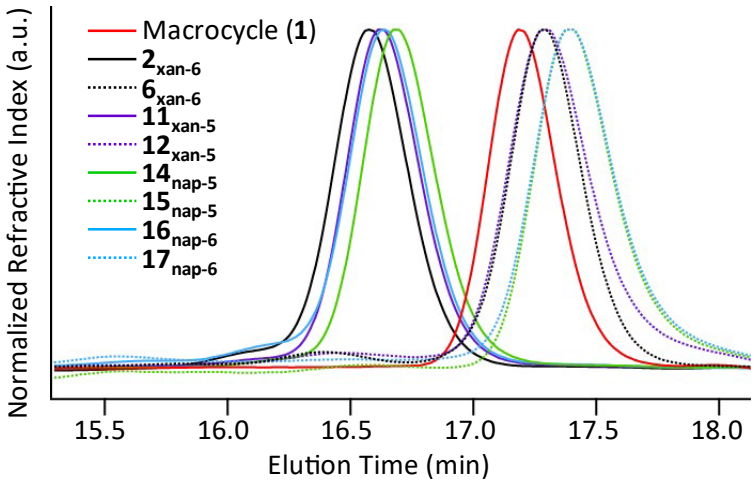

Figure 3.21 GPC traces (25% HPLC grade dimethylformamide (DMF) and 75% HPLC grade tetrahydrofuran (THF) as the eluent (1mL/min) at 25 °C) taken for the starting materials: the macrocycle (**1**), all four thread types: the original system (**2**$_{\text{xan-6}}$), **11**$_{\text{xan-5}}$, **14**$_{\text{nap-5}}$, and **16**$_{\text{nap-6}}$), and the ring closed versions of all three (**6**$_{\text{xan-6}}$, **12**$_{\text{xan-5}}$, **15**$_{\text{nap-5}}$, and **17**$_{\text{nap-6}}$).

poly[*n*]catenanes of **18$_{xan-5}$**; however, the slight disarray seen in Fractions 4$_{xan-5}$-7$_{xan-5}$ seems to suggest that cyclic and oligomeric catenanes may possess a slightly different *dn/dc*, however, as the materials could not be isolated, they cannot be calculated separately. To account for this variation, the number average degree of polymerization ($\overline{DP_n}$) values assigned to these materials are given as approximations in **Figure 3.22b**.

For the peak classification, Fractions 6$_{xan-5}$ and 7$_{xan-5}$ once again confirmed the assignments of the standards for Peaks A and B, as well as confirming the presence of unreacted **11$_{xan-5}$** within the crude sample. To assign the architecture for each of the subsequent deconvoluted peaks, $\overline{DP_n}$ and the average number of chain ends, N_c, of the fractions (Equation 2.1 and Equation 2.4) were analyzed. The N_c of the fractionated sample (Fraction 5$_{xan-5}$) that corresponds (in part) to the

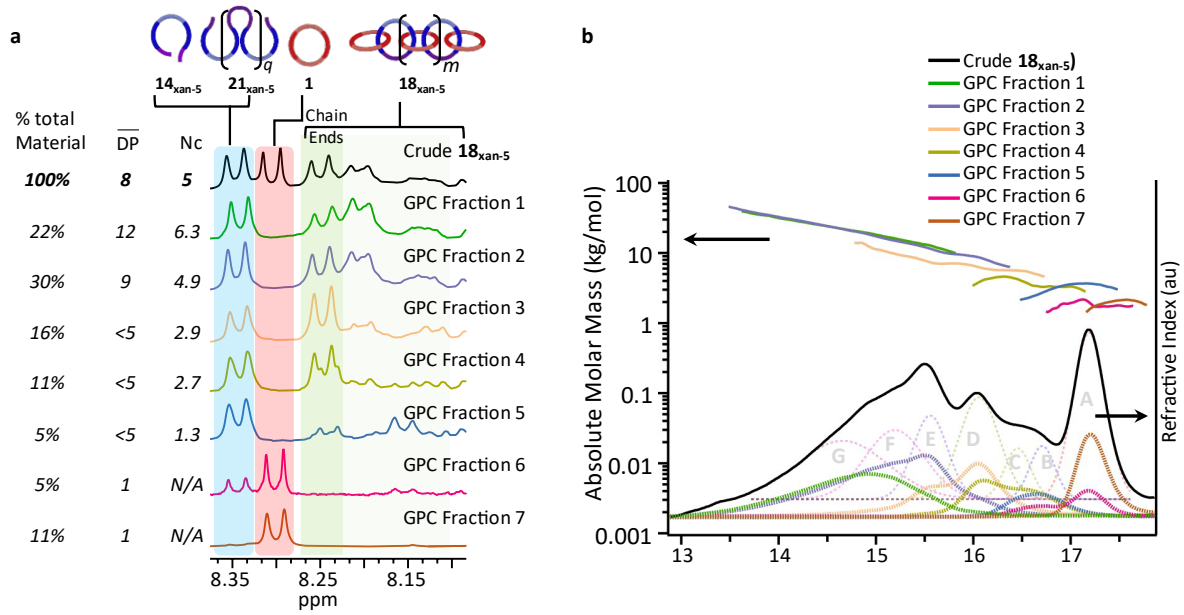

Figure 3.22 (a) ^{1}H NMR traces for all fractionated **18$_{xan-5}$** samples. (b) The GPC RI traces were collected for each fractionated sample. The combination of GPC and ^{1}H NMR was used to theorize the precise elution of the various catenane architectures in the crude GPC trace (assigned in Figure 3.20b, peaks overlayed). These assignments were obtained via analyzing the absolute molar mass of each fraction was obtain via the MALS analysis to yield the number average degree of polymerization ($\overline{DP_n}$ Equation 2.1) chain end calculations (N_c, Equation 2.4) for each fraction.

deconvoluted peak C is < 2, suggesting that cyclic poly[*n*]catenane may appear in this region. Interestingly, for all the other fractions, an $N_c > 2$ is obtained, suggesting that very little ***c*-18$_{\text{xan-5}}$** is formed in this reaction. Even if it is assumed that all of peak C corresponds to ***c*-18$_{\text{xan-5}}$**, the yield of this architecture is about half of that observed in the **3$_{\text{xan-6}}$** synthesis (**Table 3.3**). The Fraction 5$_{\text{xan-5}}$ MALS data suggests that the catenane here has a $\overline{DP_n} < 5$, therefore this peak may be a combination of both ***c*-18$_{\text{xan-5}}$** and small oligomeric [2]/[3]catenanes. Examining the ^{1}H NMR more closely, the chain-end peaks of Fraction 5$_{\text{xan-5}}$ are slightly offset (upfield). If the material was a [3]catenane, the chain end would appear as macrocycle **1**. In fact, we have shown previously[2] that the formation of the ADMET byproduct yields catenanes that are predominately terminated by macrocycle **1**. The upfield shifted chain end in Fraction 5$_{\text{xan-5}}$ suggests that this material is a **12$_{\text{xan-5}}$** terminated catenane,[2] suggesting that Peak C is may contain [2] or a [4]catenane.

Fractions 3$_{\text{xan-5}}$ and 4$_{\text{xan-5}}$ correspond predominantly to peak D, with small amounts of higher molecular weight product included. These samples have an $N_c < 3$ and, taken with the small amount of high molecular weight material, this would suggest that the N_c is consistent with this peak corresponding to a low molecular weight linear catenane ($N_c = 2$). Based on the fractions having a $\overline{DP_n} < 5$ and the primary chain ends appearing as macrocycle **1**, this peak is tentatively assigned to [3]catenane. This is in marked difference from **3$_{\text{xan-6}}$**, as no significant peak corresponding to [3]catenane was observed (**Figure 3.20a**). Peak E was assigned to the ADMET material **22$_{\text{xan-5}}$** based on a combination of its prevalence in **22$_{\text{xan-5}}$**-containing samples (Fractions 1$_{\text{xan-5}}$-4$_{\text{xan-5}}$), the percent **22$_{\text{xan-5}}$** seen in the ^{1}H NMR (**Figure 3.8**, **Table 3.3**), and the comparative assignment in the crude **3$_{\text{xan-6}}$** (**Figure 3.20a**). Finally, Fractions 1$_{\text{xan-5}}$ and 2$_{\text{xan-5}}$ which correspond predominantly to Peaks F and G, contain the highest molecular weight materials and both of these fractions have $N_c > 4$, suggesting that these materials are ***b*-18$_{\text{xan-5}}$**. It is worthy of note that, unlike

with **3**$_{\textbf{xan-6}}$, no peaks could be assigned to corresponding to a polymeric ***l*-18**$_{\textbf{xan-5}}$ (only linear species observed correspond to low molecular weight species such [2] or [3]catenane). Thus, while it is not possible to completely exclude the formation of ***l*-18**$_{\textbf{xan-5}}$, it certainly appears that shortening the alkenyl chain reduces the likelihood of the intramolecular thread cyclization of **11**$_{\textbf{xan-5}}$ in the MSP that is required to yield the linear or cyclic poly[*n*]catenanes. The consequence of which is the shorter alkenyl chain on the thread results in the formation of more branched poly[*n*]catenane, ***b*-18**$_{\textbf{xan-5}}$.

If it is just the mismatch between the shorter alkenyl chain and longer aromatic (xan) linker that is causing this significant change in product distribution, then it might be expected that the **1·14**$_{\textbf{nap-5}}$**·Zn(II)**$_{\textbf{2}}$ MSP would yield **19**$_{\textbf{nap-5}}$ with a product distribution more akin to **3**$_{\textbf{xan-6}}$. To test this hypothesis, a similar peak deconvolution analysis was performed on the crude **19**$_{\textbf{nap-5}}$ mixture (**Figure 3.20c**).

As with **18**$_{\textbf{xan-5}}$, the crude material was separated into seven fractions via preparatory GPC and analyzed by ^{1}H NMR and GPC-MALS (**Figure 3.23**). For the peak assignments, similar to the assignments for **18**$_{\textbf{xan-5}}$, Peaks A and H were assigned based on the standards shown in **Figure 3.21**. For Peak I, Fraction 5$_{\text{nap-5}}$ eluted most similarly to the Gaussian deconvolution. For Fraction 5$_{\text{nap-5}}$, the sample has an N_c ~2 and $\overline{DP} < 4$ as well as evidence of chain end peaks corresponding to both **1** terminated catenanes as well as **15**$_{\textbf{nap-5}}$ terminated catenanes; therefore Peak I was assigned to [2]catenane. GPC Fraction 4$_{\text{nap-5}}$ appears to be a combination of Peak J and unreacted thread **14**$_{\textbf{nap-5}}$, (Peak H). As Fraction 4$_{\text{nap-5}}$ has an N_c ~2 and $\overline{DP} < 4$ with primarily **1** terminated catenane, the architecture of Peak J was tentatively assigned to [3]catenane. Peak K is present to a small extent in Fraction 1$_{\text{nap-5}}$ and to a greater extent in Fractions 2$_{\text{nap-5}}$ and 3$_{\text{nap-5}}$. Based on the

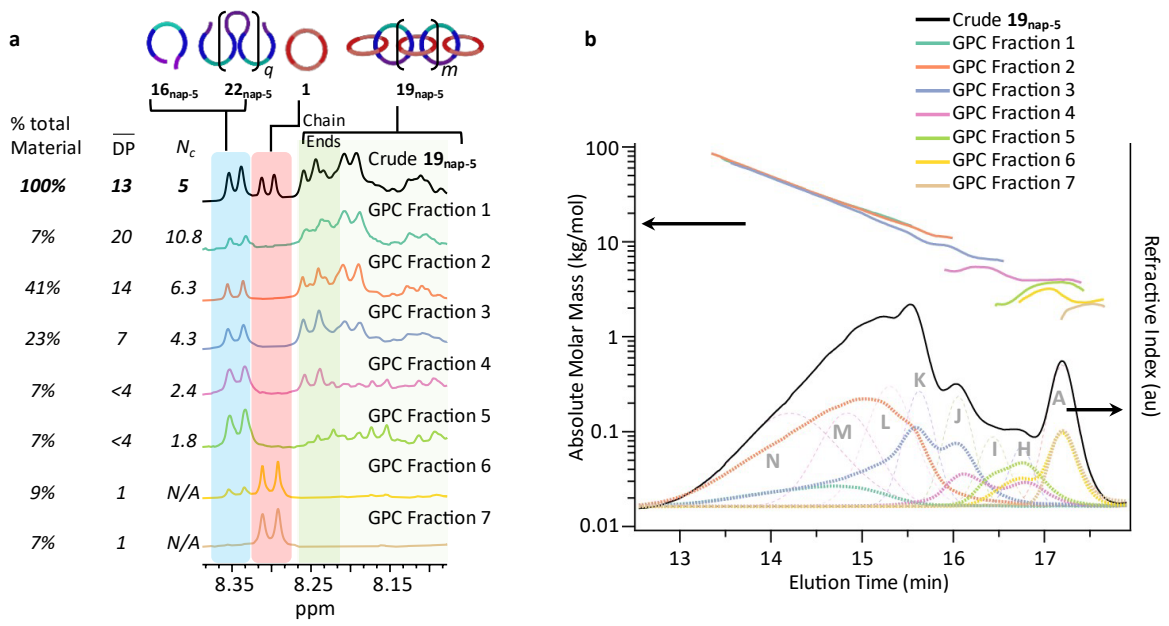

Figure 3.23 (a) ^{1}H NMR traces for all fractionated **19$_{nap-5}$** samples. (b) The GPC RI traces were collected for each fractionated sample. The combination of GPC and ^{1}H NMR was used to theorize the precise elution of the various catenane architectures in the crude GPC trace (assigned in Figure 3.20c, peaks overlayed). These assignments were obtained via analyzing the absolute molar mass of each fraction was obtain via the MALS analysis to yield the number average degree of polymerization ($\overline{DP_n}$ Equation 2.1) chain end calculations (N_c, Equation 2.4) for each fraction.

previously published work[3] and the prevalence of ADMET **22$_{nap-5}$** in the ^{1}H NMR each of these fractions, Peak K has been tentatively assigned to the ADMET byproduct **22$_{nap-5}$**. For Peaks L-M, the catenanes correspond most strongly with a combination of Fractions 1$_{nap-5}$-3$_{nap-5}$, all of which have N_c values > 4. Based on this evidence, it appears that Peaks L – M all correspond to variations of ***b*-19$_{nap-5}$**.

This analysis runs contrary to the expectation that the matching of linker and tail would cause **3$_{xan-6}$** and **19$_{nap-5}$** to have a similar distribution of architectures. In fact, the product distribution appears to more closely follows what is observed in **18$_{xan-5}$**, with the branched ***b*-19$_{nap-5}$** being the dominant poly[*n*]catenane architecture. This data suggests that the nature of the alkenyl chain plays a significant role in controlling the product architecture in the synthesis of poly[*n*]catenane

from their corresponding MSPs. It is worth noting that it is possible to use the ^{1}H NMR and GPC of the crude reaction mixture to obtain an average N_c of the entire poly[*n*]catenane sample synthesized (**Table 3.3**). Doing this shows that, irrespective the aromatic linker in the thread, the shorter 3-pentenyl tail results in a much higher N_c (4.4 or 5.4) than using the threads with the longer 4-hexenyl tail (N_c = 2.9 or 3).

Another important aspect of the product distribution analysis of $\mathbf{19_{nap\text{-}5}}$ was that no evidence was found for the formation of $\boldsymbol{c}\text{-}\mathbf{19_{nap\text{-}5}}$. This suggests that the use of the shorter $\mathbf{14_{nap\text{-}5}}$ thread makes it more difficult to form the *c*-poly[*n*]catenanes relative to the other threads. This is perhaps somewhat surprising as the MSP NMR data of the precursor $\mathbf{1{\cdot}14_{nap\text{-}5}{\cdot}Zn(II)_2}$ showed a higher percentage of *c*-MSP (**Figure 3.5b**) than in the xan-derivatives. To test this, the synthesis of $\boldsymbol{c}\text{-}\mathbf{19_{nap\text{-}5}}$ was attempted following the procedures used for creating cyclic catenane as was detailed in Chapter 2. In short, the MSP was reacted using lower reaction concentrations and Fe(II) as the templating metal ion.[2] In this experiment, no $\boldsymbol{c}\text{-}\mathbf{19_{nap\text{-}5}}$ could be isolated (**Figure 3.24**), supporting the idea that the shorter alkenyl chains disfavor the desired intramolecular ring closing reaction. It is worthwhile mentioning that the difficulty to ring-close the threads with the shorter alkenyl tails is also supported by the yields obtained for the synthesis of their corresponding macrocycles. The crude yield (from ^{1}H NMR) of $\mathbf{12_{xan\text{-}5}}$ and $\mathbf{15_{nap\text{-}5}}$ obtained from the ring closing of $\mathbf{11_{xan\text{-}5}}$ and $\mathbf{14_{nap\text{-}5}}$ were 35% and 27%, respectively. In contrast the conversion of $\mathbf{16_{nap\text{-}6}}$ to $\mathbf{17_{nap\text{-}6}}$ under similar reaction conditions occurred in a 47% crude yield.

If the shorter alkenyl chain hinders *c*- and *l*- poly[*n*]catenane formation, then it made sense to explore the formation of $\mathbf{20_{nap\text{-}6}}$, which has the longer hexenyl chain and the shorter aromatic (nap) linker. The deconvolution of **Figure 3.20d** was performed via the analysis of the fractionated samples in **Figure 3.25**. For this material, Peaks A and P were assigned based on the GPC trace of

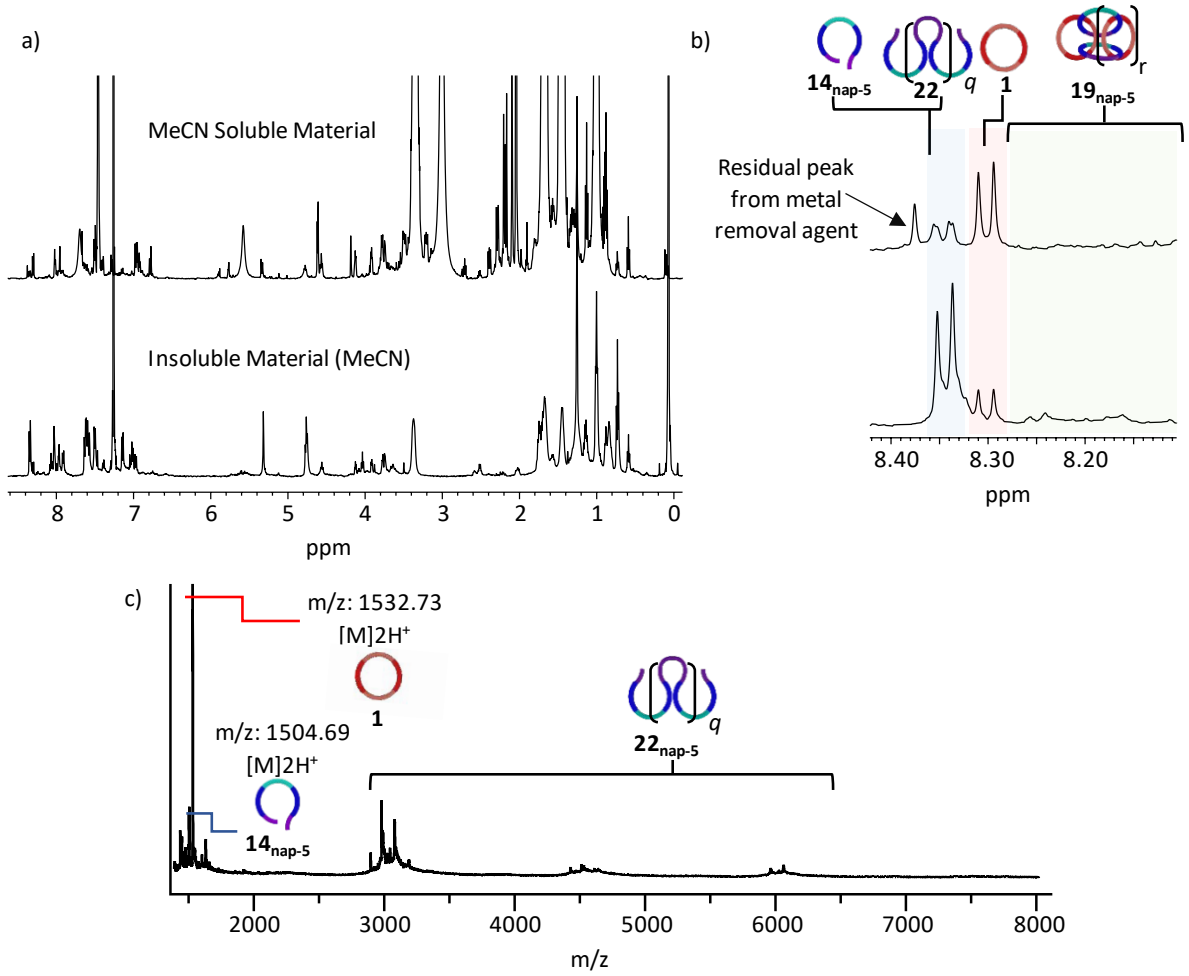

Figure 3.24 (a) Full ^{1}H NMR Spectrum for attempted synthesis of ***c*-19$_{nap-5}$**. During work-up procedure for cyclic catenane,[2] the demetallated crude mixture is washed with acetonitrile (MeCN). The majority of **1**, the Hoveyda-Grubbs catalyst, and residual demetallating agent are soluble in the MeCN and all ADMET byproduct (**22$_{nap-5}$**) and catenated material (**19$_{nap-5}$**) should crash out from the solution. The two samples (soluble and insoluble) were collected and fully dried. Both materials were fully soluble in $CDCl_3$, therefore both were able to be analyzed via ^{1}H NMR (500 MHz, $CDCl_3$, 25 °C). (b) ^{1}H NMR analysis of the H_{mpy} region (zoom). (c) Matrix-assisted laser desorption/ionization (MALDI) spectroscopy of the insoluble material to determine the ADMET (**22$_{nap-5}$**) formation.

the pure materials shown in **Figure 3.21**. Peak O was seen to correspond most closely with GPC Fraction 5$_{nap-6}$ with an N_c of 1.5 and a $\overline{DP} < 5$ (MALS). Based on the positioning of the peak, catenane content, and knowledge the previously analyzed of **3$_{xan-6}$**[3], this peak has been tentatively assigned to [2]catenane. GPC Fraction 4$_{nap-6}$ contains primarily Peak Q, with contributions from

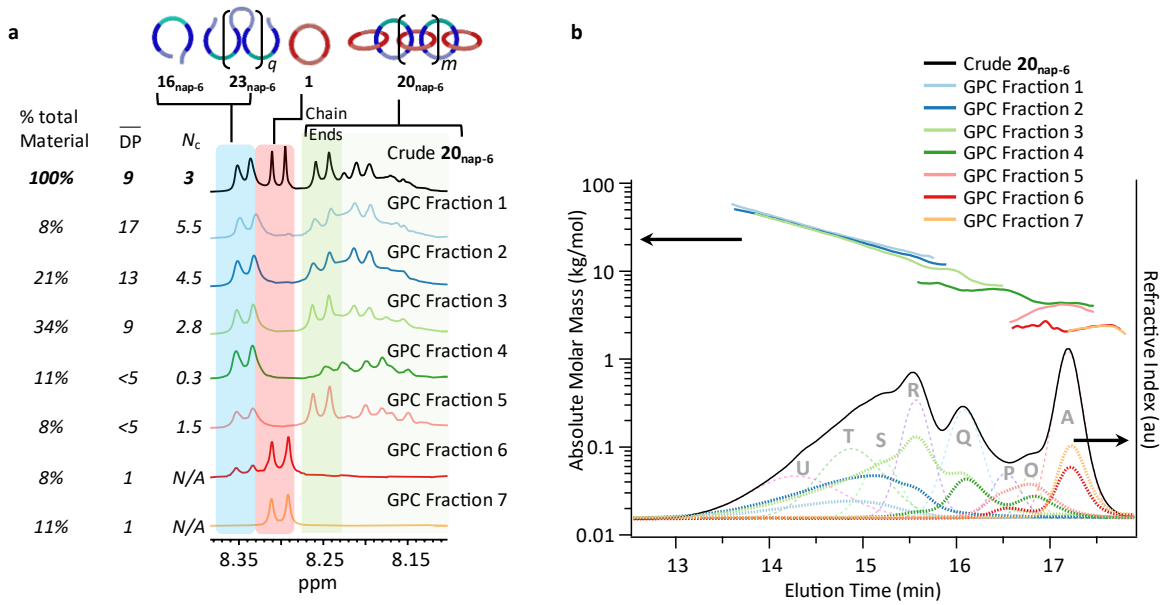

Figure 3.25 (a) ^{1}H NMR traces for all fractionated **20$_{nap-6}$** samples. (b) The GPC RI traces were collected for each fractionated sample. The combination of GPC and ^{1}H NMR was used to theorize the precise elution of the various catenane architectures in the crude GPC trace (assigned in Figure 3.20d, peaks overlayed). These assignments were obtained via analyzing the absolute molar mass of each fraction was obtain via the MALS analysis to yield the number average degree of polymerization ($\overline{DP_n}$ Equation 2.1) chain end calculations (N_c, Equation 2.4) for each fraction.

Peaks O (assigned to [2]catenane), P (**16$_{nap-6}$**), and R (tentatively assigned to ADMET **23$_{nap-6}$**). The N_c of GPC Fraction 4$_{nap-6}$ is 0.3, suggesting that majority of the catenated product in this sample is cyclic, therefore Peak Q is attributed to the ***c*-20$_{nap-6}$** product. Similar to the analysis of Peaks E and K, Peak R was assigned as the ADMET product **23$_{nap-6}$** based on the previously published work[3] and the prevalence of **23$_{nap-6}$** in the ^{1}H NMR Fractions 1$_{nap-6}$ – 4$_{nap-6}$. Peak S contains contributions from GPC Fractions 2$_{nap-6}$ and 3$_{nap-6}$. Fraction 3$_{nap-6}$ consists of primarily Peaks S and T, with contributions from peaks U, R, and Q. The N_c of Fraction 3$_{nap-6}$ is 2.8, suggesting that the primary architecture present in Fraction 3$_{nap-6}$ is ***l*-20$_{nap-6}$**, with contributions from the ***b*-20$_{nap-6}$** (which are currently attributed to the contributions from Peak U). Based on this analysis and previously published data,[3] Peak S is tentatively assigned to oligomeric ***l*-20$_{nap-6}$.** The analysis for

Peak T resembles that of Peak S, with the primary contributing GPC Fractions of $2_{nap\text{-}6}$ and $3_{nap\text{-}6}$. The increased molecular weight of this sample (as determined by MALS) is consistent with Peak T corresponding to the polymeric ***l*-20$_{nap\text{-}6}$**. Finally, Peak U corresponds most strongly with Fractions $1_{nap\text{-}6}$ and $2_{nap\text{-}6}$ that have N_c values > 4. Based on this observation, Peak U is assigned to ***b*-20$_{nap\text{-}6}$**.

The data from this analysis suggests that, while the use of the smaller nap-linker with the longer alkenyl tail result in significant drop in yield of the poly[*n*]catenane (ca. 60%), the distribution of poly[*n*]catenanes obtained (**Figure 3.20d**) appear similar to those observed in **3$_{xan\text{-}6}$**.[2,3] There are however a few notable differences. The mismatch of the shorter linker and the longer tail does yield a larger amount of the non-interlocked ADMET product (**23$_{nap\text{-}6}$**) than is observed in the **3$_{xan\text{-}6}$** synthesis, 22% vs 15% respectively based on NMR data (**Table 3.3**). A similar trend is observed in the GPC analysis, **Table 3.4**. As might be expected, a higher percentage of non-interlocked product corresponds to a drop in the overall degree of polymerization of **20$_{nap\text{-}6}$** (**Table 3.3**). However, as was the case for **3$_{xan\text{-}6}$**, the data obtained from the fractioned samples of **20$_{nap\text{-}6}$** is consistent with the formation of ***l*-**, ***c*-** and ***b*-20$_{nap\text{-}6}$** polymers. In fact, the overall product distribution of three **20$_{nap\text{-}6}$** architectures is most similar to that of the **3$_{xan\text{-}6}$**, with perhaps a slight

Table 3.4. Quantitative GPC deconvolution data for each new sample

Sample	Peak **1** (% total area)	Thread (% total area)	ADMET (% total area)	[2]Cat (% total area)	Cyclic (% total area)	[3]Cat (% total area)	Oligo (% total area)	Linear (% total area)	Branched (% total area)
3$_{xan\text{-}6}$	11	4	11	6	9	0	14	23	21
18$_{xan\text{-}5}$	23 (A)	5 (B)	12 (E)	*5*[a] (C)	*5*[a] (C)	17 (D)	0	0	38 (F,G)
19$_{nap\text{-}5}$	13 (A)	3 (H)	10 (K)	6 (I)	0	10 (J)	0	0	58 (L,M,N)
20$_{nap\text{-}6}$	21 (A)	5 (P)	16 (R)	3 (O)	13 (Q)	0	8 (S)	18 (T)	16 (U)

Peak name from Figure 5 indicated in parentheses.

(a) peak assigned as a combination of [2]catenane and cyclic catenane.

tendency to form more of the ***c*-20$_{nap-6}$**. This is consistent with the higher percentage of *c*-MSP that is formed in **1·16$_{nap-6}$·Zn(II)$_2$** relative to **1·2$_{xan-6}$·Zn(II)$_2$** (**Figure 3.5**).

3.5 Conclusions

This study has shown that MSP-templated synthetic approach to poly[*n*]catenanes is still possible with some structural variance in the thread-like monomer. The study also shows that careful design of the thread component can be employed to preferentially access different poly[*n*]catenane architectures by this approach. Perhaps the clearest example of this is the use of the shorter alkenyl tails, hinders the formation of the linear and cyclic poly[*n*]catenanes, and results in the formation of predominantly *b*-poly[*n*]catenanes. The short aromatic linker enhances this effect and thus suggest that **14$_{nap-5}$** is the thread of choice for targeting branched (or even network) polycatenanes while **2$_{xan-6}$** is still the best option for the accessing linear poly[*n*]catenanes. This type of information can be important when specifically targeting new classes of catenated polymers.

3.6 Experimental

3.6.1 Materials and Methods

Dichloromethane (DCM) was purchased from Acros Organics and distilled over CaH_2 under argon atmosphere before using. Dimethylformamide (DMF, anhydrous) was purchased from Fisher Chemical and was stored over molecular sieves. Deuterated solvents, containing tetramethylsilane (TMS) as internal standard, were purchased from Sigma Aldrich. Zinc di[bis(trifluoromethylsulfonyl)imide] was purchased from Strem Chemicals and stored in a nitrogen desiccator. All other chemicals were purchased from Sigma-Aldrich and used without further purification unless otherwise mentioned.

All silica column chromatography was performed on a Buchi Reveleris X2 Flash Chromatography System. Preparatory gel permeation chromatography was performed on a hand loaded column with Bio-Beads S-X1 gel and a mixture of 25% HPLC grade dimethylformamide (DMF) and 75% HPLC grade tetrahydrofuran (THF) as mobile phase. Silica preparatory plates were purchased from Analtech with a thickness of 1000 μm and a pore size of 6.0 Å.

NMR data was acquired on either a 400 MHz Bruker DRX spectrometer equipped with a BBO probe, using Topspin 1.3; or a 500 MHz Bruker Avance-II+ spectrometer equipped with a $^{1}H\{^{19}F, ^{13}C, ^{31}P\}$ QNP probe, using Topspin 2.1. Chemical shifts were calibrated with TMS for all measurements. Diffusion measurements were obtained using the 2D Bruker pulse program stebpgp1s, which includes a stimulated echo, bipolar gradient pulses, and one spoil gradient. The corresponding 1D pulse sequence stebpgp1s1d was used to optimize the parameters D20 ("big delta", the major diffusion delay) and P30 ("little delta", the diffusion gradient length), in accord with manufacturer-recommended methods.[6] The 2D data were acquired with a linear array of 32 diffusion gradient strengths (GPZ6 values) from 5% to 95%. ^{1}H T_1 measurements were taken using the standard Bruker inversion-recovery experiment "t1ir" with a relaxation delay D1 = 30 seconds and 16 interpulse recovery delays ranging from 0.001 to 16.0 seconds. T_1 values were obtained by fitting data to a recovery function using MestReNova software. All 1D and 2D NMR spectra were processed by either MestReNova software or Bruker Topspin 4.0.6. Diffusion coefficients were determined using the Bruker Topspin 4.0.6 direct exponential curve resolution algorithm (DECRA) plotting method.

Analytical GPC was performed on a Shimadzu Prominance LC system with PLgel Mixed-D columns using a mixture of 25% HPLC grade DMF and 75% HPLC grade THF as the eluent (1mL/min) at 25 °C. Characterization of the eluent occurred using Wyatt Dawn Helios MALS

(658 nm laser) and Wyatt Optilab T-rEX refractive index (RI) detectors. The *dn/dc* values for each new poly[*n*]catenane material were measured by injecting a series of diluted samples of each material (**18**$_{\text{xan-5}}$, **19**$_{\text{nap-5}}$, or **20**$_{\text{nap-6}}$) in 25% DMF/THF solution (concentration: 0.25, 0.5, 1.0, and 2.0 mg/mL) subsequently into the RI detector until receiving stable signal for each concentration and processed by Wyatt Astra software. The following *dn/dc* values were obtained: 0.2042 for **18**$_{\text{xan-5}}$, 0.1920 for **19**$_{\text{nap-5}}$, and 0.1829 for **20**$_{\text{nap-6}}$.

MALDI-TOF was measured by a Bruker Ultraflextreme MALDI TOF-TOF spectrometer using dithranol as the matrix and sodium trifluoroacetate as ionizer (when necessary).

3.6.2 Synthesis Procedures

3.6.2.1 Synthesis of Thread 11$_{\text{xan-5}}$

Step 1 of 2

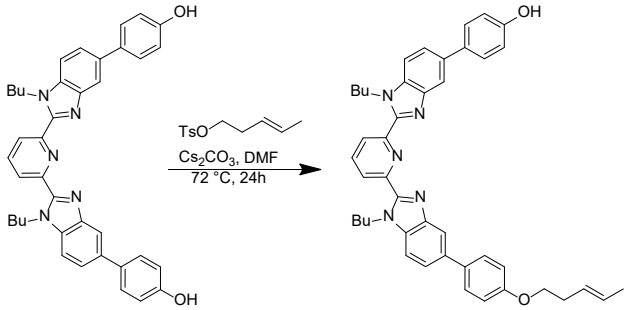

7 **24**

2 g (3.29 mmol) of **7**, 0.554 g (3.29 mmol, 1 eq.) of a literature prepared[7] tosylated 4-penten-1-ol and 3.2 g (9.82 mmol, 3 eq.) of $CsCO_3$ were added into a 50 mL round bottom flask equipped with stir bar. The flask was flushed with argon and then 22 mL anhydrous DMF was added by cannula. The reaction mixture was stirred at 72 °C for 24 hours. DMF was then removed under vacuum and the solid was stirred with chloroform and filtered. The filtrate was collected and the solvent removed under reduced pressure. The product was purified via flash column chromatography on silica gel (120 g) with a chloroform/methanol gradient from 100/0 to 97/3 (v/v) as the mobile phase (85 mL/min, 1 hour) followed by recrystallization in a mixture of chloroform and methanol. **S2**

was isolated as yellow crystals in 36% yield. ^{1}H NMR (400 MHz, $CDCl_3$) δ_H (ppm) 8.34 (d, J = 7.9 Hz, 2H), 8.07 (t, J = 7.9 Hz, 1H), 8.02 (dd, J = 8.0, 1.6 Hz, 2H), 7.65 – 7.53 (m, 6H), 7.50 (dd, J = 8.5, 1.6 Hz, 2H), 7.02 (d, J = 8.7 Hz, 2H), 6.96 (d, J = 8.7 Hz, 2H), 5.69 – 5.49 (m, 2H), 4.76 (t, J = 7.3 Hz, 4H), 4.03 (t, J = 6.9 Hz, 2H), 2.51 (q, J = 6.7 Hz, 2H), 1.76 (q, J = 7.5 Hz, 4H), 1.71 (dd, J = 5.9, 1.3 Hz, 3H), 1.15 (h, J = 7.4 Hz, 4H), 0.73 (t, J = 7.3 Hz, 6H). ^{13}C NMR (101 MHz, $CDCl_3$) δ_C (ppm) 158.4, 156.3, 150.6, 150.5, 149.8, 149.7, 143.1, 142.9, 138.4, 136.7, 136.4, 135.3, 135.2, 134.1, 133.5, 128.6, 128.4, 127.8, 126.8, 125.7, 123.3, 117.9, 117.8, 116.2, 115.0, 110.6, 68.0, 44.8, 32.6, 32.2, 19.9, 18.1, 13.5. MALDI-TOF MS: m/z 676 ($[M]H^+$).

Step 2 of 2

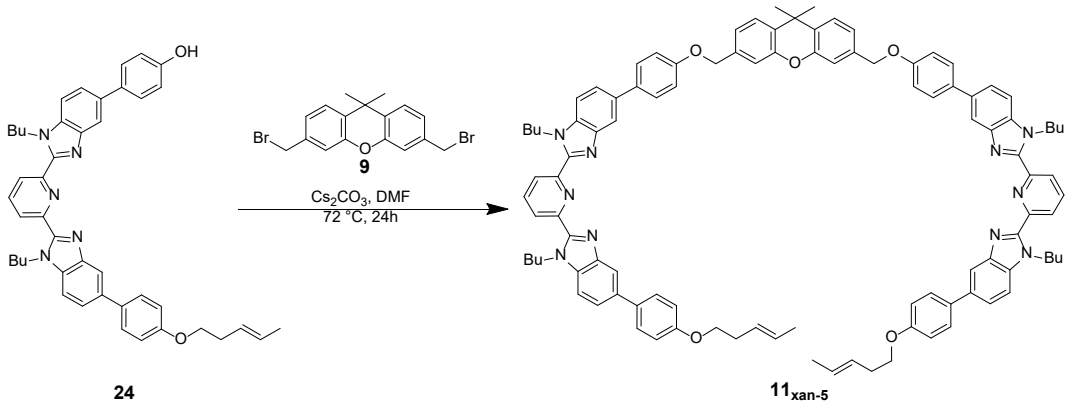

Step 2: To a 10 mL round bottom flask equipped with stir bar, 500 mg (0.74 mmol) of **24**, 146 mg (0.37 mmol, 0.5 eq.) of **9** and 352 mg (1.08 mmol, 1.5 eq.) of anhydrous cesium carbonate was added, followed by flushing with argon. Then 3 mL anhydrous DMF was injected into the reaction. The mixture was stirred at 72 °C for 24 hours. DMF was then removed under vacuum and the solid was stirred with chloroform and filtered. The filtrate was collected and the solvent removed under reduced pressure. The product purified by flash column chromatography on silica gel (80 g) with a chloroform/methanol gradient from 99.5/0.5 to 99/1 (v/v) as the mobile phase (60 mL/min, 30

minutes), followed by recrystallization in a mixture of chloroform and methanol. Yield of **11**$_{xan-5}$: 38% as an off-white solid. ^{1}H NMR (400 MHz, $CDCl_3$) δ_H (ppm) 8.35 (d, J = 7.9 Hz, 4H), 8.07 (t, J = 7.9 Hz, 2H), 8.03 (dd, J = 3.8, 1.6 Hz, 4H), 7.67 – 7.54 (m, 12H), 7.54 – 7.43 (m, 6H), 7.20 (dd, J = 6.3, 1.9 Hz, 4H), 7.12 (d, J = 8.9 Hz, 4H), 7.02 (tt, J = 8.7, 7.0, 6.6 Hz, 4H), 5.69 – 5.48 (m, 4H), 5.12 (s, 4H), 4.76 (t, J = 7.3 Hz, 8H), 4.03 (t, J = 6.8 Hz, 4H), 2.56 – 2.46 (m, 4H), 1.75 (p, J = 8.7, 7.5, 6.5 Hz, 8H), 1.71 (d, J = 5.5 Hz, 6H), 1.15 (h, J = 7.4 Hz, 8H), 0.73 (t, J = 7.4 Hz, 12H). ^{13}C NMR (101 MHz, $CDCl_3$) δ_C (ppm) 157.3, 157.1, 149.71, 149.68, 149.5, 149.0, 142.4, 137.2, 135.7, 135.2, 135.1, 134.5, 134.5, 133.6, 133.2, 128.6, 127.4, 127.3, 126.7, 125.7, 125.6, 124.5, 122.1, 122.1, 121.1, 117.1, 117.0, 114.4, 114.2, 113.9, 109.5, 109.4, 68.5, 66.9, 43.8, 32.9, 31.5, 31.2, 18.9, 17.1, 12.5. MALDI-TOF MS: m/z 1587 ([M]2H^{+}).

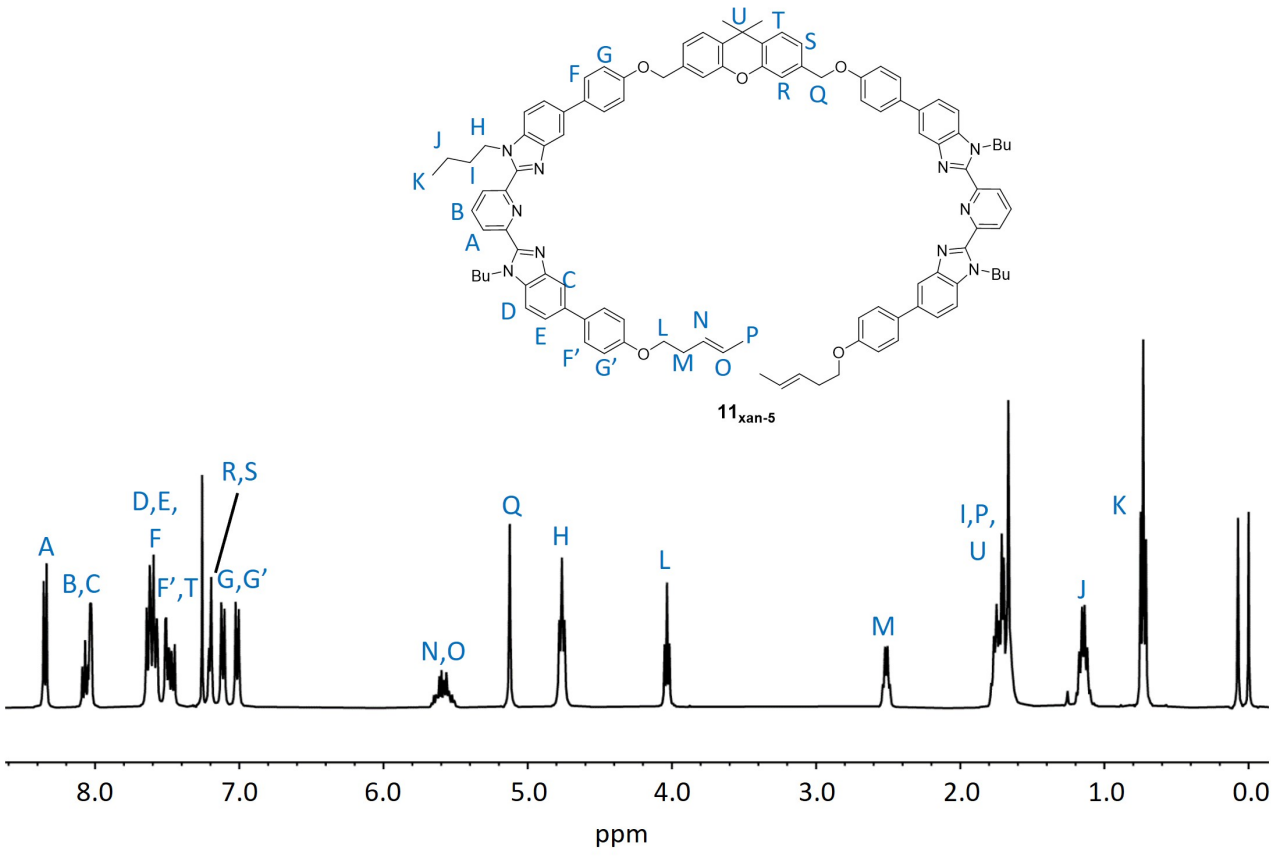

3.6.2.2 Synthesis of Thread $14_{nap\text{-}5}$

Step 1 of 2[8]

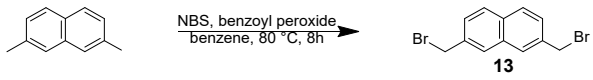

2,7-dimethylnaphthalene (500 mg, 3.2 mmol) was dissolved in benzene (64 mL, 50 mM) and stirred under argon at room temperature. *N*-bromosuccinimide (NBS) was then added (1.31 g, 7.4 mmol), followed by benzoyl peroxide (387 mg, 1.6 mmol). The solution was stirred and heated at reflux (80 °C) for 8 hours. After completely reacting, the reaction was cooled to 0 °C and was filtered to remove precipitated succinimide. The filtrate was concentrated under pressure and dissolved in a minimal amount of warm $CHCl_3$, followed by a generous amount of hexanes at RT. The suspension was cooled in the freezer overnight, and the resulting precipitate was filtered. Yield of **13**: 33%, beige solid. ^{1}H NMR (500 MHz, $CDCl_3$) δ_H (ppm) 7.82 (d, J = 8.6 Hz, 2H), 7.81 (d, J = 1.8 Hz, 2H), 7.52 (dd, J = 8.4, 1.8 Hz, 2H), 4.66 (s, 4H). ^{13}C NMR (101 MHz, $CDCl_3$) δ_C (ppm) 135.86, 133.0, 132.7, 128.6, 127.9, 127.5, 33.8.

Step 2 of 2

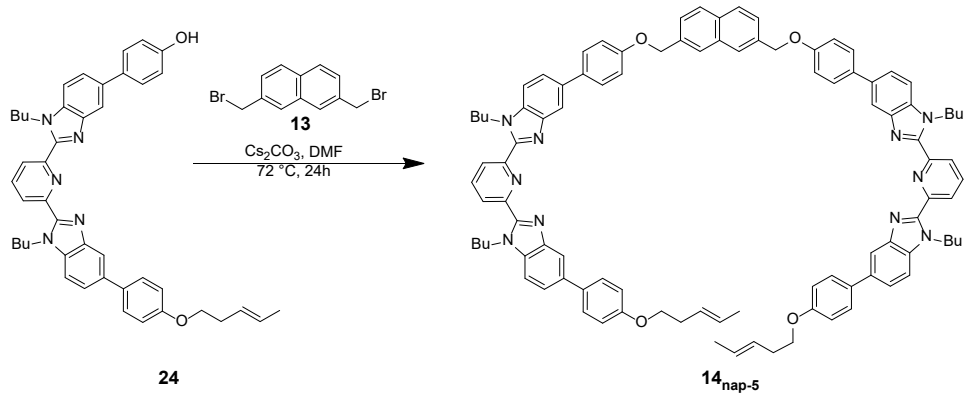

To a 10 mL round bottom flask equipped with stir bar, 500 mg (0.74 mmol) of **24**, 116 mg (0.37 mmol, 0.5 eq.) of **9**, and 689 mg (1.08 mmol, 1.5 eq.) of anhydrous cesium carbonate was added,

followed by flushing with argon. Then 3 mL anhydrous DMF was injected into the reaction. The mixture was stirred at 72 °C for 24 hours. DMF was then removed under vacuum and the solid was stirred with chloroform and filtered. The filtrate was collected and the solvent removed under reduced pressure. The product purified via flash column chromatography on silica gel (80 g) with a chloroform/methanol gradient from 100/0 to 98/2 (v/v) as the mobile phase (60 mL/min, 35 minutes), followed by recrystallization in a mixture of chloroform and methanol. Yield of **14**$_{\textbf{nap-5}}$: 36%, white solid. ^{1}H NMR (400 MHz, $CDCl_3$) δ_H (ppm) 8.35 (d, J = 7.9 Hz, 4H), 8.07 (t, J = 7.8 Hz, 2H), 8.03 (d, J = 2.8 Hz, 4H), 7.96 (s, 2H), 7.91 (d, 8.3 Hz, 2H), 7.65-7.56 (overlapped, 14H), 7.50 (dd, J = 3.5 Hz, 4H), 7.14 (d, J = 8.6 Hz, 4H), 7.01 (d, J = 8.6 Hz, 4H), 5.58 (m, J = 6.3 Hz, 4H), 5.32 (s, 4H), 4.76 (t, J = 7.3 Hz, 8H), 4.03 (t, J = 6.8 Hz, 4H), 2.51 (q, J = 6.6 Hz, 4H), 1.75 (p-overlapped, 8H), 1.70 (d- overlapped, 6H) 1.15 (h, J = 7.5 Hz, 8H), 0.73 (t, J = 7.3 Hz, 12H). ^{13}C NMR (101 MHz, $CDCl_3$) δ_C (ppm) 158.5, 158.3, 150.9, 150.8, 150.2, 150.1, 143.6, 138.3, 136.4, 136.2, 135.7, 135.6, 135.2, 134.8, 134.3, 133.4, 132.9, 128.6, 128.5, 128.5, 127.9, 126.9, 126.5, 125.7, 125.6, 123.3, 123.2, 118.3, 118.2, 115.5, 115.1, 110.7, 110.6, 70.4, 68.1, 44.9, 32.7, 32.32, 20.0, 18.2, 13.7. MALDI-TOF MS: m/z 1505 ([M]2H$^+$).

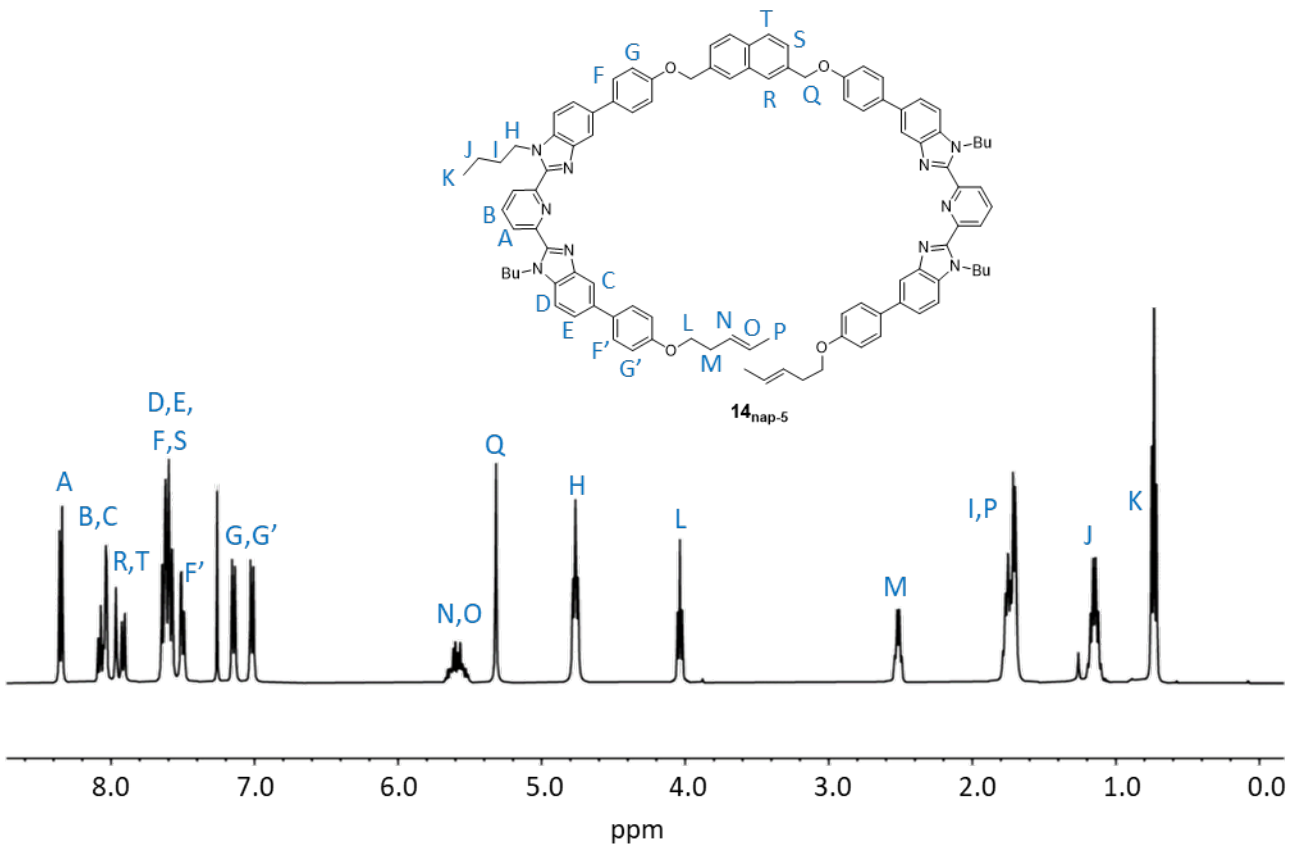

3.6.2.3 Synthesis of Thread 16_{nap-6}

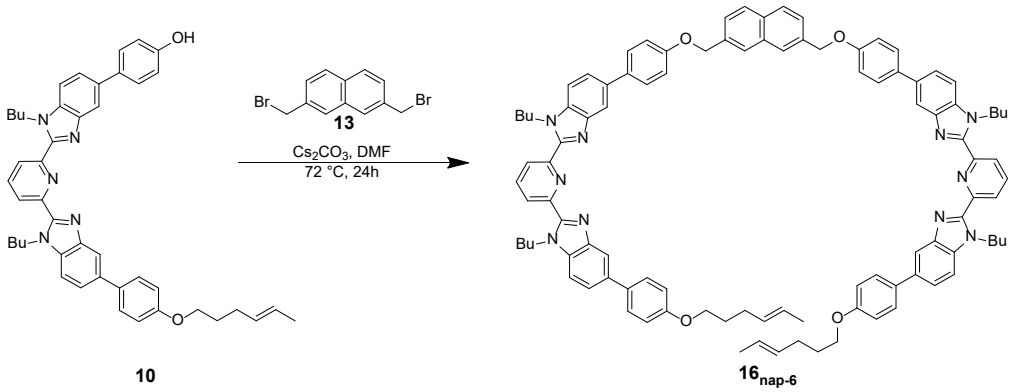

To a 10 mL round bottom flask equipped with stir bar, 500 mg (0.74 mmol) of **10**, 113 mg (0.37 mmol, 0.5 eq.) of **13** and 352 mg (1.08 mmol, 1.5 eq.) of anhydrous cesium carbonate was added, followed by flushing with argon. Then 3 mL anhydrous DMF was injected into the reaction. The mixture was stirred at 72 °C for 24 hours. DMF was then removed under vacuum and the solid

was stirred with chloroform and filtered. The filtrate was collected and the solvent removed under reduced pressure. The product purified via column chromatography on silica gel (80 g) with a chloroform/methanol gradient from 100/0 to 97/3 (v/v) as the mobile phase (60 mL/min, 40 minutes), followed by recrystallization in a mixture of chloroform and methanol. Purified yield of **16**$_{\textbf{nap-6}}$: 33% as a yellow solid. ^{1}H NMR (400 MHz, $CDCl_3$) δ 8.35 (d, J = 7.9 Hz, 4H), 8.07 (t, J = 7.9 Hz, 2H), 8.03 (d, J = 1.3 Hz, 4H), 7.96 (s, 2H), 7.91 (d, 8.4 Hz, 2H), 7.65-7.56 (overlapped, 14H), 7.50 (dd, J = 3.4 Hz, 4H), 7.14 (d, J = 8.7 Hz, 4H), 7.01 (d, J = 8.7 Hz, 4H), 5.50 (m, J = 3.4 Hz, 4H), 5.31 (s, 4H), 4.76 (t, J = 7.3 Hz, 8H), 4.02 (t, J = 6.5 Hz, 4H), 2.19 (q, J = 6.5 Hz, 4H), 1.88 (p, J = 6.9 Hz, 4H), 1.74 (p, J = 7.3 Hz, 8H), 1.66 (d, J = 4.3 Hz, 6H) 1.15 (h, J = 7.5 Hz, 8H), 0.73 (t, J = 7.3 Hz, 12H). ^{13}C NMR (101 MHz, $CDCl_3$) δ 158.6, 158.2, 150.9, 150.8, 150.2, 150.1, 143.5, 138.3, 136.3, 136.2, 135.7, 135.6, 135.2, 134.8, 134.2, 133.3, 132.9, 130.4, 128.6, 128.5, 128.4, 126.5, 125.8, 125.6, 125.6, 123.2, 118.2, 118.2, 110.6, 110.5, 70.3, 67.5, 44.9, 32.3, 29.2, 29.1, 20.0, 18.1, 13.6. MALDI-TOF MS: m/z 1533 ([M]2H^{+}).

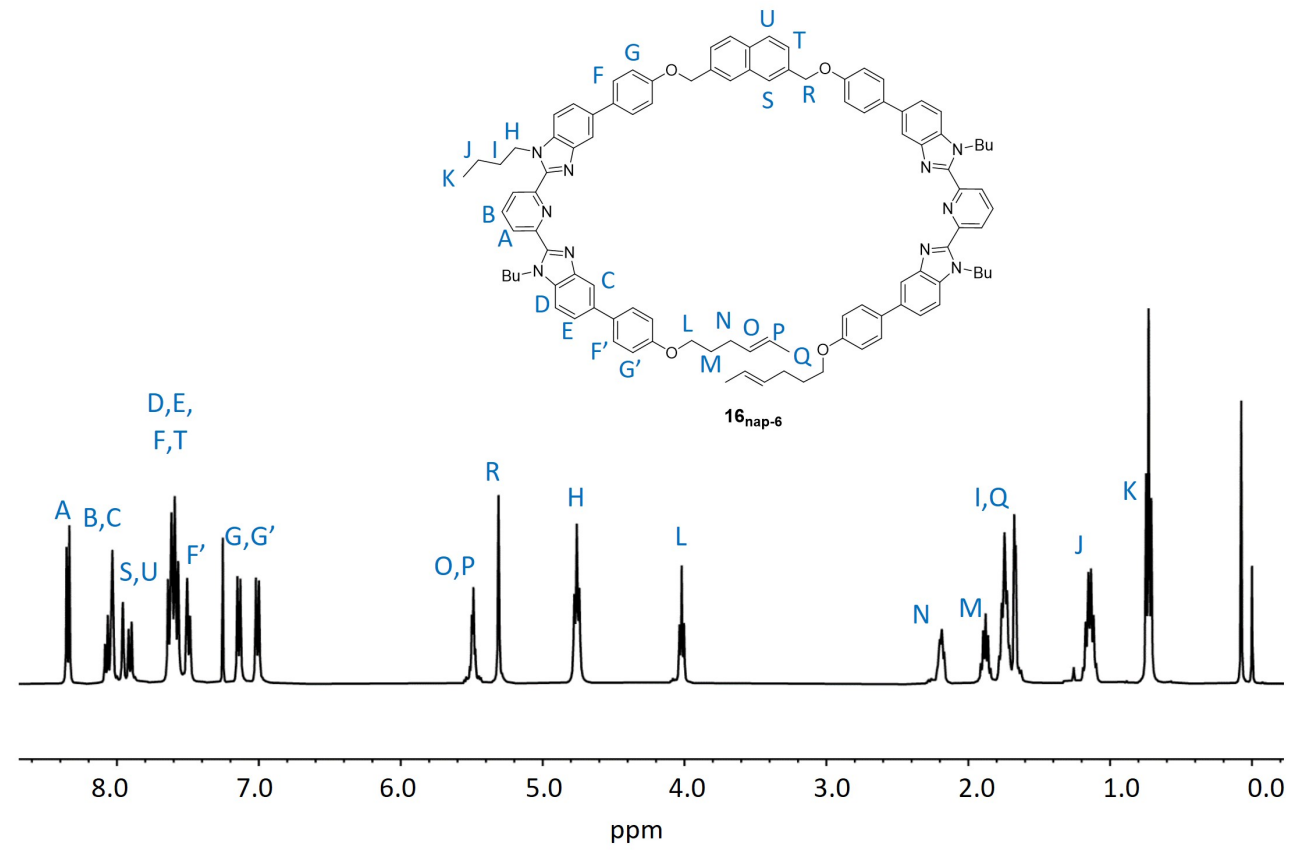

3.6.2.4 Synthesis of $12_{xan\text{-}5}$

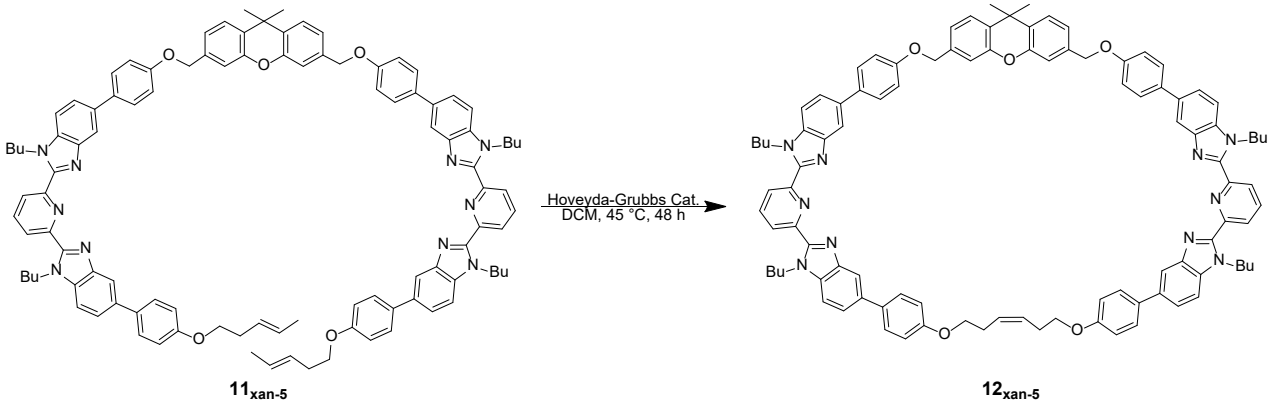

In a 250 mL round bottom flask equipped with stir bar and water condenser, 250 mg (0.158 mmol) of **11**$_{xan\text{-}5}$ was dissolved in 50 mL of DCM. The solution was stirred and heated to reflux followed by bubbling argon for 30 minutes to degas the solvent. The Hoveyda-Grubbs catalyst (12.6 mg) was injected in additional solvent to return the solution to the initial concentration (to account for

any solvent lost during the initial bubbling step, approximately 2 mL of DCM). After the catalyst, a second degassing argon bubbling step for approximately 30 minutes the reaction was allowed to react for 24 hours. After 24 hours, a second catalyst addition step occurred (following the same degassing and addition procedure as before). When purging is stopped, the evaporation of DCM is negligible and the total concentration of $\mathbf{11}_{\mathbf{xan\text{-}5}}$ remains approximately constant (ca. 2.5 mM) through the entire reaction. The reaction solution was kept at reflux for another 24 hours. At which point the solution was cooled to room temperature followed by the addition of excess ethyl vinyl ether (~1mL) to deactivate the catalyst. The solvent was removed under vacuum and the product purified by repeated column chromatography (the flash column system was not used, column was run by hand) with triethylamine neutralized silica gel and a chloroform/methanol gradient from 100/0 to 98/2 (v/v) as the mobile phase (one hour at 100/0, 45 minutes at 99.5/0.5, 45 minutes at 99/1, 45 minutes at 98/2) and repeated recrystallization with a mixture of chloroform and methanol. Crude ^{1}H NMR Yield of $\mathbf{12}_{\mathbf{xan\text{-}5}}$: 35% Isolated yield: 5%. The product is white waxy solid which is a mixture of cis and trans isomers. ^{1}H NMR (400 MHz, $CDCl_3$, *cis/trans* isomers are partially overlapped) δ_H (ppm) 8.30 (dd, J = 7.8, 3.7 Hz, 4H), 8.05 – 7.95 (m, 4H), 7.93 (s, 2H), 7.54 – 7.44 (m, 12H), 7.44 – 7.35 (m, 6H), 7.16 – 7.06 (m, 4H), 7.01 – 6.88 (m, 8H), 5.74 – 5.66 (m, 2H), 5.25 (s, 4H), 4.66 (p, J = 14.8, 7.3 Hz, 8H), 4.06 (t, J = 5.9 Hz, 4H), 2.58 – 2.43 (m, 4H), 1.72 – 1.60 (m, 16H), 1.10 – 1.02 (m, 8H), 0.68 – 0.57 (m, 12H). ^{13}C NMR (101 MHz, $CDCl_3$, *cis/trans* isomers are partially overlapped) δ_C (ppm) 158.65, 157.61, 150.74, 150.68, 150.61, 150.16, 143.54, 143.47, 138.23, 137.62, 136.33, 136.28, 135.58, 134.57, 134.28, 129.37, 129.26, 128.52, 128.42, 126.81, 125.59, 123.35, 121.26, 118.14, 115.77, 115.48, 115.20, 114.63, 110.56, 69.29, 68.05, 44.81, 33.97, 32.70, 32.61, 32.27, 29.86, 22.85, 19.96, 14.27, 13.63, 13.62. MALDI-TOF MS: m/z 1531 ([M]2H^{+}).

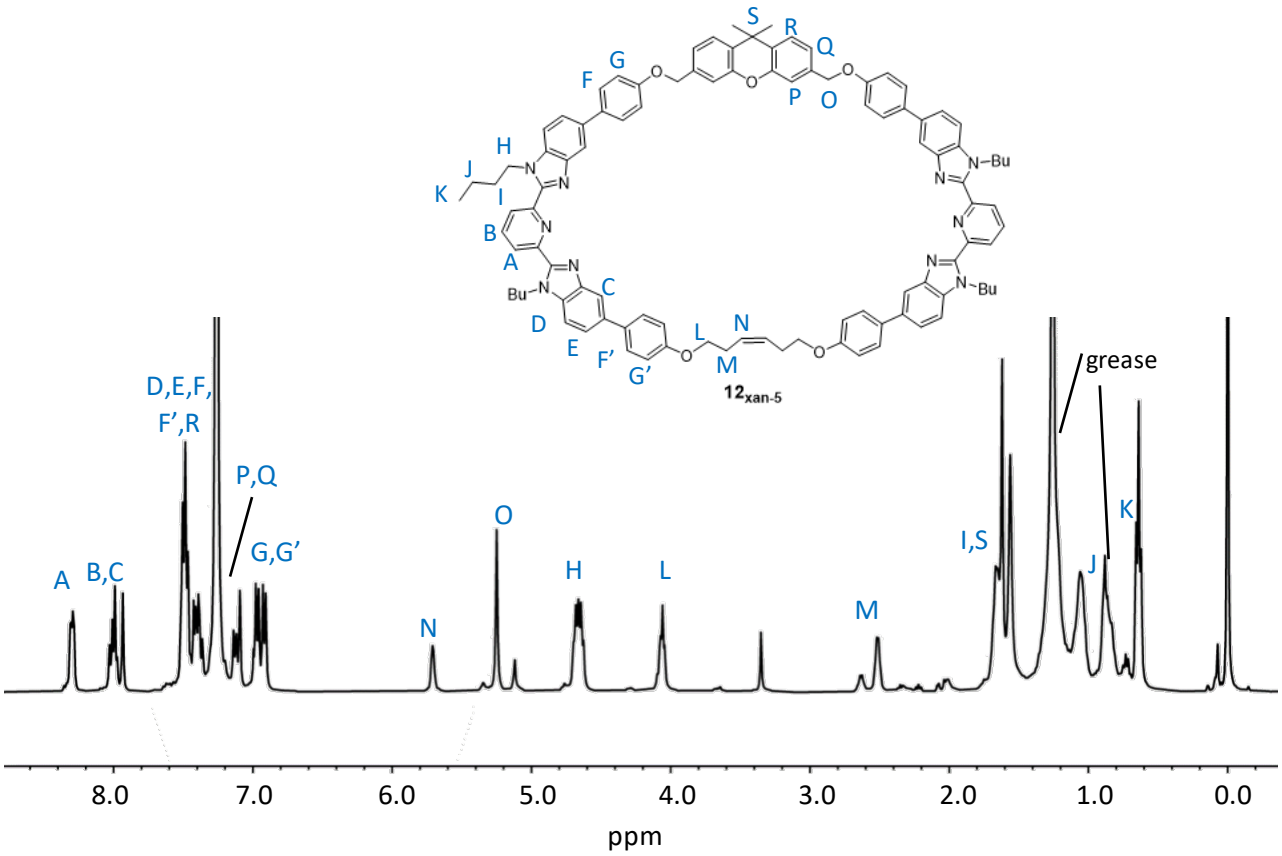

3.6.2.5 Synthesis of $15_{nap\text{-}5}$

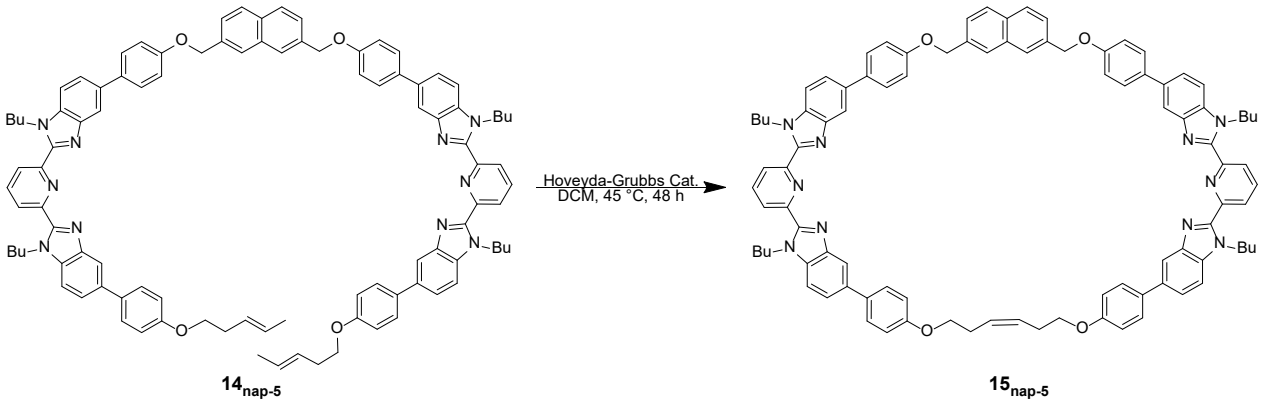

$15_{nap\text{-}5}$ was synthesized in the same way as **$12_{xan\text{-}5}$** with 472 mg of **$14_{nap\text{-}5}$** (0.308 mmol) dissolved in 123 mL of DCM with 24.6 mg of catalyst in 4 mL DCM for each addition. The product purified by repeated column chromatography (the flash column system was not used, column was run by

hand) with triethylamine neutralized silica gel and a chloroform/methanol gradient from 100/0 to 99/1 (v/v) as the mobile phase (one hour at 100/0, 45 minutes at 99.5/0.5, one hour at 99/1) and repeated recrystallization with a mixture of chloroform and methanol. Crude ^{1}H NMR Yield of **15$_{nap\text{-}5}$**: 27% Isolated yield: 4% as a white waxy solid that is a mixture of *cis* and *trans* isomers. ^{1}H NMR (400 MHz, $CDCl_3$, *cis/trans* isomers are partially overlapped) δ_H (ppm) 8.32 – 8.25 (m, 4H), 8.07 – 7.95 (m, 4H), 7.93 – 7.90 (m, 2H), 7.88 – 7.79 (m, 4H), 7.57 – 7.38 (m, 16H), 7.34 (d, J = 8.5 Hz, 2H), 7.01 (d, J = 8.6 Hz, 4H), 6.91 (d, J = 8.4 Hz, 4H), 5.71 (d, J = 4.5 Hz, 2H), 5.43 (s, 4H), 4.63 (dt, J = 16.1, 7.2 Hz, 8H), 4.14 – 3.98 (m, 4H), 2.57 (dd, J = 47.9, 5.8 Hz, 4H), 1.72 – 1.59 (m, 8H), 1.11 – 0.97 (m, 8H), 0.68 – 0.57 (m, 12H). ^{13}C NMR (101 MHz, $CDCl_3$, *cis/trans* isomers are partially overlapped)) δ_C (ppm) 158.67, 157.69, 150.70, 150.16, 143.46, 138.22, 136.32, 136.16, 135.94, 135.55, 134.62, 134.34, 134.25, 133.44, 129.30, 128.64, 128.53, 128.48, 128.40, 128.34, 125.57, 124.65, 123.34, 118.11, 118.08, 115.98, 115.49, 115.22, 110.58, 110.52, 70.16, 68.09, 67.59, 44.82, 32.60, 32.25, 32.08, 29.86, 22.84, 19.95, 14.27, 13.62. MALDI-TOF MS: m/z 1448 ([M]2H^{+}).

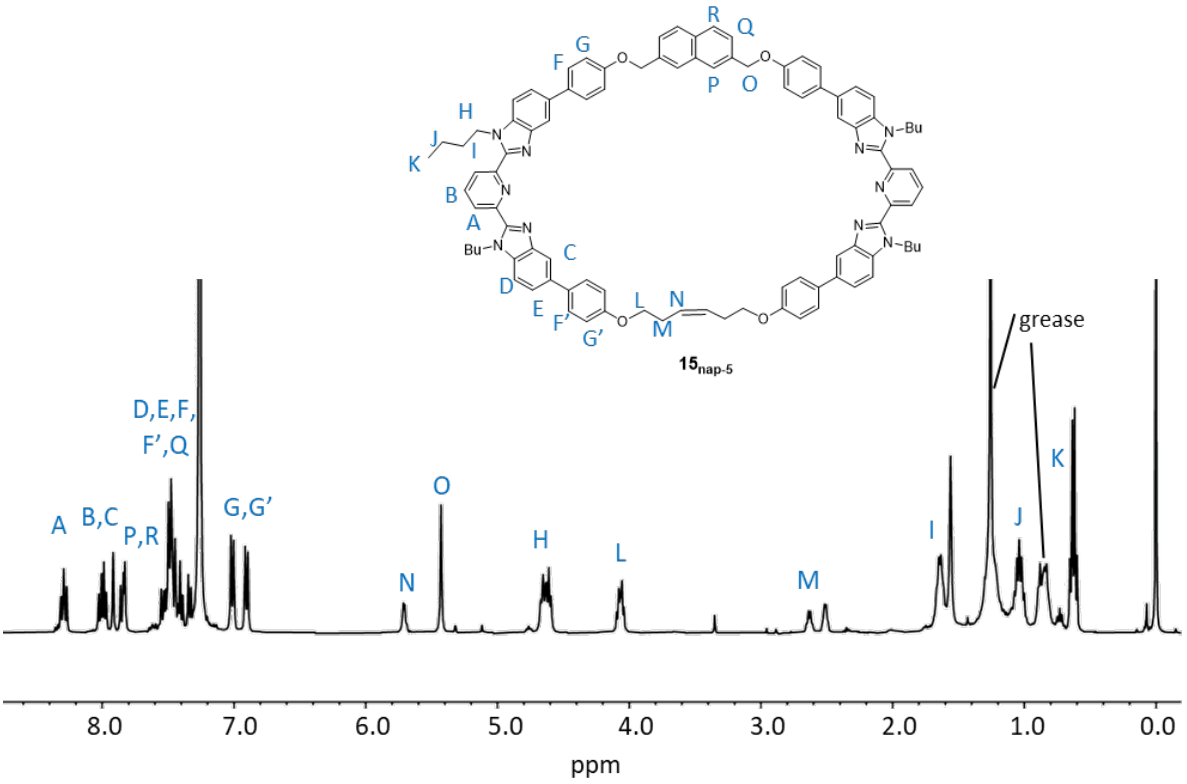

3.6.2.6 Synthesis of 17_{nap-6}

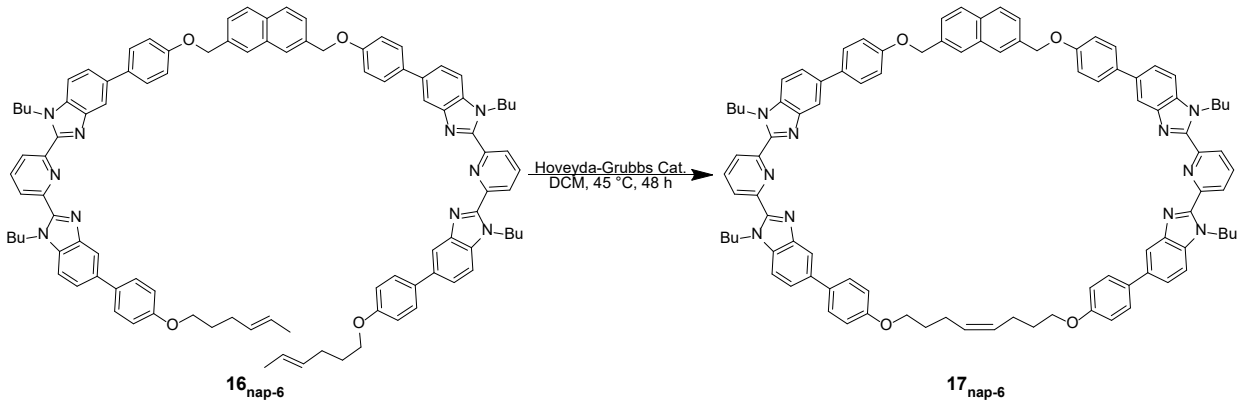

This compound was synthesized in the same way as **12**$_{xan-5}$ with 350 mg of **16**$_{nap-6}$ (0.233 mmol) dissolved in 93 mL of DCM with 18.6 mg of catalyst in 3 mL DCM for each addition. The product purified by repeated column chromatography (the flash column system was not used, column was run by hand) with triethylamine neutralized silica gel and a chloroform/methanol gradient from 100/0 to 99/1 (v/v) as the mobile phase (one hour at 100/0, 45 minutes at 99.5/0.5, one hour at

99/1) and repeated recrystallization with a mixture of chloroform and methanol. Crude ^{1}H NMR Yield: 46% Isolated yield: 4% as white waxy solid which is a mixture of *cis* and *trans* isomers. ^{1}H NMR (400 MHz, $CDCl_3$, *cis/trans* isomers are partially overlapped) δ_H (ppm) 8.33 – 8.23 (m, 4H), 8.06 – 7.96 (m, 4H), 7.94 – 7.89 (m, 2H), 7.88 – 7.77 (m, 4H), 7.58 – 7.36 (m, 16H), 7.32 (d, J = 8.3 Hz, 2H), 7.02 (d, J = 8.6 Hz, 4H), 6.94 (d, J = 8.7 Hz, 4H), 5.59 – 5.48 (m, 2H), 5.43 (s, 4H), 4.63 (dt, J = 19.2, 7.3 Hz, 8H), 4.00 (t, J = 6.5 Hz, 4H), 2.31 – 2.19 (m, 4H), 1.90 (p, J = 6.7 Hz, 4H), 1.76 – 1.60 (m, 8H), 1.03 (hept, J = 15.1, 7.5 Hz, 8H), 0.68 – 0.56 (m, 12H). ^{13}C NMR (126 MHz, $CDCl_3$, *cis/trans* isomers are partially overlapped) δ_C (ppm) 158.50, 157.68, 150.73, 150.60, 150.15, 143.50, 143.46, 138.22, 136.29, 136.16, 135.90, 135.54, 135.51, 134.62, 134.13, 133.42, 132.64, 130.60, 128.63, 128.52, 128.48, 128.43, 125.62, 125.58, 125.56, 124.65, 123.33, 118.08, 116.02, 115.99, 115.05, 110.60, 110.52, 70.15, 66.86, 44.84, 44.76, 32.27, 32.24, 29.86, 28.76, 28.62, 19.94, 13.62, 13.61. MALDI-TOF MS: m/z 1476 ([M]2H^{+}).

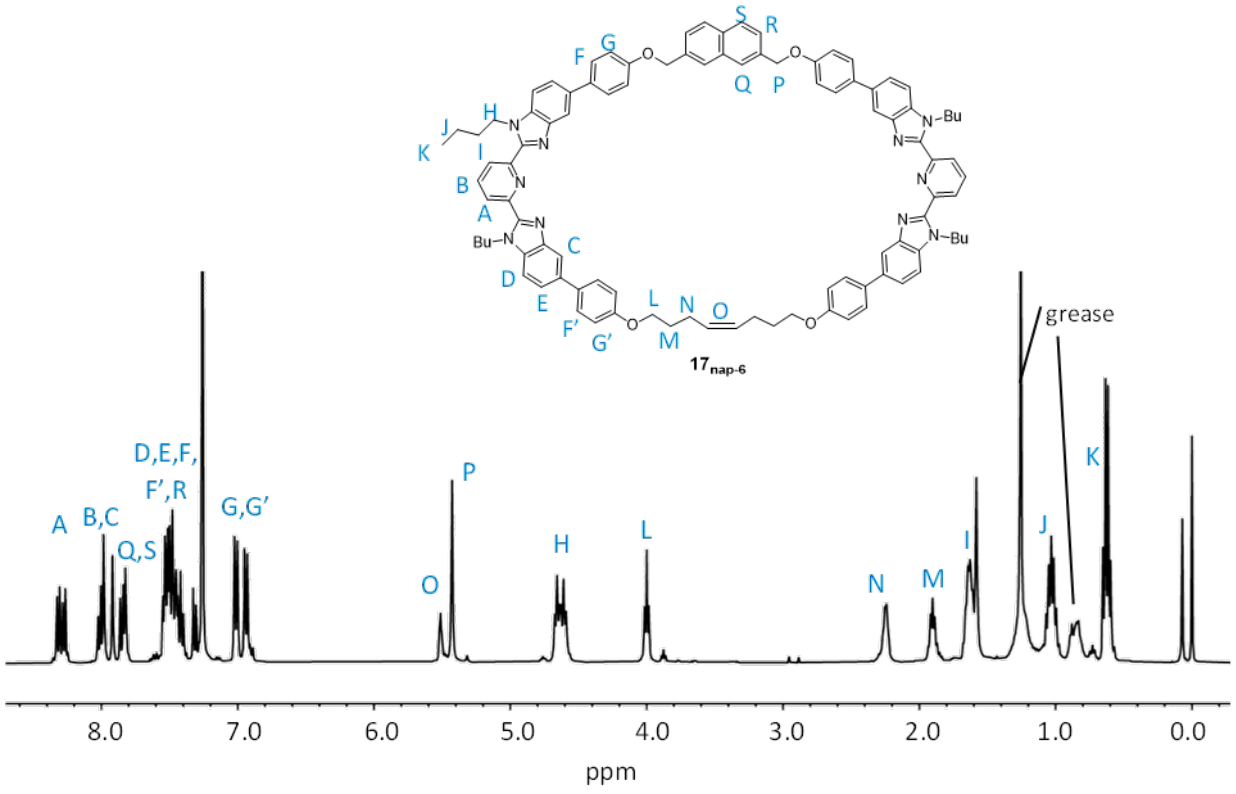

3.6.2.7 Synthesis of $\mathbf{21}_{\mathbf{xan\text{-}5}}$, $\mathbf{22}_{\mathbf{nap\text{-}5}}$, $\mathbf{23}_{\mathbf{nap\text{-}6}}$

In a 5 mL conical vial equipped with stir bar and water condenser, 50 mg (0.033 mmol) of $\mathbf{11}_{\mathbf{xan\text{-}5}}$ was dissolved in 0.66 mL of DCM. The solution was stirred and heated to reflux followed by bubbling argon for 5 minutes to remove dissolved oxygen. Then 0.26 mg of catalyst (dissolved in 0.2 mL of DCM) was injected, and the solution was bubbled with argon for additional 10 mins. After 24 hours, 0.26 mg of catalyst (dissolved in 0.2mL of DCM) was injected, and the solution was bubbled with argon for additional 10 mins. During each argon purging step ~0.2 mL of DCM was lost due to evaporation, which is offset by the addition of the catalyst in 0.2 mL of DCM. When purging is stopped, the evaporation of DCM was negligible and the concentration remains approximately constant (ca. 50 mM with respect to $\mathbf{11}_{\mathbf{xan\text{-}5}}$ and repeat units derived from $\mathbf{11}_{\mathbf{xan\text{-}5}}$) through the entire reaction. The reaction solution was kept at reflux for another 24 hours for a total of 48 hours reacting. At which point the solution was cooled to room temperature followed by the addition of excess ethyl vinyl ether (~0.2 mL) to deactivate the catalyst. Then, the reaction mixture was precipitated into 20 mL cold MeCN under stirring. The suspension was cooled in a freezer (–18 °C) overnight to allow complete precipitation. The product was collected by filtration and washed three times with cold MeCN. Yield is quantitative and the product ($\mathbf{21}_{\mathbf{xan\text{-}5}}$) is obtained as a brown solid. The color is due to the trace amount of residue deactivated catalyst.

The procedure was repeated with both $\mathbf{22}_{\mathbf{nap\text{-}5}}$ and $\mathbf{23}_{\mathbf{nap\text{-}6}}$.

$\mathbf{21}_{\mathbf{xan\text{-}5}}$ ^{1}H NMR (400 MHz, $CDCl_3$) δ_H (ppm) 8.35 (d, J = 7.9 Hz, 4H), 8.07 (t, J = 7.8 Hz, 2H), 8.03 (s, 4H), 7.66 – 7.55 (m, 12H), 7.48 (dd, J = 16.4, 8.5 Hz, 6H), 7.23 – 7.08 (m, 10H), 7.03 (d, J = 8.4 Hz, 4H), 5.81-5.65 (m, 2H), 5.12 (s, 4H), 4.76 (t, J = 7.3 Hz, 8H), 4.08 (t, J = 6.3 Hz, 4H), 2.70-2.59 (m, 4H), 1.74 (q, J = 7.5 Hz, 4H), 1.60 (s, 6H), 1.14 (h, J = 7.3 Hz, 8H), 0.73 (t, J

= 7.3 Hz, 12H). ^{13}C NMR (101 MHz, $CDCl_3$) δ_C (ppm) 158.4, 158.3, 150.9, 150.6, 150.2, 149.6, 143.6, 138.3, 136.8, 136.4, 136.3, 135.7, 135.6, 134.8, 134.5, 129.8, 128.7, 128.6, 128.5, 126.7, 125.7, 123.3, 122.3, 118.3, 115.6, 115.4, 115.1, 110.6, 69.7, 67.9, 44.9, 34.1, 32.7, 32.3, 20.0, 13.7.

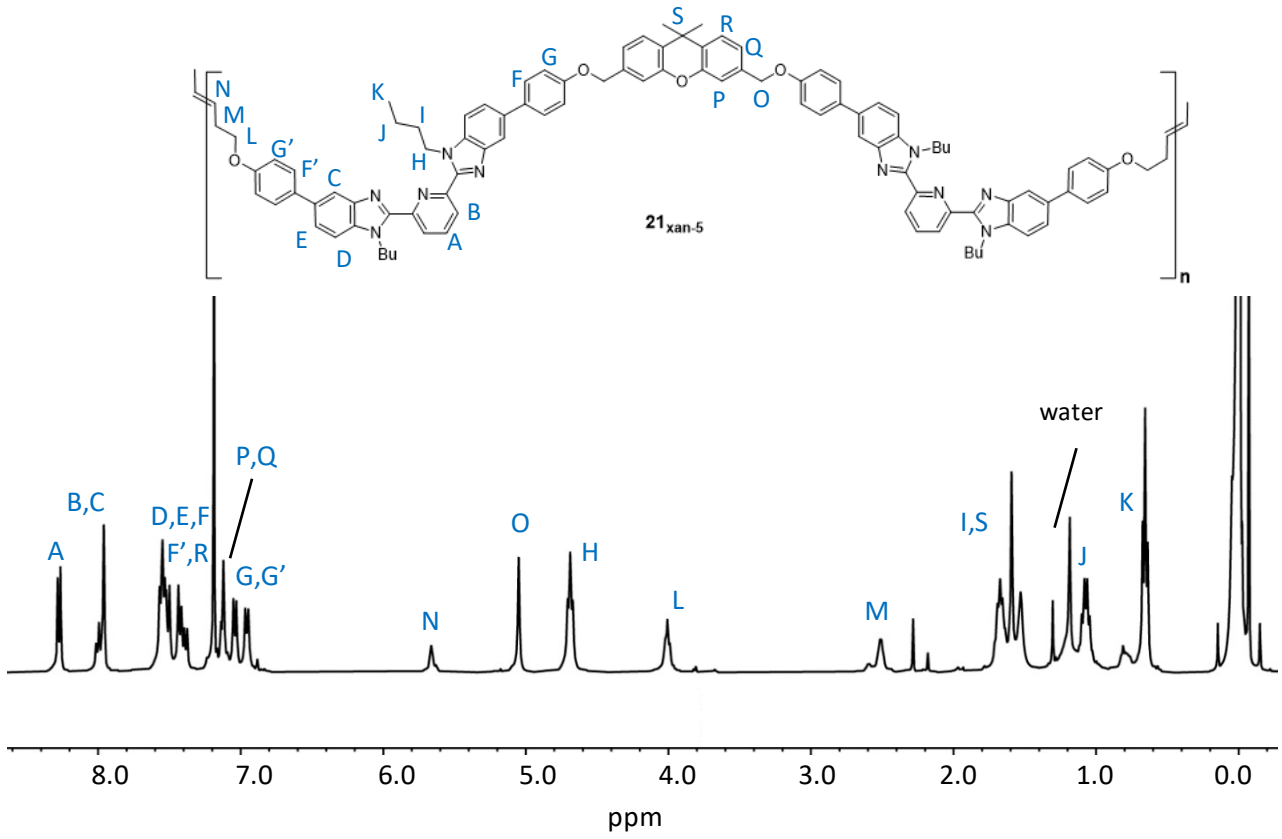

22$_{nap-5}$: ^{1}H NMR (400 MHz, $CDCl_3$) δ_H (ppm) 8.35 (d, J = 7.9 Hz, 4H), 8.07 (t, J = 7.8 Hz, 2H), 8.04 – 8.02 (m, 4H), 7.96 (s, 2H), 7.91 (d, J = 8.5 Hz, 2H), 7.66 – 7.55 (m, 14H), 7.50 (d, J = 8.6 Hz, 4H), 7.14 (d, J = 8.5 Hz, 4H), 7.03 (d, J = 8.4 Hz, 4H), 5.78 – 5.67 (m, 2H), 5.31 (s, 4H), 4.76 (t, J = 7.3 Hz, 8H), 4.08 (t, J = 6.5 Hz, 4H), 2.61 – 2.55 (m, 2H), 1.75 (p, J = 7.4 Hz, 8H), 1.14 (h, J = 7.4 Hz, 8H), 0.73 (t, J = 7.3 Hz, 12H) ^{13}C NMR (101 MHz, $CDCl_3$) δ_C (ppm) 158.4, 158.3, 150.9, 150.8, 150.2, 143.6, 138.3, 136.4, 136.3, 135.7, 135.6, 135.2, 134.8, 134.4, 133.4,

132.9, 128.7, 128.6, 128.5, 127.9, 126.5, 125.7, 123.3, 118.3, 118.2, 115.5, 115.1, 110.6, 70.4, 67.9, 44.9, 32.8, 32.3, 30.1, 20.0, 13.7.

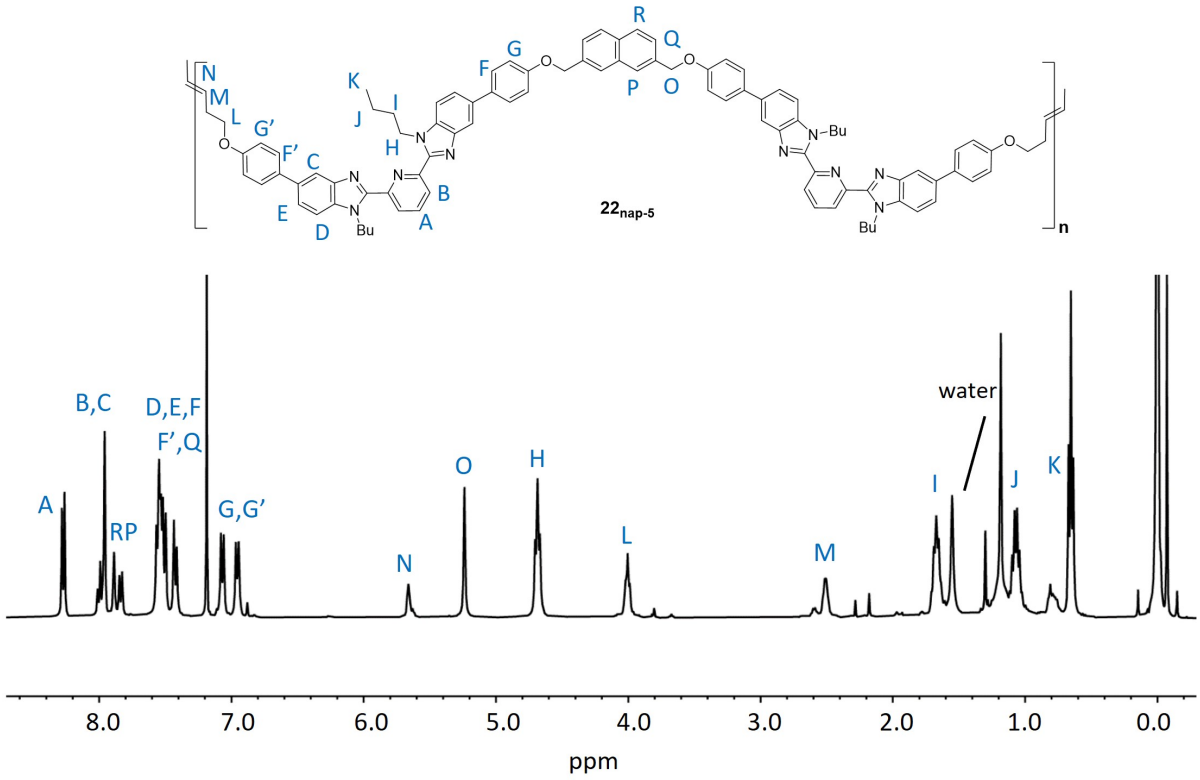

23$_{\text{nap-6}}$: ^{1}H NMR (400 MHz, $CDCl_3$) δ_H (ppm) 8.35 (d, J = 7.9 Hz, 4H), 8.08 (t, J = 8.2 Hz, 2H) 8.04 (s, 4H), 7.96 (s, 2H), 7.91 (d, J = 8.5 Hz, 2H)7.67 – 7.55 (m, 14H), 7.50 (d, J = 7.3 Hz, 4H), 7.13 (d, J = 8.4 Hz, 4H), 7.02 (d, J = 8.6 Hz, 4H), 5.60 – 5.46 (m, 2H), 5.31 (s, 4H), 4.76 (t, J = 7.0 Hz, 8H), 4.03 (q, J = 9.8, 8.0 Hz, 4H), 2.36 – 2.17 (m, 2H), 1.89 (q, J = 6.7 Hz, 4H), 1.79 – 1.70 (m, 8H), 1.15 (h, J = 14.9, 7.4 Hz, 8H), 0.73 (t, J = 7.3 Hz, 12H). ^{13}C NMR (101 MHz, $CDCl_3$) δ_C (ppm) 158.6, 158.3, 150.8, 150.1, 143.6, 138.3, 136.4, 136.2, 135.7, 135.2, 134.8, 134.3, 133.4, 132.9, 130.3, 128.6, 128.5, 126.5, 125.7, 123.3, 118.3, 115.5, 115.0, 110.6, 70.4, 67.5, 44.9, 32.3, 29.3, 29.1, 20.0, 13.7.

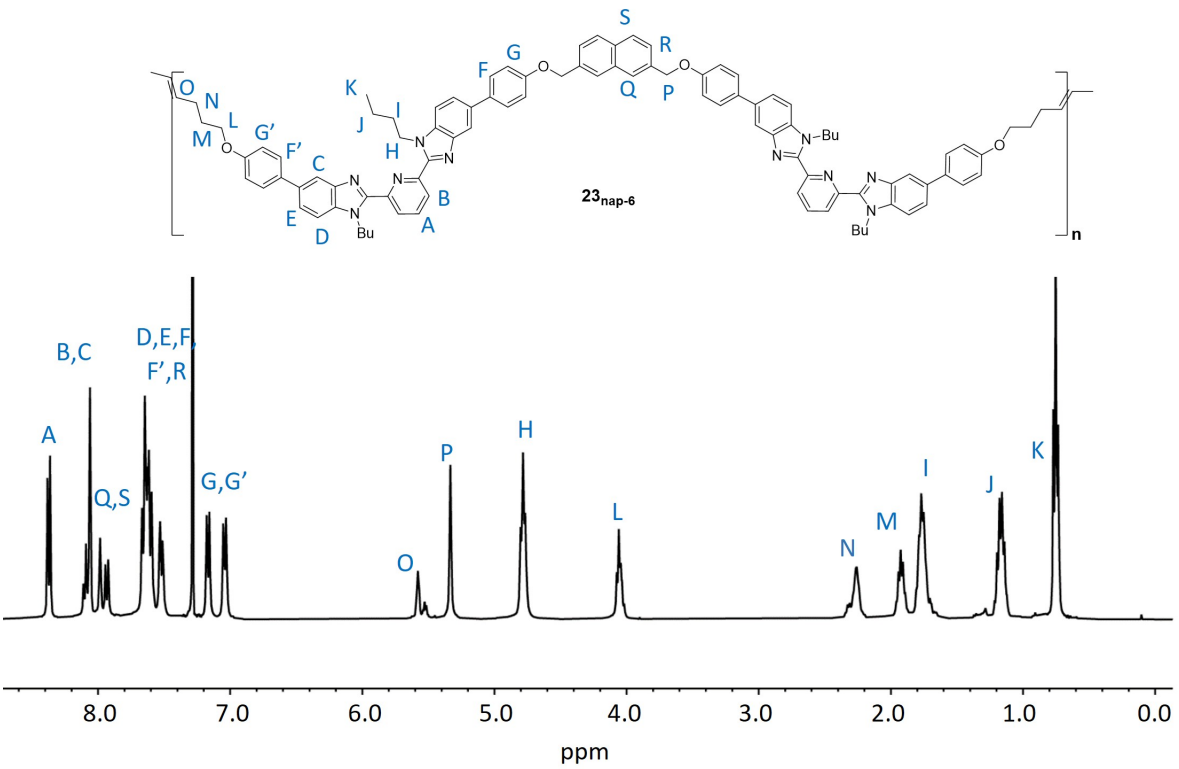

3.6.2.8 Poly[*n*]catenane synthesis $18_{xan\text{-}5}$

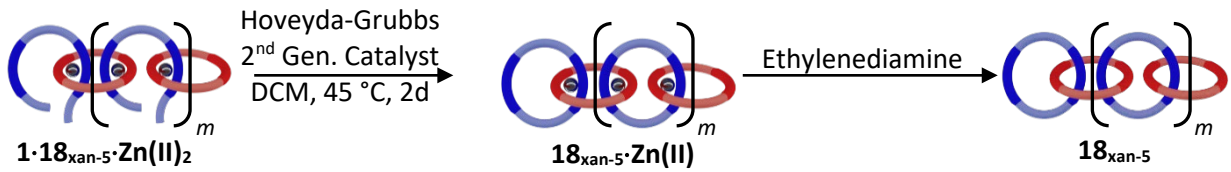

Poly[*n*]catenane synthesis followed the same procedures as Section 2.6.2.4. Briefly, MSP **1·18$_{xan\text{-}5}$·Zn(II)$_2$** (40 mg) was added to the dried vessel and dissolved in DCM (at a concentration of 2.5 mM wrt **1**). The solution was stirred and heated to reflux (45°C) followed by bubbling argon for 30 minutes to remove dissolved oxygen. Then Hoveyda-Grubbs second generation catalyst in DCM (0.32 mM) was added to the solution. To account for any solvent evaporation during the bubbling steps, additional DCM was added as required to maintain the original concentration (2.5 mM). While still under reflex, the solution was bubbled with argon for additional 30 mins. The

Argon purge and catalyst addition was repeated 24 hours after the first addition. The reaction was carried out for a further 24 hours before the solution was cooled to room temperature and ethyl vinyl ether (~1mL) was added to deactivate the catalyst. To demetallate the reaction products, 50 μL of ethylenediamine was added to the reaction and allowed to stir. The resulting mixture was washed with 5 aliquots of water or until the aqueous wash was no longer basic. The organic layer was passed through a 0.45 μm PTFE syringe filter and the solvent was removed under vacuum. The resulting demetallated reaction mixture was obtained as a yellow or slightly brown solid.

For the purposes of characterization, **18**$_{\textbf{xan-5}}$ was purified to the greatest extent that could be achieved. The crude sample of **18**$_{\textbf{xan-5}}$ was fractionated via preparatory gel permeation chromatography (prep-GPC) using a mobile phase of 25% HPLC grade dimethylformamide (DMF) and 75% HPLC grade tetrahydrofuran (THF). After this step, the individual fractions were characterized fully via ^{1}H NMR and GPC-MALS.

After prep-GPC, fractions 1-3 were recombined and partially re-metalated with $Zn(NTf_2)_2$ until ca. 30% of **18**$_{\textbf{xan-5}}$ was metalated as observed by ^{1}H NMR. The sample was fully dried under vacuum and washed 8 times with a solution of 2:1 chloroform:hexanes to remove the non-metal-containing compounds. The remaining metalated compounds were dissolved in DCM and demetallated using 50 μL of diethylenetriamine. The resulting mixture was washed with 5 aliquots of water or until the sample was no longer basic. After removal of residual water, the final material was collected. **18**$_{\textbf{xan-5}}$ was isolated in 85% purity with the residual byproduct identified as **21**$_{\textbf{xan-5}}$.

Polycatenane **18**$_{\textbf{xan-5}}$ (84% pure) ^{1}H NMR (500 MHz, $CDCl_3$) δ_H (ppm) 8.28 – 8.10 (m, 8H), 7.98 – 7.81 (m, 12H), 7.46 – 7.29 (m, 36H, overlapped with $CDCl_3$), 7.11 (d, J = 8.7 Hz, 2H), 6.98 (s, 2H), 6.89 – 6.75 (m, 8H), 6.71 – 6.54 (m, 8H), 5.58 – 5.27 (m, 2H), 5.07 – 4.93 (m, 4H), 4.63 –

4.42 (m, 16H), 4.04 – 3.95 (m, 4H), 3.92 – 3.47 (m, 32H), 1.68 – 1.61 (m, 16H, overlapped), 1.46 – 1.38 (m, 6H), 0.92 – 0.78 (m, 16H), 0.64 – 0.46 (m, 24H).

21$_{\textbf{xan-5}}$ Byproduct (16%) 8.35 (d), 8.07 (t), 8.03 (s), 7.66 – 7.55 (m), 7.48 (dd), 7.23 – 7.08 (m), 7.03 (d), 5.81-5.65 (m), 5.12 (s), 4.76 (t), 4.08 (t), 2.70-2.59 (m), 1.74 (q), 1.60 (s), 1.14 (h), 0.73 (t). For full ^{1}H NMR and ^{13}C NMR information on **21**$_{\textbf{xan-5}}$, see page Section 3.6.2.7.

3.6.2.9 Poly[*n*]catenane synthesis 19$_{\textbf{nap-5}}$

19$_{\textbf{nap-5}}$ was synthesized in the same manner as **18**$_{\textbf{xan-5}}$ using 40 mg of **1·14**$_{\textbf{nap-5}}$**·Zn(II)**$_2$.

For the purposes of characterization, **19**$_{\textbf{nap-5}}$ was purified to the greatest extent that could be achieved. The crude sample of **19**$_{\textbf{nap-5}}$ was fractionated via prep-GPC using a mobile phase of 25% DMF and 75% THF. After this step, the individual fractions were characterized fully via ^{1}H NMR and GPC-MALS.

After prep-GPC, fraction 2 was purified via silica-preparative plates that had undergone pretreatment with TEA, eluted with a solution of 5% MeOH in $CHCl_3$.The bottom fraction was collected and washed three times in 30% MeOH in $CHCl_3$. The solvent was removed under reduced pressure and the material was redissolved in pure chloroform. The solution was passed through a 0.2 μm PTFE syringe filter to remove residual silica. The chloroform was removed under pressure and the material was washed with pure hexanes to remove grease and other residual byproducts from the prep-TLC plate. The final material was collected to yield a sample of **19**$_{\textbf{nap-5}}$ in 95% purity with the residual byproduct identified as **22**$_{\textbf{nap-5}}$, though this byproduct was nearly negligible via ^{1}H NMR.

Polycatenane (96% pure) ^{1}H NMR (500 MHz, $CDCl_3$) δ_H (ppm) 8.27 – 8.08 (m, 8H), 7.93 – 7.82 (m, 12H), 7.72 – 7.56 (m, 4H), 7.45 – 7.30 (m, 16H), 7.30 – 7.27 (m, 10H), 7.23 – 7.14 (m, 8H), 6.86 (d, J = 7.8 Hz, 4H), 6.79 (dd, J = 25.9, 8.1 Hz, 8H), 6.58 (t, J = 8.3 Hz, 4H), 5.56 – 5.50 (m, 2H), 5.24 – 5.10 (m, 4H), 4.61 – 4.41 (m, 16H), 3.99 – 3.83 (m, 4H), 3.81 – 3.45 (m, 32H), 2.40 – 2.30 (m, 4H), 1.65 – 1.46 (m, 16H), 1.03 – 0.91 (m, 16H), 0.63 – 0.50 (m, 24H).

3.6.2.10 Poly[*n*]catenane synthesis $\mathbf{20_{nap\text{-}6}}$

$\mathbf{20_{nap\text{-}6}}$ was synthesized in the same manner as $\mathbf{18_{xan\text{-}5}}$ using 40 mg of $\mathbf{1{\cdot}16_{nap\text{-}6}{\cdot}Zn(II)_2}$. All purification procedures for $\mathbf{18_{xan\text{-}5}}$ were similarly repeated. In brief, the crude sample $\mathbf{20_{nap\text{-}6}}$ was fractionated using prep-GPC with a mobile phase of 25% DMF and 75% THF. The first three fractions were partially remetallated using $Zn(NTf_2)_2$ and the sample was washed with a mixture of chloroform/hexanes to remove the unmetalated byproducts. After demetallation, the mixture was found to be a mixture of $\mathbf{20_{nap\text{-}6}}$ (76%) and the ADMET byproduct $\mathbf{23_{nap\text{-}6}}$.

Polycatenane $\mathbf{20_{nap\text{-}6}}$ (76% pure) ^{1}H NMR (500 MHz, $CDCl_3$) δ_H (ppm) 8.29 – 8.13 (m, 8H), 7.95 – 7.83 (m, 12H, overlapped with **6**), 7.76 – 7.66 (m, 4H), 7.46 – 7.31 (m, 26H, overlapped with $CDCl_3$), 7.24 – 7.17 (m, 8, overlapped with $CDCl_3$), 6.88 (d, J = 8.6 Hz, 4H), 6.81 (dd, J = 21.1, 8.1 Hz, 8H), 6.62 (d, J = 8.8 Hz, 4H), 5.50 – 5.36 (m, 2H, overlapped with **6**), 5.26 – 5.16 (m, 4H), 4.64 – 4.43 (m, 16H), 4.00 – 3.95 (m, 4H), 3.81 – 3.45 (m, 32H), 2.48 – 2.37 (m, 4H), 2.10 – 1.99 (m, 4H), 1.64 – 1.51 (m, 16H), 1.05 – 0.92 (m, 16H), 0.63 – 0.52 (m, 24H).

Byproduct $\mathbf{23_{nap\text{-}6}}$ (23%) 8.35 (d), 8.08 (t), 8.04 (s), 7.96 (s), 7.67 – 7.55 (m), 7.50 (d), 7.15 (d), 7.02 (d), 5.60 – 5.46 (m), 5.31 (s), 4.76 (t), 4.03 (q), 2.36 – 2.17 (m), 1.89 (q), 1.79 – 1.70 (m), 1.15 (h), 0.73 (t). For full ^{1}H NMR and ^{13}C NMR information on $\mathbf{23_{nap\text{-}6}}$, see page Section 3.6.2.7.

3.7 References

1 R. J. Wojtecki, Q. Wu, J. C. Johnson, D. G. Ray, L. S. T. J. Korley and S. J. Rowan, *Chem. Sci.*, 2013, **4**, 4440–4448.

2 Q. Wu, P. M. Rauscher, X. Lang, R. J. Wojtecki, J. J. de Pablo, M. J. A. Hore and S. J. Rowan, *Science (80-.).*, 2017, **358**, 1434–1439.

3 M. M. Tranquilli, Q. Wu and S. J. Rowan, *Chem. Sci.*, 2021, **12**, 8722–8730.

4 J. A. Semlyen, in *Mechanisms of Polyreactions-Polymer Characterization*, Springer Berlin Heidelberg, Berlin, Heidelberg, pp. 41–75.

5 P. C. Hiemenz and T. P. Lodge, in *Polymer Chemistry*, CRC press, Boca Raton, Second., 2007.

6 *1D and 2D Experiments Step-by-step Tutorial; Advanced Experiments User Guide, vers. 002*, Bruker Biospin, 2006.

7 V. Polic, K. J. Cheong, F. Hammerer and K. Auclair, *Adv. Synth. Catal.*, 2017, **359**, 3983–3989.

8 M. B. Andrus, K. C. Harper, M. A. Christiansen and M. A. Binkley, *Tetrahedron Lett.*, 2009, **50**, 4541–4544.

Chapter 4: Macrocycle Structural Effects on the Synthesis of Poly[*n*]catenanes

* This chapter was adapted from: Tranquilli, M.M.[‡]; Rawe, B.W.[‡]; Liu, G.; Sun, M.; Rowan, S.J. Macrocycle Structural Effects on the Synthesis of Poly[*n*]catenanes. [*in preparation*]

4.1 Introduction

In the early analyses of poly[*n*]catenane **3**, several computational models were employed by Dr. Phillip Rauscher to understand the solution dynamics of **3**.[1] In his investigations of the behavior of the poly[*n*]catenane structure, Dr. Rauscher investigated the dynamics of the metalated catenane structure (**3·Zn(II)**). This model was used to determine variations in the inter-metal distances (M–M) between each Bip–metal complex within the poly[*n*]catenane (**3·Zn(II)**) (**Figure 4.1**). These M–M distances demonstrated the variations between the macrocycle (**1**) and the closed thread (**6**). **Figure 4.1** shows the relative probability of the M–M distances; within this analysis there is a distinctive difference between the probability populations for **1** and **6**. Macrocycle **6** exhibits a larger average M–M distance and a narrower probability distribution, indicating greater rigidity in the structure. In contrast, macrocycle **1** demonstrates a disperse distribution with a lower average M–M distance, demonstrating flexibility within the macrocycle. From a synthetic perspective, the

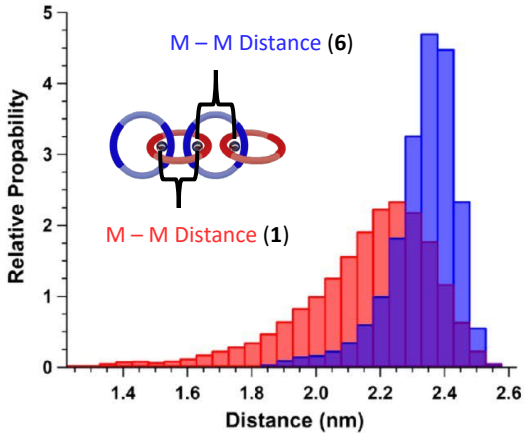

Figure 4.1 Relative probability of inter-metal distances for **1** (red) and **6** (blue) in a [4]catenane (only interior rings considered).[1]

flexibility of the metalated macrocycle (**1**) suggests that the motions in solution may affect the frequency of side reactions in synthesis, yielding the ADMET byproduct **5**. **Figure 4.2** demonstrates several paths that may be taken to yield the non-interlocked byproducts **1** and **5**. Of these, the undesired metatheses reactions seen in ***l*-3·Zn(II)** and ****l*-3·Zn(II)** may be affected by the structure of the macrocycle **1**: the back-biting type reaction that leads to the formation of ***l*-3·Zn(II)** and ****l*-3·Zn(II)** may be promoted by the flexibility of the macrocycle **1** in solution.

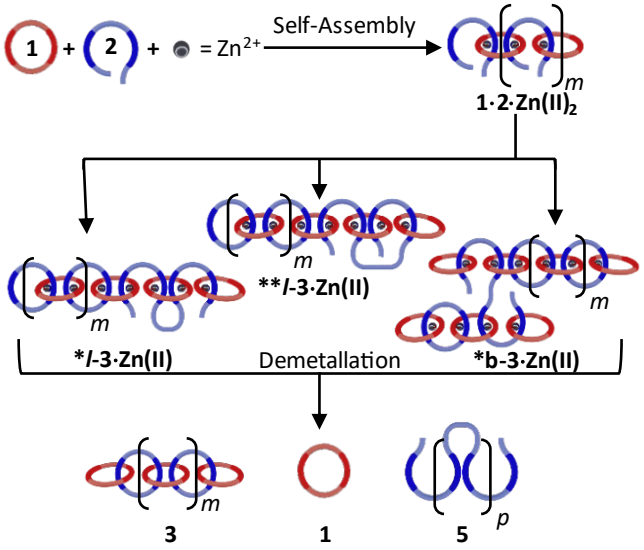

Figure 4.2 Synthetic pathways that employ incorrected ring closure of MSP ***l*-1·2·Zn(II)$_2$** to yield the non-interlocked byproducts **1** and **5**.

Examining the chemical structure of **1**, there are two main components that make up the macrocycle (**Figure 4.3**): the Bip ligand (**7**) and the tetraethylene glycol "linker" (**8**$_{4EG}$). As the ring closed (RC) component (**6**) similarly contains two Bip ligands, the disperse probability distribution must be a direct result of the flexible tetraethylene glycol linker (**8**$_{4EG}$). To understand the effects of flexibility on the formation of ***l*-3·Zn(II)** and ****l*-3·Zn(II)**, therefore, the rigidity of the linker component must be altered.

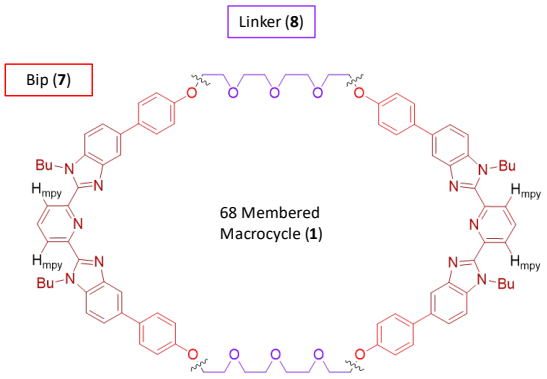

Figure 4.3 Chemical structure for the macrocycle (**1**) with the ligand highlighted in red and the linker component highlighted in purple.

Similarly, the formation of ***l*-3·Zn(II)** and ****l*-3·Zn(II)** may be related to the size of the macrocycle component. One commonly accepted method for classifying the size of a macrocycle is to count the number of atoms that compose the inner ring of the macrocycle. For example, when the linker component is the tetraethylene glycol (**8**$_{4EG}$), the ring size of **1** is 68. To fully understand the effect of size, therefore, an ideal sample of macrocycles would include linkers that create macrocycles both smaller and larger than the original 68-membered ring.

Based on this analysis, a series of macrocycles were synthesized with variations to the linker component to fully test the effects of both size and flexibility on the poly[*n*]catenane synthesis reaction with a particular focus on how the rigidity of the macrocycle affects the yield of the non-interlocking byproducts.

4.2 Selection and Synthesis of New Macrocycle Components

To test the effects of the macrocycle size and flexibility on the synthesis of poly[*n*]catenane we sought to create a large library that would offer the full breadth of analysis of both size and rigidity (**Figure 4.4,** linkers **25-32**). Linkers **25**$_{2EG}$ and **26**$_{3EG}$ most closely resemble the original

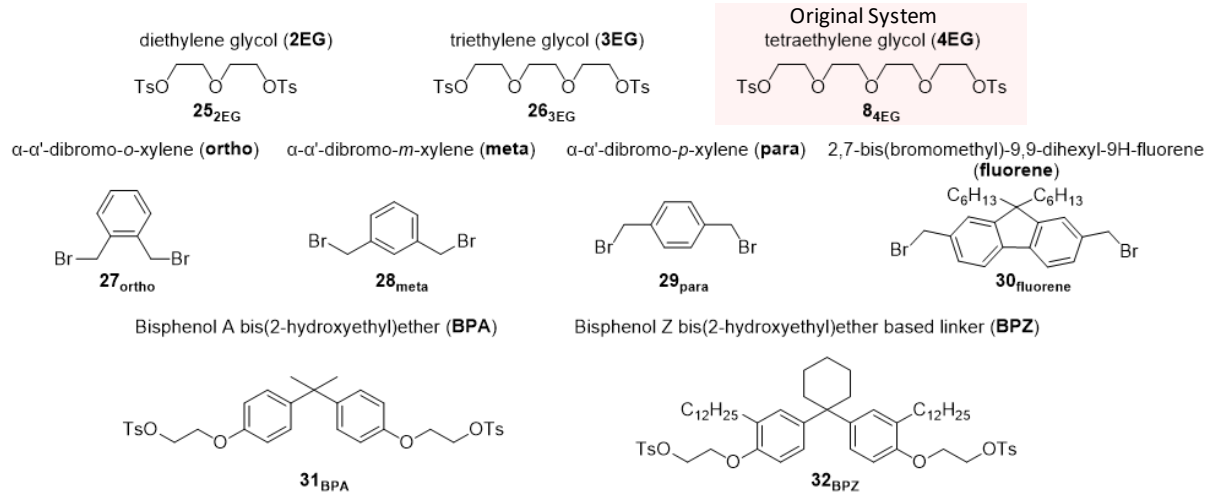

Figure 4.4 Chemical structures of the linkers used to create a full library of macrocycles for catenane synthesis testing.

linker **8**$_{4EG}$ their chemical composition and relative flexibility. With these ethylene glycol-based linkers, the only variation given is the length of the linker. The **25**$_{2EG}$, **26**$_{3EG}$ linker series was selected (a) to keep the chemical similarity of the macrocycles as close to the original system as possible; and (b) to test if the smaller macrocycle size increases the formation of the byproducts. Linkers **25**$_{2EG}$ and **26**$_{2EG}$ were synthesized in a similar manner to the original linker (**8**$_{4EG}$) and full synthetic procedures for the resulting macrocycles (**33**$_{2EG}$, **34**$_{EG}$) can be found in the experimental section.

The second set of xylene- based linkers (**27**$_{ortho}$, **28**$_{meta}$, **29**$_{para}$) were selected for their size and rigidity. The size variations between **27**$_{ortho}$-**29**$_{para}$ are small (**Table 4.1**), with 54, 56 or 58 atoms, allowing for a more precise analysis of how size can affect the overall yield of the poly[*n*]catenane synthesis. These macrocycles (**35**$_{ortho}$, **36**$_{meta}$, **37**$_{para}$) were synthesized in a similar manner to the previous macrocycles (see Experimental Section); however, upon further purification, the macrocycle **35**$_{ortho}$ was found to be insoluble in the solvents required for characterization and

synthesis (namely $CHCl_3$ and DCM). As a result, the ortho macrocycle **35$_{ortho}$** was removed from further analysis and was not able to form a poly[*n*]catenane.

The next linker (2,7-bis(bromomethyl)-9,9-dihexyl-9H-fluorene) **30$_{fluorene}$** was selected based on the extreme rigidity of the fluorene base. This macrocycle (**38$_{fluorene}$**) is particularly unique as it (a) is only slightly larger than the largest xylene-based macrocycle (**37$_{para}$**), allowing for analysis of the direct progression between size and yield for the rigid systems; (b) is similar in size to macrocycle **26$_{3EG}$**, allowing for a close comparison between the rigid and flexible systems; and (c) is the rigid macrocycle with a ring size closest to the original macrocycle (**1$_{4EG}$**) (**Table 4.1**).

Table 4.1 Size and rigidity classifications of the macrocycles synthesized from the linkers in Figure 4.4

Linker	Macrocycle Size	Rigid or Flexible?
25$_{2EG}$	56	F
26$_{3EG}$	62	F
8$_{4EG}$	68	F
27$_{ortho}$	54	R
28$_{meta}$	56	R
29$_{para}$	58	R
30$_{fluorene}$	64	R
31$_{BPA}$	76	R/F?
32$_{BPZ}$	76	R/F?

The final set of linkers are based on bisphenol compounds were selected with the intention of creating a larger, more rigid set of macrocycles. BPA (Bisphenol A) is a common monomer used access high T_g polycarbonate materials.[2] Though the bisphenol-based linkers (**31$_{BPA}$**, **32$_{BPZ}$**) are the same size, several variations were built into the linkers. The BPA based linker **31$_{BPA}$** was selected for ease of synthesis and simplicity. However, concerns over the solubility of this macrocycle also led to the selection of a Bisphenol Z based linker. BPZ (**32$_{BPZ}$**) was given the long greasy dodecyl alkane chain to enhance the solubility of the macrocycle and the resulting MSP.

These bisphenol-based linkers were able to form macrocycles (**39**$_{\mathbf{BPA}}$, **40**$_{\mathbf{BPZ}}$) and were soluble in the required solvents.

At this time, it is worth discussing several linkers that were also tested but will not be explored in this study (**Figure 4.5**). Each of these linkers were excluded at various stages in the testing process: the biphenol based linker, BPA based linker, and 6EG linker (three top) were all found to self-bind (see next section for more details on self-binding); the carbazole based linker (bottom left) was unstable due to radical reactions that occur naturally during the linker synthesis; and finally the BPZ based linker (bottom right) was found to yield very little catenanted material compared to the analyzed BPZ linker (**40**$_{\mathbf{BPZ}}$). Though each linker in **Figure 4.5** was disqualified at a different stage in the synthesis process, they were removed from the in-depth discussions in this chapter for the sake of brevity. However, it is important to note the failure of these structures for any future poly[*n*]catenane testing.

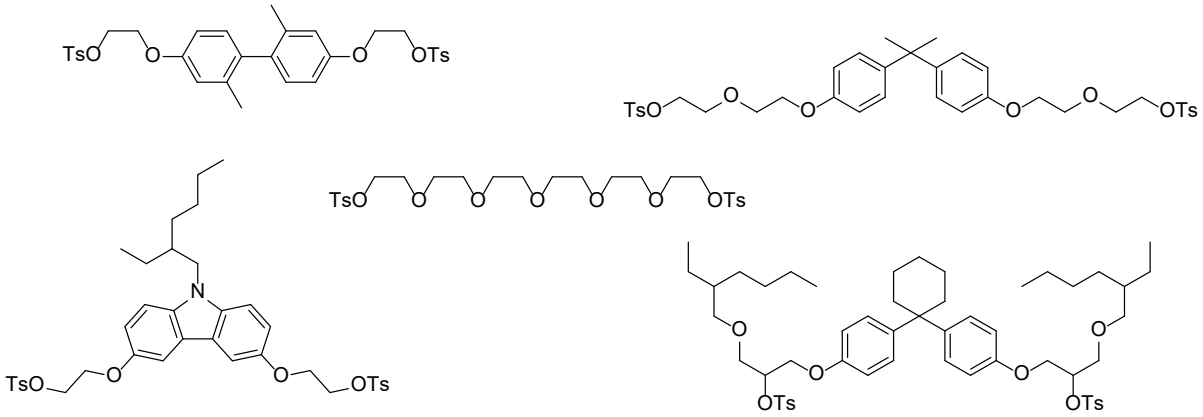

Figure 4.5 A series of other structures tested for linkers in this study but were abandoned due to synthetic difficulties or self-binding of the constructed macrocycles.

4.3 Macrocycle Binding Tests

Apart from size and solubility, a key parameter in macrocycle viability is the ability to bind two Zn(II) ions in a single macrocycle. While these macrocycles may all visually appear to have this ability when structured in 2D, the 3D complexation of a macrocycle may impair this. The enthalpic self-assembly of the polycatenane components will ensure that each Zn(II) ion is bound to as many ligand centers as possible. Therefore, the 3D twisting of the macrocycle may force both Bip ligand centers within the macrocycle to bind to the same Zn(II) molecule (**Figure 4.6a**). This self-binding would impair MSP formation and lead to subsequent failure of the poly[*n*]catenane reaction.

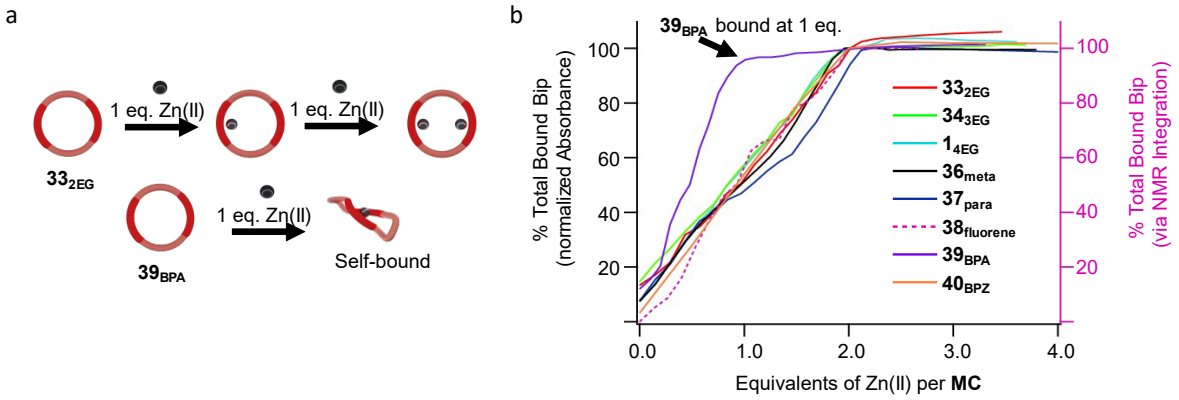

Figure 4.6 (a) Cartoon representation of how a self-binding event occurs within a macrocycle. (b) Titration data for all tested macrocycles to determine self-binding tendencies. The left axis corresponds to the UV-vis titration data collected for all samples with solid-line plots. The right axis corresponds to the dashed-line of **38fluorene**, that was tested via an ^{1}H NMR titration rather than UV-vis.

To test the self-binding tendencies of the synthesized macrocycles, the UV activity of the Bip ligand was exploited. The Bip ligand fluoresces with λ_{max} = 336 nm. Upon binding to a Zn(II) ion, the Bip fluorescence shifts to a λ_{max} ca. 382 nm. Therefore, to test the self-binding ability of **33$_{2EG}$**, a solution at 40 μM of **33$_{2EG}$** was prepared in 9:1 $CHCl_3$:MeCN. A second solution containing both **33$_{2EG}$** at 40 μM and $Zn(Tf_2N)_2$) 1 mM was also prepared. The **33$_{2EG}$·Zn(II)** solution was

slowly titrated into the pure macrocycle solution in 15 µL increments. After each addition, the mixture was agitated and allowed to equilibrate for approximately 5 minutes. Once equilibrated, a UV-vis spectrum was collected; the sample of **33_{2EG}** was slowly titrated until the solution reached 4 equivalents of Zn(II) per **33_{2EG}** (i.e. 2 equivalents of Zn(II) per Bip ligand) (**Figure 4.7**).

This experiment was repeated for the each of the other purified macrocycles, with the exception of **$38_{fluorene}$**. When the UV-vis data was collected for the **$38_{fluorene}$,** the fluorescence of linker **$30_{fluorene}$** interfered with the data collection at 382 nm.[3] As a result, an ^{1}H NMR titration experiment of fluorene was undertaken where proton "G" was followed and integrated after each addition, the key data points are picture in **Figure 4.8**. Once titration data was collected for all macrocycle samples, the **39_{BPA}** showed a marked difference from the other samples (**Figure 4.6b**): rather than

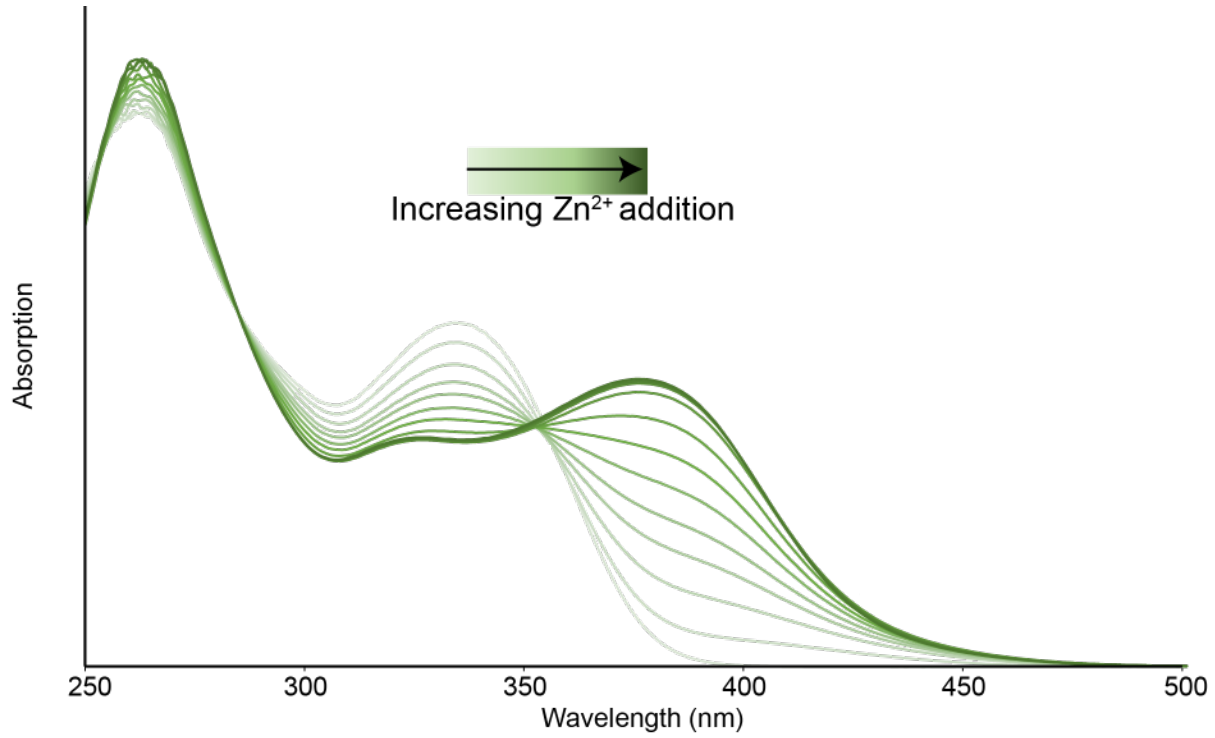

Figure 4.7 UV-vis titration data for **33_{2EG}.**

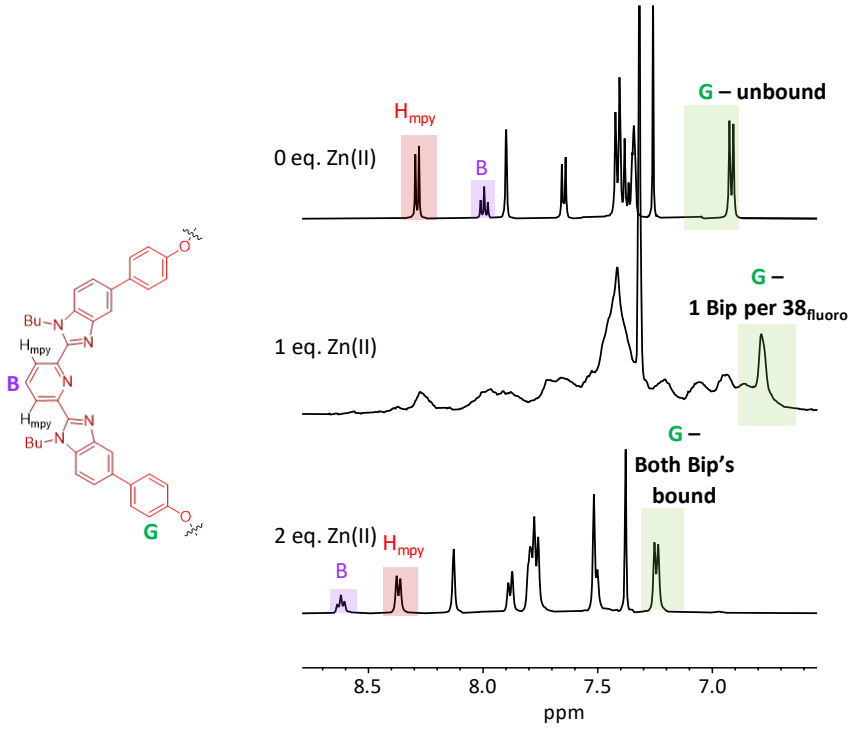

Figure 4.8 ^{1}H NMR titration data from **38$_{fluorene}$.** Proton "G" was monitored, and the 3 placements of the proton were integrated at each titration point. At 50% titration, the sample was a combination of unbound, singly bound, and doubly bound **38$_{fluorene}$** (middle). At 2 equivalents of Zn(II) the ^{1}H NMR resolution returned to high quality and the G proton had entirely shifted downfield (bottom).

reaching its maximum absorbance at 2 eq. of Zn(II) per MC, **39$_{BPA}$** reached its maximum absorbance at 1 eq. of Zn(II) per **39$_{BPA}$**. This data would indicate that the two Bip moieties in **39$_{BPA}$** are able to bind to the same Zn(II) ion, and that **39$_{BPA}$** is able to self-bind as depicted in **Figure 4.6a**. This would suggest that **39$_{BPA}$** would not be able to efficiently form the desired **39$_{BPA}$·2·Zn(II)$_2$** MSP necessary for the poly[*n*]catenane synthesis. As such, macrocycle **39$_{BPA}$** was excluded from further experiments.

4.4 MSP Analyses

Based on the confirmation of the utility of macrocycles **33$_{2EG}$, 34$_{3EG}$, 36$_{meta}$, 37$_{para}$, 38$_{fluorene}$,** and **40$_{BPZ}$**, each of the new macrocycles were used to create an MSP using thread **2**. Each MSP

was formed as previously detailed in Chapter 2. In short, the selected macrocycle (e.g. **33_{2EG}**) was dissolved in $CDCl_3$ and a solution of **2** was slowly titrated in until the integrations of the H_{mpy} peaks was exactly 1:1. **36_{meta}** and **40_{BPZ}** were exceptions to this method, as the H_{mpy} chemical shift for **36_{meta}** and **40_{BPZ}** is further downfield than the H_{mpy} of any of that of the other macrocycles tested (8.32 and 8.35 ppm), overlapping closely with the H_{mpy} shift of **2**. For this titration, the 1:1 mixture was monitored by integrating the triplets at 4.79 (**2**) and 4.55 (**36_{meta}**) or 4.36 (**40_{BPZ}**). After the 1:1 mixture was attained, $Zn(NTf_2)_2$ was added slowly until all H_{mpy} peaks shifted downfield, indicating that all Bip moieties had been bound to Zn(II). This shift occurs at approximately 2 full equivalents of zinc, yielding the new MSPs (**33_{2EG}·2·Zn(II)$_2$**, **33_{3EG}·2·Zn(II)$_2$**, **33_{meta}·2·Zn(II)$_2$**, **33_{para}·2·Zn(II)$_2$**, **$33_{fluorene}$·2·Zn(II)$_2$**).

After removal of the solvent, a portion of the MSP was dissolved in a solution of 4:1 CD_2Cl_2 at a concentration of 2.5 mM w.r.t. **2**. To confirm the formation of the MSP, each sample was examined using diffusion ordered spectroscopy (DOSY) to determine the diffusion coefficient. Although the exact value of diffusion coefficient of polymers obtained by DOSY can be inaccurate due to the dispersity of polymers with the same chemical shift,[4] the diffusion coefficient obtained for these regions was smaller ($1.10\text{-}4.51\times10^{-10}$ m^2s^{-1}) than that of the individual components ($4.66\text{-}6.31\times10^{-10}$ m^2s^{-1}), confirming the polymeric nature of the MSP (**Table 4.2**). Further evidence for polymer formation was that the NMR signals were broader than the corresponding components and that each solution remained highly viscous, even at 2.5 mM.

Based on the data from Chapters 2 and 3, we have previously established that the shape of the H_{mpy} peak in the MSP has a strong correlation to the architecture of the MSP (cyclic vs. linear). The ^1H NMR data for each new MSP is shown in **Figure 4.9**.

Table 4.2 Diffusion coefficients of each MSP as determined by DOSY analysis of the region from 8.70-8.85 ppm (region i)

MSP	Diffusion coefficient (x 10^{-10} m^2s^{-1})
33_{2EG}·2·Zn(II)$_2$	4.51e-10
34_{3EG}·2·Zn(II)$_2$	1.74e-10
1_{4EG}·2·Zn(II)$_2$	1.10e-10
36_{meta}·2·Zn(II)$_2$	2.57e-10
37_{para}·2·Zn(II)$_2$	3.04e-10
$38_{fluorene}$·2·Zn(II)$_2$	2.63e-10
40_{BPZ}·2·Zn(II)$_2$	2.02e-10

Figure 4.9 shows the series of MSPs examined for this study at a concentration of 2.5 mM wrt **2.** In **Figure 4.9a**, a trend in the H_{mpy} proton can be observed as the size of the macrocycle changes: at the smallest macrocycle size (in **33_{2EG}·2·Zn(II)$_2$** and **36_{meta}·2·Zn(II)$_2$**), the H_{mpy} protons for the two organic components are distinct: the H_{mpy} corresponding to the macrocycle has a different shift from thread **2**. This is very much in line with what has been seen in the past with small macrocycles[5]: decreasing the size of the macrocycle changes the chemical environment of the H_{mpy} proton and makes it distinct from the H_{mpy} proton seen in the thread (**2**). As the macrocycle increases in size (in **33_{3EG}·2·Zn(II)$_2$** and **36_{para}·2·Zn(II)$_2$**) the H_{mpy} peak of the organic compounds become less distinct; however, it is not until the larger macrocycle sizes are reached (in **34_{3EG}·2·Zn(II)$_2$** and **$36_{fluorene}$·2·Zn(II)$_2$**) that the peaks appear as a single defined multiplet.

In Chapter 2 and 3, variations in regions i and ii were attributed to the differences between *c*-MSP and *l*-MSP, based on cyclic yields in the final materials and diffusion coefficients obtained from DOSY.[6] In Chapter 2 these regions were shown to contain the same integrations in both 1:4 d-MeCN:$CDCl_3$ and in d-DCM. Due to the increased resolution in the ^{1}H-NMR data, therefore, the integrations of regions i and ii were taken in d-DCM (**Figure 4.9b**). For **34_{3EG}·2·Zn(II)$_2$**, the diffusion coefficient of region ii was able to be calculated (3.5×10^{-10} m^2s^{-1}), confirming that the

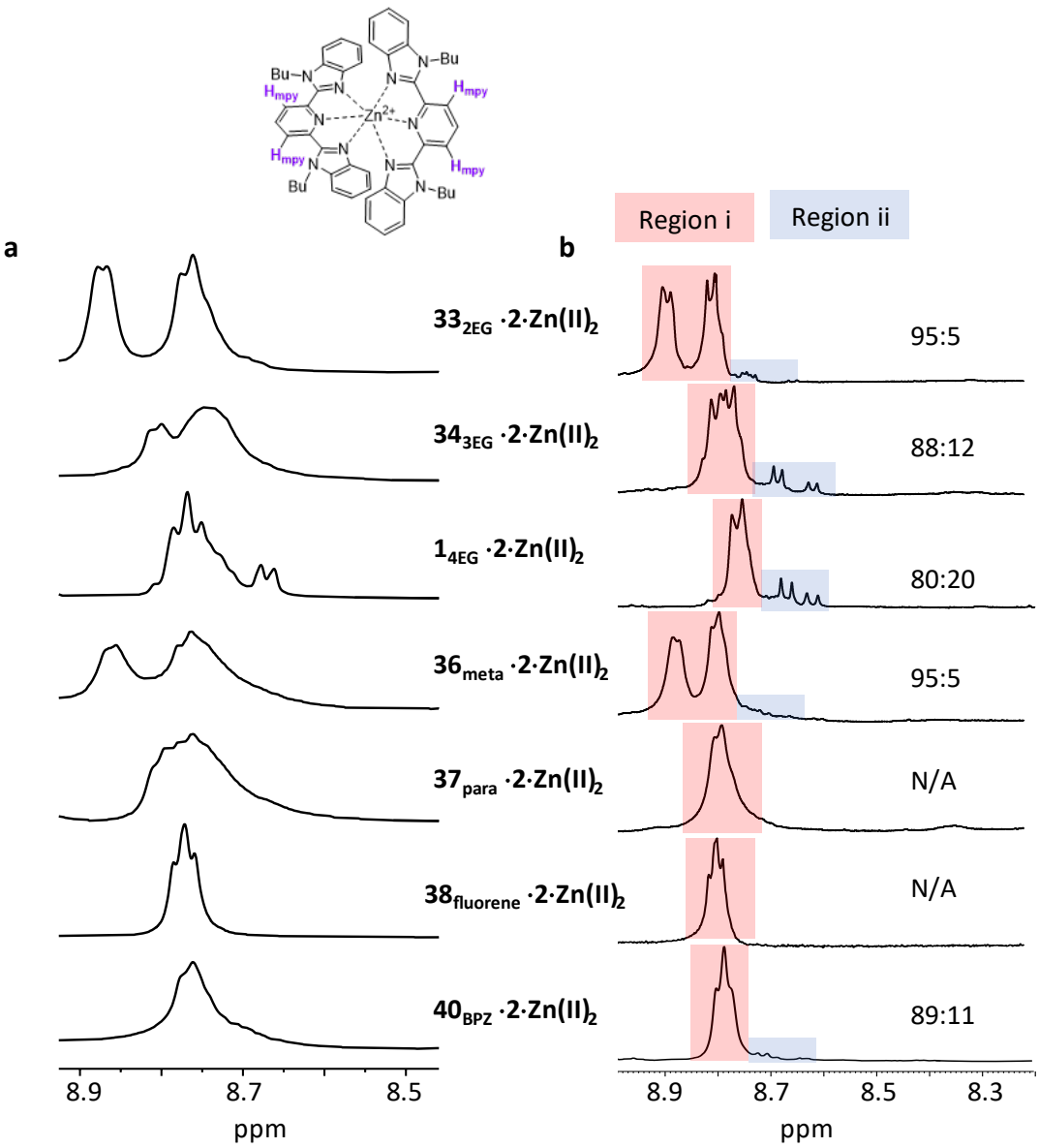

Figure 4.9 ^{1}H NMR of all MSPs at 2.5 mM wrt **2**: (a) 500 MHz, 1:4 d-MeCN:$CDCl_3$, 25 °C and (b) 500 MHz, CD_2Cl_2, 25 °C.

material in this region has a smaller hydrodynamic radius than that in region i (1.74×10^{-10} m^2s^{-1}). Based on the similar trends to those seen for **1_{4EG}·2·Zn(II)$_2$**, the variation in regions i and ii seems likely to correspond to a similar trend in the architecture of the materials. Unfortunately, the area of region ii for samples **33_{2EG}·2·Zn(II)$_2$**, **36_{meta}·2·Zn(II)$_2$**, and **40_{BPZ}·2·Zn(II)$_2$** makes up less than

10% of the total MSP and the peaks are low and broad, making determining a precise diffusion coefficient difficult for this region.

However, the general trends between region ii and the rigidity of the macrocycle paint an interesting picture of the link between *c*-MSP and flexibility. Within the most flexible macrocycle (**1**$_{4EG}$), the MSP shows the greatest percent of peak area in region ii, suggesting that the flexible linkers allow for easier formation of this small, cyclic structure. As the linker shortens (**34**$_{3EG}$**, 33**$_{2EG}$), confining the flexibility of the macrocycle, the amount of peak area seen in region ii decreases from 20% (**1**$_{4EG}$**·2·Zn(II)**$_2$) to 12% (**34**$_{3EG}$**·2·Zn(II)**$_2$) and finally down to 5% (**33**$_{2EG}$**·2·Zn(II)**$_2$). This is further emphasized in the more rigid structures, where the **40**$_{BPZ}$ structure shows the most area in region ii (10%), likely due to the flexibility of the ethylene glycol arms on the linker (**32**$_{BPZ}$, **Figure 4.4**). However, as the macrocycle grows more confined and rigid, the peak population in region ii disappears entirely (**37**$_{para}$**·2·Zn(II)**$_2$ and **38**$_{fluorene}$**·2·Zn(II)**$_2$).

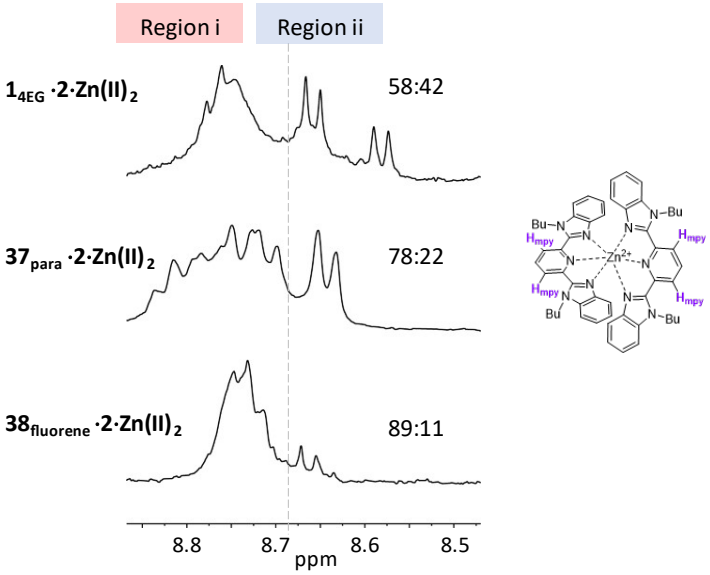

Figure 4.10 ^{1}H NMR (500 MHz, CD_2Cl_2, 25 °C) of **1**$_{4EG}$**·2·Zn(II)**$_2$, **37**$_{para}$**·2·Zn(II)**$_2$, and **38**$_{fluorene}$**·2·Zn(II)**$_2$ at 0.25 mM wrt **2**.

To further confirm the rigid macrocycles' aversion to forming *c*-MSP, **37$_{para}$·2·Zn(II)$_2$** and **38$_{fluorene}$·2·Zn(II)$_2$** were diluted to 0.25 mM in CD_2Cl_2 and tested via ^{1}H NMR (**Figure 4.10**). At this concentration, the **1$_{4EG}$·2·Zn(II)$_2$** shows 43% of the peak population in region ii, suggesting that nearly 90% of the MSP appears as cyclic.[6] However, at the same concentration, **37$_{para}$·2·Zn(II)$_2$** and **38$_{fluoro}$·2·Zn(II)$_2$** only show 22% and 11%, respectively. While the low concentrations will favor a cyclic MSP structure, both of these rigid macrocycles inhibit the efficient assembly of the c-MSP.[6] However, it is worth pointing out the possibility that the rigid macrocycles may form larger *c*-MSPs that have a different chemical shift, so complete exclusion of cyclic catenanes cannot be confirmed at this stage. Additionally, the complexity of the **37$_{para}$·2·Zn(II)$_2$** H_{mpy} peak in **Figure 4.10** may suggest that some *c*-MSP is being created, but it is displaying a different shift than what is typically observed for **1$_{4EG}$·2·Zn(II)$_2$**.

4.5 NMR Analysis

For each of the analyzed MSPs, a ring-closing reaction was performed at a concentration of 2.5 mM wrt **2** in dry DCM, following the procedures detailed in the Experimental Section (consistent with the procedures used in Chapters 2 and 3). After the metathesis reaction and further work-up, the crude reaction mixtures were collected for complete analysis. As with all previous analysis of poly[*n*]catenane materials detail so far, ^{1}H NMR spectroscopy (**Figure 4.11**) was used to analyze the crude products. For each reaction, the H_{mpy} region shows the three primary regions typically seen in poly[*n*]catenane synthesis: the free macrocycle (a doublet located between 8.29-8.35 ppm, depending on the macrocycle used), a thread-based byproduct at 8.35 ppm (doublet, attributed to the free thread, **2**, or the ADMET material, **5**), and a new set of peaks located between 8.05-8.27 ppm, tentatively attributed to catenated materials **41$_{2EG}$, 42$_{3EG}$, 43$_{meta}$, 44$_{para}$,** or **45$_{fluorene}$**. **46$_{BPZ}$** was analyzed somewhat differently (**Figure 4.12**): this synthesis was conducted at a time

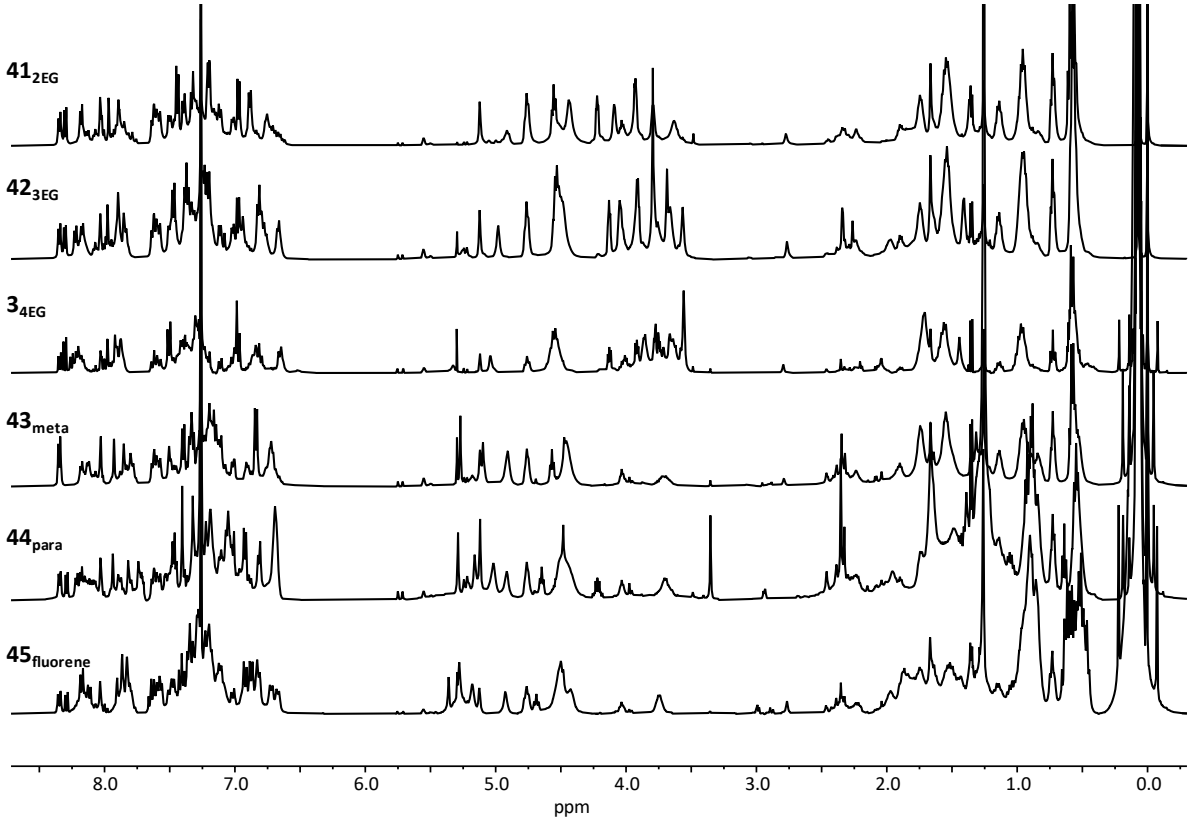

Figure 4.11 Full ^{1}H NMR spectrum (500 MHz, $CDCl_3$, 25 °C) for the crude samples of the analyzed poly[*n*]catenanes: **3$_{4EG}$, 41$_{2EG}$, 42$_{3EG}$, 43$_{meta}$, 44$_{para}$,** and **45$_{fluorene}$.**

when analysis of the crude materials was not the primary goal of the reaction. In this material, tetrabutylammonium hydroxide was used to demetallate the crude reaction mixture and the product was crashed out into acetonitrile. The Zn(II) and a portion of the **40$_{BPZ}$** remained in the acetonitrile, while **5** and **46$_{BPZ}$** was collected externally. Though this sample showed evidence of the new set of peaks located between 8.05-8.27 ppm, suggesting that catenated material was formed for this reaction, a combination of faulty GPC running procedures (see section 2.4 for more details) and complications in the synthesis of linker **32$_{BPZ}$** meant that this avenue of research was not pursued further. At this time, analysis of **46$_{BPZ}$** will no longer be discussed in this chapter.

To limit the amount of macrocyclic byproducts affecting the material analysis, each of the crude reactions were partially purified using the previously established metalation procedures.

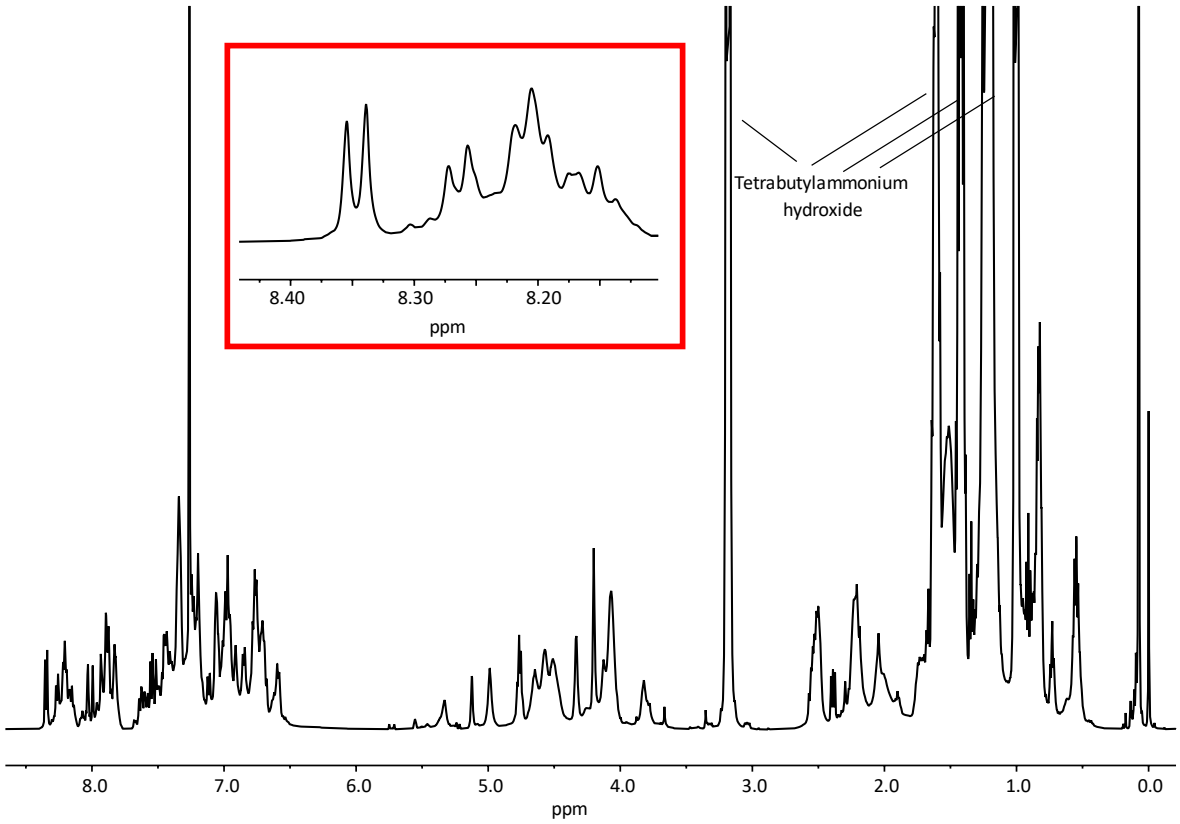

Figure 4.12 Full ^{1}H NMR spectrum (500 MHz, $CDCl_3$, 25 °C) for the partially purified sample of **46$_{BPZ}$.** Inset: H_{mpy} focus showing evidence of peaks in the region that historically has been attributed to poly[*n*]catenane (8.05-8.27 ppm).

Briefly: the crude materials were slowly titrated with metal and the principle of maximum site occupancy[7] ensured that the metal would preferentially bind with the interlocked materials rather than the free rings. The dried sample was washed with a 2:1 $CHCl_3$:hexanes mixture and monitored by UV lamp: the material fluoresced green while unmetalled fluoresced blue. The $CHCl_3$: hexanes mixture was only able to solubilize the non-metalated materials. Once only metalated materials remained, the sample was demetallated and dried.

Each new purified material was then subjected to COSY analysis to confirm the assignment of all new material peaks (**Figure 4.13-4.17**). Similar to the analysis performed in Chapter 3, the COSY analysis demonstrates that the peaks located between 8.05-8.27 ppm do correspond to the

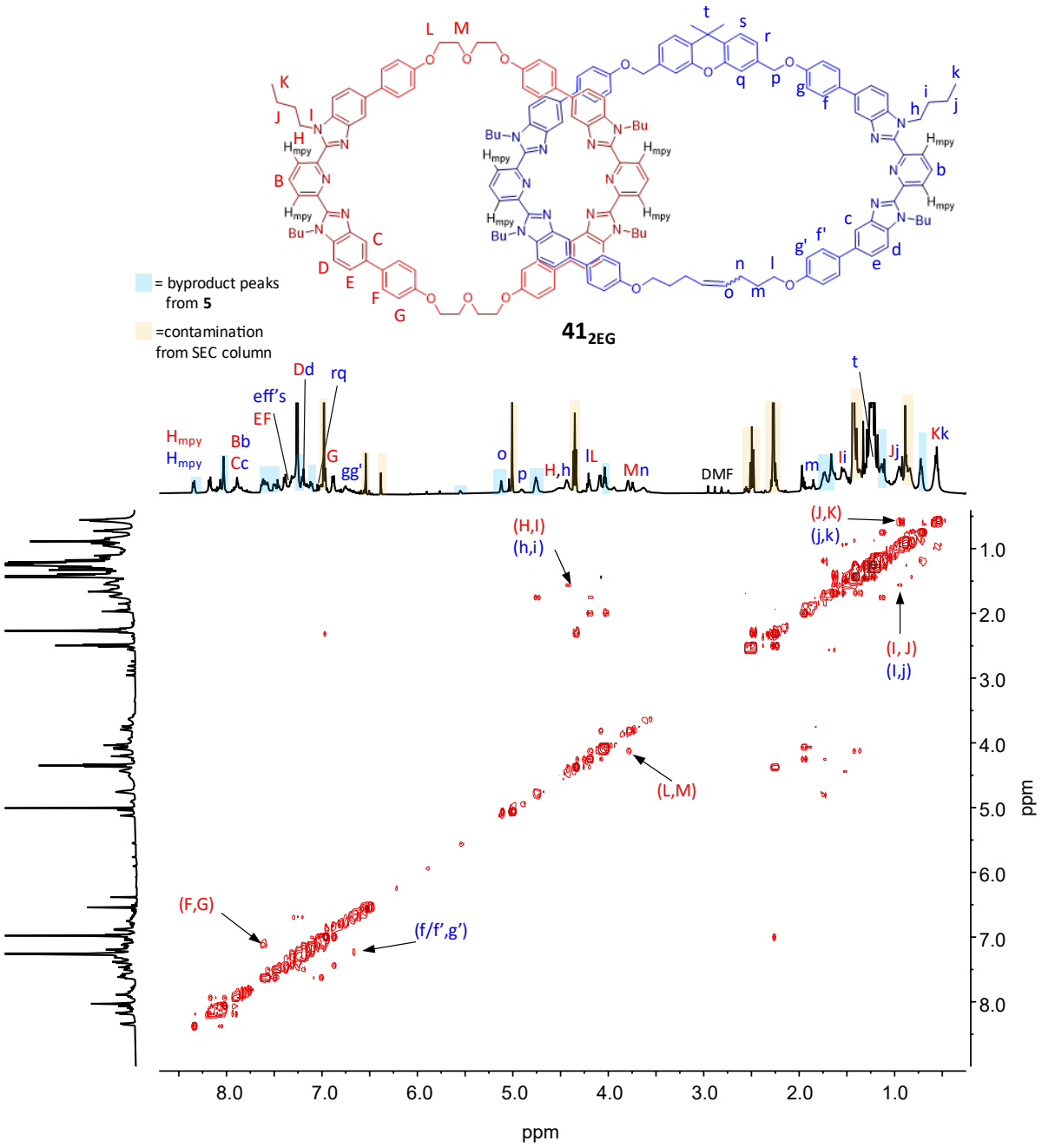

Figure 4.13 ^{1}H-^{1}H homonuclear correlation spectroscopy (COSY) (500 MHz, $CDCl_3$, 25 °C) of **41$_{2EG}$** (68% purified, 10 mg/mL). Peaks corresponding to the residual byproduct (**5**) are indicated via blue highlight.

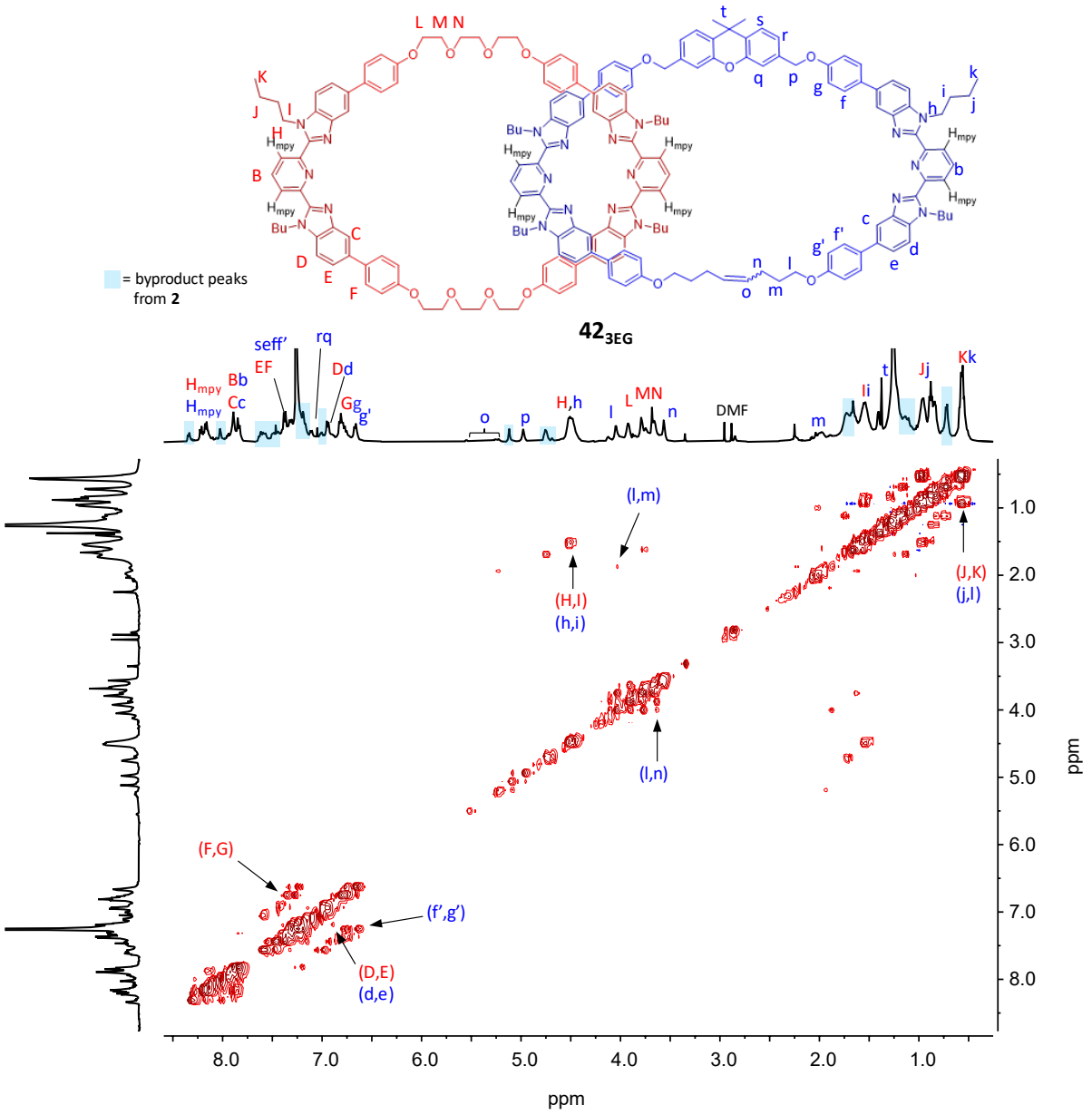

Figure 4.14 ^{1}H-^{1}H homonuclear correlation spectroscopy (COSY) (500 MHz, $CDCl_3$, 25 °C) of **42**$_{3EG}$ (83% purified, 10 mg/mL). Peaks corresponding to the residual byproduct (**5**) are indicated via blue highlight.

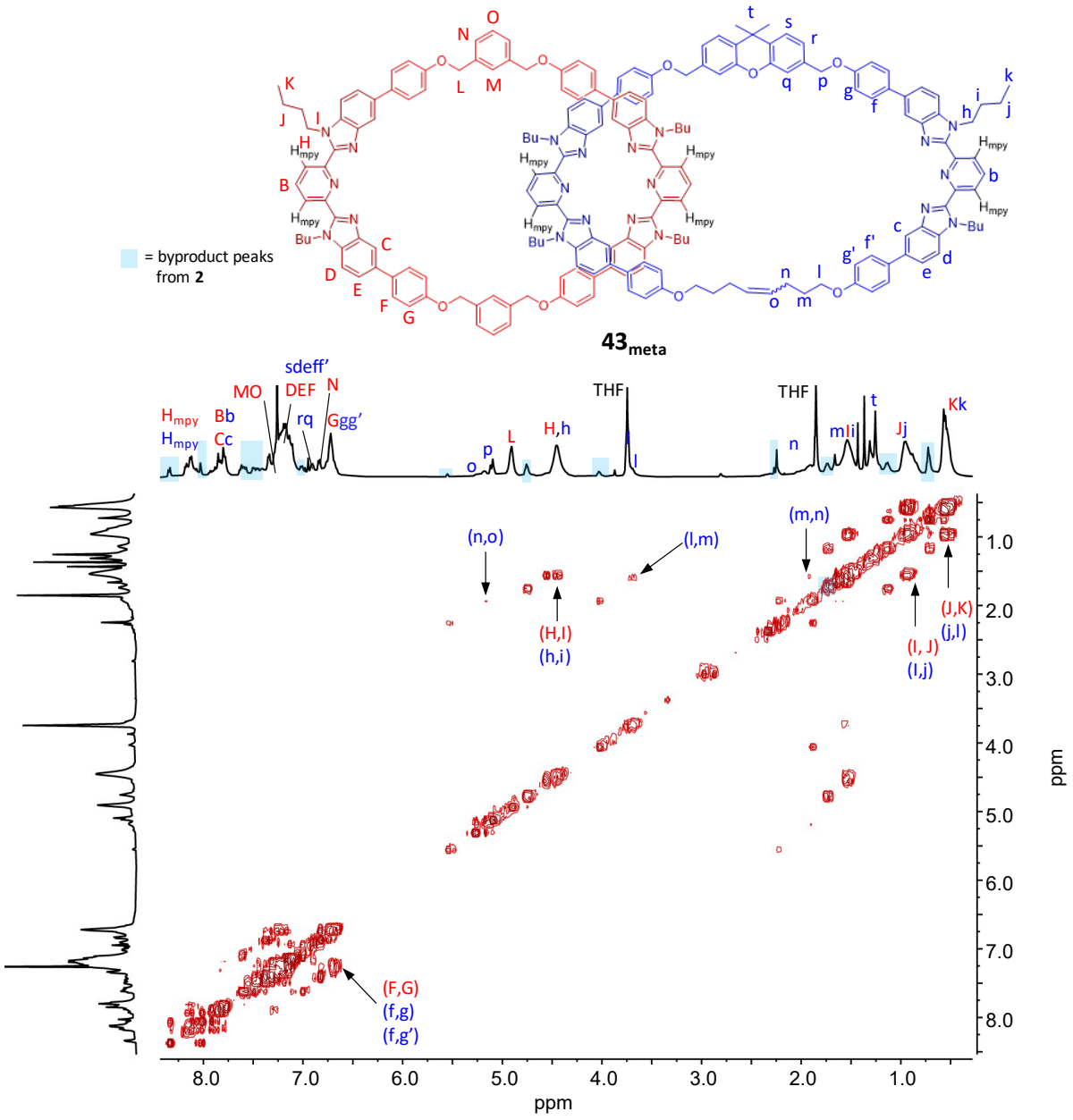

Figure 4.15 ^{1}H-^{1}H homonuclear correlation spectroscopy (COSY) (500 MHz, $CDCl_3$, 25 °C) of **43**$_{\mathbf{meta}}$ (87% purified, 10 mg/mL). Peaks corresponding to the residual byproduct (**5**) are indicated via blue highlight.

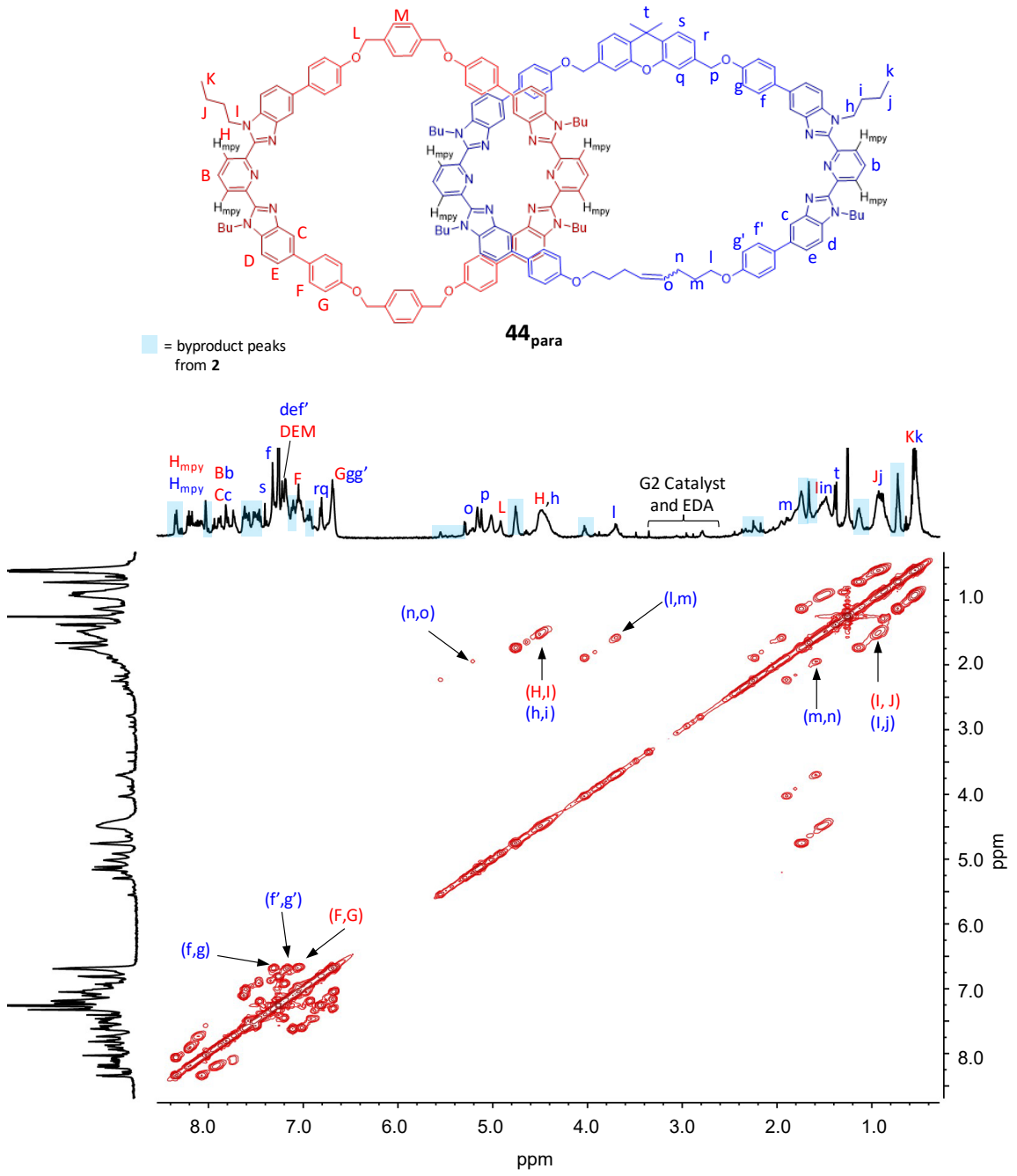

Figure 4.16 ^{1}H-^{1}H homonuclear correlation spectroscopy (COSY) (500 MHz, $CDCl_3$, 25 °C) of **44**$_{\mathbf{para}}$ (75% purified, 10 mg/mL). Peaks corresponding to the residual byproduct (**5**) are indicated via blue highlight.

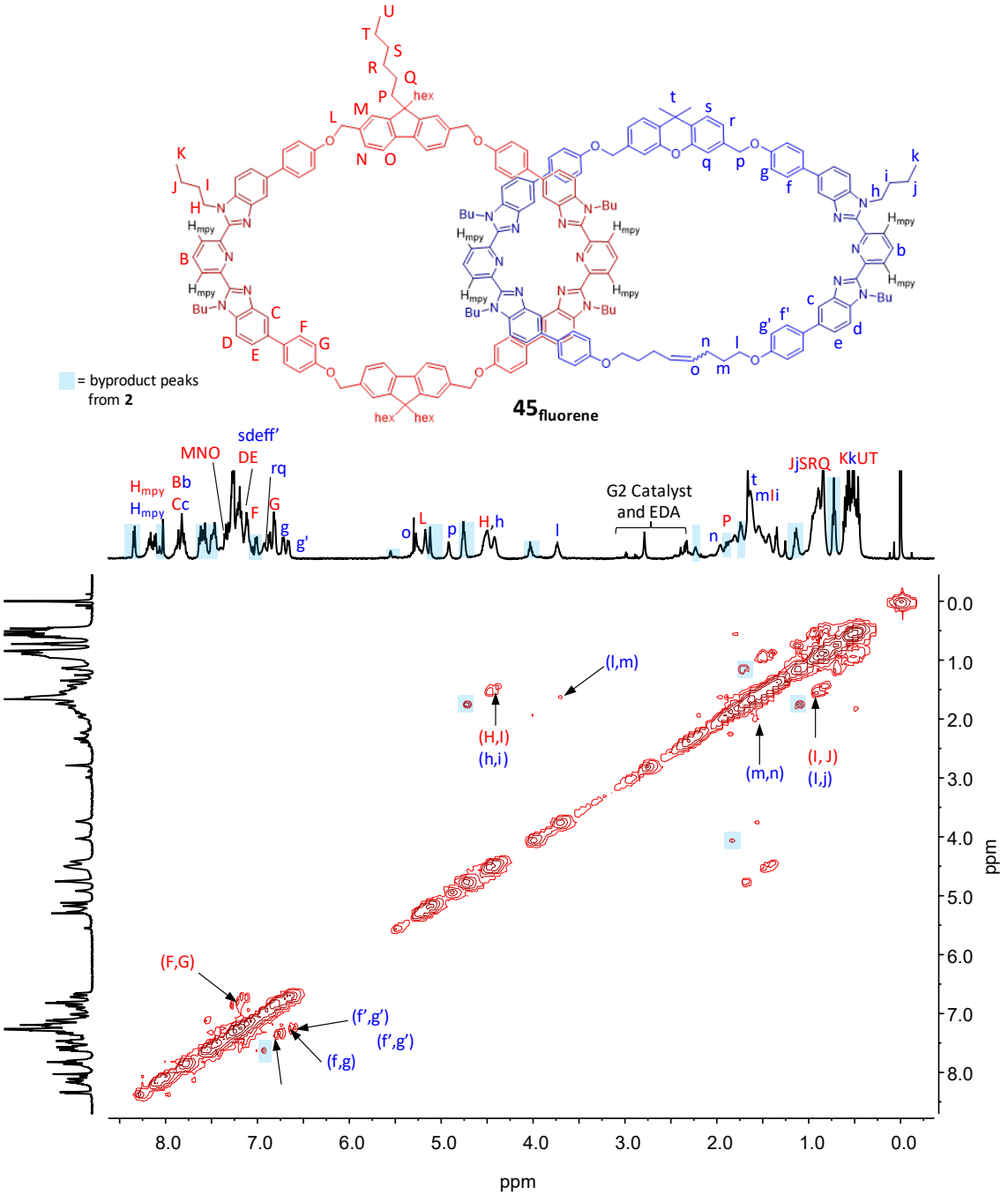

Figure 4.17 ^{1}H-^{1}H homonuclear correlation spectroscopy (COSY) (500 MHz, $CDCl_3$, 25 °C) of **45**$_{\text{fluorene}}$ (79% purified, 10 mg/mL). Peaks corresponding to the residual byproduct (**5**) are indicated via blue highlight.

new materials (**41_{2EG}-46_{BPZ}**) for all new materials. In each sample, ADMET **5** could not be fully removed from the sample and all peaks corresponding to this byproduct are highlighted in blue.

To confirm the interlocked nature of each new material, low temperature NOESY was employed. NOESY analysis allows for detection of cross-peaks between protons across space (non-bonded) within 5Å. Via this NMR method, cross-peaks between the non-covalently bonded interlocked components can be identified to confirm the interlocked nature of each new material, as was used in Chapter 3. For **41_{2EG}**, the NOESY analysis can be seen in **Figure 4.18**, with the cross-peaks between the interlocked components highlighted by the addition of black boxes. The presences of the cross-peaks between components proves the interlocked nature of the **41_{2EG}**.

Identical analyses were performed for **42_{3EG}, 43_{meta}, 44_{para},** and **45_{fluoro}**, as seen in **Figures 4.19-4.22**. Upon looking at these figures, it becomes evident that some of the catenanes have more apparent cross-peaks than others. This trend may be attributed to a couple of different factors. For example, macrocycles with many distinctive peaks in less-populated areas are more likely to show clean cross-peaks between rings (i.e. the peaks corresponding to LMN in **42_{3EG}, Figure 4.19**), than a compound like **$45_{fluorene}$,** where the peaks that are distinctive to the macrocycle overlap often with other peaks (i.e. all cross-peaks at 0.65 – 0.42 ppm may be attributed to either the hexyl chain of linker or the butyl chains of both macrocycles, **Figure 4.22**). To ensure accurate reporting, only peaks that *cannot* be intra-ring are highlighted as cross-peaks in **Figures 4.19-4.22**, however additional cross-peaks that are not highlighted may exist between components. Additionally, the frozen conformation of the catenanes does appear to change based on the structure. This is particularly noticeable with **44_{para}**, where the peaks corresponding to the closed alkene chain (lmno) show a clear association with the Bip protons of the macrocycle (C) that aren't seen in the

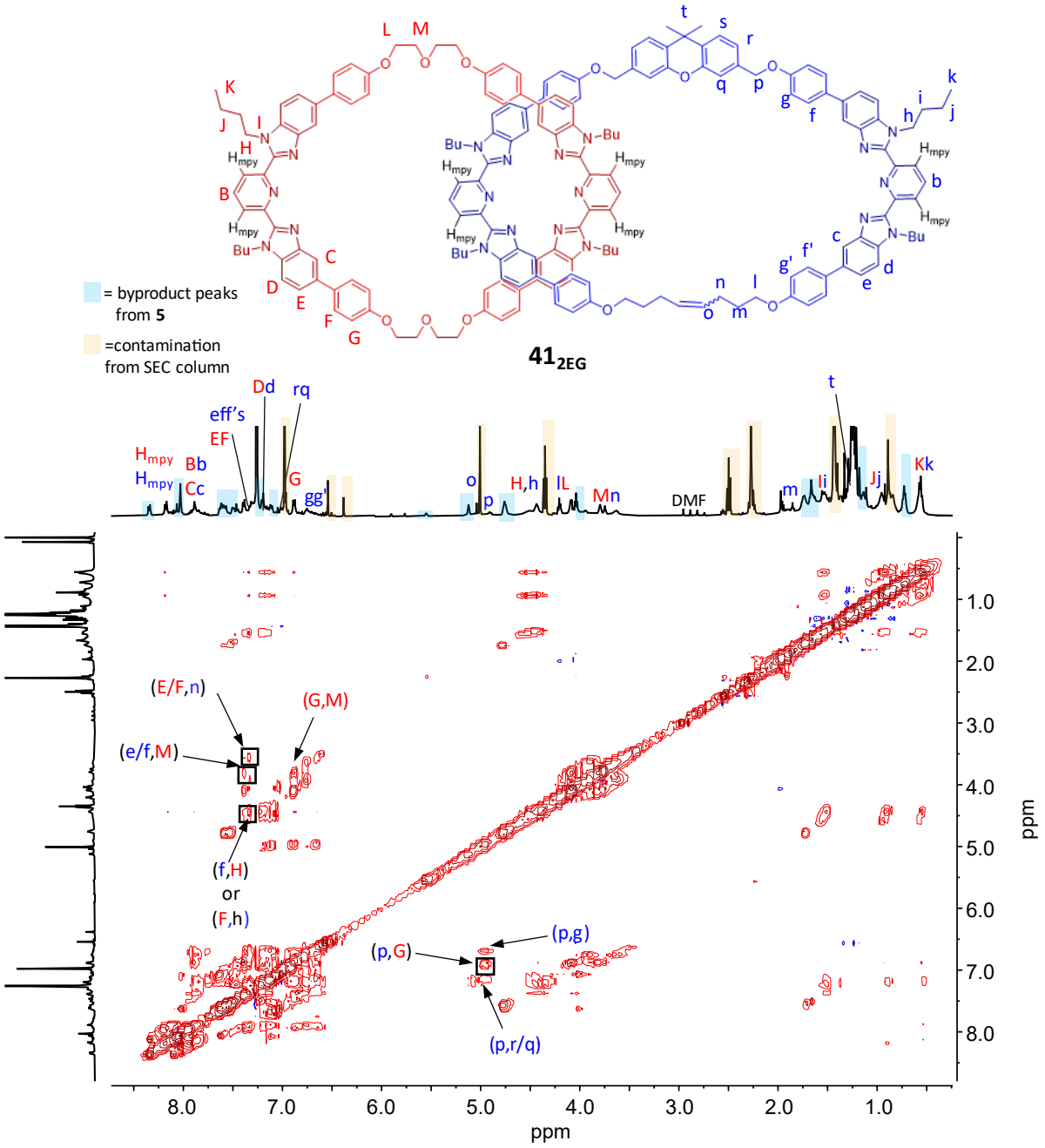

Figure 4.18 Nuclear Overhauser Effect Spectroscopy (NOESY) (500 MHz, $CDCl_3$, -25 °C) of **41**$_{2EG}$ (68% purified, 10 mg/mL) for confirmation of interlocked structure. A selection of the interlocked cross-peaks are identified with black boxes.

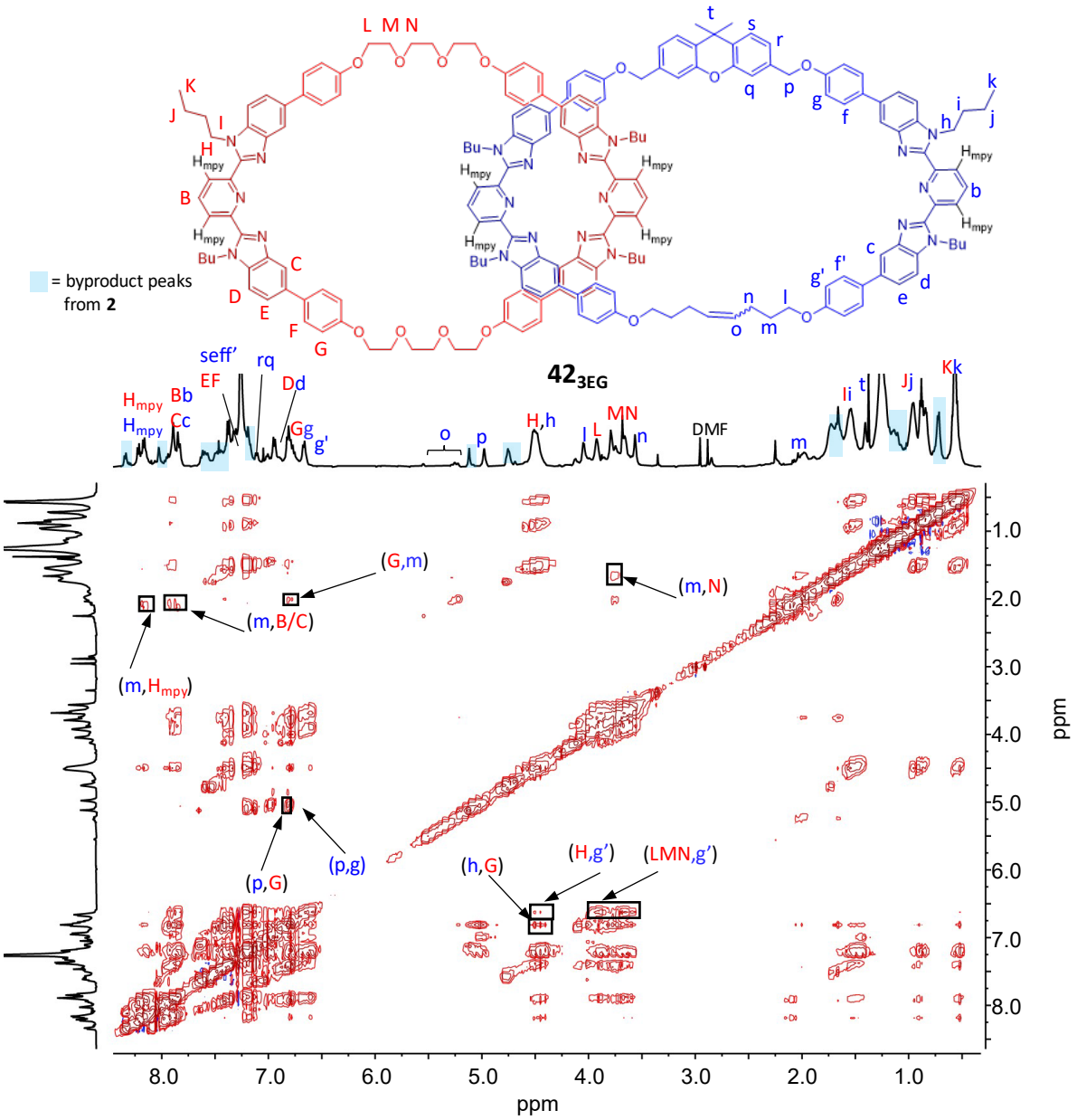

Figure 4.19 Nuclear Overhauser Effect Spectroscopy (NOESY) (500 MHz, $CDCl_3$, -25 °C) of **42**$_{3EG}$ (83% purified, 10 mg/mL) for confirmation of interlocked structure. A selection of the interlocked cross-peaks are identified with black boxes.

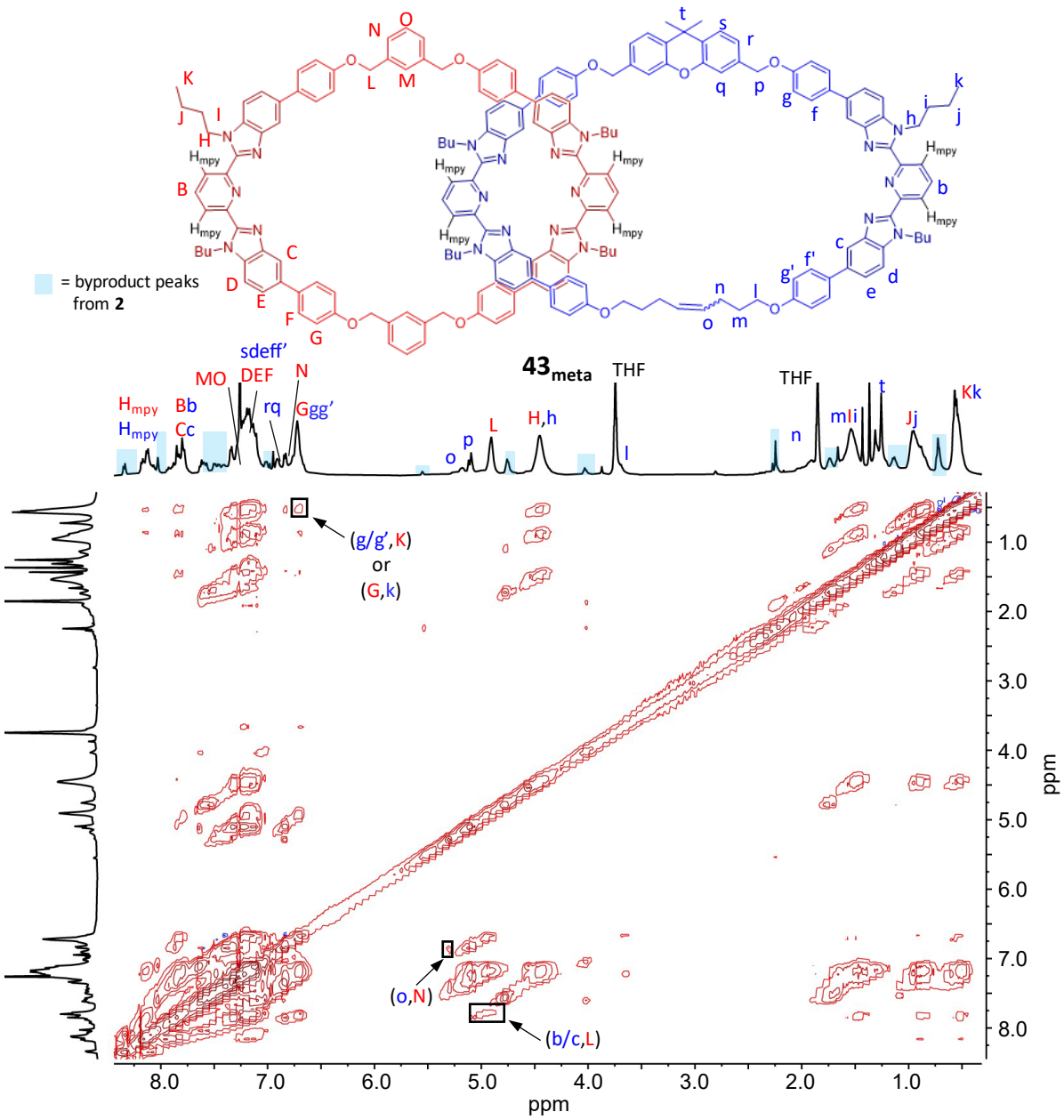

Figure 4.20 Nuclear Overhauser Effect Spectroscopy (NOESY) (500 MHz, $CDCl_3$, -25 °C) of **43**$_{meta}$ (73% purified, 10 mg/mL) for confirmation of interlocked structure. A selection of the interlocked cross-peaks are identified with black boxes.

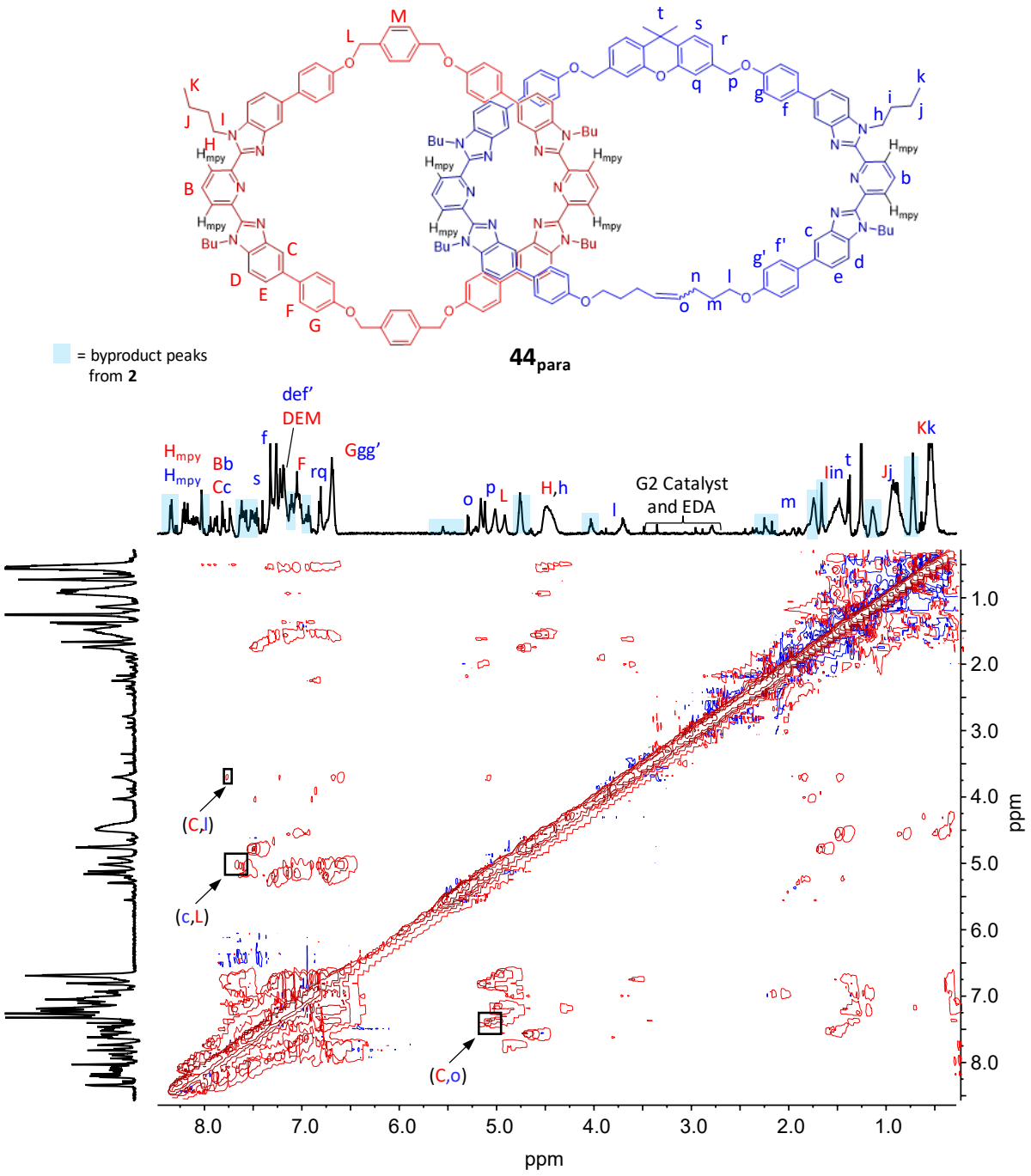

Figure 4.21 Nuclear Overhauser Effect Spectroscopy (NOESY) (500 MHz, $CDCl_3$, -25 °C) of **44**$_{para}$ (75% purified, 10 mg/mL) for confirmation of interlocked structure. A selection of the interlocked cross-peaks are identified with black boxes.

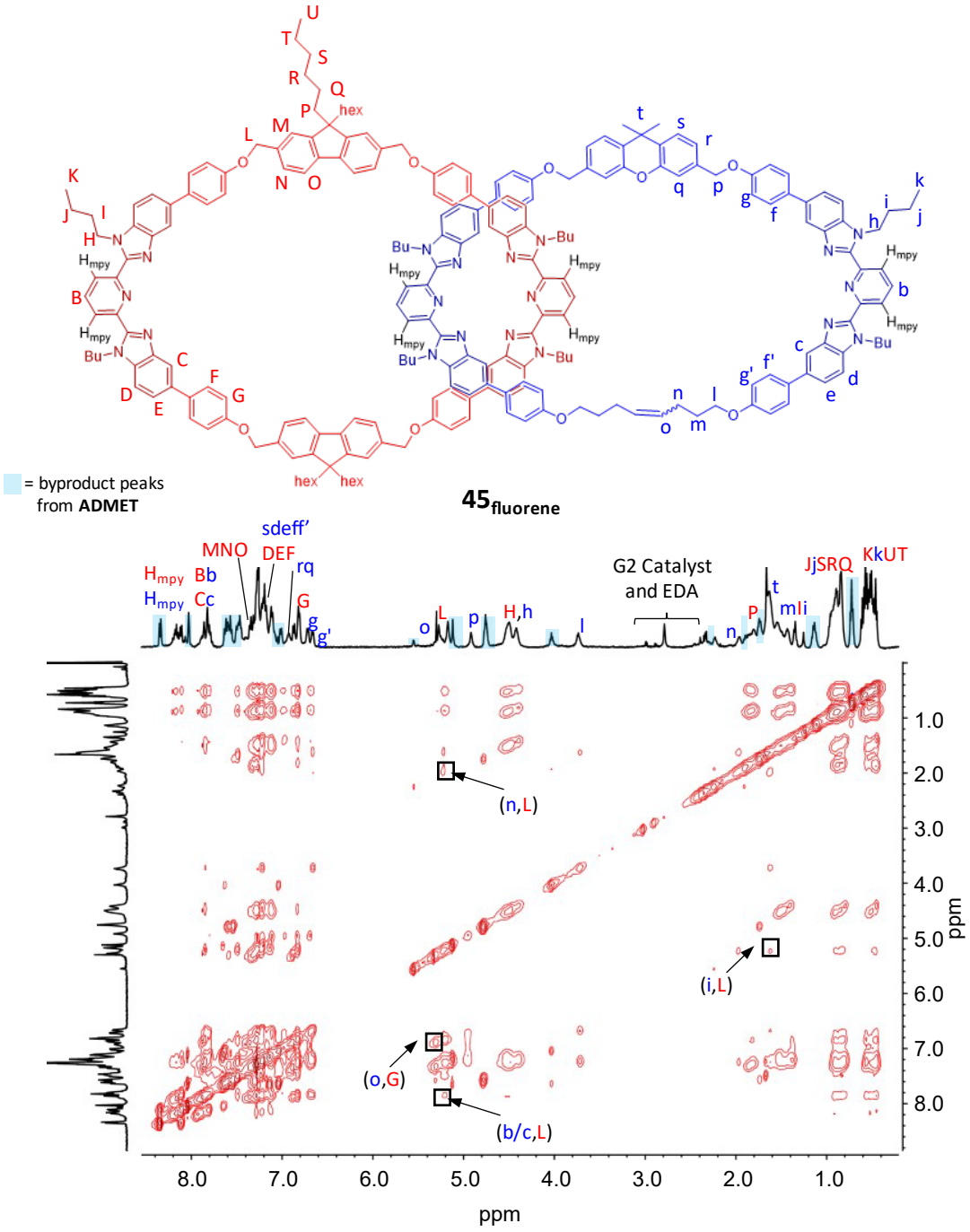

Figure 4.22 Nuclear Overhauser Effect Spectroscopy (NOESY) (500 MHz, $CDCl_3$, -25 °C) of **45**$_{\textbf{fluorene}}$ (79% purified, 10 mg/mL) for confirmation of interlocked structure. A selection of the interlocked cross-peaks are identified with black boxes.

other catenanes (**Figure 4.21**). However, even with these complexities and rigorous standards, inter-ring cross-peaks were identified for all new poly[*n*]catenane structures. This extensive NOESY analysis confirms that all the tested materials were able to form catenated materials.

With the H_{mpy} material assignments confirmed, the yield of poly[*n*]catenane can be analyzed (**Figure 4.23, Table 4.3**) by integrating the byproduct peaks (8.29-8.35 ppm) against the

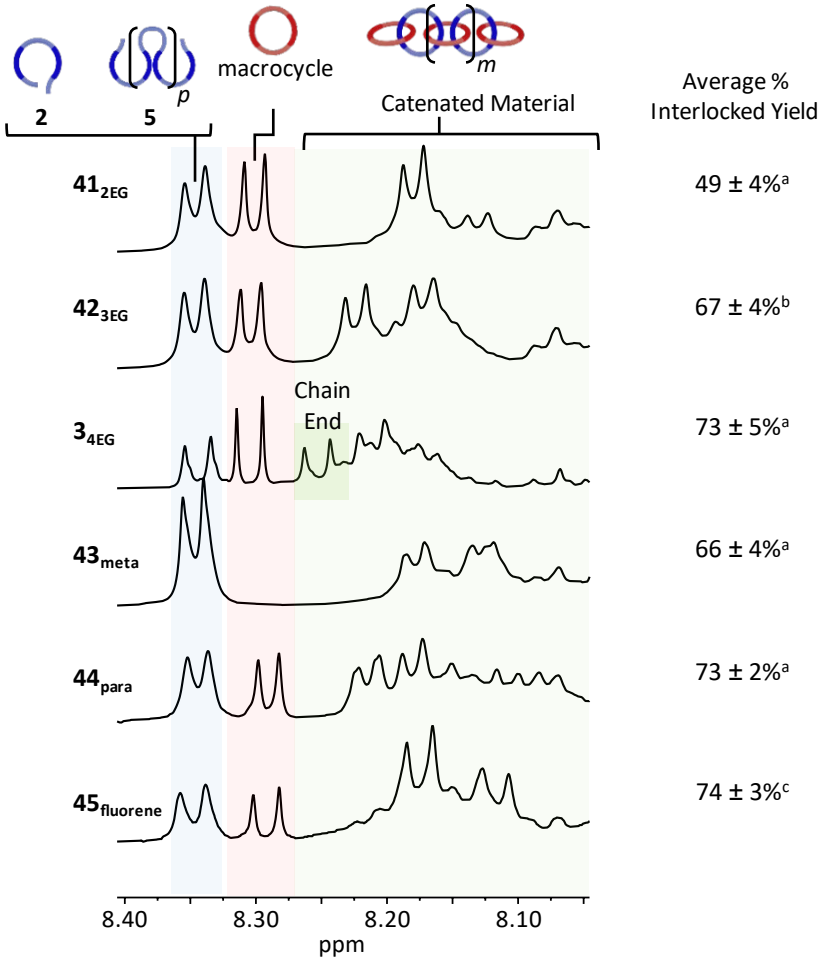

Figure 4.23 ^{1}H NMR (500 MHz, $CDCl_3$, 25 °C) for the crude samples of each new poly[*n*]catenane (**3**$_{4EG}$, **41**$_{2EG}$, **42**$_{3EG}$, **43**$_{meta}$, **44**$_{para}$, **45**$_{fluorene}$) with a focus on the H_{mpy} region. The byproducts corresponding to thread are highlighted in blue (**2**, **5**). The residual macrocycle (**33**$_{2EG}$, **34**$_{3EG}$, **1**$_{4EG}$, **37**$_{para}$, or **38**$_{fluorene}$) is highlighted in red. For the **36**$_{meta}$ based material, the doublets for **2** and **36**$_{meta}$ overlap exactly at 8.35 ppm (4th spectrum from the top). The interlocked materials (**41**$_{2EG}$, **42**$_{3EG}$, **3**$_{4EG}$, **43**$_{meta}$, **44**$_{para}$, or **45**$_{fluorene}$) are highlighted in green.
[a] Error for data set taken at 95% confidence interval (n=6).
[b] Error for data set taken at 95% confidence interval (n=3).
[c] Error for data set taken at 95% confidence interval (n=2).

interlocked material peaks (8.05-8.27 ppm). For each sample, any potential overlap between the catenane H_{mpy} peak and the byproduct was accounted for via Equation 4.1 and Equation 4.2:

$$\%\ Interlocked\ Yield = \frac{Integration\ ((8.05-8.27\ ppm)-(Triplet\ from\ \mathbf{6}\ at\ 8.07\ ppm))}{Intergration\ (8.05-8.38ppm)} \times 100 \qquad \text{Equation 4.1}$$

$$\%\ Interlocked\ \ \mathbf{43}_{\boldsymbol{meta}} = \frac{I\ ((8.05-8.27\ ppm)-I(T\ \mathbf{6}\ at\ 8.07\ ppm+T\ \mathbf{36}_{\boldsymbol{meta}}\ at\ 8.06\ ppm)}{I\ (8.05-8.38ppm)} \times 100 \qquad \text{Equation 4.2}$$

By comparing the integrals from the crude reaction mixtures to make **41**$_{2EG}$**, 42**$_{3EG}$ and **3**$_{4EG}$ (49 ± 4, 73 ± 5, and 67 ± 4%, respectively), it is clear that an increase in ring size (from 56, to 62, to 68 atoms) within the MSP increases the ratio of catenated products when the linkers between the Bip units in the macrocycle are flexible (i.e. ethylene glycol units). Moving to more rigid macrocycles does appear to result in an improvement in the polycatenane yield. For example, **43**$_{meta}$ and **44**$_{para}$**,** are both higher yielding (**43**$_{meta}$= 66 ± 4%, **44**$_{para}$= 73 ± 2%) than **41**$_{2EG}$ despite having with the same/similar atom sizes to **41**$_{2EG}$ (**43**$_{meta}$=56 atoms, **44**$_{para}$=58 atoms). This observation seems to align with the theory postulated in **Figure 4.2**, where the more rigid macrocycles may hinder the formation of the back-biting side reactions, ***l*-3·Zn(II)** and ****l*-3·Zn(II),** and increase the overall poly[*n*]catenane yield. It is worthy of note that a small increase in macrocycle size, the change from **36**$_{meta}$ (56 atoms) to **37**$_{para}$ (58 atoms) can result in a fairly significant increase in the interlocked yield (66% → 73%). Therefore, the ideal macrocycle for this reaction would be assumed to be a rigid structure that is larger than the **37**$_{para}$. Based on this data, **38**$_{fluorene}$ (64 atoms) represents an very interesting candidate to explore. However, **45**$_{fluorene}$ appears to have yields fairly similar to both **3**$_{4EG}$ and **44**$_{para}$ (74 ± 3 %), indicating that the yield improvements with the rigid macrocycles do not scale linearly.

Unlike the poly[*n*]catenane materials containing **1**$_{4EG}$ as a monomeric unit, the new materials do not necessarily have easily identifiable chain ends (chain ends for **3**$_{4EG}$ highlighted in **Figure 4.23**). Attempts to isolate the chain end were performed on the **44**$_{para}$ H_{mpy}: a titration with Zn(II) was conducted to take advantage of the catenand effect (**Figure 4.24**).[8,9] Briefly, the binding

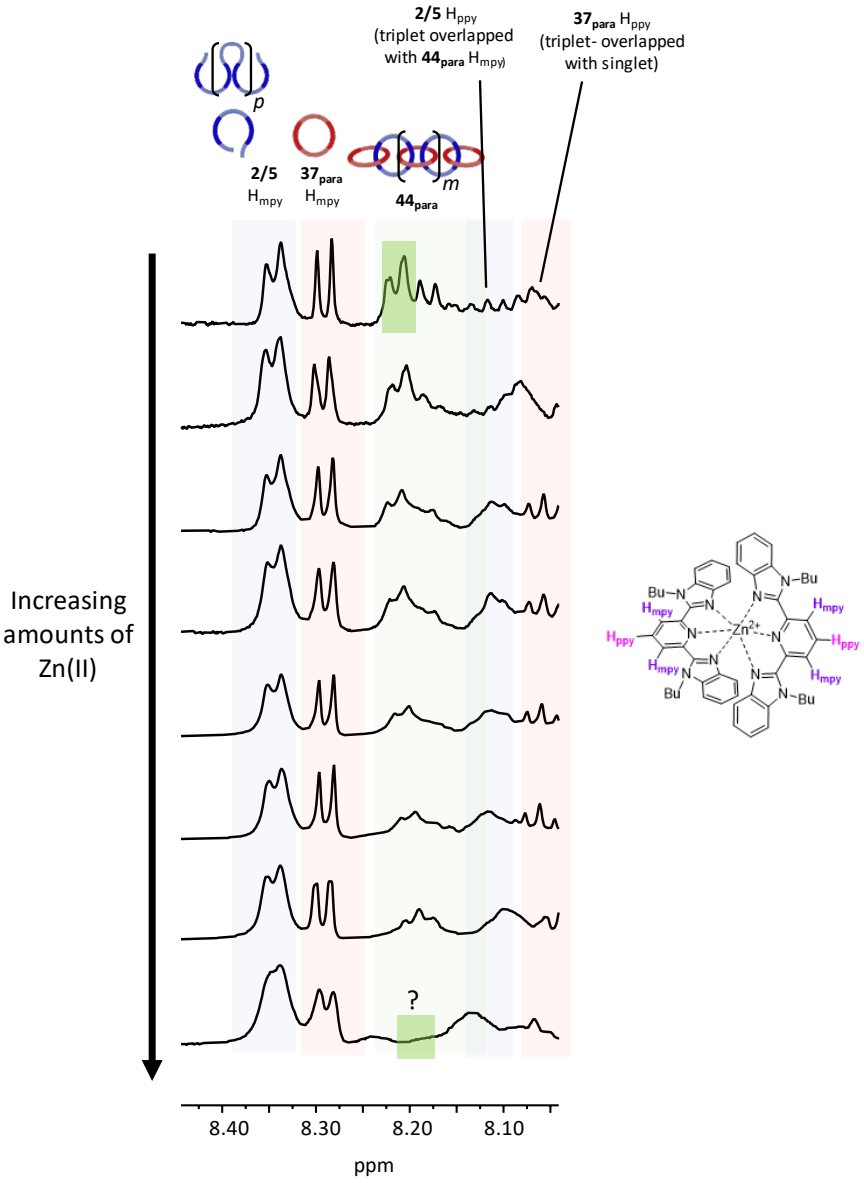

Figure 4.24 ^{1}H NMR (500 MHz, $CDCl_3$, -20 °C) of the crude **44**$_{para}$ material undergoing slowly Zn(II) titration. The furthest downfield peaks of the **44**$_{para}$ H_{mpy} appear to be final component metalated, suggesting that they may correspond to the chain ends of the catenane.

constant for the catenane pocket is such that the Zn(II) will preferentially bind to the catenated structure. By this reasoning, the free chain ends would be less likely to bind and would persist (to some degree) the longest when monitoring via ^{1}H NMR. The results in **Figure 4.24** show that, for **44$_{\mathbf{para}}$**, the most downfield shifted doublet is the final part of the catenated H_{mpy} to be metalated (emphasized in dark green). This is consistent with what was observed in the original **3$_{\mathbf{4EG}}$** system, where the most deshielded chain ends peaks correspond with the most downfield shifted doublet of the catenane. Unfortunately, for this material, the doublet in question appears to be overlapped with non-chain ends protons. Qualitative analysis of **41$_{\mathbf{2EG}}$**, **42$_{\mathbf{3EG}}$**, **43$_{\mathbf{meta}}$**, and **45$_{\mathbf{fluorene}}$** as well as T1 experiments of the crude materials seems to suggest similar struggles: the doublet that corresponds to the chain ends cannot be isolated in the same way as the **3$_{\mathbf{4EG}}$** material. As a result, the following GPC analysis can elucidate information about molecular weight and $\overline{DP}$, however exact architecture breakdowns as seen in Chapters 2 and 3 are not possible for these materials.

4.6 GPC Analysis

In addition to each of the NMR analyses, GPC-MALS offers the clearest picture of the variations of the new poly[*n*]catenane syntheses. To gain a more accurate representation of the molecular weight of the polymeric materials, *dn/dc* values for each new catenane were obtained via an analysis of a series of concentrations of the partially purified materials. These numbers were applied to the GPC-MALS data of each crude reaction mixture. Based on the information obtained from the MALS, **Table 4.3** lists the calculated molecular weight data for each new polycatenane system. From the previously materials (Chapters 2 and 3), analysis of the crude (unpurified) reaction mixture has been shown to give the most representative molecular weight data for polycatenanes. As a result, the crude samples for each catenane were used to provide an accurate representation of each polycatenane via GPC-MALS (**Figure 4.25**).

Table 4.3 Quantitative data of poly[*n*]catenane obtained via ^{1}H NMR and GPC-MALS

Polymer	Atom Size of Macrocycle	Average Catenane Yield (%)[a]	$\overline{M}_n$[b]	$\overline{DP}$[c]
41$_{2EG}$	56	49 ± 4[d]	10200	7
42$_{3EG}$	62	67 ± 4[e]	11700	8
3$_{4EG}$	68	73 ± 5[e]	17100	11
43$_{meta}$	56	66 ± 4[e]	14400	10
44$_{para}$	58	73 ± 2[e]	15600	11
45$_{fluorene}$	64	74 ± 3[f]	16800	10

(a) Average catenane yield. (b) GPC-MALS (3:1 THF:DMF solvent mixture) individual *dn/dc* values determined for each catenane. Molecular weight is determined taking the area of the GPC trace at elution time up to but not including the residual macrocycle. (c) Number average degree of polymerization calculated from Equation 2.1. (d) Error for data set taken at 95% confidence interval (n=6). (e) Error for data set taken at 95% confidence interval (n=3). (f) Error for data set taken at 95% confidence interval (n=2).

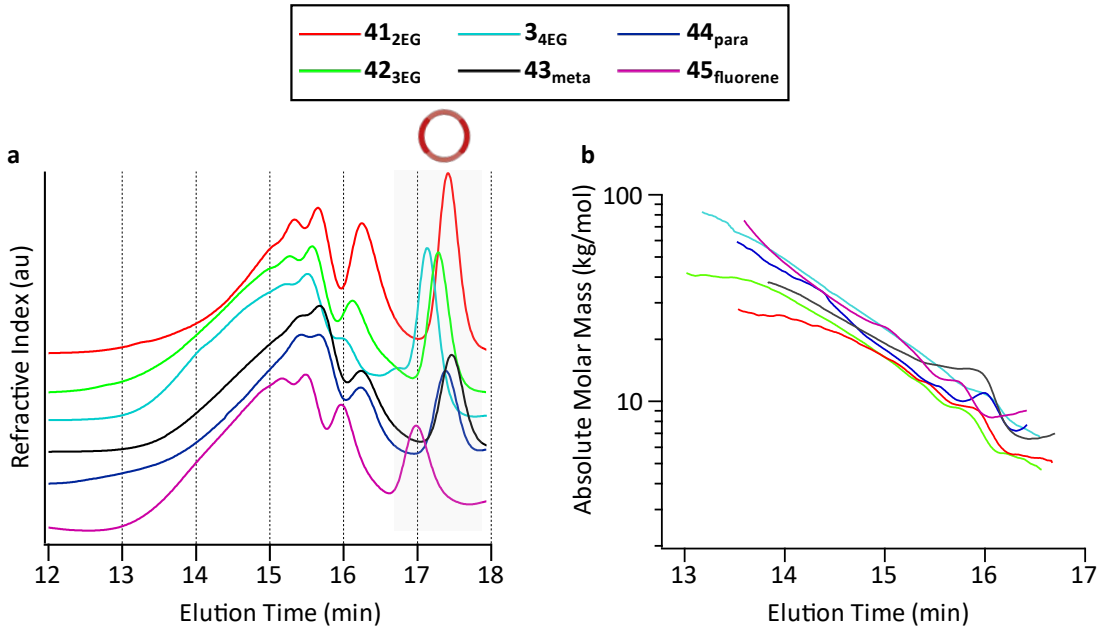

Figure 4.25 a) GPC (mobile phase - 25% DMF in THF) refractive index traces for (top to bottom) **41**$_{2EG}$, **42**$_{3EG}$, **3**$_{4EG}$, **43**$_{meta}$, **44**$_{para}$, and **45**$_{fluorene}$. b) Absolute molar mass for each new poly[*n*]catenane sample.

Though complete deconvolution was not carried out for each sample, samples of the starting materials can be compared to the traces to isolate these components. RI traces for pure **33**$_{2EG}$, **34**$_{3EG}$, **36**$_{meta}$, **37**$_{para}$, and **38**$_{fluorene}$ were collected (**Figure 4.26**) and seen to elute at approximately 17-18 minutes, corresponding to the sharp signals in each crude sample at this time (**Figure 4.25a**).

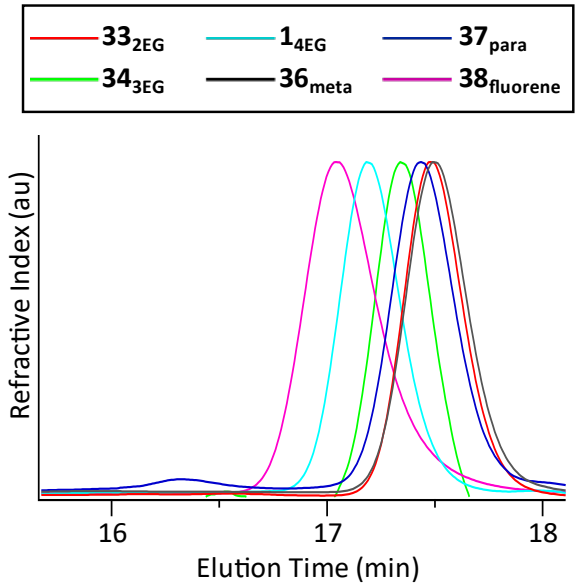

Figure 4.26 GPC traces (25% HPLC grade dimethylformamide (DMF) and 75% HPLC grade tetrahydrofuran (THF) as the eluent (1mL/min) at 25 °C) taken for the starting materials: the thread-like monomer (**2**) and each macrocycle used in poly[*n*]catenane synthesis: **33**$_{2EG}$**, 34**$_{3EG}$**, 1**$_{4EG}$**, 36**$_{meta}$**, 37**$_{para}$**,** and **38**$_{fluorene}$**.**

Based on this result, this region is assumed to contain no interlocked materials and was excluded from the molecular weight analysis seen in **Table 4.3**. Analysis of the GPC-MALS appear to show that there is a correlation between interlocked yield and molecular weight (**Figure 4.25b**). This is certainly most evident when inspecting the reaction mixture of **41**$_{2EG}$, which gave the lowest yield of interlocked products (49%) and forms the smallest polymers (10,200 g mol^{-1}). This is not a surprise: for a step growth polymerization, a lower extent of reaction (i.e. ring-closing metathesis) will drastically decrease the molecular weight of the obtained polymers. Based on the molecular weight analysis, the **44**$_{para}$ and the **45**$_{fluorene}$ seem to have been the most successful syntheses of large molecular weight catenanes, apart from the original **3**$_{4EG}$ materials.

4.7 Conclusions and Future Directions

The synthesis of a large library of macrocycles has allowed insight into the parameters that affect poly[*n*]catenane synthesis (size, rigidity, etc.) and proof that the synthesis of poly[*n*]catenanes does not require the use of macrocycle **1$_{4EG}$**. This study represents the largest collection of poly[*n*]catenane materials made (**Figure 4.11** and **4.12**) and included multiple tests that show the limitations of the macrocycles accessible for poly[*n*]catenane synthesis (**Figure 4.5**). The final aim of this project will be to explore the synthesis of **44$_{para}$** or **45$_{fluorene}$** at a lower synthesis concentration (ideally 0.5 or 1.0 mM) to see if these materials may result in the exclusion of *c*- and *b*- catenanes.

4.8 Experimental

4.8.1 Materials and Methods

Dichloromethane (DCM) was purchased from Acros Organics and distilled over CaH_2 under argon atmosphere before using. Dimethylformamide (DMF, anhydrous) was purchased from Fisher Chemical and was stored over molecular sieves. Deuterated solvents, containing tetramethylsilane (TMS) as internal standard, were purchased from Sigma Aldrich. Zinc di[bis(trifluorenemethylsulfonyl)imide] was purchased from Strem Chemicals and stored in a nitrogen desiccator. All other chemicals were purchased from Sigma-Aldrich and used without further purification unless otherwise mentioned. All silica column chromatography was performed on a Buchi Reveleris X2 Flash Chromatography System. Preparatory gel permeation chromatography was performed on a hand loaded column with Bio-Beads S-X1 gel and a mixture of 25% HPLC grade dimethylformamide (DMF) and 75% HPLC grade tetrahydrofuran (THF) as mobile phase.

NMR data was acquired on either a 400 MHz Bruker DRX spectrometer equipped with a BBO probe, using Topspin 1.3; or a 500 MHz Bruker Avance-II+ spectrometer equipped with a $^{1}H\{^{19}F, ^{13}C, ^{31}P\}$ QNP probe, using Topspin 2.1. Chemical shifts were calibrated with TMS for all measurements. Diffusion measurements were obtained using the 2D Bruker pulse program stebpgp1s, which includes a stimulated echo, bipolar gradient pulses, and one spoil gradient. The corresponding 1D pulse sequence stebpgp1s1d was used to optimize the parameters D20 ("big delta", the major diffusion delay) and P30 ("little delta", the diffusion gradient length), in accord with manufacturer-recommended methods.[10] The 2D data were acquired with a linear array of 32 diffusion gradient strengths (GPZ6 values) from 5% to 95%. All 1D and 2D NMR spectra were processed by either MestReNova software or Bruker Topspin 4.0.6. Diffusion coefficients were determined using the Bruker Topspin 4.0.6 direct exponential curve resolution algorithm (DECRA) plotting method.

Analytical GPC was performed on a Shimadzu Prominance LC system with PLgel Mixed-D columns using a mixture of 25% HPLC grade DMF and 75% HPLC grade THF as the eluent (1mL/min) at 25 °C. Characterization of the eluent occurred using Wyatt Dawn Helios MALS (658 nm laser) and Wyatt Optilab T-rEX refractive index (RI) detectors. The *dn/dc* values for each new poly[*n*]catenane material were measured by injecting a series of diluted samples of each material (**41**$_{2EG}$**, 42**$_{3EG}$**, 43**$_{meta}$**, 44**$_{para}$**,** or **45**$_{fluorene}$) in 25% DMF/THF solution (concentration: 0.25, 0.5, 1.0, and 2.0 mg/mL) subsequently into the RI detector until receiving stable signal for each concentration and processed by Wyatt Astra software. The following *dn/dc* values were obtained: 0.1974 for **41**$_{2EG}$, 0.2117 for **42**$_{3EG}$, 0.2330 for **43**$_{meta}$, 0.2930 for **44**$_{para}$, and 0.2094 for **45**$_{fluorene}$.

MALDI-TOF was measured by a Bruker Ultraflextreme MALDI TOF-TOF spectrometer using dithranol as the matrix and sodium trifluoreneacetate as ionizer (when necessary). UV-vis

measurements were collected on a Shimadzu UV-3600 Plus UV-VIS-NIR spectrophotometer with a resolution of 0.1 nm.

4.8.2 Synthesis Procedures

4.8.2.1 Synthesis of macrocycle 33_{2EG}

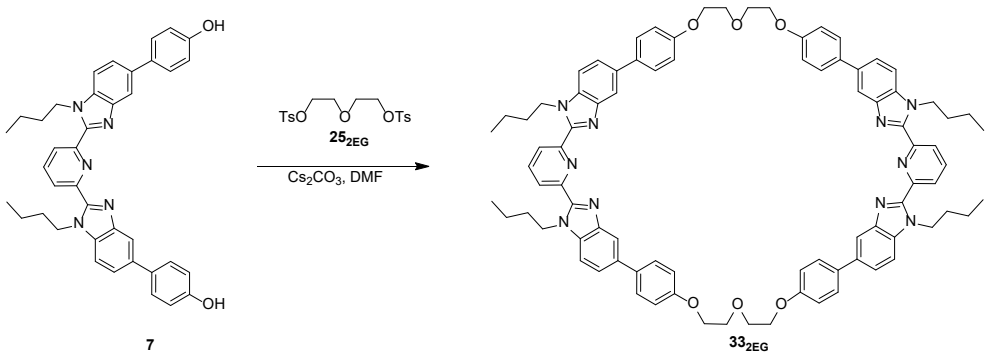

A 500 L addition funnel containing the linker $\mathbf{25_{2EG}}$ (diethylene glycol di-p-toluenesulfonate, synthesized as linker $\mathbf{8_{4EG}}$ in Chapter 2.6.2.2, 1.80 g, 4.34 mmol) in 500 mL of anhydrous DMF was fitted to a 2 L two-necked round bottom flask containing **7** (2.64 g, 4.34 mmol) and Cs_2CO_3 (5.66 g, 17.4 mmol, 4 eq.) and a stir bar. The reaction vessel was flushed with argon before anhydrous DMF (630 mL) was added by cannula. The reaction was submerged in a silicone oil bath and heated to 75 °C while rapidly stirring. Over the course of 3 days, $\mathbf{25_{2EG}}$ was added dropwise to the reaction vessel. The reaction was stirred at 75°C for an additional 4 days (for a total of 7 days), after which the solvent was removed, the crude product was triturated with $CHCl_3$, and the insoluble salt was removed via filtration. The filtrate was collected and solvent was removed under vacuum. The resulting residue was purified by flash chromatography (1% methanol in chloroform, TEA treated silica, multiple columns) followed by recrystallization in chloroform to yield the desired macrocycle as a white solid in 22% yield.

^{1}H NMR (500 MHz, $CDCl_3$) δ_H (ppm) 8.30 (d, J = 7.8 Hz, 4H), 8.02 (t, J = 7.8 Hz, 2H), 7.96 (d, J = 1.2 Hz, 4H), 7.44 (d, J = 8.6 Hz, 8H), 7.32 (dd, J = 8.4 Hz, 1.5 Hz, 4H), 7.20 (d, J = 8.5 Hz, 4H), 6.97 (d, J = 8.6 Hz, 8H), 4.55 (t, J = 7.2 Hz, 8H), 4.23 – 4.20 (m, 8H), 3.94 (m, 8H), 1.56 (m, 8H), 0.98-0.91 (m, 8H), 0.59 (t, J = 7.20 Hz 6H). ^{13}C NMR (126 MHz, $CDCl_3$) δ_C (ppm): 158.0, 150.4, 150.0, 143.3, 138.1, 136.0, 135.3, 134.3, 128.2, 125.4, 123.3, 117.8, 115.8, 110.4, 70.0, 68.0, 44.5, 32.0, 19.7, 13.5. MALDI-MS: m/z 1356 ($[M]H^+$).

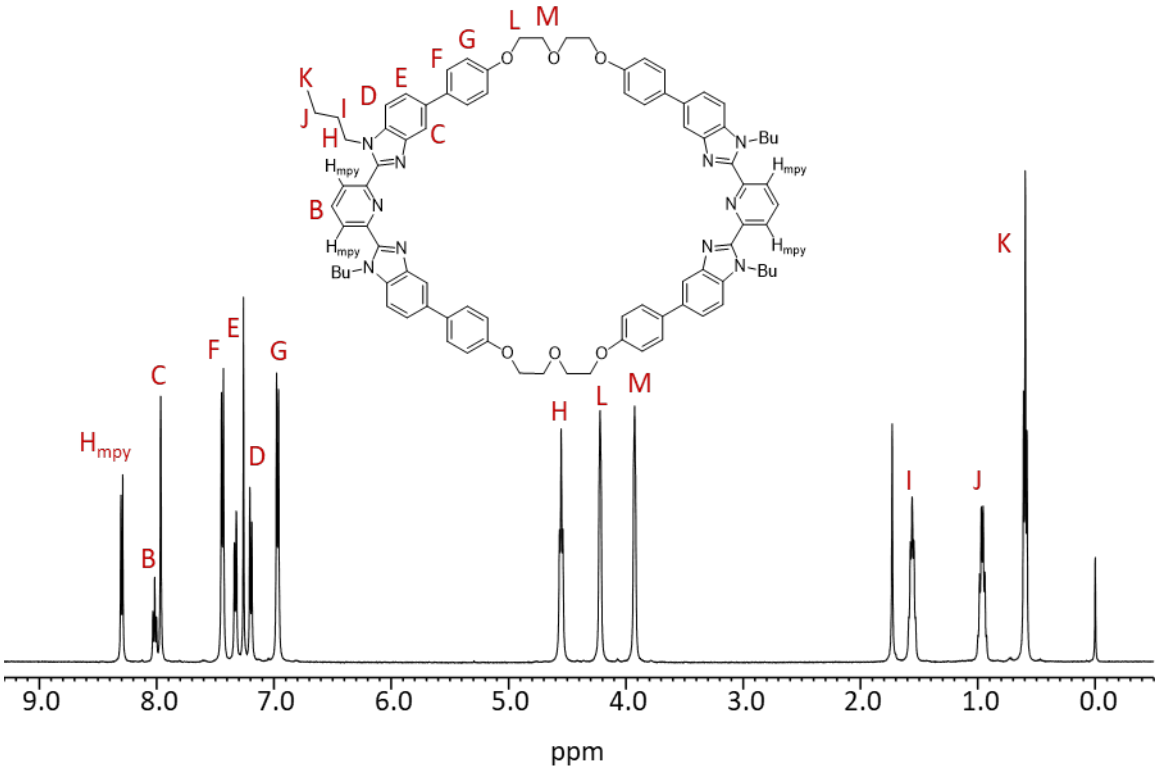

4.8.2.2 Synthesis of macrocycle 34_{3EG}

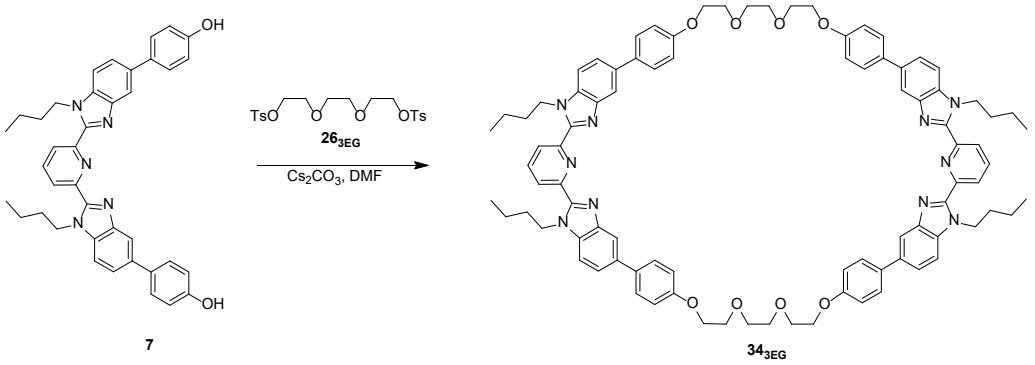

Macrocycle $\mathbf{34_{3EG}}$ was synthesized in a similar fashion to macrocycles $\mathbf{1_{4EG}}$ and $\mathbf{33_{2EG}}$. Briefly, $\mathbf{26_{3EG}}$ (1.51g, 3.3 mmol) was dissolved in 430 mL of anhydrous DMF in an addition funnel and slowly (3 days) dripped into a mixture of **7** (2.0 g, 3.3 mmol) and Cs_2CO_3 (4.29 g, 13.2 mmol, 4 eq.) in 430 mL DMF. The synthesis ran for a total of 7 days while heating at 75 °C. After cooling to room temperature, the solvent was removed, the crude product was triturated with $CHCl_3$, and the insoluble salt was removed via filtration. The filtrate was collected and solvent was removed under vacuum. The resulting residue was purified by flash chromatography (0.5 - 2% gradient in methanol/ chloroform, on TEA treated silica, multiple columns) followed by recrystallization in chloroform to yield the desired macrocycle as a white solid in 9.5% yield. ^{1}H NMR (500 MHz, $CDCl_3$) δ_H (ppm) 8.30 (d, J = 7.9 Hz, 4H), 7.99 (t, J = 7.8 Hz, 2H), 7.98 (s, 4H), 7.47 (d, J = 8.6 Hz, 8H) 7.36 (dd, J = 8.4 Hz, J = 1.1 Hz, 4H), 7.22 (d, J = 8.5 Hz, 4H), 6.97 (d, J = 8.6 Hz, 8H), 4.54 (t, J = 7.2 Hz, 8H), 4.13 (t, J = 9.3 Hz, 8H), 3.91 (t, J = 9.3 Hz, 8H), 3.79 (s, 8H), 1.54 (m, 4H, CH_2), 0.93 (m, 4H, CH_2), 0.58 (t, J = 7.4 Hz, 6H). ^{13}C NMR (122 MHz, $CDCl_3$) δ_C (ppm) 158.2, 150.4, 150.0, 143.3, 138.0, 135.9, 135.4, 134.1, 128.2, 125.5, 123.1, 117.8, 115.3, 110.4, 71.1, 69.9, 67.7, 44.5, 32.0, 19.7, 13.4. MALDI-MS: m/z 1444 ($[M]H^+$).

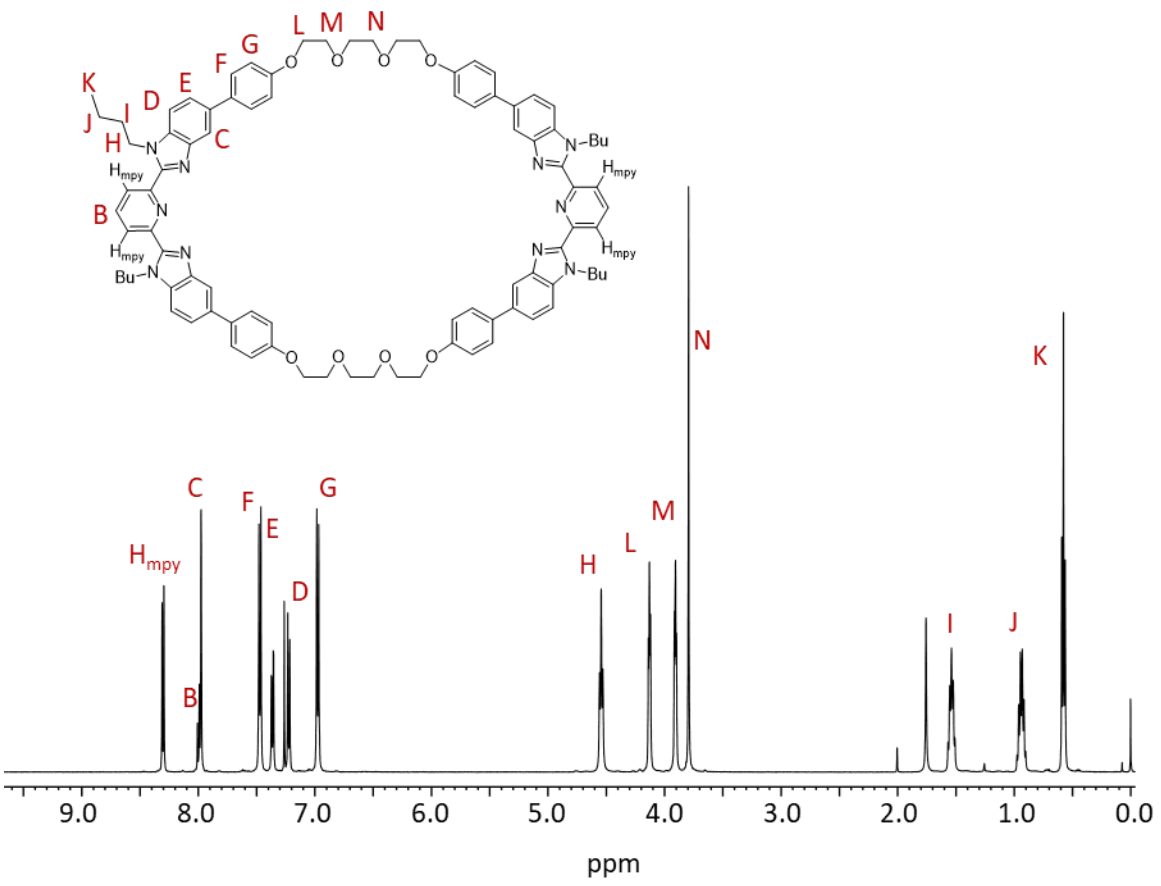

4.8.2.3 Synthesis of Ortho (**35**$_{ortho}$), Meta (**36**$_{meta}$), and Para (**37**$_{para}$) Macrocycles

A 500 mL addition funnel containing 435 mg (1.65 mmol) of a commercially available α,α'-dibromo-xylene material (**27**$_{ortho}$**, 28**$_{meta}$**,** or **29**$_{para}$) in 206 mL of anhydrous DMF was fitted to a 1 L two-necked round bottom flask containing **7** (1.0 g, 1.65 mmol, 1 eq.) and Cs_2CO_3 (2.15 g, 6.6 mmol, 4 eq.) and a stir bar. The reaction vessel was flushed with argon before anhydrous DMF (206 mL) was added to the flask. The reaction was submerged in a silicone oil bath and heated to 75 °C while rapidly stirring. Over the course of 3 days, the xylene (**27, 28,** or **29)** was added dropwise to the reaction vessel. The reaction was stirred at 75°C for an additional 4 days (for a total of 7 days), after which the solvent was removed, the crude product was triturated with $CHCl_3$, and the insoluble salt was removed via filtration. The filtrate was collected and solvent was

removed under vacuum. Each crude mixture was purified by column chromatography on TEA treated silica with a mobile phase gradient of 0-1% MeOH/$CHCl_3$ over 20 CV. Final purification steps varied based on material.

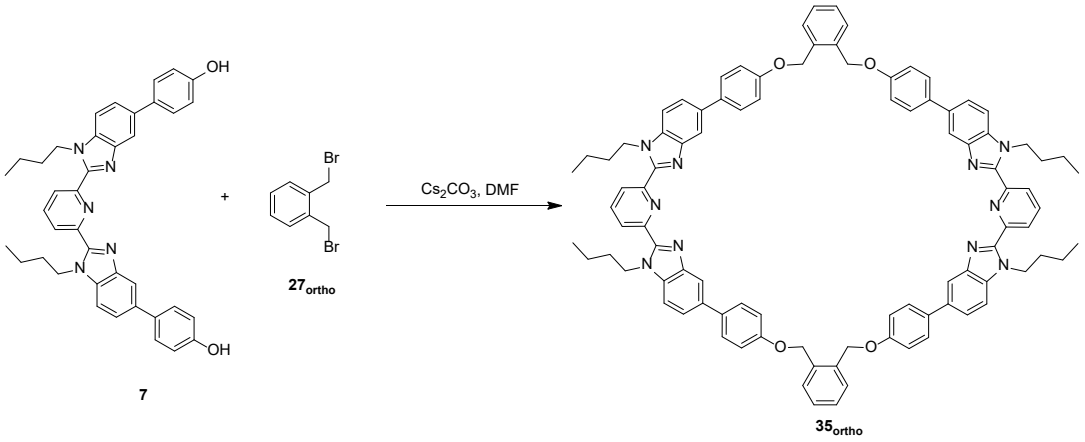

7 27_{ortho} 35_{ortho}

35_{ortho} work up: The material was recrystallized in a combination of $CHCl_3$ and MeOH. After recrystallization and column, **35_{ortho}** became insoluble and studies on this macrocycle were not continued.

50% pure, highly insoluble ^{1}H NMR (400 MHz, $CDCl_3$) δ_H (ppm) 8.34 (d, J = 7.9 Hz, 4H), 8.30 (d, J = 7.8 Hz, 4H), 8.10 – 8.03 (m, 4H), 8.04 – 7.99 (m, 4H), 7.93 (d, J = 1.6 Hz, 4H), 7.67 – 7.34 (m, 48H), 7.26 (d, J = 8.5 Hz, 4H), 7.17 – 7.08 (m, 8H), 6.94 – 6.87 (m, 8H), 5.27 (d, J = 1.9 Hz, 4H), 5.23 (d, J = 2.9 Hz, 12H), 4.76 (t, J = 7.2 Hz, 8H), 4.58 (t, J = 7.3 Hz, 8H), 1.75 (q, J = 7.5 Hz, 8H), 1.65 (q, J = 7.4 Hz, 8H), 1.25 (s, 2H), 1.14 (h, J = 7.4 Hz, 8H), 1.02 (dt, J = 14.8, 7.4 Hz, 8H), 0.72 (t, J = 7.4 Hz, 12H), 0.64 (t, J = 7.3 Hz, 12H). MALDI-MS: m/z 1421 ([M]2H+), 2131 (trimer), 2841 (quatramer).

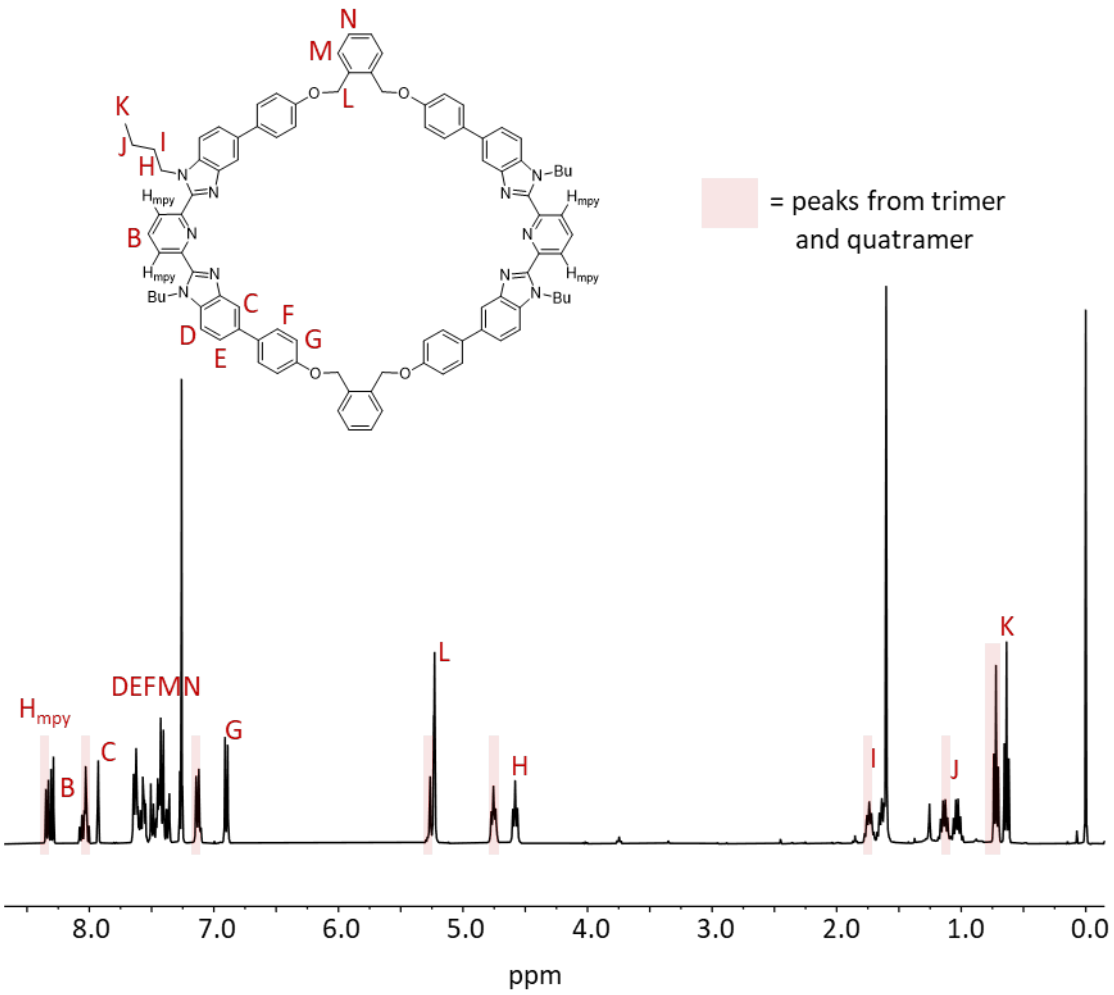

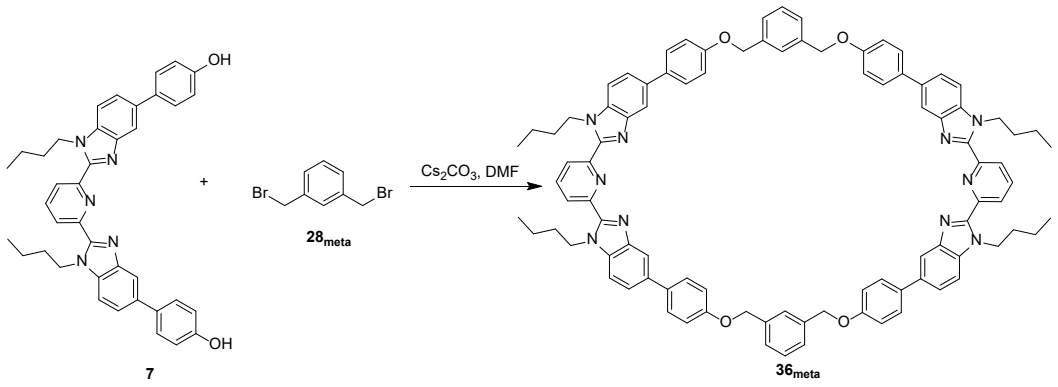

36$_{meta}$ work up: After the column, the **36**$_{meta}$ containing fractions were collected and recrystallized repeatedly in a combination of $CHCl_3$ and MeOH. The final macrocycle was collected as a white

solid in 18.7% yield. ^{1}H NMR (400 MHz, $CDCl_3$) δ_H (ppm) 8.32 (d, J = 7.9 Hz, 4H), 8.05 (t, J = 7.9 Hz, 2H), 7.92 (d, J = 1.6 Hz, 4H), 7.50 (s, 2H), 7.43 – 7.29 (m, 20H), 7.16 (d, J = 8.5 Hz, 4H), 6.84 (d, J = 8.7 Hz, 8H), 5.27 (s, 8H), 4.55 (t, J = 7.2 Hz, 8H), 1.62 – 1.50 (m, 8H), 0.94 (h, J = 7.4 Hz, 8H), 0.58 (t, J = 7.3 Hz, 12H). ^{13}C NMR (101 MHz, $CDCl_3$) δ_C (ppm) 157.4, 150.4, 150.0, 143.2, 138.4, 138.2, 136.3, 135.3, 134.3, 129.2, 128.2, 126.1, 125.7, 125.6, 123.5, 117.8, 116.2, 110.6, 69.9, 44.7, 32.1, 19.8, 13.5. MALDI-TOF MS: m/z 1421 ([M]2H+).

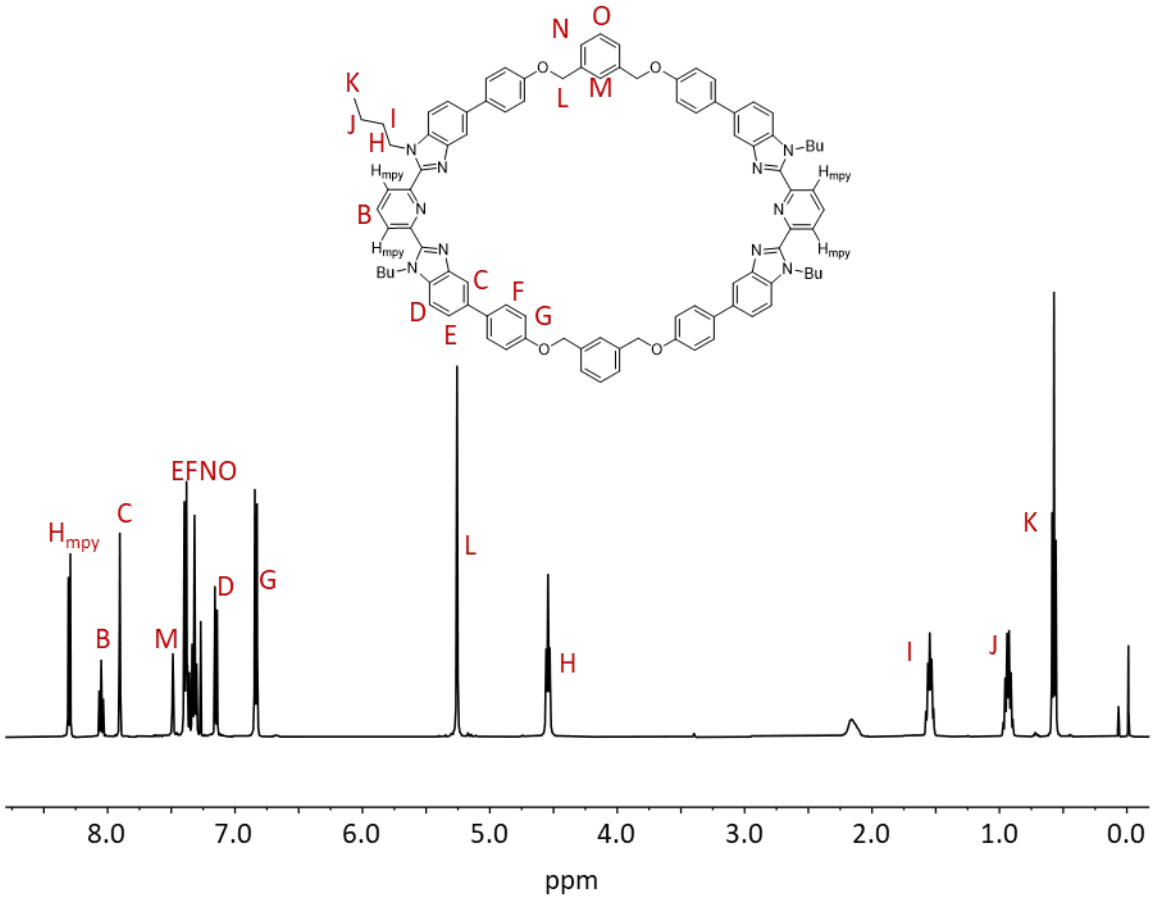

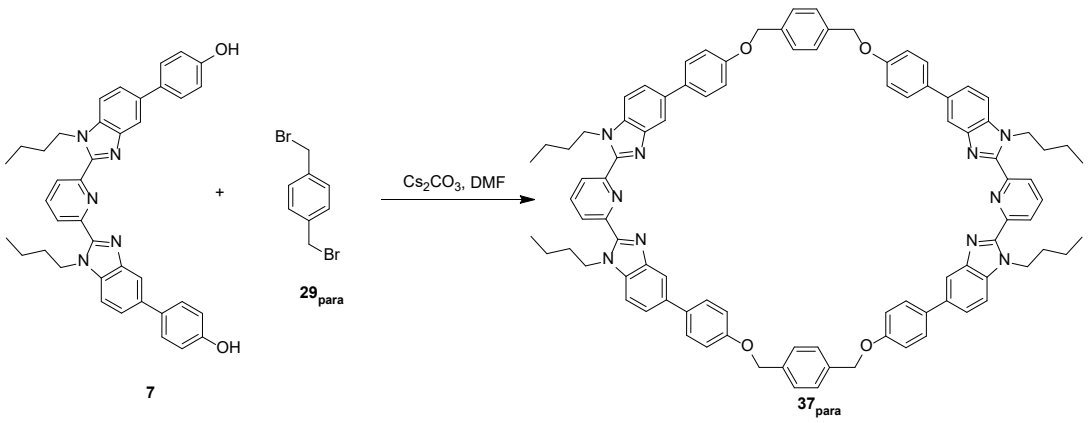

7 29_{para} 37_{para}

37_{para} work up: After the column, the **37_{para}** containing fractions were collected and recrystallized repeatedly in a combination of $CHCl_3$ and MeOH. The final macrocycle was collected as a white solid in 11.5% yield. ^{1}H NMR (400 MHz, $CDCl_3$) δ_H (ppm) 8.29 (d, J = 7.9 Hz, 4H), 8.02 (t, J = 7.9 Hz, 2H), 7.93 (d, J = 1.6 Hz, 4H), 7.50 – 7.42 (m, 12H), 7.40 (s, 12H), 6.92 (d, J = 8.6 Hz, 8H), 5.29 (s, 8H), 4.65 (t, J = 7.3 Hz, 8H), 1.71 – 1.59 (m, 8H), 1.05 (q, J = 7.5 Hz, 8H), 0.64 (t, J = 7.4 Hz, 12H). ^{13}C NMR (101 MHz, $CDCl_3$) δ_C (ppm) 157.4, 150.7, 150.0, 143.4, 138.2, 137.3, 136.1, 135.5, 134.4, 128.4, 126.9, 125.5, 123.3, 118.0, 116.5, 115.8, 110.6, 69.4, 44.8, 32.2, 29.8, 19.9, 13.6. MALDI-TOF MS: m/z 14201 ([M]2H+).

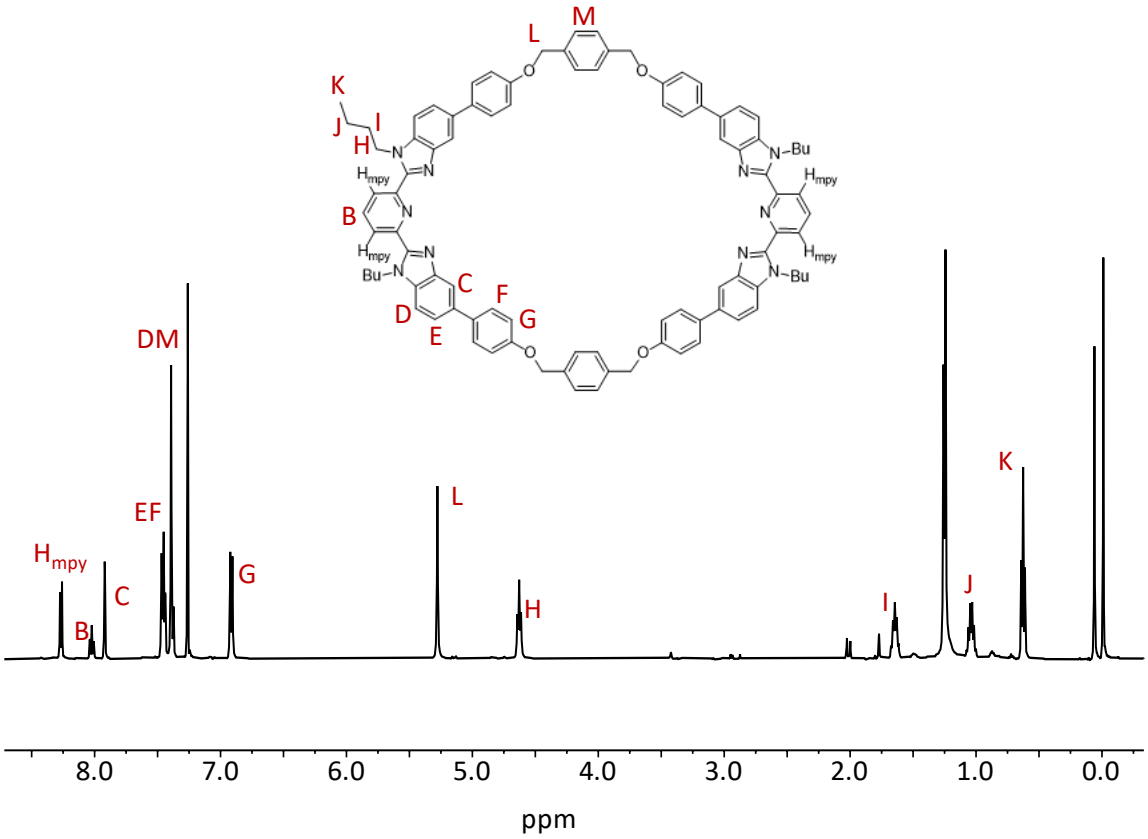

4.8.2.4 Synthesis of Fluorene Macrocycle (38$_{fluorene}$)

Step 1 of 3

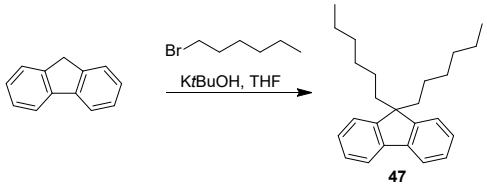

Compound **47** was synthesized according to literature.[11] Briefly, 16.6 g of fluorene (0.1 mol) and *n*-hexyl bromide (36.3 g, 0.22 mol, 2.2eq.) were combined in a 250 mL round bottom flask under argon and dissolved in 120 mL of dry THF. Potassium *tert*-butoxide (33.7 g, 0.3 mol, 3eq.) was added portion-wise to the mixture. After all of the base had been added, the reaction was stirred at

45 °C for 24 hours. After 24 hours, the reaction was cooled to room temperature and crashed out into water. The product was extracted with diethyl ether and purified by column chromatography. **47** was isolated as a yellow oil in 78% yield. ^{1}H NMR (400 MHz, $CDCl_3$) δ_H (ppm) 7.72 – 7.65 (m, 2H), 7.37 – 7.21 (m, 8H), 1.99 – 1.91 (m, 4H), 1.17 – 0.96 (m, 12H, overlapped), 0.61 (t, J = 6.8 Hz, 6H), 0.67 – 0.55 (m, 4H). ^{13}C NMR (101 MHz, $CDCl_3$) δ_C (ppm) 150.8, 141.2, 127.1, 126.8, 123.0, 119.8, 77.4, 55.1, 40.5, 31.6, 29.9, 23.9, 22.7, 14.1.

Step 2 of 3

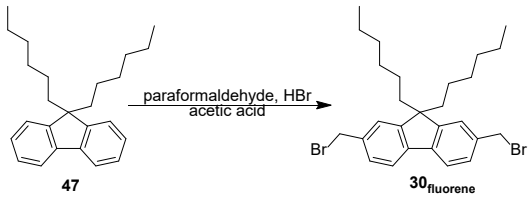

Compound **30$_{fluorene}$** was synthesized using a modified literature procedure.[12] 11 g of **47** (34 mmol) and paraformaldehyde (10.2 g, 280 mmol) were combined in a round bottom flask and heated in 50 mL of acetic acid at 80 °C. After the reaction reached 80 °C, 100 g of 33% HBr solution in acetic acid was added to the reaction. The reaction was stirred at 80 °C for 24 hours before cooling to room temperature and pouring into 500 mL of water. The product was extracted from the water using DCM and the organic layer was washed with water, sodium bicarbonate, and brine. The material was purified on a column run in pure hexanes to give **30$_{fluorene}$** as a colorless oil in 34% yield. ^{1}H NMR (400 MHz, $CDCl_3$) δ_H (ppm) 7.64 (d, J = 7.8 Hz, 2H), 7.35 (d, J = 7.5 Hz, 4H), 4.60 (s, 4H), 2.01 – 1.86 (m, 5H), 1.19 – 1.06 (m, 6H), 1.05 (d, J = 3.1 Hz, 8H), 0.76 (t, J = 7.0 Hz, 6H), 0.66 – 0.55 (m, 5H). ^{13}C NMR (101 MHz, $CDCl_3$) δ_C (ppm) 151.8, 140.9, 137.1, 128.2, 123.8, 120.2, 55.3, 40.2, 34.6, 31.5, 29.7, 23.8, 22.6, 14.1.

Step 3 of 3

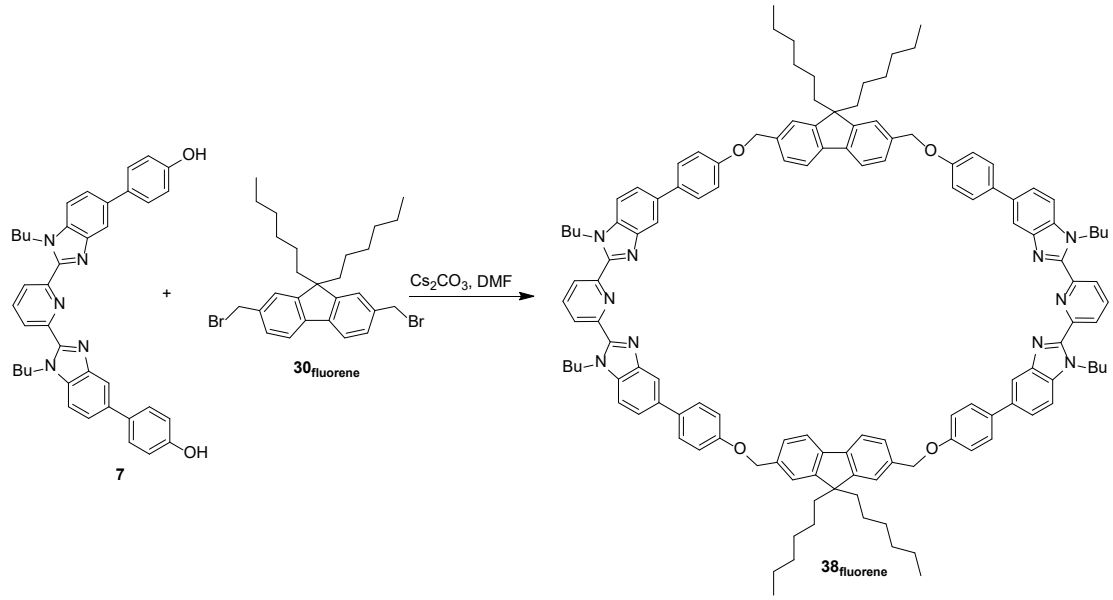

All glassware was dried overnight to ensure water free condition. A 500 mL addition funnel containing **30fluorene** (3.4 g, 6.5 mmol, 1eq.) in 500 mL of anhydrous DMF was fitted to a 2 L two-necked round bottom flask containing **7** (4.0 g, 6.5 mmol, 1 eq.) and Cs_2CO_3 (8.6 g, 26 mmol, 4 eq.) and a stir bar. The reaction vessel was flushed with argon before anhydrous DMF (1.13 L) was added by cannula. The reaction was submerged in a silicone oil bath and heated to 75 °C while rapidly stirring. Over the course of 3 days, **30fluorene** was added dropwise to the reaction vessel. The reaction was stirred at 75 °C for an additional 4 days (for a total of 7 days), after which the solvent was removed, the crude product was triturated with $CHCl_3$, and the insoluble salt was removed via filtration. The filtrate was collected and solvent was removed under vacuum. The resulting solid was purified by an iterative combination of column chromatography (TEA pretreated silica gel, 0.0-2.0% MeOH/CH_2Cl_2 gradient) and recrystallization (method 1: heat-dissolve in CH_2Cl_2,, add MeCN until product begins to precipitate, allow to settle at -7 °C; method 2: heat-dissolve in CH_2Cl_2,, add hexanes until product begins to precipitate, allow to settle at -

7 °C;) to yield **38**$_{\textbf{fluorene}}$ as white solid powder. Crude ^{1}H NMR Yield = 9%, Isolated yield 1.6%. ^{1}H NMR (400 MHz, $CDCl_3$) δ_H (ppm) 8.29 (d, J = 7.9 Hz, 4H), 7.99 (t, J = 7.9 Hz, 2H), 7.91 – 7.89 (m, 4H), 7.65 (d, J = 8.2 Hz, 4H), 7.46 – 7.35 (m, 16H), 7.37 – 7.30 (m, 8H), 6.92 (d, J = 8.8 Hz, 8H), 5.36 (s, 8H), 4.68 (t, J = 7.3 Hz, 8H), 1.92 – 1.85 (m, 8H), 1.70 – 1.60 (m, 8H), 1.04 (h, J = 7.7, 7.2, 7.2 Hz, 8H), 0.97 (p, J = 6.8 Hz, 8H), 0.90 (q, J = 4.4, 3.4 Hz, 16H), 0.62 (dt, J = 10.1, 7.3 Hz, 24H), 0.52 – 0.42 (m, 8H). ^{13}C NMR (126 MHz, $CDCl_3$) δ_C (ppm) 157.4, 151.5, 150.7, 150.1, 143.5, 140.4, 138.2, 136.8, 136.2, 135.5, 134.5, 128.2, 125.6, 125.5, 123.2, 121.5, 120.0, 118.1, 116.4, 110.4, 70.6, 55.1, 53.6, 44.8, 40.5, 32.2, 31.6, 29.8, 29.8, 23.8, 22.6, 19.9, 14.0, 13.6. MALDI-TOF MS: m/z 1933 ([M]2H+).

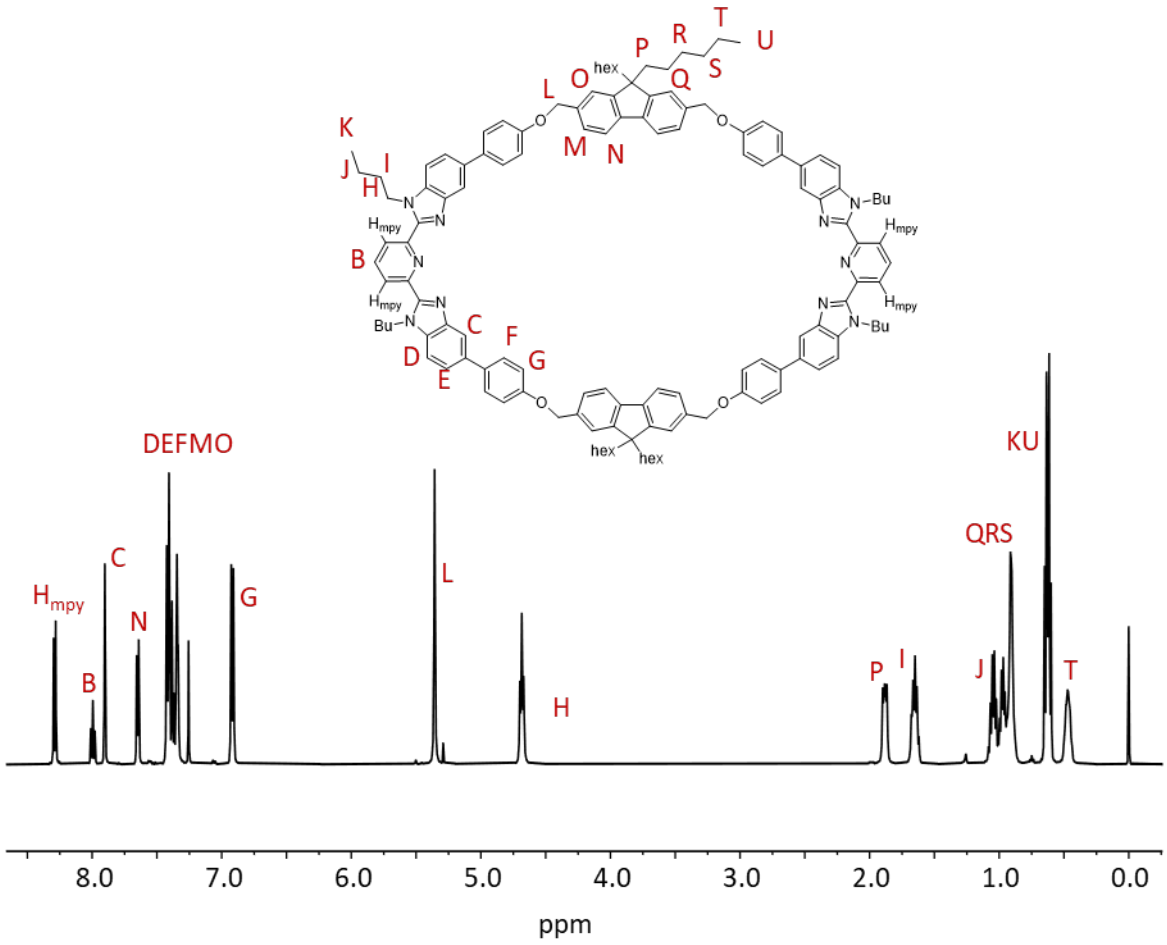

4.8.2.5 Synthesis of BPA Macrocycle (39_{BPA})

Step 1 of 3

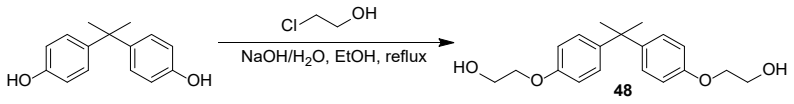

5 g of Bisphenol A (4,4′-(Propane-2,2-diyl)diphenol, 22 mmol) was dissolved in 112 mL of ethanol (200 mM) in 250 mL round bottom flask equipped with a stir bar and condenser. A solution of NaOH (260 mg, 66 mmol, 3 eq.) in water (15 mL) was added to the mixture and stirred. After 10 minutes of stirring, chloroethanol (5.3g, 66 mmol, 3 eq.) was added. The mixture was heated to reflux and allowed to stir at reflux for 3 days. After cooling to room temperature, the solvent was removed under pressure. The material was washed with H_2O and dichloromethane. The product was collected as a white crystal in 95% yield. ^{1}H NMR (500 MHz, $CDCl_3$) δ_H (ppm) 7.14 (d, J = 8.7 Hz, 4H), 6.82 (d, J = 8.8 Hz, 4H), 4.08 – 4.05 (m, 4H), 3.97 – 3.92 (m, 4H), 2.03 (t, J = 6.3 Hz, 2H), 1.64 (s, 6H).

Step 2 of 3

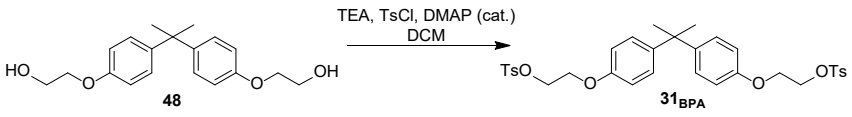

In a 250 mL round bottom flask equipped with a stir bar under argon atmosphere, **48** (5 g, 15.7 mmol, 1 eq.) was combined with triethylamine (14.3 g, 141 mmol, 9 eq.), and 4-dimethylaminopyridine (0.03 g, 0.15 mmol, 0.01 eq.) in dry dichloromethane (53 mL) and stirred at 0 °C. 4-Toluenesulfonyl chloride (8.9 g, 44 mmol, 3 eq.) was stirred in dry dichloromethane (52 mL) and added to the reaction flask after it had stirred for some time at 0 °C. The reaction was allowed to slowly warm to rt over 24 hours of reaction after which the solvent was removed. The

mixture was redissolved in ethylacetate and filtered to remove salt. Product **31$_{BPA}$** was purified via column chromatography (0-3% $CHCl_3$/MeOH) to yield the tosylated product as white solid in 73% yield. ^{1}H NMR (500 MHz, $CDCl_3$) δ_H (ppm) 7.81 (d, J = 8.3 Hz, 4H), 7.33 (d, J = 8.1 Hz, 4H), 7.08 (d, J = 8.8 Hz, 4H), 6.68 (d, J = 8.8 Hz, 4H), 4.38 – 4.30 (m, 4H), 4.13 – 4.09 (m, 4H), 2.43 (s, 6H), 1.60 (s, 6H).^{13}C NMR (126 MHz, $CDCl_3$) δ_C (ppm) 155.98, 145.04, 143.89, 133.02, 129.96, 128.13, 127.84, 114.08, 68.31, 65.54, 41.83, 31.09, 21.77. ESI MS: m/z 647.2 ([M]Na^+).

Step 3 of 3

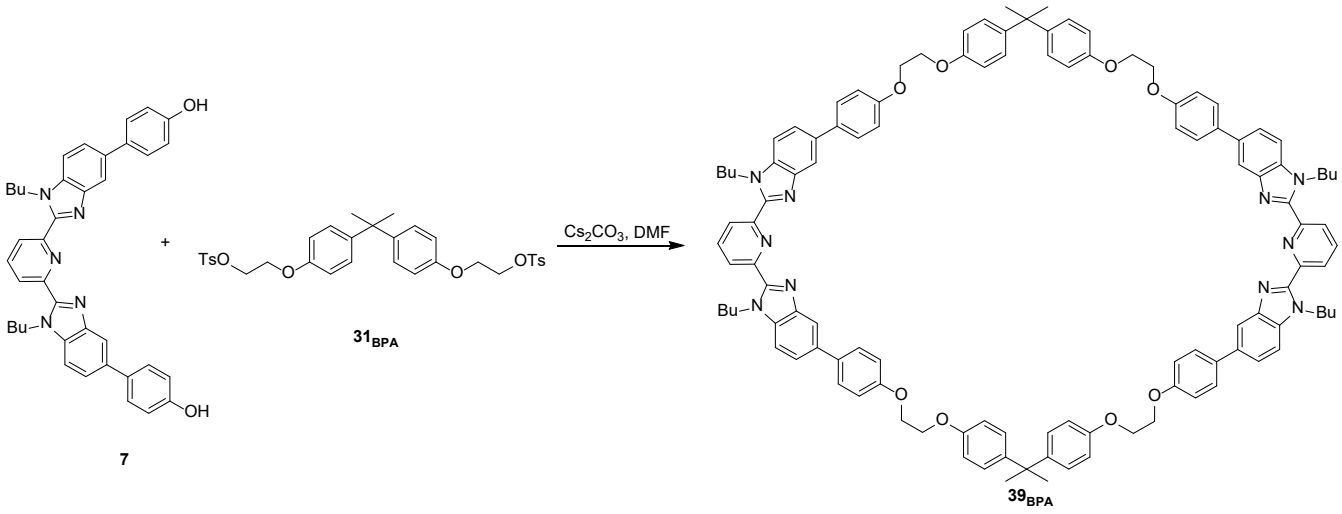

A 2 L round bottom flask equipped with a stir bar was dried overnight and assembled with a 500 mL addition funnel under argon. To the flask, a mixture of **7** (2.18 g, 3.6 mmol) and Cs_2CO_3 (4.7 g, 14.4 mmol, 4 eq.) in 450 mL anhydrous DMF was added. The addition funnel was filled with **31$_{BPA}$** (2.15 g, 3.6 mmol) in 450 mL of anhydrous DMF. The contents of the addition funnel were slowly (3 days) dripped into the round bottom flask while heating at 75 °C. After the contents of the addition funnel were completely added, the reaction continued for an additional 4 days while heating, resulting in a total of 7 days. After cooling to room temperature, the solvent was removed, the crude product was triturated with $CHCl_3$, and the insoluble salt was removed via filtration. The

filtrate was collected and solvent was removed under vacuum. The resulting residue was purified by flash chromatography (0-1.5% gradient in methanol/ chloroform, on TEA treated silica, multiple columns) followed by recrystallization in chloroform to yield the desired macrocycle as a white solid in 1.5% yield. ^{1}H NMR (400 MHz, $CDCl_3$) δ_H (ppm) 8.31 (d, J = 7.9 Hz, 4H), 8.04 (t, J = 7.8 Hz, 2H), 8.00 (d, J = 1.6 Hz, 4H), 7.57 (d, J = 8.5 Hz, 8H), 7.58 – 7.42 (m, 8H), 7.14 (dd, J = 8.5, 4.2 Hz, 8H), 7.02 (dd, J = 8.5, 4.2 Hz, 8H), 6.87 (d, J = 8.4 Hz, 8H), 4.71 (t, J = 7.3 Hz, 8H), 4.36 (tt, J = 5.2, 2.5 Hz, 16H), 1.75 – 1.62 (m, 8H), 1.26 (s, 12H), 1.09 (p, J = 7.5 Hz, 8H), 0.69 (t, J = 7.4 Hz, 12H). ^{13}C NMR (101 MHz, $CDCl_3$) δ_C (ppm) MALDI-TOF MS: m/z 1777 ([M]2H+).

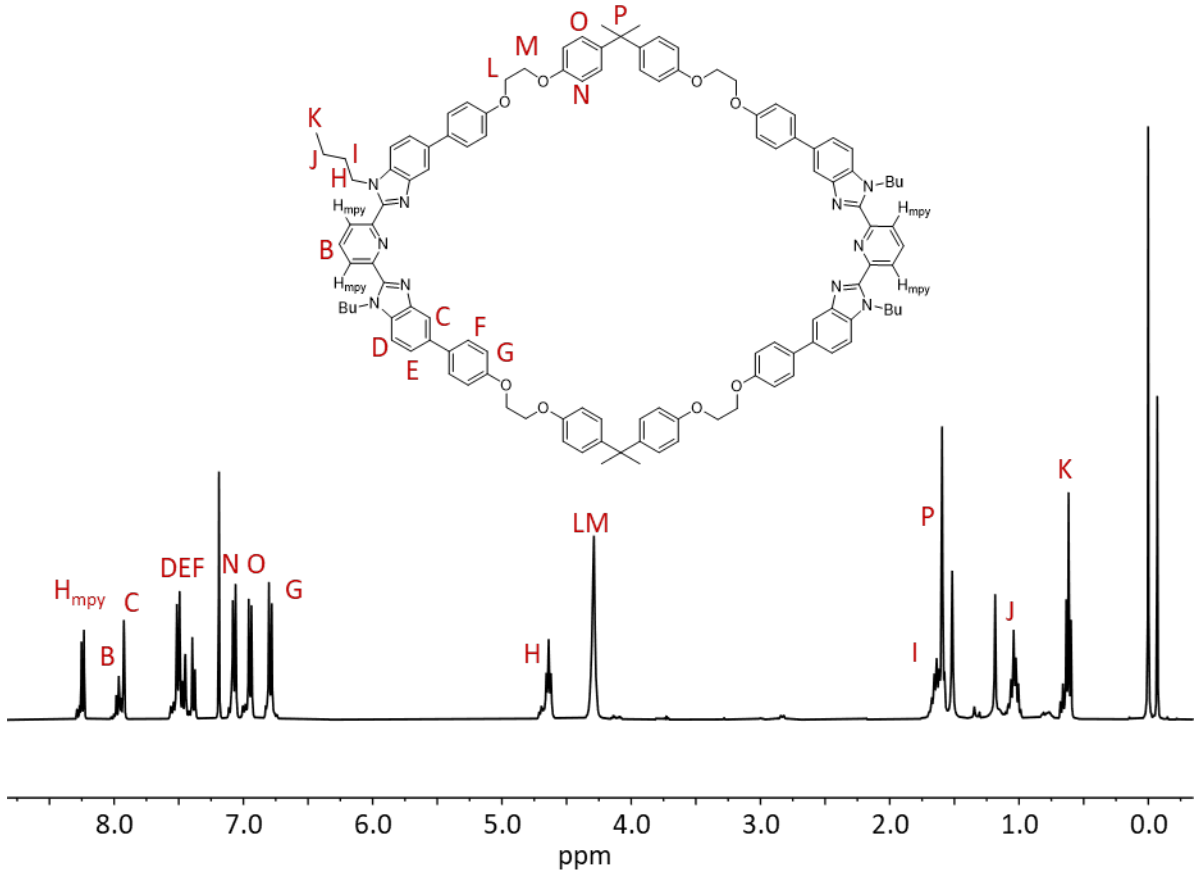

4.8.2.6 Synthesis of Dodecyl Macrocycle (40$_{BPZ}$)

Step 1 of 4

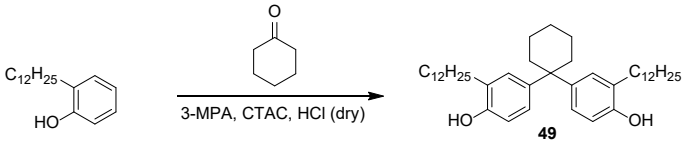

To a 25 mL two-neck round bottom flask equipped with stir bar and condenser, 10 g (38 mmol) of 2-dodecylphenol, 40 mg (0.1 eq., 0.38 mmol) of 3-mercaptopropionic acid (3-MPA) and 120 mg (0.01 eq, 0.38 mmol) of cetyltrimethylammonium chloride (CTAC) was added. The flask was heated to 55 °C under argon atmosphere to melt the 2-dodecylphenol, and a homogenous melt was obtained after stirring. Dry HCl gas (prepared by adding concentrated HCl solution dropwise into solid anhydrous calcium chloride) was bubbled into the melt by a cannula for 30 minutes. The HCl was removed from the solution and 1.87g (0.5 eq., 19 mmol) of cyclohexanone was added into the melt dropwise. The reaction mixture was stirred at 55 °C under argon atmosphere for 24 hours, while under HCl gas. After cooling down to room temperature, the crude product was dissolved in diethyl ether, washed with 1M potassium carbonate solution (three times) and water (three times) followed by drying over anhydrous sodium sulfate and filtration. The filtrate was collected and the solvent was removed under vacuum. The crude product was purified by chromatography (silica gel, 5% EtOAc/ hexanes). Yield: 24.7%, white waxy solid. ^{1}H NMR (500 MHz, $CDCl_3$) δ_H (ppm) 6.99 (d, J = 2.4 Hz, 2H), 6.92 (dd, J = 8.4, 2.4 Hz, 2H), 6.64 (d, J = 8.4 Hz, 2H), 2.57 – 2.51 (m, 4H), 2.19 (t, J = 5.7 Hz, 4H), 1.62 – 1.41 (m, 10H), 1.32 – 1.22 (m, 36H), 0.88 (t, J = 6.8 Hz, 6H). ^{13}C NMR (126 MHz, $CDCl_3$) δ_C (ppm) 150.9, 129.0, 127.8, 125.7, 114.8, 45.1, 37.5, 32.0, 30.3, 29.9, 29.8, 29.7, 29.6, 29.5, 29.4, 26.5, 23.0, 22.7, 14.1. ESI MS: m/z 627.2 ([M]Na^+).

Step 2 of 4

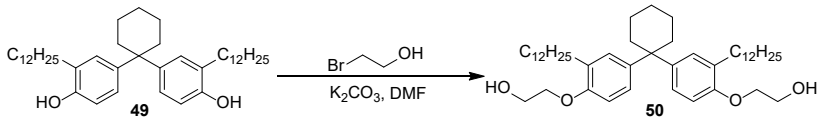

3.29 g (5.42 mmol) of **49**, 5.24 g (43.4 mmol, 8 eq.) of 2-bromoethanol, 3.0 g (21.7 mmol, 4 eq.) of K_2CO_3, a catalytic amount of potassium iodide, and 22 mL of anhydrous DMF was combined in a 25 mL pressure flask equipped with stir bar. The pressure flask was sealed (and the O-ring was wrapped in Teflon) and the mixture was stirred at 100 °C for 24 hours. Caution: appropriate safety shield must be used for reaction in glassware under pressure. After cooling down, the mixture was poured into 100 mL of deionized water. The product was extracted with diethyl ether 4 times, followed by removing solvent under vacuum and column chromatography with a 10-30% hexane/DCM gradient as eluent. Yield: 51%, white waxy solid. ^{1}H NMR (500 MHz, $CDCl_3$) δ_H (ppm) 7.04 (d, J = 2.5 Hz, 2H), 6.98 (dd, J = 8.5, 2.5 Hz, 2H), 6.72 (d, J = 8.5 Hz, 2H), 4.04 (dd, J = 5.2, 3.9 Hz, 4H), 3.93 (q, J = 4.9 Hz, 4H), 2.56 (dd, J = 8.5, 6.7 Hz, 4H), 2.24 – 2.18 (m, 4H), 1.60 – 1.51 (m, 10H), 1.33-1.20 (m, 36H), 0.88 (t, J = 6.9 Hz, 6H). ^{13}C NMR (126 MHz, $CDCl_3$) δ_C 154.0, 130.8, 129.1, 125.5, 111.2, 69.3, 61.9, 45.2, 37.5, 32.1, 30.7, 30.2, 29.87, 29.86, 29.83, 29.72, 29.70, 29.5, 26.6, 23.1, 22.8, 14.3. ESI MS: m/z 715.6 ([M]Na^+).

Step 3 of 4

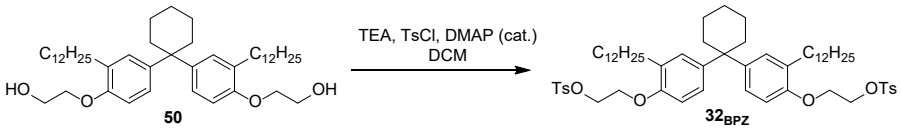

In a 25 mL round bottom flask equipped with a stir bar under argon atmosphere, **50** (634 mg, 0.91 mmol, 1 eq.) was combined with triethylamine (829 mg, 8.2 mmol, 9 eq.), and 4-dimethylaminopyridine (cat., 0.01 eq.) in dry dichloromethane (3 mL) and stirred at 0 °C. 4-

Toluenesulfonyl chloride (696 mg, 3.65 mmol, 3 eq.) was stirred in dry dichloromethane (3 mL) and added to the reaction flask after it had stirred for some time at 0 °C. The reaction was allowed to slowly warm to rt over 24 hours of reaction after which the solvent was removed. The mixture was redissolved in ethylacetate and filtered to remove salt. Product **32$_{BPZ}$** was purified via column chromatography with a 5-30% hexane/DCM gradient as eluent.to yield the tosylated product as a colorless oil in 87% yield. ^{1}H NMR (500 MHz, $CDCl_3$) δ_H (ppm) 7.80 (dd, *J* = 8.2, 1.5 Hz, 4H), 7.31 (d, *J* = 8.1 Hz, 4H), 7.00 (d, *J* = 2.6 Hz, 2H), 6.95 – 6.90 (m, 2H), 6.59 (dd, *J* = 7.3, 2.0 Hz, 2H), 4.33 (t, *J* = 4.8 Hz, 4H), 4.11 (t, *J* = 5.6 Hz, 4H), 2.48 – 2.41 (m, 10H), 2.18 (t, *J* = 5.4 Hz, 4H), 2.05 (d, *J* = 1.2 Hz, 5H), 1.55 – 1.43 (m, 6H), 1.33 – 1.17 (m, 36H), 0.88 (t, 7.1 Hz, 6H). 13C NMR (126 MHz, CDCl3) δ 153.4, 144.8, 132.9, 130.9, 129.9, 128.9, 127.9, 125.2, 110.8, 68.3, 65.4, 45.0, 37.4, 32.0, 30.4, 29.9, 29.8, 29.7, 29.6, 29.5, 29.4, 26.4, 22.9, 22.7, 21.7, 14.2. MALDI-TOF MS: 1001 ([M]H+).

Step 4 of 4

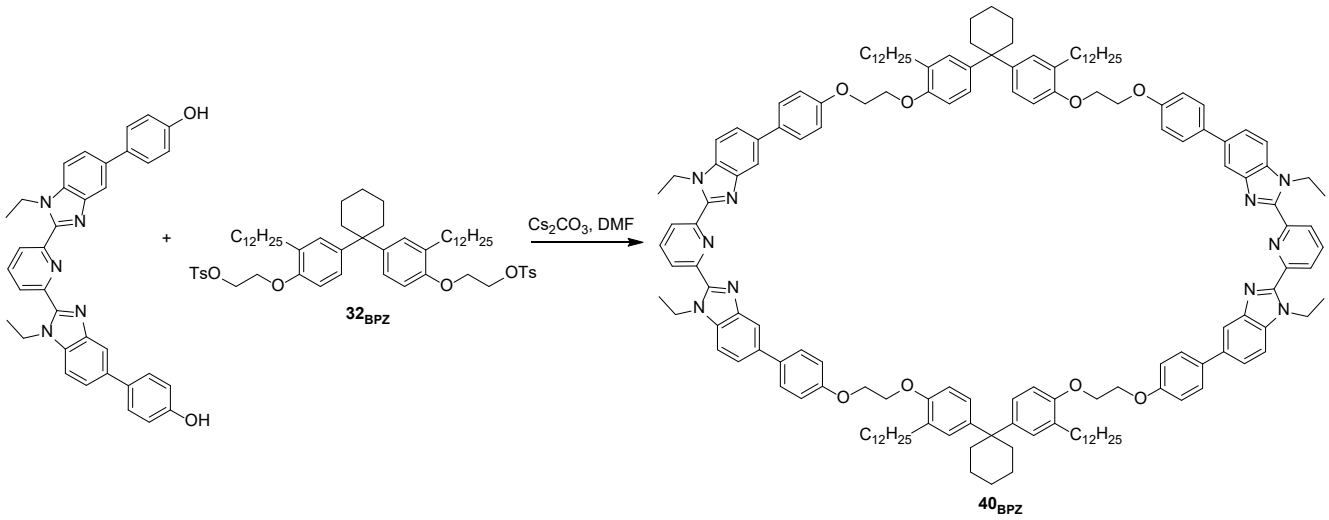

32$_{BPZ}$ **40$_{BPZ}$**

All glassware was dried overnight to insure water free condition. A 250 mL addition funnel containing **32$_{BPZ}$** (630 mg g, 0.78 mmol, 1eq.) in 97 mL of anhydrous DMF was fitted to a 500

mL two-necked round bottom flask containing a slightly different 2,6-bisbenzimidazolylpyridine ligand (synthesized by literature procedures[13]) (415 mg, 0.78 mmol, 1 eq.) and Cs_2CO_3 (1.02 g, 3.1 mmol, 4 eq.) and a stir bar. The reaction vessel was flushed with argon before anhydrous DMF (97 mL) was added by cannula. The reaction was submerged in a silicone oil bath and heated to 75 °C while rapidly stirring. Over the course of 3 days, **32$_{BPZ}$** was added dropwise to the reaction vessel. The reaction was stirred at 70 °C for an additional 4 days (for a total of 7 days), after which the solvent was removed, the crude product was triturated with $CHCl_3$, and the insoluble salt was removed via filtration. The resulting solid was purified by an iterative combination of column chromatography (TEA pretreated silica gel, 0.0-1.3, 2.5% MeOH/$CHCl_3$ gradient) and recrystallization (heat-dissolve in CH_2Cl_2, add MeCN until product begins to precipitate, allow to settle at -7 °C) to yield **40$_{BPZ}$** as white solid powder in 7.0 % yield. ^{1}H NMR (500 MHz, $CDCl_3$) δ_H (ppm) 8.37 (d, *J* = 7.8 Hz, 4H), 8.06 (t, *J* = 7.9 Hz, 2H), 8.02 (d, *J* = 1.5 Hz, 4H), 7.60 – 7.56 (m, 8H), 7.55 (dd, *J* = 8.4, 1.7 Hz, 4H), 7.47 (d, *J* = 8.4 Hz, 4H), 7.07 (d, *J* = 2.5 Hz, 4H), 7.02 (dd, *J* = 12.2, 8.7 Hz, 12H), 6.80 (d, *J* = 8.6 Hz, 4H), 4.78 (q, *J* = 7.2 Hz, 8H), 4.36 (tt, *J* = 5.2, 2.7 Hz, 16H), 2.59 (t, *J* = 8.5, 6.8 Hz, 8H), 2.27 (p, *J* = 5.7 Hz, 8H), 1.63-1.48 (m, 20H), 1.37 (t, *J* = 7.2 Hz, 12H), 1.32 – 1.20 (m, 72H), 0.87 (t, *J* = 6.9 Hz, 12H). ^{13}C NMR (126 MHz, $CDCl_3$) δ_C (ppm) 158.1, 154.0, 150.4, 150.1, 143.6, 141.4, 138.2, 136.3, 135.3, 134.6, 131.4, 128.9, 128.5, 125.8, 125.2, 123.3, 118.2, 115.3, 111.5, 110.4, 66.9, 66.7, 45.1, 40.0, 37.2, 32.1, 30.7, 30.1, 29.90, 29.88, 29.8, 29.7, 29.6, 29.5, 26.6, 23.1, 22.8, 15.6, 14.3. MALDI-TOF MS: m/z 2420 ([M]4H+).

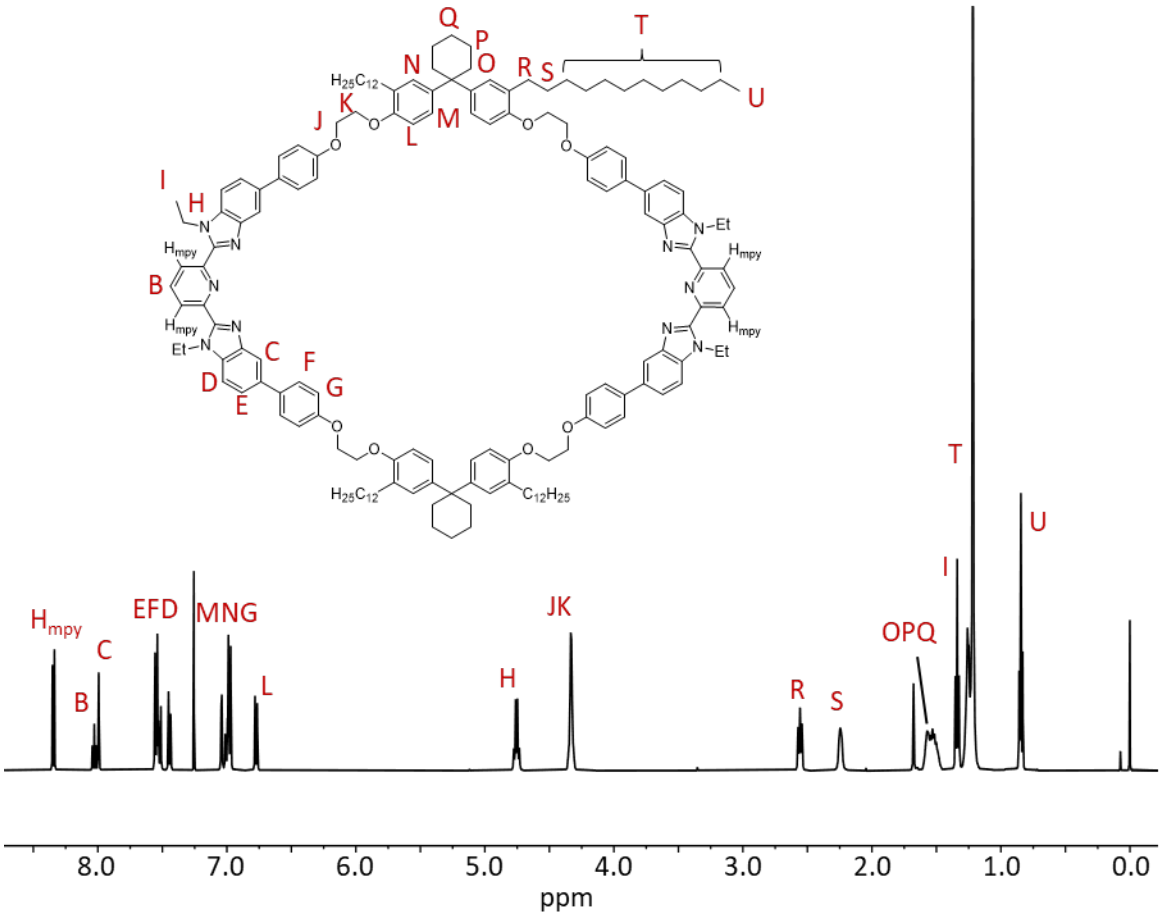

4.8.2.7 Synthesis of 46$_{BPZ}$

MSP **40$_{BPZ}$·2·Zn(II)$_2$** (66 mg) was added to the dried vessel and dissolved in 5 mL DCM (at a concentration of 2.5 mM wrt **2**). The solution was stirred and heated to reflux (45°C) followed by bubbling argon for 30 minutes to remove dissolved oxygen. Then 1.0 mg Hoveyda-Grubbs second generation catalyst in DCM (0.32 mM wrt final reaction volume) was added to the solution. To account for any solvent evaporation during the bubbling steps, additional DCM was added as required to maintain the original concentration (2.5 mM wrt **2**). While still under reflux, the solution was bubbled with argon for additional 30 mins. The argon purge and catalyst addition was repeated 24 hours after the first addition. The reaction was carried out for a further 24 hours before the solution was cooled to room temperature and ethyl vinyl ether (~1mL) was added to deactivate

the catalyst. The material was dried under pressure while metalated and then dissolved in MeCN. ~1 mL of tetrabutylammonium hydroxide was added to the solution and the insoluble residue was collected by filtration. The filtrate contained a combination of the catalyst and some of the macrocycle byproduct, therefore no accurate crude characterization was obtained.

Polycatenane **46$_{BPZ}$** ^{1}H NMR (500 MHz, $CDCl_3$) δ_H (ppm): 8.29 – 8.11 (m, 8H), 7.98 – 7.79 (m, 12H), 7.43 – 7.29 (m, 18H), 7.26 – 7.15 (m, 12H), 7.09 – 7.03 (m, 8H), 6.94 – 6.88 (m, 4H), 6.85 (d, J = 7.9 Hz, 4H), 6.80 – 6.66 (m, 16H), 6.64 – 6.55 (m, 4H), 5.42 – 5.26 (m, 2H), 4.99 (s, 4H), 4.68 – 4.45 (m, 16H), 4.15 – 3.99 (m, 16H), 3.85 – 3.75 (m, 4H), 2.54 – 2.46 (m, 8H), 2.25 – 2.16 (m, 8H), 2.09 – 1.93 (m, 4H), 1.78 – 1.69 (m, 4H) 1.56 – 1.48 (m, 28H), 1.28 – 1.14 (m, 86H), 0.89 – 0.77 (m, 20H), 0.55 (p, J = 6.9 Hz, 12H).

ADMET byproduct **5**: ^{1}H NMR (500 MHz, $CDCl_3$) δ_H (ppm) 8.35 (d) 8.07 (t), 8.03 (s), 7.65 – 7.55 (m), 7.50 (dd), 7.46 (d), 7.20 (m), 7.11 (d), 7.01 (d), 5.56 – 5.48 (m), 5.12 (s), 4.76 (t), 4.03 (t), 2.32-2.21 (m), 1.89 (p), 1.74 (p), 1.66 (s), 1.14 (p), 0.73 (t).

4.8.2.8 Synthesis procedure for 43$_{meta}$, 44$_{para}$, 45$_{fluorene}$

Poly[*n*]catenane synthesis followed the same procedures as Section 2.6.2.4. Briefly, MSP **36$_{meta}$·2·Zn(II)$_2$** (90 mg) was added to the dried vessel and dissolved in 8.5 mL DCM (at a concentration of 2.5 mM wrt **2**). The solution was stirred and heated to reflux (45°C) followed by bubbling argon for 30 minutes to remove dissolved oxygen. Then 1.7 mg Hoveyda-Grubbs second generation catalyst in DCM (0.32 mM wrt final reaction volume) was added to the solution. To account for any solvent evaporation during the bubbling steps, additional DCM was added as required to maintain the original concentration (2.5 mM wrt **2**). While still under reflux, the solution was bubbled with argon for additional 30 mins. The argon purge and catalyst addition was

repeated 24 hours after the first addition. The reaction was carried out for a further 24 hours before the solution was cooled to room temperature and ethyl vinyl ether (~1mL) was added to deactivate the catalyst. To demetallate the reaction products, 50 μL of ethylenediamine was added to the reaction and allowed to stir. The resulting mixture was washed with 5 aliquots of water or until the aqueous wash was no longer basic. The organic layer was passed through a 0.45 μm PTFE syringe filter and the solvent was removed under vacuum. The resulting demetallated reaction mixture was obtained as a yellow or slightly brown solid.

After characterization of the crude mixture, residual macrocycle was removed a partial re-metalated process. The polycatenanes were titrated with $Zn(NTf_2)_2$ until ca. 30% of **43$_{meta}$** was metalated as observed by ^{1}H NMR. The sample was fully dried under vacuum and washed 8 times with a solution of 2:1 chloroform:hexanes to remove the non-metal-containing compounds. The remaining metalated compounds were dissolved in DCM and demetallated using 50 μL of ethylenediamine. The resulting mixture was washed with 5 aliquots of water or until the sample was no longer basic. After removal of residual water, the final material was collected. For samples **43$_{meta}$, 44$_{para}$,** and **45$_{fluorene}$**, all purified characterizations were taken at this stage.

Polycatenane **43$_{meta}$** (87% pure) ^{1}H NMR (500 MHz, $CDCl_3$) δ_H (ppm): 8.20 – 8.05 (m, 8H), 7.94 – 7.72 (m, 12H), 7.37 – 7.06 (m, 38H), 6.92 – 6.88 (m, 4H), 6.84 (d, J = 8.4 Hz, 4H), 6.79 – 6.63 (m, 16H), 5.44 – 5.14 (m,23H), 5.14 – 5.06 (m, 4H), 4.91 (s, 8H), 4.53 – 4.34 (m, 16H), 3.72 – 3.66 (m, 4H), 2.01 – 1.88 (m, 4H), 1.69 – 1.63 (m, 4H), 1.61 – 1.47 (m, 16H), 1.26 (s, 6H), 1.03 – 0.79 (m, 16H), 0.60 – 0.45 (m, 24H).

Polycatenane **44$_{para}$** (76% pure): ^{1}H NMR (500 MHz, $CDCl_3$) δ_H (ppm) 8.24 – 8.07 (m, 8H), 7.96 – 7.70 (m, 12H), 7.36 – 7.14 (m, 34H), 7.08 – 6.99 (m, 8H), 6.81 (d, J = 7.9 Hz, 4H), 6.69 (d, J = 7.1 Hz, 8H), 5.23 – 5.19 (m, 26H), 5.16 – 5.10 (m, 10H), 5.06 – 4.89 (m, 14H), 4.60 – 4.28 (m,

34H), 3.78 – 3.60 (m, 8H), 2.04 – 1.86 (m, 4H), 1.67 – 1.44 (m, 20H), 1.41 (s, 6H), 0.90 (dt, *J* = 20.8, 7.3 Hz, 16H), 0.61 – 0.45 (m, 24H).

Polycatenane **45$_{fluorene}$** (79% pure): ^{1}H NMR (500 MHz, $CDCl_3$) δ_H (ppm) 8.24 – 8.09 (m, 8H), 7.93 – 7.74 (m, 12H), 7.37 – 7.28 (m, 12H), 7.26 – 7.15 (m, 26H), 7.11 (d, *J* = 8.0 Hz, 8H), 6.95 – 6.90 (m, 4H), 6.81 (d, *J* = 7.9 Hz, 8H), 6.72 (d, *J* = 7.8 Hz, 4H), 6.66 (d, *J* = 8.1 Hz, 4H), 5.53 – 5.31 (m, 2H), 5.29 – 5.14 (m, 8H), 4.92 (s, 4H), 4.63 – 4.34 (m, 16H), 3.79 – 3.68 (m, 4H), 2.05 – 1.91 (m, 4H), 1.86 – 1.77 (m, 8H), 1.63 – 1.23 (m, 26H), 1.01 – 0.80 (m, 40H), 0.65 – 0.42 (m, 44H).

All Catenanes include peaks from ADMET byproduct **5**: ^{1}H NMR (500 MHz, $CDCl_3$) δ_H (ppm) 8.35 (d) 8.07 (t), 8.03 (s), 7.65 – 7.55 (m), 7.50 (dd), 7.46 (d), 7.20 (m), 7.11 (d), 7.01 (d), 5.56 – 5.48 (m), 5.12 (s), 4.76 (t), 4.03 (t), 2.32-2.21 (m), 1.89 (p), 1.74 (p), 1.66 (s), 1.14 (p), 0.73 (t).

4.8.2.9 Synthesis procedures for 41$_{2EG}$, 42$_{3EG}$

Poly[*n*]catenane synthesis followed the same procedure for synthesis and work-up as for **43$_{meta}$, 44$_{para}$,** and **45$_{fluorene}$**. However, after the partial metalation purification, further purification procedures were conducted on the material. The partially purified sample of **41$_{2EG}$** was fractionated via C using a mobile phase of 25% DMF and 75% THF. The early fractions containing primarily **41$_{2EG}$** were used for characterization.

The same procedure was repeated for **42$_{3EG}$**.

Polycatenane **41$_{2EG}$** (68% pure): ^{1}H NMR (500 MHz, $CDCl_3$) δ_H (ppm) 8.20 – 8.08 (m, 8H), 7.95 – 7.70 (m, 12H), 7.43 – 7.28 (m, 24H), 7.20 – 7.17 (m, 4H), 7.15 (d, *J* = 8.0 Hz, 4H), 7.06 – 6.99 (m, 4H), 6.88 (d, *J* = 8.3 Hz, 8H), 6.79 – 6.57 (m, 8H), 5.08 – 5.03 (m, 2H), 4.96 – 4.87 (m, 4H), 4.60 – 4.39 (m, 16H), 4.22 – 4.17 (m, 4H), 4.09 (d, *J* = 6.2 Hz, 8H), 3.83 – 3.56 (m, 12H), 1.88 –

1.82 (m, 4H), 1.57 – 1.50 (m, 16H), 1.21 (d, J = 3.1 Hz, 6H), 1.01 – 0.92 (m, 16H), 0.59 – 0.53 (m, 24H).

Polycatenane **42$_{3EG}$** (83% pure): ^{1}H NMR (500 MHz, $CDCl_3$) δ_H (ppm) 8.25 – 8.11 (m, 8H), 7.98 – 7.77 (m, 12H), 7.44 – 7.18 (m, 26H), 7.02 – 6.99 (m, 4H), 6.94 (d, J = 8.3 Hz, 8H), 6.85 – 6.74 (m, 12H), 6.67 (d, J = 8.2 Hz, 4H), 5.57 – 5.17 (m, 2H), 4.98 (s, 4H), 4.60 – 4.38 (m, 16H), 4.09 – 3.99 (m, 4H), 3.96 – 3.63 (m, 24H), 3.58 – 3.55 (m, 4H), 2.09 – 1.92 (m, 4H), 1.64 – 1.46 (m, 16H), 1.26 (s, 6H), 0.99 – 0.90 (m, 16H), 0.56 (t, J = 8.5 Hz, 24H).

All Catenanes include peaks from ADMET byproduct **5**: ^{1}H NMR (500 MHz, $CDCl_3$) δ_H (ppm) 8.35 (d) 8.07 (t), 8.03 (s), 7.65 – 7.55 (m), 7.50 (dd), 7.46 (d), 7.20 (m), 7.11 (d), 7.01 (d), 5.56 – 5.48 (m), 5.12 (s), 4.76 (t), 4.03 (t), 2.32-2.21 (m), 1.89 (p), 1.74 (p), 1.66 (s), 1.14 (p), 0.73 (t).

4.9 References

1 Q. Wu, P. M. Rauscher, X. L. Lang, R. J. Wojtecki, J. J. de Pablo, M. J. A. Hore and S. J. Rowan, *Science (80-.).*, 2017, **358**, 1434–1439.

2 J. P. Mercier, J. J. Aklonis, M. Litt and A. V. Tobolsky, *J. Appl. Polym. Sci.*, 1965, **9**, 447–459.

3 M.-Y. Yuen, S. C. F. Kui, K.-H. Low, C.-C. Kwok, S. S.-Y. Chui, C.-W. Ma, N. Zhu and C.-M. Che, *Chem. – A Eur. J.*, 2010, **16**, 14131–14141.

4 P. Groves, *Polym. Chem.*, 2017, **8**, 6700–6708.

5 J. E. Hertzog, V. J. Maddi, L. F. Hart, B. W. Rawe, P. M. Rauscher, K. M. Herbert, E. P. Bruckner, J. J. de Pablo and S. J. Rowan, *Chem. Sci.*, , DOI:10.1039/D2SC01486F.

6 M. M. Tranquilli, Q. Wu and S. J. Rowan, *Chem. Sci.*, 2021, **12**, 8722–8730.

7 R. Kramer, J. M. Lehn and A. Marquis-Rigault, *Proc. Natl. Acad. Sci.*, 1993, **90**, 5394–5398.

8 J. E. M. Lewis, M. Galli and S. M. Goldup, *Chem. Commun.*, 2017, **53**, 298–312.

9 A. M. Albrecht-Gary, Z. Saad, C. O. Dietrich-Buchecker and J.-P. Sauvage, *J. Am. Chem. Soc.*, 1985, **107**, 3205–3209.

10 *1D and 2D Experiments Step-by-step Tutorial; Advanced Experiments User Guide, vers. 002*, Bruker Biospin, 2006.

11 M.-Y. Yuen, S. C. F. Kui, K.-H. Low, C.-C. Kwok, S. S.-Y. Chui, C.-W. Ma, N. Zhu and C.-M. Che, *Chem. - A Eur. J.*, 2010, **16**, 14131–14141.

12 M. G. Murali, P. Naveen, D. Udayakumar, V. Yadav and R. Srivastava, *Tetrahedron Lett.*, 2012, **53**, 157–161.

13 B. M. McKenzie, A. K. Miller, R. J. Wojtecki, J. C. Johnson, K. A. Burke, K. A. Tzeng, P. T. Mather and S. J. Rowan, *Tetrahedron*, 2008, **64**, 8488–8495.

Chapter 5: The future of poly[*n*]catenanes: toward poly[*n*]catenane networks and co-polymeric materials

5.1 Introduction

* the computational analysis in this section has been adapted from: Liu, G.; Rauscher, P.M.; Rawe, B.W.; Tranquilli, M.M.; Rowan, S.J. *Chem. Soc. Rev*. **2022**, DOI: 10.1039/d2cs00256f.

The synthesis of all poly[*n*]catenane materials discussed in this thesis have represented the cutting edge of entirely catenated synthetic polymers.[1] However, these materials are still limited for use as functional polymers due to their relatively low molecular weights. The high T_g of the poly[*n*]catenane (97 °C for linear sample, 104 °C for branched sample as given by differential scanning calorimetry (DSC))[2] yields a polymer that is extremely brittle at room temperature and unable to undergo material testing. These comparatively low molecular weights yield materials below the entanglement threshold for the poly[*n*]catenane, limiting the rheological and materials testing that can be performed on the poly[*n*]catenanes. This limitation appears particularly pronounced when regarding the properties of the catenane when explored by computational theory.

Work done by Dr. Phillip Rauscher on poly[*n*]catenane materials has shown great insight into the the dynamics of polycatenanes in solution, the melt, and under nanoscale confinement. Interestingly, the mechanical bond causes a slow-down in dynamics at the length scale of the overall ring – no matter how large. For instance, in solution, the overall ring relaxation in poly[*n*]catenanes is an order of magnitude slower compared to free rings, whether the ring contains ten repeat units or a hundred.[3] These same results hold in the melt[4] and for polymeric [2]catenanes in solution, and are essentially unaffected by the inclusion of hydrodynamic interactions.[5]

Dr. Rauscher's work has shown that the poly[*n*]catenanes demonstrate unusual rheological behaviour that is strongly contrasting with typical polymer melts; for these interlocked systems, the viscosity decreases with increasing ring size and molecular weight (**Figure 5.1**).[6] This surprising trend continues up to a critical ring size, above which the viscosity increases with increasing molecular weight (ring size). It has been suggested that inter-ring correlations between catenated moieties may be a key cause for this behaviour. In fact, more complex catenated structures can even lead to a jamming transition as the ring size decreases.[7] Similarly, the dynamics of catenated rings were recently analysed in terms of a "topological friction," which couples the motion of the interlocked portions of the molecules.[8] These findings suggest a rich phenomenology and motivate further synthetic and experimental advances so that these predictions can be tested and studied in the laboratory as well as the computer.

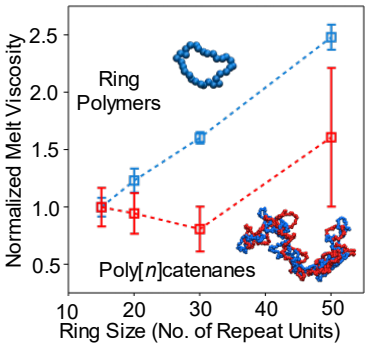

Figure 5.1 Normalized viscosities of ring polymer and poly[*n*]catenane melts as a function of the ring size demonstrating the unique viscosity behavior of the poly[*n*]catenane materials in simulation.

In service of advancing the dynamics and rheology of these materials in a laboratory setting, several pathways to large poly[*n*]catenane polymers and networks have been proposed (**Figure 5.2)**. The variations to the synthesis would lead to a complex series of interesting polymers. Though no large strides have been made in the synthesis of these materials, preliminary reactions have been undertaken in for each pathway (**Figure 5.2a-d**). This chapter will detail the preliminary

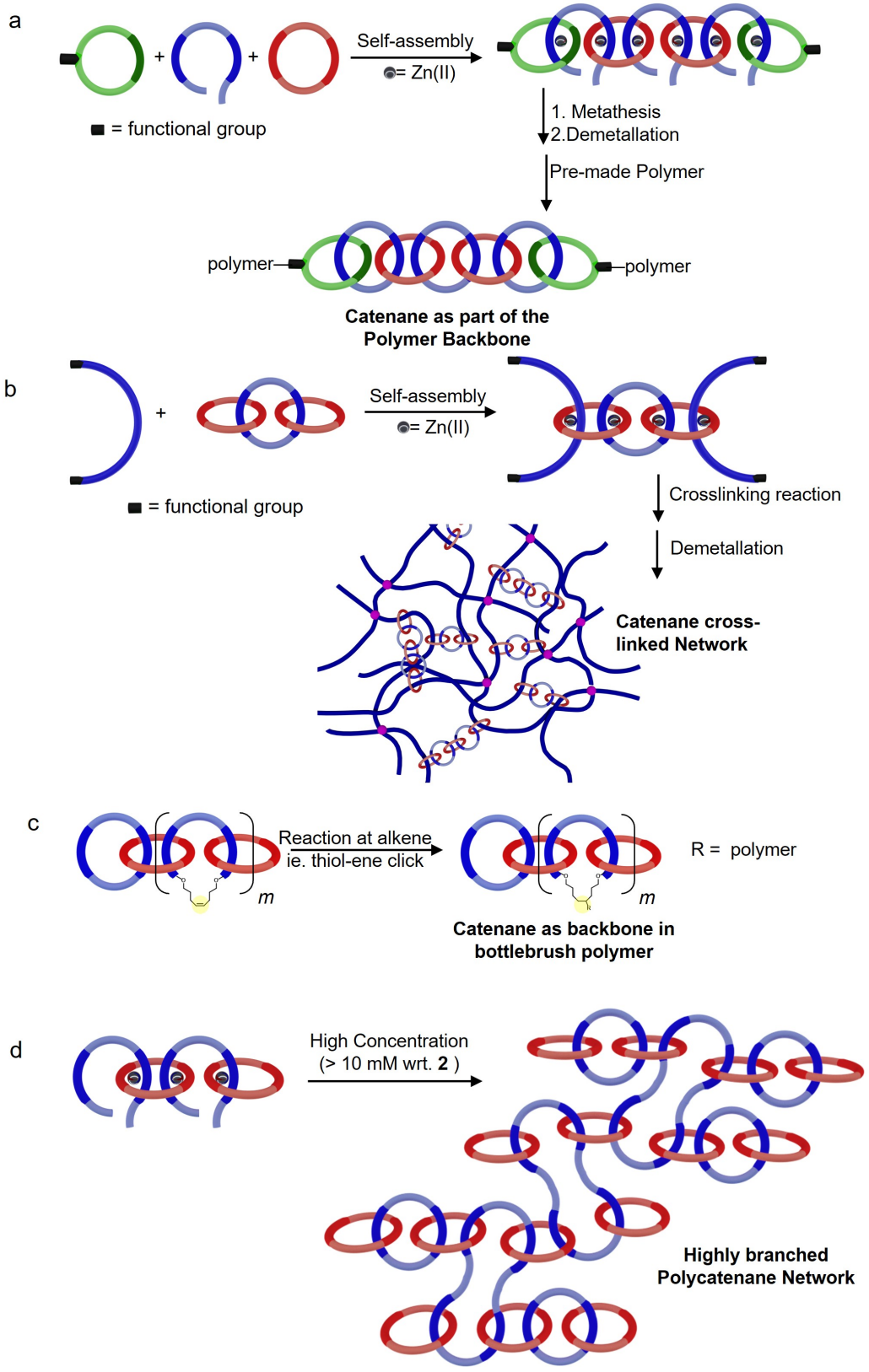

Figure 5.2 Four unique pathways to complex poly[*n*]catenane polymers capable of more in depth materials testing (tensile, rheological).

work done in each avenue, the obstacles in the synthesis, and the outlook of each material for future researchers. This work detailed in this chapter is not intended as a completed research analysis nor as the final word in the creation of these materials; rather, it is meant as a guide for future researchers and a collection of chemistries attempted as well as the lessons learned from these attempts.

5.2 Functionalized Catenanes for Co-Polymerization

While many of the pathways in **Figure 5.2** depict materials derived from the synthesis of the original poly[*n*]catenane **3**, **Figure 5.2a** depicts a polymer that results from a fundamentally different MSP. In this material, a new macrocycle monomer (**Figure 5.3**, **51**) is created similar to the [3]catenane synthesis published in the Rowan group previously.[9] This new macrocycle, **51**, was synthesized previously (see Synthesis Procedures). **51** differs from all macrocycles seen in this thesis previously because it only contains a single Bip ligand and also contains a functionalized group (carboxylate ester). If **51** is included in a controlled quantity with **1** and **2** during MSP synthesis, **51** would act as a chain terminating agent during the self-assembly of **$(\mathbf{1{\cdot}2{\cdot}Zn(II)_2})_n{\cdot}\mathbf{51}_2$.** After ring-closing and demetallation, the resulting oligomer could undergo a reduction reaction at the carboxylate ester and subsequent reaction with a secondary functionalized polymer to form a

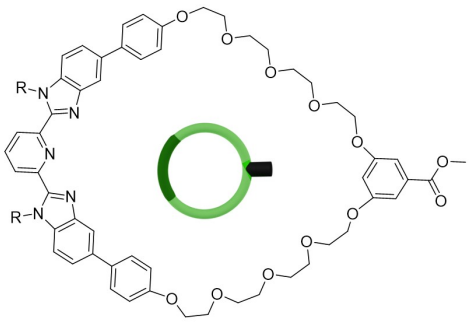

51

Figure 5.3 Chemical structure for macrocycle **51**: containing a single Bip ligand and a carboxylate ester functional group for later reduction and reaction.

co-polymer. Though macrocycle **51** was created for preliminary studies, the bulk of this project was transferred to a different researcher and later abandoned in a similarly early synthetic phase.

This system would be of particular interest when exploring atomic force microscopy (AFM) based single-molecule force spectroscopy (SMFS). This method has been used on [2]catenanes in the past[10] and has shown that the mobility of a single [2]catenane has a measurable change in the persistence length of the material and the sub-molecular dynamics of the material. Similar studies in the poly[*n*]catenane have proven difficult due to the length of ***l*-3** and lack of an easy polymer "handle" for the AFM tip to grip to; a potential collaboration with Jilin University (who had experience in AFM-SMFS with poly[2]catenane materials[11]) attempted to study the current poly[*n*]catenane material **3**, however the gripping difficulties prevented this from garnering any usable results. The synthesis of this catenane co-polymer would allow for more complex SMFS studies on poly[*n*]catenane. A similar structure has recently been utilized by Barnes and co-workers to make a [2]catenane gel.[12] Progress in the method detailed in this section would allow for [n]catenane crosslinks in a similar structure for easy analysis of the influence of increasing the number of mechanical bonds within a catenated cross-linked gel.

This researcher believes that the current tendency to form the ADMET byproduct **5** may inhibit the viability of this synthetic route (**Figure 5.4**). This route, therefore, may hold greater potential with an alternate ligand system if the byproduct reaction can be eliminated.

5.3 Catenane as mobile cross-links

The use of mobile cross-links in polymeric materials is a well-studied area in the field of slide-ring materials using the rotaxane functionality.[13–15] It is unsurprising, therefore, that the desire to

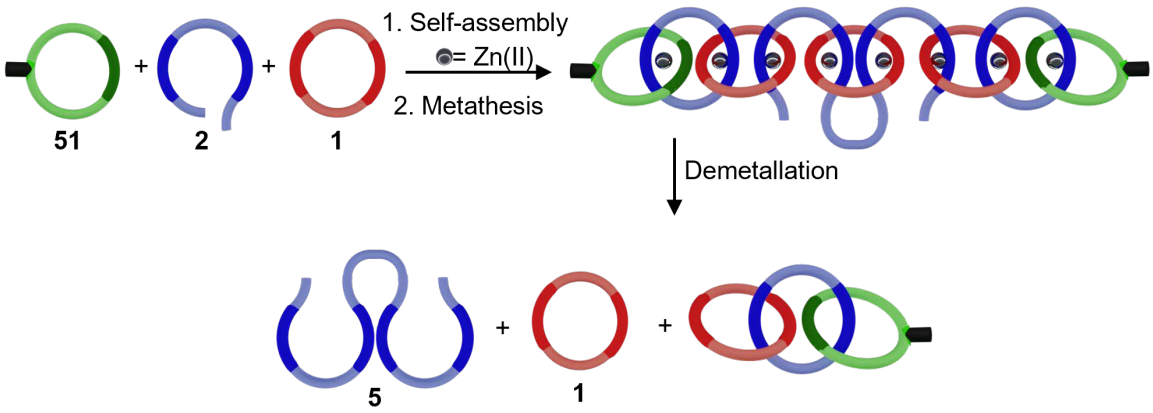

Figure 5.4 Graphical depiction as to how the formation of ADMET **5** would severely interfere with the production of the catenane co-polymer synthesis.

combine the properties of the slide-ring material with the complexity of the polycatenane structure has given rise to a proposed mobile catenane crosslink, as seen in **Figure 5.2b**.

In short project done in collaboration with Dr. Qiong Wu, crosslinked polydimethylsiloxane (PDMS) based gels were synthesized according to **Figure 5.5**. In this process, a 4-6% (mercaptopropyl)methylsiloxane – dimethylsiloxane co-polymer (PDMS-r-MMS) was reacted with an alkene terminated crosslinker (**Figure 5.5a)** under thiol-ene click conditions[16,17] to yield a cross-linked gel **52**. Based on this synthesis, a pseudorotaxane **1·53$_2$·Zn(II)$_2$** was incorporated into a new reaction to act as a second cross-linking point. In this method (**Figure 5.5b**), both the covalent crosslink and **53** were employed at a ratio of 4:1 (such that 20% of the cross-link would be the mobile interlocked crosslink). The synthesis of this gel attempted via two different catalytic methods.[18] Initially, Dr. Wu employed a camphorquinone (CQ) photoinitiator under blue light to complete the thiol-ene click reaction in a single step. However, by virtue of this synthetic method, all four alkenes of **1·53$_2$·Zn(II)$_2$** must fully react into order to complete the full crosslink. If even 1 out of the 4 alkene remains unreacted, the material will de-thread upon demetallation and render the interlocked cross-link obsolete. Therefore, when the CQ initiated gel was demetallated using tetrabutylammonium

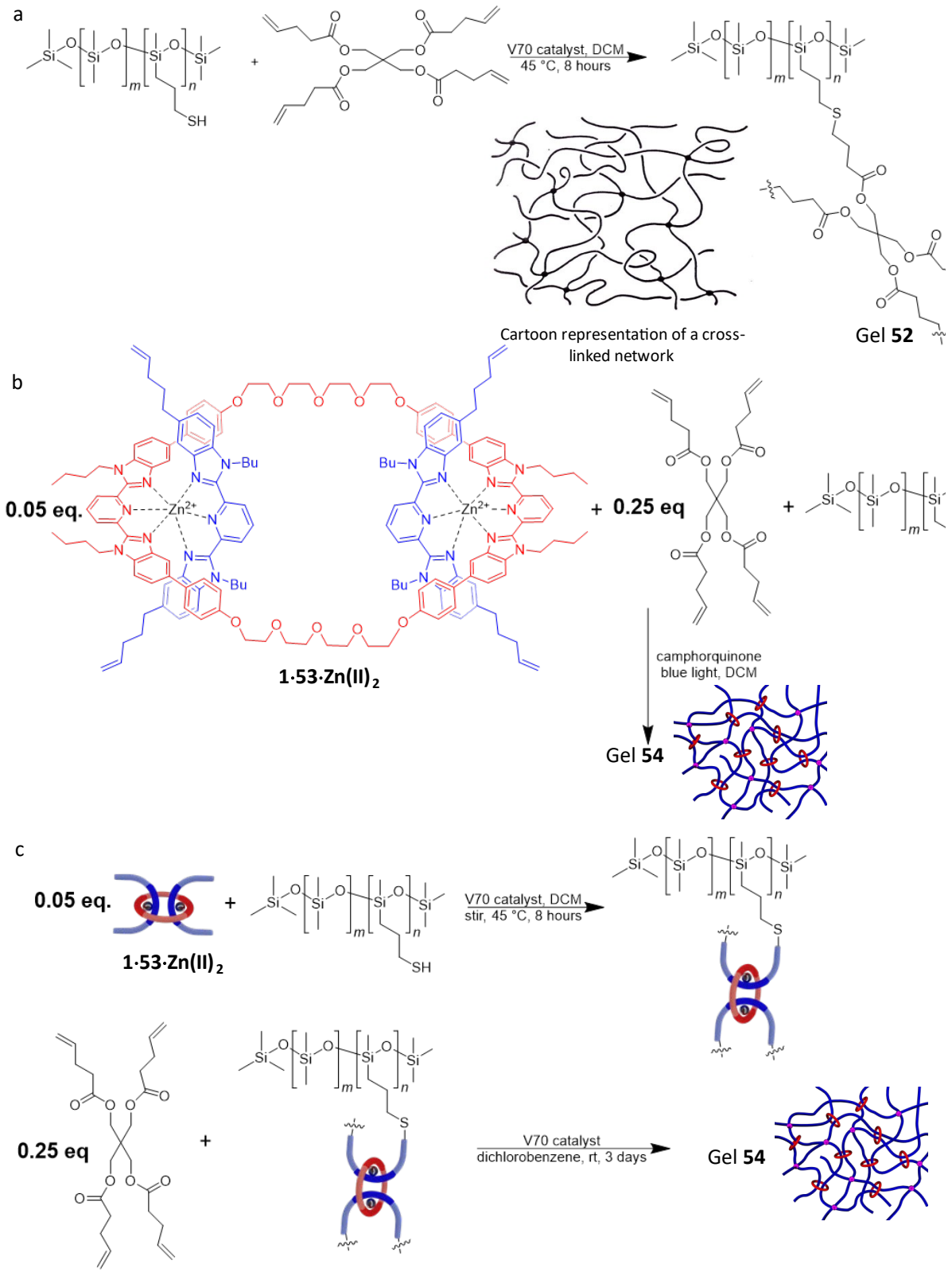

Figure 5.5 (a) Synthetic method for the formation of the covalent gel **52**. (b) and (c) depict the two synthetic methods employed to create the interlocked gel **54**.

hydroxide (TBAH), over 50% of the material was lost.

To attempt to overcome this, we sought to separate out the two cross-linking steps (**Figure 5.5c**). To maximize the amount of reacted chain-ends in **1·53$_2$·Zn(II)$_2$**, the pseudorotaxane and the polymer were reacted for 8 hours while stirring. After this reaction, the mixture was poured into a petri dish, was placed under argon, and allowed to react with the covalent crosslink and catalyst in o-dichlorobenzene (see Synthetic Procedures). The resulting metalated material (**54·Zn(II)**) is pictured in **Figure 5.6**. Unfortunately, this material was also unable to hold its fully shape once exposed to the demetallating agent (TBAH). The incomplete reaction was attributed to radical reaction used in this synthesis. Based on this work (as well as work done by other researchers in the group), we ascertained that materials containing metalated-Bip (**7**) severely hindered the progress of any radial-based reaction.

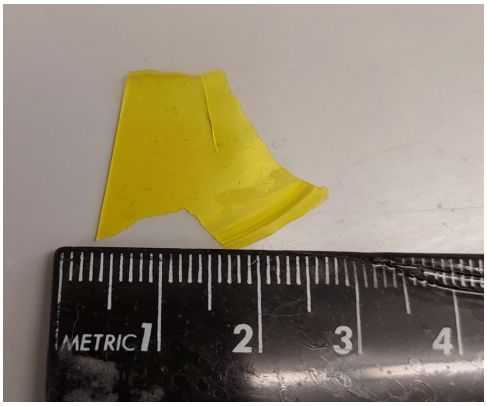

Figure 5.6 Image of a segment of the metalated gel **54·Zn(II)**.

Based on this information, work by Laura Hart has continued to explore the viability of a similar reaction, using a new system with a nitrile-oxide alkyne click reaction rather than the radial initiated V70. These materials incorporate polyethylene oxide as well as a new macrocyclic component into the system to make more complex slide-ring materials which may be viable for created catenated networks as seen in **Figure 5.2b**.

5.4 Functionalization of pre-made poly[*n*]catenanes

In Section 5.2 the co-polymerization of poly[*n*]catenane was attempted by installing a new functionality on to the material; however, poly[*n*]catenane **3** already contains an active site for reactions: the alkene moiety of monomer **6**. After the completed metathesis reaction of **2**, each monomer **6** contains a single alkene where the metathesis reaction occurred (**Figure 5.7**). Therefore, it is conceivable that this alkene can be exploited to create a bottle-brush type polymer off of the completed poly[*n*]catenane structure as in **Figure 5.2c**. Unlike the materials discussed in Section 5.3, the completed poly[*n*]catenane does not contain metalated **7**, therefore radical based initiators would be a viable avenue for this work. As thiol-ene click reactions are common among

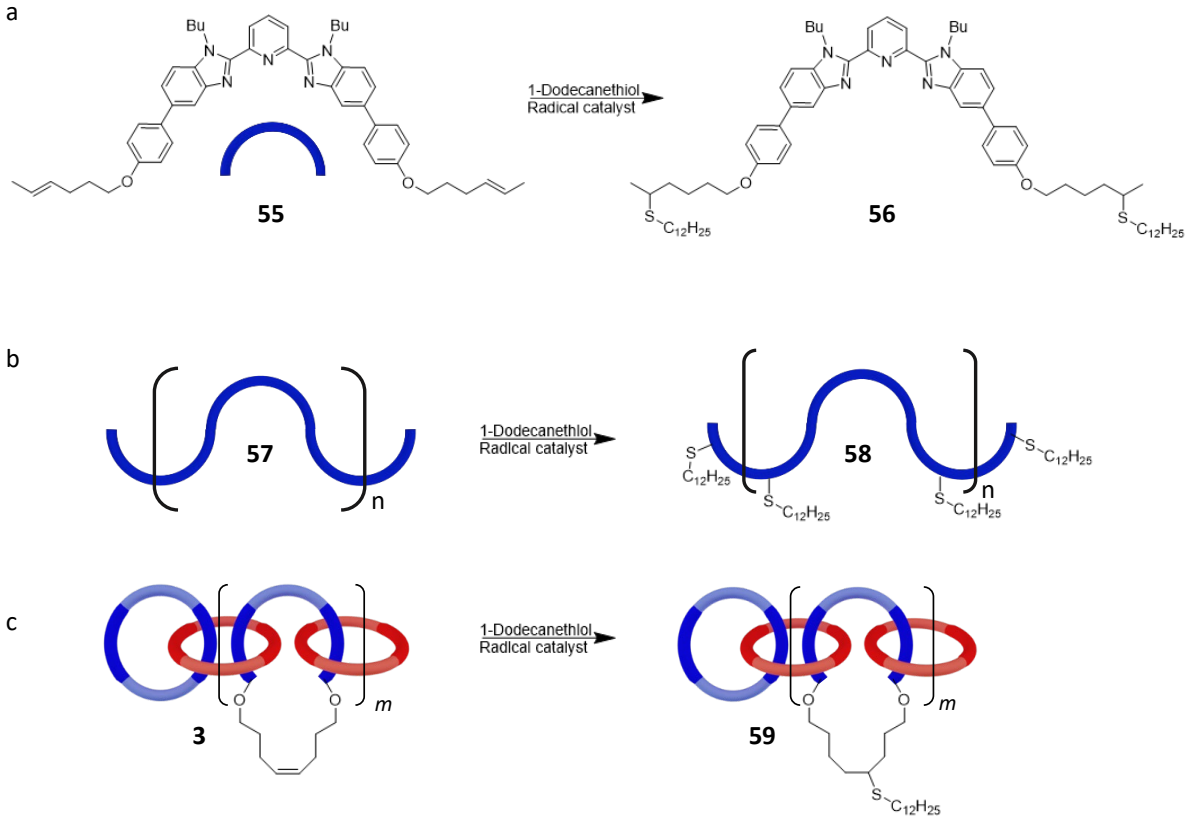

Figure 5.7 Step-wise testing of the viability of the thiol-ene click reaction for functionalizing poly[*n*]catenane materials: (a) small molecule, (b) covalent polymer, and (c) poly[*n*]catenane.

the group and have been show to work on 1,2-disubstituted alkenes,[19] a thiol-ene click reaction was proposed for this reaction.

To test the viability of this method, a series of trial reactions were proposed (**Figure 5.7**). In the initial test reactions (**Figure 5.7a**) two primary factors were tested: (1) whether the internal alkene a small molecule Bip-containing compound (**55**) was able to undergo a radical thiol-ene click reaction and (2) which reactions conditions were preferable for this reaction. Two different catalysts were tested: Azobisisobutyronitrile (AIBN) and V70 (**Figure 5.8**). In this reaction, both catalysts were able to perform the thiol-ene click reaction; however, the V70 was shown to be a

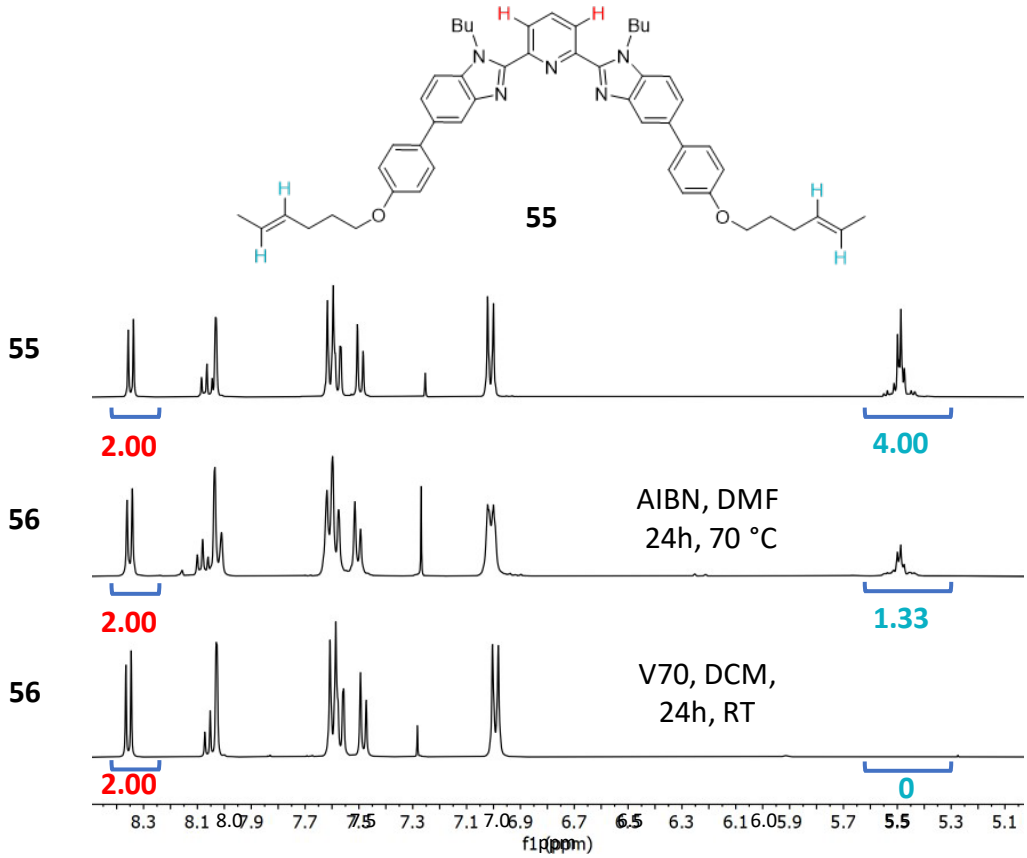

Figure 5.8 ^{1}H NMR analysis of the functionalization reactions showing the difference between the original material **55** (top), synthesis of **56** using an AIBN catalyst (middle), and synthesis of **56** using a V70 catalyst (bottom).

better catalyst for the formation of **56**, with all of the alkene peaks having fully reacted within 24 hours.

Based on the success of the formation of **56**, an oligomer of **55** was created to test the viability of this reaction in a more complex and hindered environment (**Figure 5.7b**). Based on the results from success of V70 in the synthesis of **56**, the same reaction conditions were used for the synthesis of **58**. After 24 hours, an aliquot of the reaction was removed and characterized; at this time point, only 34 % of the alkene had reacted. Additional catalyst was added and the reaction was allowed to run for an additional 24 hours and was similarly characterized (**Figure 5.9**). After a total of 48 hours, only 38% of the alkene had reacted. While this result was not ideal, the synthesis of the bottlebrush structure **59** did not require all alkenes to react, so testing progressed to **Figure 5.7c**.

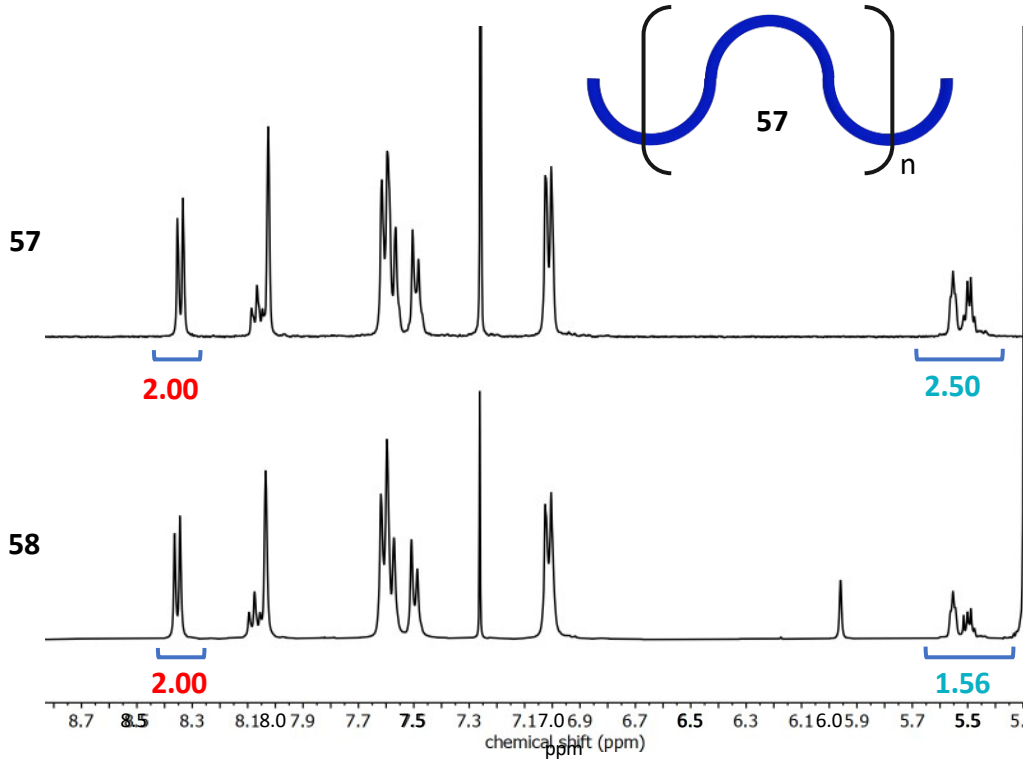

Figure 5.9 ^{1}H NMR analysis of the functionalization reactions of an oligomer showing the difference between the original material **57** (top) and after 48 hours of reaction with a V70 catalyst to yield **58** (bottom).

A sample of partially purified **3** was allowed to react under the same conditions as **57** to yield the material **59**. Based on the integration of the alkene protons, it was evident that the ADMET byproduct **5** was more reactive than the poly[*n*]catenane; however, integration of the poly[*n*]catenane alkene clearly showed evidence of reaction (34%).

Based on these preliminary results, this methodology seems a viable route for functionalization and creation of new catenane co-polymers. However, due to the low rates of reaction, it may be worth exploring other chemistries if this structure is to be explored further: for instance, the nitrile-oxide alkyne click reaction being explored for the procedure in **5.3** may have potential in this avenue as well.

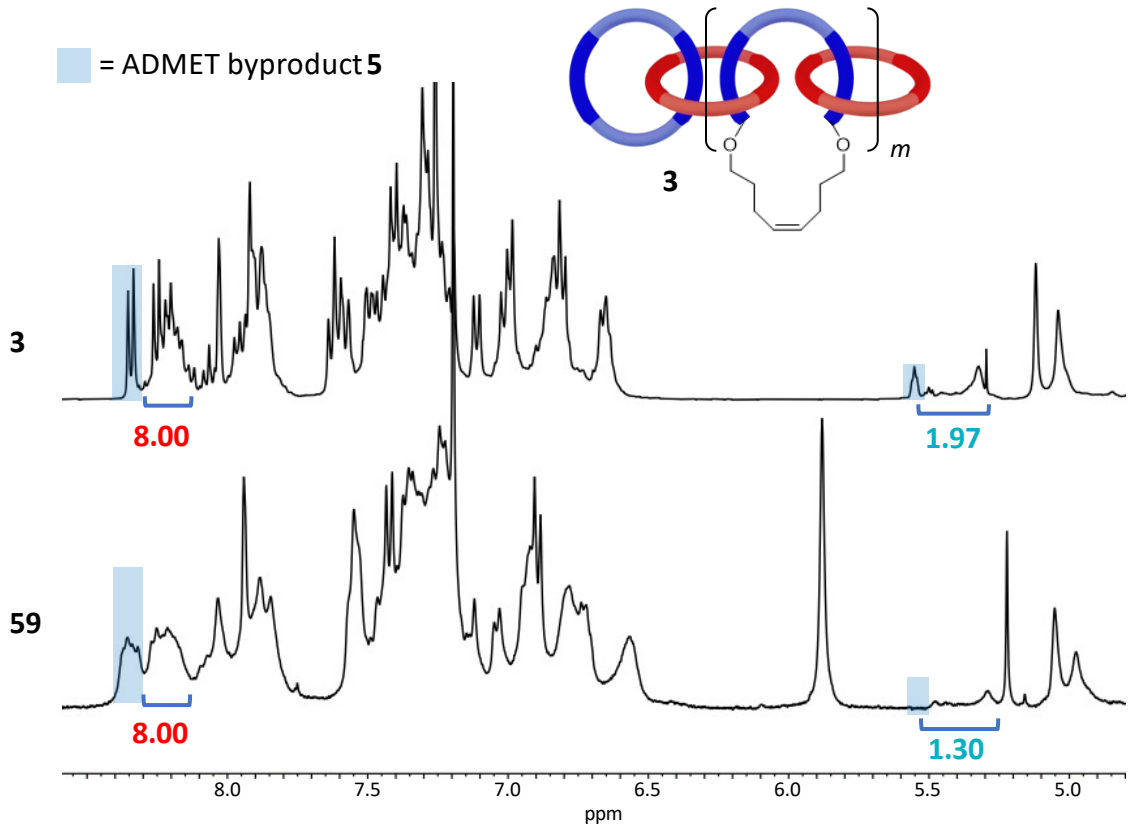

Figure 5.10 ^{1}H NMR analysis of the functionalization reactions of poly[*n*]catenane **3** showing the difference between the original material **3** (top) and after 48 hours of reaction with a V70 catalyst to yield **59** (bottom).

5.5 Progress toward fully catenated networks

The final method of creating larger, more complex catenane materials is the only material that is composed only of interlocked rings: the network catenane material (**Figure 5.2d**). As was discussed in Chapter 1 of this thesis, entirely catenated networks (Olympic gels) have been seen in the literature before.[20–23] However, in each of the examples discussed, the catenane network is formed in a random manner, either as a byproduct in a polymerization or as a random network of varying ring sizes. There is no evidence in the literature of an entirely synthetic controlled synthesis of poly[*n*]catenane networks.

There is a significant amount of evidence that the method used to synthesize poly[*n*]catenane in this thesis can lead to network polycatenanes. In the past, several catenane syntheses have yielded unidentifiable thin film-like substances (**Figure 5.11**). During the synthesis of **3**, at concentrations of 2.5, 5.0, and 10.0 mM, different samples of **1·2·Zn(II)$_2$** have yielded the swellable gel seen in **Figure 5.11a**. These gels have undergone the full metathesis reaction and were isolated from the soluble products. To ensure that the gelation of these materials was not due to metalation, the swollen gels were allowed to soak in a solution of DCM and ethylenediamine overnight to ensure full demetallation. This, taken with the blue fluorescence that the material

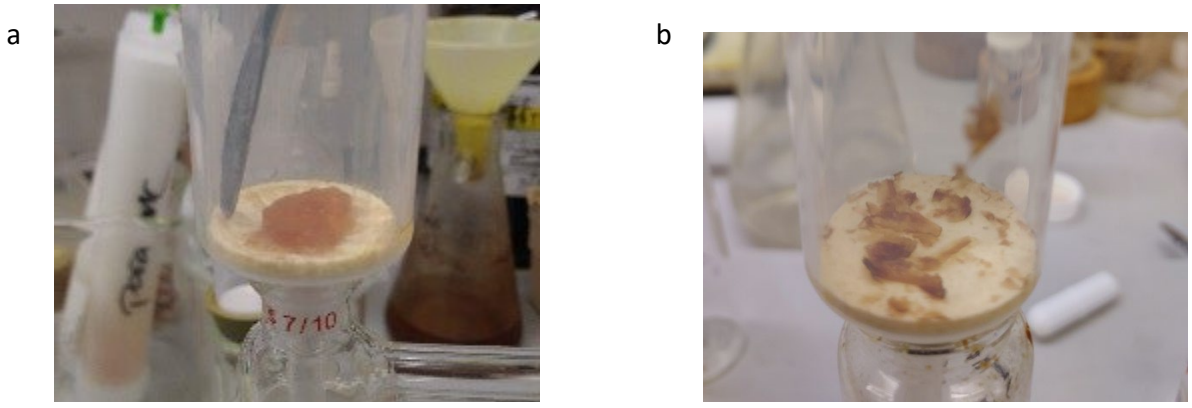

Figure 5.11 Images of insoluble gels resulting from the poly[*n*]catenane synthesis of (a) **3** and (b) **43$_{meta}$**.

exhibited when under UV light, indicated that these gels were not metallopolymers, but genuine gels. These materials were also seen in other poly[*n*]catenane synthesis, as in the metathesis of **36**$_{meta}$**·2·Zn(II)**$_2$ (**Figure 5.11b**). The gels were seen to swell in a variety of organic solvents, including chloroform, DCM, acetone, and THF. Unfortunately, without the ability to solubilize the gels, the materials could not be characterized via typical catenane characterization procedures so, at this time, there is no explicit evidence that these are interlocked gels; however, due to the ratio of **1**:**2** (or **36**:**2**) in the soluble materials, the insoluble material must contain an equal ratio of **1**:**2** (or **36**:**2**), therefore, the best explanation at present is that these materials are, in fact, olympic gels.

In an attempt to recreate these gels, a polycatenane reaction was performed using **1·2·Zn(II)**$_2$ in unique conditions: to create a film for testing, the material was not stirred in DCM, rather, **1·2·Zn(II)**$_2$ was dissolved in tetrachloroethane and allowed to react without stirring. To increase the likelihood of film formation, **1·2·Zn(II)**$_2$ was dissolved at a concentration of 20 mM wrt **1**. After addition of the Hoveyda-Grubbs GII catalyst, the material quickly formed an insoluble gel (**RINGO, Figure 5.12a**). The gel was allowed to react for the full two-day catenane reaction period, with addition of catalyst after 24 hours. After completion of the reaction and deactivation of the

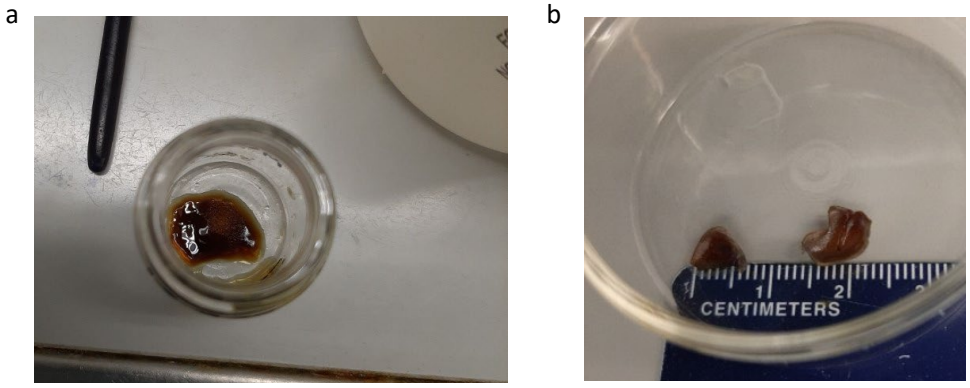

Figure 5.12 Images of the metalated **RINGO**, the first attempt at targeting an Olympic gel using this synthetic method. **RINGO** is pictured after the reaction (a) and after drying (b).

catalyst, **RINGO** dried, yielding the metalated gel pictured in **Figure 5.12b**. However, exposure to the demetallating base (ethylenediamine) in DCM, **RINGO** quickly separated and dissolved in the DCM. ^{1}H NMR characterization of the material demonstrated that < 30% of the starting material had been converted into catenane (**Figure 5.13**). As with many cross-linking reactions, once the material reached a minimum number of linking sights, the network was no longer soluble. Unfortunately, since **1·2·Zn(II)$_2$** is supported by the metal bonding of the MSP, the number of crosslinks required to form a gel with this material is not the same as that of the final gel (**RINGO**). The mechanism of the metathesis reaction required that the alkenes remain in solution to undergo the proper ring-closing reaction. Without this, the material ended up as seen in **Figure 5.13**, with the majority of the material completely unreacted.

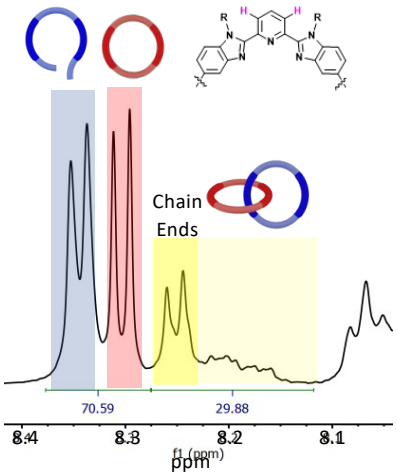

Figure 5.13 ^{1}H NMR characterization of the demetallated **RINGO** demonstrating that only 30 % of the material was catenated, while 70 % remained as the two starting materials. This ^{1}H NMR additionally shows large chain end peaks, suggesting that the material formed may be primarily [2]catenane.

To overcome this, the ideal next steps for the formation of this gel requires a reaction that does not need the alkene chain-ends to remain in solution for the duration of the reaction. A photo-catalyzed reaction may aid the formation of future generations of these materials. It is also of interest that the materials seen in **Figure 5.11** are not seen for every catenane reaction; therefore,

the MSP starting material must play a role in when and how much of this material appears. During MSP synthesis, precise ratios are monitored via ^{1}H NMR, however, slight variations (ie. 0.99:1 ratio of **1**:**2**) may occur. If the conditions that lead to the formation of the insoluble gels in **Figure 5.11** can be pinpointed, perhaps these materials can be targeted with more precision in the future.

5.6 Conclusions

The processes described in this chapter are all, unfortunately, early in their conception; however, the contents of this work will likely form the basis for the future of poly[*n*]catenane materials. The ultimate goal of this project has always been to move from polymerization innovation to materials characterization, in order to gain an understanding of the physical properties that poly[*n*]catenane materials can offer the world of polymer chemists. The information gleaned in Chapters 2-4 will likely steer the course of how future poly[*n*]catenanes will be made, however the work in this chapter will hopefully form the basis for the complex and interesting materials that these polymers are capable of creating.

5.7 Synthesis procedures for preliminary products

5.7.1 Synthesis of Macrocycle 51

Step 1 of 4

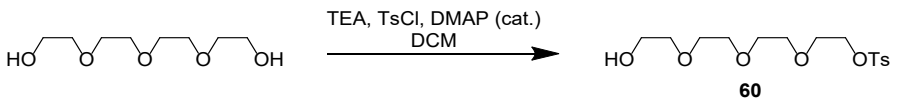

60

In a 1 L round bottom flask equipped with a stir bar under argon atmosphere, tetraethylene glycol (40.0 g, 206 mmol, 1 eq.) was combined with triethylamine (62.5 g, 618 mmol, 3 eq.), and 4-

dimethylaminopyridine (0.50 g, 4 mmol, 0.01 eq.) in dry dichloromethane (685 mL) and stirred at 0 °C. 4-Toluenesulfonyl chloride (39.27 g, 206 mmol, 1 eq.) was stirred in dry dichloromethane (685 mL) and added to the reaction flask after it had stirred for some time at 0 °C. The reaction was allowed to slowly warm to rt over 24 hours of reaction after which the solvent was removed. The mixture was redissolved in ethylacetate and filtered to remove salt. Product **60** was purified via column chromatography (90% EtOAc/ hexanes) to yield the tosylated product as a clear viscous liquid in 35% yield.

^{1}H NMR (500 MHz, $CDCl_3$) δ_H (ppm) 7.83 (d, J = 8.3 Hz, 2H), 7.37 (d, J = 8.0 Hz, 2H), 4.19 (t, J = 5.0, 4.5 Hz, 2H), 3.75 – 3.70 (m, 6H), 3.70 – 3.64 (m, 6H), 3.63 (t, J = 4.3 Hz, 2H), 2.47 (s, 3H).

Step 2 of 4

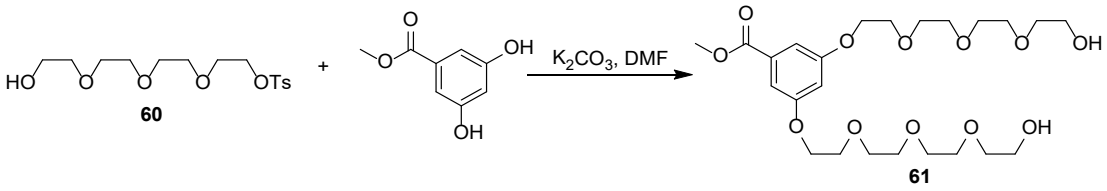

In a 250 mL round bottomed flask equipped with a stir bar, methyl 3,5-dihydroxybenzoate (3.2 g, 19 mmol), product **60** (20 g, 3 eq,, 57 mmol), and K_2CO_3 (7.9 g, 3 eq., 57 mmol) were combined in dry DMF (70 mL) under argon. The mixture was stirred at 72 °C for 24 hours before being cooled to room temperature. The DMF was removed under pressure and the resulting material was dissolved in $CHCl_3$ and filtered. The filtrate was collected and concentrated then purified via column chromatography (0-3 % MeOH/ EtOAc). Yield = 49 %.

^{1}H NMR (500 MHz, $CDCl_3$) δ_H (ppm) 7.22 (d, *J* = 2.4 Hz, 2H), 6.74 (t, *J* = 2.4 Hz, 1H), 4.22 – 4.15 (m, 4H), 3.90 – 3.85 (m, 4H), 3.79 – 3.67 (m, 24H), 3.66 – 3.60 (m, 4H), 1.72 – 1.63 (m, 3H).

Step 3 of 4

61 62

In a 250 mL round bottom flask equipped with a stir bar under argon atmosphere, **61** (4.7 g, 9.5 mmol) was combined with triethylamine (8.7 g, 85.5 mmol, 9 eq.), and 4-dimethylaminopyridine (0.10 g, 0.05 mmol, 0.01 eq.) in dry dichloromethane (32 mL) and stirred at 0 °C. 4-Toluenesulfonyl chloride (5.4 g, 28.5 mmol, 3 eq.) was stirred in dry dichloromethane (32 mL) and added to the reaction flask after it had stirred for some time at 0 °C. The reaction was allowed to slowly warm to rt over 24 hours of reaction after which the solvent was removed. The mixture was redissolved in ethylacetate and filtered to remove salt. The filtrate was collected and the solvent removed under reduced pressure yielding yellow-brown oil. The resulting material was purified by column chromatography (20% EtOAc/ hexanes) to yield **62** in a 31% yield

^{1}H NMR (500 MHz, $CDCl_3$) δ_H (ppm) 7.81 (d, J = 8.3 Hz, 4H), 7.38 – 7.33 (m, 4H), 7.21 (d, J = 2.4 Hz, 2H), 6.70 (t, J = 2.4 Hz, 1H), 4.16 (ddd, J = 10.6, 5.4, 4.1 Hz, 12H), 3.87 (dd, J = 5.6, 3.9 Hz, 4H), 3.80 – 3.62 (m, 16H), 2.46 (s, 6H), 1.67 (s, 3H).

Step 4 of 4

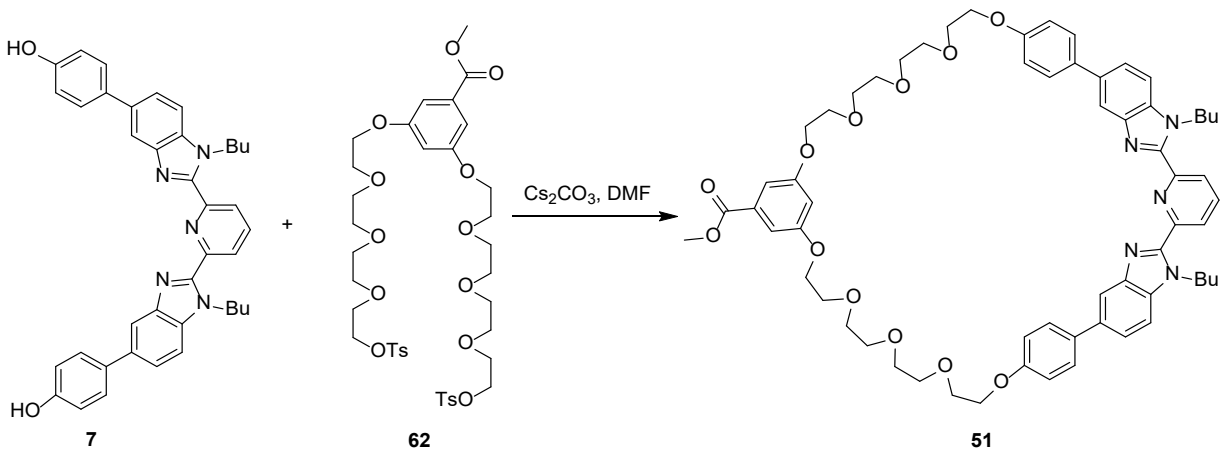

7 **62** **51**

A 250 mL additional funnel containing **62** (2 g, 2.4 mmol) and **7** (1.45 g, 2.4 mmol) in 157 mL of DMF was fitted to a 500 mL round bottom flask containing Cs_2CO_3 (7.0 g, 21.6 mmol) and stir bar in anhydrous DMF (240 mL). The mixture was stirred at 72 °C for 24 hours while the mixture within the addition funnel was gradually added. After the entire mixture was combined, the material was allowed to react for an additional 72 hours. The DMF was removed under pressure; the mixture was dissolved in $CHCl_3$, filtered, and the filtrate was collected as a yellow/brown solid. Pure product was not isolated for this reaction.

5.7.2 Reaction Conditions for PDMS gel 54

A pentene terminated product from **7** was synthesized according to the literature to yield **53**.[24] A solution of **1** was titrated with **53** an monitored by ^{1}H NMR until a precise 1:2 ratio of **1**:**53** was achieved. The material was titrated with $Zn(Tf_2N)_2$ until a precise 1:2:2 ratio was reached, yielding the doubly threaded pseudorotaxane **1·53$_2$·Zn(II)$_2$** (pictured in **Figure 5.5**).

1.69 g of 4-6% (mercaptopropyl)methylsiloxane – dimethylsiloxane was combined with **1·53$_2$·Zn(II)$_2$** (180 mg, 0.05 eq., 0.0423 mmol) in a dried round bottom flask under argon. 16.9

mL of dried DCM (2.5 mM) was added to the reaction. The DCM was degassed for 20 minutes before addition of the V70 catalyst (13 mg). The reaction was stirred for 24 hours at 45 °C.

After 24 hours, 3.39 mL of o-dichlorobenzene (DCB) was added to the reaction and the DCM was removed under pressure. To the mixture in DCB, the alkene terminated crosslinker (77.4 mg, 0.25 eq., 0.17 mM) and a second portion of the V70 catalyst (20.88 mg) was added. The entire mixture was transferred to a petri dish. The reaction vessel was rinsed with an additional 3.9 mL of DCB and added to the dish (final concentration 100 mM). The dish was placed in a chamber under argon for 24 hours. The DCB was removed via vacuum after reaction to yield the gel **54**.

5.7.3 Synthesis of ADMET 57

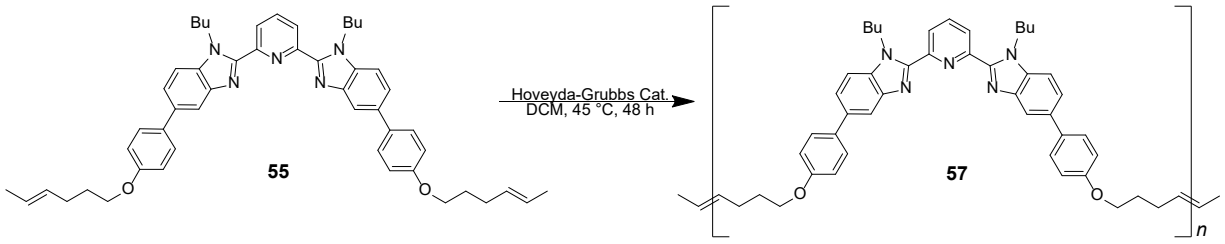

In a 25 mL round-bottomed flask equipped with stir bar and condenser, 500 mg (0.65 mmol) of **55** (collected as a byproduct in the synthesis of **14**, see **2.6.2.3**) was dissolved in 13 mL of DCM (50 mM). The DCM was degassed with argon before the addition of 2.6 mg of Hoveyda-Grubbs G2 catalyst (0.32 mM) in DCM. The amount of DCM added accounted for any evaporation during the degassing. The reaction was degassed for an additional 30 minutes and the solvent level was maintained throughout to keep the proper concentration. After 24 hours the degassing and catalyst addition was repeated. After a total of 48 hours reacting, the reaction was allowed to cool to room temperature and 1 mL of ethyl vinyl ether was injected to deactivate the catalyst. After stirring for 30 minutes, the 13 mL of reaction mixture was precipitated into 200 mL of cold MeCN. The

reaction vial was rinsed twice with 1.0 mL of DCM, which were also precipitated in to MeCN. The suspension was allowed to sit in the fridge overnight to fully precipitate. The product (**57**) was collected by filtration and washed three times with cold MeCN. Yield is quantitative and the product is light brown solid. The color is due to the trace amount residue deactivated catalyst.

^{1}H NMR (400 MHz, $CDCl_3$) δ_H 8.35 (d, J = 7.8 Hz, 2H), 8.07 (td, J = 7.8, 1.5 Hz, 1H), 8.02 (s, 2H), 7.59 (dd, J = 11.4, 8.2 Hz, 6H), 7.53 – 7.46 (m, 2H), 7.01 (d, J = 8.9 Hz, 4H), 5.59 – 5.41 (m, 3H), 4.76 (t, J = 7.3 Hz, 4H), 4.07 – 3.97 (m, 4H), 2.24 (m, 2H), 1.96 – 1.82 (m, 4H), 1.74 (d, J = 7.7 Hz, 4H), 1.70 – 1.61 (m, 3H), 1.15 (q, J = 7.4 Hz, 4H), 0.77 – 0.68 (m, 6H).

5.7.4 AIBN reaction conditions (for 56)

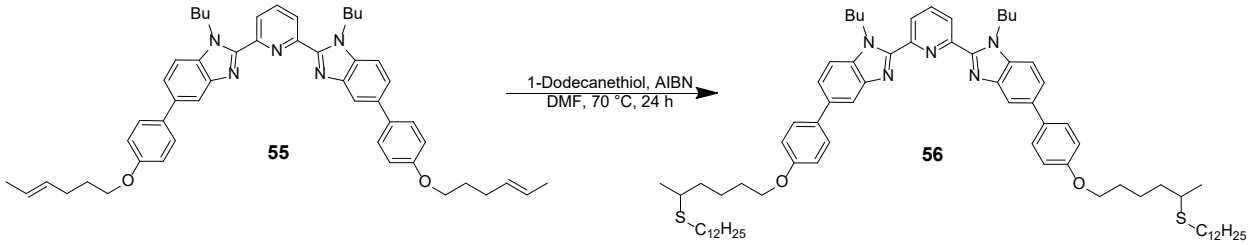

In a 5 mL conical reaction flask equipped with stir bar, 100 mg (0.13 mmol) of **55** (collected as a byproduct in the synthesis of **14**, see **2.6.2.3**) was dissolved in 1 mL of dry DMF, placed under argon, and heated to 70 °C. After fully dissolving, 1-dodecanethiol (52 mg, 2 eq., 0.26 mM) was injected into the reaction and the AIBN catalyst was added (2.13 mg, 0.1 eq. 0.013 mM). The reaction was stirred under argon at 70 °C for 24 hours. After cooling to room temperature, the DMF was removed. All NMR analysis was performed on the crude reaction mixture.

^{1}H NMR (400 MHz, $CDCl_3$) δ_H 8.35 (d, J = 7.8 Hz, 2H), 8.08 (t, J = 7.9 Hz, 1H), 8.06 – 7.99 (m, 2H), 7.65 – 7.55 (m, 6H), 7.50 (d, J = 8.5 Hz, 2H), 7.04 – 6.97 (m, 4H), 5.55 – 5.41 (m, 1H), 4.76 (t, J = 7.3 Hz, 4H), 4.03 (dt, J = 9.4, 6.5 Hz, 4H), 2.75 – 2.54 (m, 3H), 2.22 – 2.12 (m, 1H), 1.95

– 1.82 (m, 2H), 1.85 – 1.70 (m, 4H), 1.74 – 1.52 (m, 6H), 1.30 (t, *J* = 6.5 Hz, 4H), 1.26 (s, 22H), 1.20 – 1.05 (m, 4H), 0.88 (t, *J* = 6.5 Hz, 6H), 0.73 (t, *J* = 7.3 Hz, 6H).

5.7.5 V70 Reaction Conditions (for 56, 58, 59)

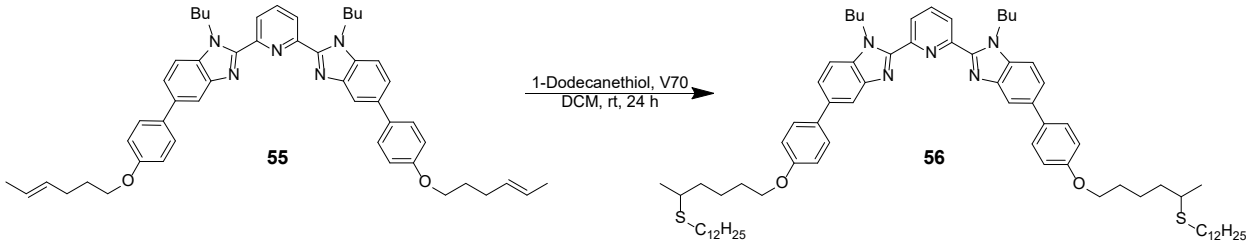

In a 5 mL conical reaction flask equipped with stir bar, 100 mg (0.13 mmol) of **55** (collected as a byproduct in the synthesis of **14**, see **2.6.2.3**) was dissolved in 1 mL of DCM and stirred. After fully dissolving, 1-dodecanethiol (52 mg, 2 eq., 0.26 mM) was injected into the reaction and the V70 catalyst was added (2.13 mg, 0.1 eq. 0.013 mM). The reaction was stirred under argon for 24 hours upon which the DCM was removed under vacuum. The resulting product, **56**, was characterized crude.

56: ^{1}H NMR (400 MHz, $CDCl_3$) δ_H 8.35 (d, *J* = 7.8 Hz, 2H), 8.07 (t, *J* = 7.9 Hz, 1H), 8.03 (d, *J* = 1.6 Hz, 2H), 7.64 – 7.54 (m, 6H), 7.50 (d, *J* = 8.5 Hz, 2H), 7.01 (d, *J* = 8.7 Hz, 4H), 4.76 (t, *J* = 7.3 Hz, 4H), 4.04 (q, *J* = 6.1 Hz, 4H), 2.08 – 1.92 (m, 2H), 1.88 – 1.67 (m, 4H), 1.66 – 1.54 (m, 6H), 1.44 – 1.35 (m, 4H), 1.27 (m, 22H), 1.23 – 1.02 (m, 4H), 1.01 (d, J = 7.3 Hz, 2H), 0.88 (t, *J* = 6.7 Hz, 6H), 0.73 (t, *J* = 7.3 Hz, 6H).

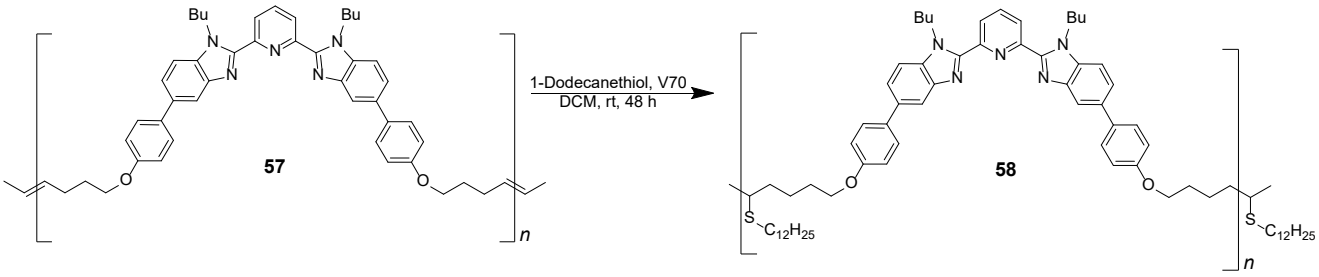

For the synthesis of **58**, a 5 mL conical reaction flask equipped with stir bar, 100 mg (0.14 mmol) of **57** was dissolved in 1 mL of DCM and stirred. After fully dissolving, 1-dodecanethiol (28 mg, 1 eq., 0.14 mM) was injected into the reaction and the V70 catalyst was added (43 mg, 1 eq. 0.14

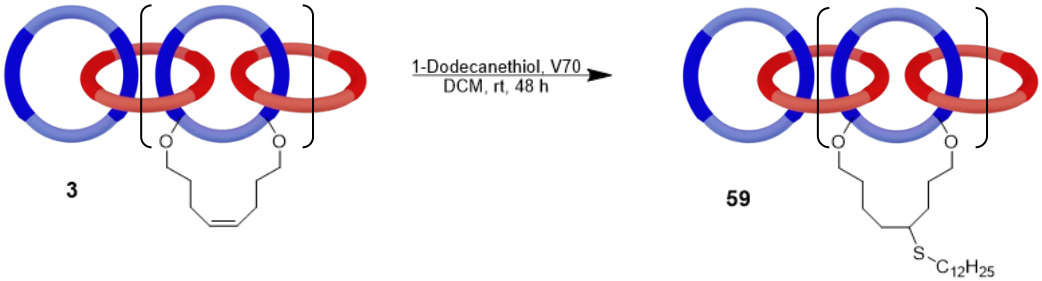

mM). The reaction was stirred under argon for 24 hours upon which an additional 43 mg of V70 was added to the reaction. After another 24 hours of reaction (total reaction time—48 hours) the DCM was removed under vacuum. The resulting product, **58**, was characterized crude (see **Figure 5.9** for the ^{1}H NMR).

For the synthesis of **59**, a 5 mL conical reaction flask equipped with stir bar, 30 mg of **3** was dissolved in 1 mL of DCM and stirred. After fully dissolving, 1-dodecanethiol (1.7 mg, 1 eq., 0.008 mM) was injected into the reaction and the V70 catalyst was added (2.6 mg, 1 eq. 0.008 mM). The reaction was stirred under argon for 24 hours upon which an additional 2.6 mg of V70 was added to the reaction. After another 24 hours of reaction (total reaction time—48 hours) the DCM was removed under vacuum. The resulting product, **59**, was characterized crude (see **Figure 5.10** for the ^{1}H NMR).

5.7.6 RINGO Synthetic Conditions

To a 20 mL vial, 72 mg of **1·2·Zn(II)$_2$** was added and placed under argon. 0.5 mL of dichloroethane was added to the vial and the reaction was heated to 45 °C to fully dissolve the **1·2·Zn(II)$_2$**. After reaching the final temperature, 0.32 mg of Hoveyda-Grubbs G2 catalyst (0.64 mM) in 0.3 mL of DCE (to bring the final concentration to 20 mM wrt **2**) was injected into the vial. After a slight agitation to distribute the catalyst, the reaction was allowed to sit under argon at 45 °C for 24 hours. After 24 hours, a second addition of catalyst (0.32 mg) was injected. After a total of 48 hours of reaction, the reaction was cooled to room temperature and 0.3 mL of ethyl vinyl ether was injected to deactivate the catalyst. The vial was dried on vacuum and reswollen in DCM to yield the metalated gel, **RINGO**. After **RINGO** was allowed to sit in ethylenediamine, the gel was disrupted and yielded the mixture of products seen in **Figure 5.13**.

5.8 References

1. Hart, L. F. *et al.* Material properties and applications of mechanically interlocked polymers. *Nat. Rev. Mater.* (2021) doi:10.1038/s41578-021-00278-z.
2. Wu, Q. *et al.* Poly[*n*]catenanes: Synthesis of molecular interlocked chains. *Science (80-.).* **358**, 1434–1439 (2017).
3. Rauscher, P. M., Rowan, S. J. & De Pablo, J. J. Topological Effects in Isolated Poly[n]catenanes: Molecular Dynamics Simulations and Rouse Mode Analysis. *ACS Macro Lett.* **7**, 938–943 (2018).
4. Rauscher, P. M., Schweizer, K. S., Rowan, S. J. & De Pablo, J. J. Thermodynamics and Structure of Poly[n]catenane Melts. *Macromolecules* **53**, 3390–3408 (2020).
5. Rauscher, P. M., Rowan, S. J. & De Pablo, J. J. Hydrodynamic interactions in topologically linked ring polymers. *Phys. Rev. E* **102**, 032502 (2020).
6. Rauscher, P. M., Schweizer, K. S., Rowan, S. J. & de Pablo, J. J. Dynamics of poly[n]catenane melts. *J. Chem. Phys.* **152**, 214901 (2020).
7. Hagita, K., Murashima, T. & Sakata, N. Mathematical Classification and Rheological Properties of Ring Catenane Structures. *Macromolecules* **55**, 166–177 (2021).
8. Amici, G., Caraglio, M., Orlandini, E. & Micheletti, C. Topological Friction and Relaxation Dynamics of Spatially Confined Catenated Polymers. *ACS Macro Lett.* **13**, 1–6 (2021).
9. Wojtecki, R. J. *et al.* Optimizing the formation of 2,6-bis(N-alkyl-benzimidazolyl)pyridine-containing [3]catenates through component design. *Chem. Sci.* **4**, 4440–4448 (2013).
10. Van Quaethem, A., Lussis, P., Leigh, D. A., Duwez, A. S. & Fustin, C. A. Probing the mobility of catenane rings in single molecules. *Chem. Sci.* **5**, 1449–1452 (2014).
11. Xing, H. *et al.* Mechanochemistry of an Interlocked Poly[2]catenane: From Single Molecule to Bulk Gel. *CCS Chem.* **2**, 513–523 (2020).
12. Nosiglia, M. A. *et al.* Metalation/Demetalation as a Postgelation Strategy To Tune the Mechanical Properties of Catenane-Crosslinked Gels. *J. Am. Chem. Soc.* (2022) doi:10.1021/jacs.2c03166.
13. Hart, L. F. *et al.* Material properties and applications of mechanically interlocked polymers. *Nat. Rev. Mater.* **6**, 508–530 (2021).
14. Bin Imran, A. *et al.* Extremely stretchable thermosensitive hydrogels by introducing slide-ring polyrotaxane cross-linkers and ionic groups into the polymer network. *Nat. Commun.* **5**, 5124 (2014).
15. Ito, K. Novel Cross-Linking Concept of Polymer Network: Synthesis, Structure, and Properties of Slide-Ring Gels with Freely Movable Junctions. *Polym. J.* **39**, 489–499 (2007).

16. Lowe, A. B. Thiol-ene “click” reactions and recent applications in polymer and materials synthesis. *Polym. Chem.* **1**, 17–36 (2010).

17. Nilsson, C., Simpson, N., Malkoch, M., Johansson, M. & Malmström, E. Synthesis and thiol-ene photopolymerization of allyl-ether functionalized dendrimers. *J. Polym. Sci. Part A Polym. Chem.* **46**, 1339–1348 (2008).

18. Uygun, M., Tasdelen, M. A. & Yagci, Y. Influence of Type of Initiation on Thiol-Ene “Click” Chemistry. *Macromol. Chem. Phys.* **211**, 103–110 (2010).

19. Claudino, M., Johansson, M. & Jonsson, M. Thiol–ene coupling of 1,2-disubstituted alkene monomers: The kinetic effect of cis/trans-isomer structures. *Eur. Polym. J.* **46**, 2321–2332 (2010).

20. Endo, K., Shiroi, T., Murata, N., Kojima, G. & Yamanaka, T. Synthesis and Characterization of Poly(1,2-dithiane). *Macromolecules* **37**, 3143–3150 (2004).

21. Yamanaka, T. & Endo, K. Network Formation of Interlocked Copolymer Obtained from Copolymerization of 1,2-Dithiane and Lipoic Acid by Metal Salt. (2007) doi:10.1295/polymj.PJ2007069.

22. Hu, P., Madsen, J., Huang, Q. & Skov, A. L. Elastomers without covalent cross-linking: Concatenated rings giving rise to elasticity. *ACS Macro Lett.* **9**, 1458–1463 (2020).

23. Kim, Y. S. *et al.* Gelation of the genome by topoisomerase II targeting anticancer agents. *Soft Matter* **9**, 1656–1663 (2013).

24. McKenzie, B. M. *et al.* Metallo-Responsive Liquid Crystalline Monomers and Polymers. *Chem. Mater.* **23**, 3525–3533 (2011).